بِسْمِ ٱللَّهِ ٱلرَّحْمَٰنِ ٱلرَّحِيمِ

Sudan University of Science and Technology

Colleague of Graduate Studies

Development of Electromagnetic Field Exposure Model for Multi-Technology Mobile Networks using Optimal Weighted Antenna Angle

تطوير نموذج التعرض للمجال الكهرومغناطيسي لشبكات الهاتف المحمول متعددة التقنيات باستخدام زاوية الهوائي الموزونة المثلى

A Thesis Submitted in Fulfilment of the Requirements for the Degree of Doctor of Philosophy in Electronic and Communication Engineering

By:

Mohammed Suleiman Elbasheir Mohammed

Supervisor:

Prof. Dr. Rashid Abdelhaleem Saeed

Co-Supervisor:

Dr. Salaheldin Mohamed Ibrahim Edam

October 2024

Approval Page

Sudan University of Science & Technology
College of Graduate Studies

جامعة السودان للعلوم والتكنولوجيا
كلية الدراسات العليا

Approval Page

Name of Candidate: **Mohammed Suleiman Elbasheir Mohammed**

Thesis Title:

Development of Electromagnetic Field Exposure Model for Multi-Technology Mobile Networks using Optimal Weighted Antenna Angle

Approved by:

1. External Examiner

Name: **Dr. Abdulgodus Alsamee** Signature: Date: **6/10/2024**

2. Internal Examiner

Name **Dr. Jacquline J. Faraj** Signature: Date: **6/10/2024**

3. Supervisor

Name **Prof. Dr. Rashid A. Saeed** Signature: Date: **6/10/2024**

cgs @ sustech edu. البريد الإلكتروني 83 769363 /فاكس ص.ب 407

Dedication

This thesis is dedicated to the soul of ***my father Suleiman Elbasheir****, my first teacher, who formed my character, and worked hard to support us during his whole life.*

Acknowledgment

For most, thanks to my God the most merciful and most gracious.

I would like to thank ***my supervisor Prof. Rashid Abdelhaleem Saeed*** *for his great supervision and support, canalized guidance, dedication, constant inspiration and encouragement.*

I also extend the thanks to ***my co-supervisor Dr. Salaheldin Mohamed Ibrahim Edam*** *for his wise guidance and support.*

A very special thanks to all my family members specially ***my mother, my wife, my brothers and sister, and my daughters and sun*** *for their unconditional love, support, patience and encouragement.*

Table of Contents

Abstract

Mobile networks are expanding quickly as a result of development in wireless technologies, especially with the recent introduction of the Fifth Generation New Radio (5G NR). The growth in mobile networks requires the installation of massive number of base stations (BSs) that bring concerns about increasing overall electromagnetic field (EMF) radiation exposure levels. The International Commission on Non-Ionizing Radiation Protection (ICNIRP) has published guidelines that have been adopted by many regulators in many countries to control the overall radiation from EMF transmitters. This research started with comprehensive review for recent works focused on BS EMF radiation assessment for BSs from different perspectives including review for standard limits. An enhanced formula is developed and proposed to accurately calculate the compliance distance (CD) considering more factors such as power reduction factor and system load. In situ measurements are conducted to validate the formula. The results show that CD has shorter distances when the power factor is considered. Also, the study investigated the compliance distance of shared sites by a group of Mobile Network Operators (MNO). The results shows that, compared with a single MNO, the CD increased by 41% in the case of two MNOs, 73% for three MNOs, and 100% for four MNOs. Additionally, sharing scale-up formula is driven and proposed to estimate the increase in CDs for N number of MNOs assuming that all MNOs use the same site configuration. Finally, a design model is developed and proposed to de-concentrate and reduce the total exposure ration (TER) from sectorized antennas of the multi-technology BS with no drawbacks on site coverage level and capacity. The model applies the concept of weighted antenna's azimuth to spread the total exposure among the horizontal direction. A set of simulations and field measurements were done in a life network to validate the proposed solution. The pre-and-post results show the TER and CD are reduced after applying the proposed model. Overall, the system records show no significant impacts were observed on site's coverage level and capacity.

المستخلص

تتوسع شبكات الهاتف المحمول بسرعة نتيجة للتطور في الحلول اللاسلكية خاصة مع طرح الجيل الخامس. تتطلب شبكات الهاتف المحمول تركيب أعداد هائلة من محطات البث التي تثير المخاوف بشأن زيادة مستويات التعرض للإشعاع في المجال الكهرومغناطيسي. بدأ هذا البحث بمراجعة شاملة للدراسات الحديثة التي تركز على تقييم إشعاع المجال الكهرومغناطيسي لمحطات البث و حدود التعرض القياسية المعتمدة من قبل بعض الهيئات التنظيمية . فتم تقييم مستويات التعرض للمجالات الكهرومغناطيسية لمحطة تبث بموجات لتقنيات متعددة، بما في ذلك الجيل الثاني والثالث والجيل الثالث و الرابع ة الخامس. تم إجراء محاكاة و قياسات و أظهرت النتائج أن نسبة التعرض الإجمالية كانت منخفضة جدًا مقارنة بحدود التعرض القياسية. تم تطوير واقتراح صيغة محسنة لحساب المسافة الامنة مع الأخذ في الاعتبار المزيد من العوامل في الحسابات مثل عامل تقليل الطاقة وحمولة النظام للحصول، وتم إجراء قياسات ميدانية للتحقق من صحة صيغة الحساب. وأظهرت النتائج أن المسافة أقصر عند أخذ عامل الطاقة في الاعتبار، وأن الجيل الخامس يمثل أعلى مساهمة في إجمالي نسبة التعريض عند المسافة الامنة في الاتجاهات الرئيسية للهوائي. تناولت الدراسة مسافة الامتثال الامنة للمواقع المشتركة وأظهرت النتائج أنه بالمقارنة مع مشغل واحد، ارتفع معدل مسافة الامتثال الامنة بنسبة 41% في حالة مشغلين اثنين، و73% لثلاثة مشغلين، و100% لأربعة مشغلين. بالإضافة إلى ذلك، تم تطوير صيغة تقريبية لتقدير الزيادة في المسافة الامنة لعدد N من المشغلين على افتراض أن جميع مشغلي شبكات الجوال يستخدمون نفس تكوين الموقع. أخيرًا، تم تطوير واقتراح نموذج تصميم لتقليل التركيز مستوي التعرض الإجمالي من الهوائيات للمحطة متعددة التقنيات دون أي تأثير سلبي في مستوى تغطية الموقع وسعته. يطبق االتصميم المقترح مفهوم استخدام زوايا حسب توزيع مستوي الانبعاث من كل هوائي و ذلك عن طريق فصل الهوائيات المثبتة أفقيا. تم إجراء مجموعة من عمليات المحاكاة لحساب الانخفاض في إجمالي نسبة التعرض الكلية و كذلك تم إجراء قياسات ميدانية لتقييم مستوى ونسبة التعرض الإجمالي و المسافة الامنة. أظهرت النتائج انخفاض ونسبة التعرض الإجمالي و المسافة الامنة بعد تطبيق النموذج المقترح. بشكل عام، تظهر سجلات االشبكة عدم ملاحظة أي آثار سلبية على مستوى تغطية الموقع وقدرتها الاستيعابية بعد تطبيق النموذج.

List of Figures

List of Tables

List of Abbreviations

1G	First Generation
2G	Second Generation
3G	Third Generation
4G	Fourth Generation
5G	Fifth Generation
5G-NSA	5G Non-Stand-Alone
5G-SA	5G Stand-Alone
6G	Six Generation
AAU	Active Antenna Unit
BBU	Base-Band Unit
BCCH	Broadcast Common Control Channel
BS	Base Station
BTS	Base Transceiver Station
CD	Compliance Distance
COST	Cooperation in Science and Technology
CoW	Cell On Wheel
CPE	Customer Premises Equipment
CPRI	Common Public Radio Interface
CSSR	Call Setup Success Rate
DAS	Distributed Antenna System
DCS	Digital Cellular System
DL	Down Link
E-Field	Electric Field
EIRP	Equivalent isotropic radiated power
EMF	Electromagnetic Field
ER	Exposure Ratio
FCC	Federal Communications Commission
FDD	Frequency Division Duplexing
FDTD	Finite Difference Tim Domain
GB	Giga Bytes
Gbps	Giga bit per second
GE	General Public

GHz	Giga Herts
GPS	Global Positioning System
GSM	Global System for Mobile Communication
H-Field	Magnetic Field
HO	Handover
HOSR	Handover Success Rate
IBS	Indoor Based Solution
ICNIRP	International Commission on Non-Ionizing Radiation Protection
IEC	International Electrotechnical Commission
IoT	Internet of Things
kHz	Kilo Hertz
LOS	Line of Sight
LTE	Long-Term Evolution
Mbps	Mega bit per second
ME	Mean Error
MHz	Mega Hertz
MIMO	Multi-Input-Multi-Output
mMIMO	massive Multi-Input-Multi-Output
MNO	Mobile Network Operator
MOCN	Multi Operator Core Network
MORAN	Multi Operator Radio Access Network
MPE	Maximum Permissible Exposure
MW	Microwave
NAPP	Normalized Average Power Pattern
NB-IoT	Narrow Band -Internet of Things
NLOS	Non-Line of Sight
NR	New Radio
OSS	Operation Support System
OW	Occupational Worker
PD	Power Density
PLMN	Public Land Mobile Network
PRB	Physical Resource Block
RAN	Radio Access Network

RF	Radio Frequency
RRU	Radio Remote Unit
RSCP	Received Signal Code Power
RSRP	Reference Signal Received Power
RX	Received Power
SAR	Specific Absorption Rate
SS-RSRP	Secondary Synchronization Reference Signal Received Power
SSS	Site Sharing Scale
TB	Tera Bytes
TDD	Time Division Duplexing
TEMS	Test of Ericson for Mobile Station
TER	Total Exposure Ratio
TX	Transmitted Power
UE	User Equipment
UL	Up Link
UMa	Urban Macro
UMTS	Universal Mobile Telecommunications System
USD	user distribution scenario
WHO	World Health Organization
WiFi	Wireless Fidelity
WLAN	Wireless Local Area Networks

Chapter One: Introduction

1.1. General Overview

Currently, the world is witnessing rapid development and growth in the Mobile wireless communication industry, this growth is followed by a significant increase in the installation of transmitting base stations (BS) inside and outside cities to ensure network coverage and service access to the public, there is huge demand and use of mobile and internet services everywhere from the world, which led to an increase in the number of subscribers and consumers of mobile communication services, the expectations indicate that increase in data usage through mobile networks will increase by 7,990% by year 2030 to reach 5,012 million TeraBytes (TB) per month compared to 62 million TB per month for the year 2020 [1, 2].

The increasing demand for the use of mobile phone networks has led to great progress in the development of network technology and solutions, starting from the first generation (1G), the second generation (2G) of Global System of Mobile communication (GSM) , the third generation (3G) of Universal Mobile Telecommunications System (UMTS), the fourth generation (4G) of Long-Term Evolution (LTE) ,and currently we are witnessing the deployment of the fifth generation (5G) of New Radion and Internet of things (IoT). It is expected end of this decade to see the introduction of the six-generation (6G). The service providers, network operators, and vendors are installing large numbers of new base stations and expanding existing ones to meet the increasing demand of consumers, which has raised questions about effects of electromagnetic waves and radiation from Mobile BSs on human health side.

Many scientific studies have been done over the past years to determine limits and high levels of electromagnetic field (EMF) radiation, it's used to set up controls and guides to regulate the amount of radiation transmitted from BSs. There are guidelines and controls adopted and issued by reliable international organizations, the most important of which is the one issued by the International Commission on Non-Ionizing Radiation Protection ICNIRP [3], and the USA Federal Communications Commission FCC [4], which both are recommended by World Health Organization (WHO) and adopted by national regulators in many countries.

Investigating the exposure to Radio Frequency (RF) radiation is a hot topic and research will continue as well as mobile technologies continue developing. The situation of adding more layers co-located in the same site and also the site sharing between operators need investigations to assess and predict the accumulated increase in radiation considering all technologies transmitting with maximum power and considering new induced solutions such as the massive Multi-Input-Multi-Output mMIMO transmitters (mMIMO). There is a high expectation that 5G technology will be the system of general-purposes technology [7], therefore deployment of 5G base stations requires balancing and optimization of both the cost and signal coverage [5], this balance is done by operators during the network planning design stage by which operators decide their strategy for deployment to go for 5G stand-alone (SA) or non-stand-alone (NSA) sites on existing co-location with 4G and 3G [6], according the results will have a different effect of total EMF output exposure levels.

1.2. Problem Statement

This study addresses an important problem that has three points related to total accumulated EMF radiation levels emitted from mobile network base station in the situation of the co-existing multi-technology transmitting from the same site.

- First, determining and quantifying the increase in EMF exposure levels in terms of Total Exposure Ratio (TER) due to the addition of ongoing 5G mMIMO deployments on existing sites as the situation of multi-technology co-located site, where most of the current related works (found in the literature) investigated the situation of single-technology.

- Second, the accuracy of the equation designed to calculate the compliance distances can be improved by developing an enhanced equation that considers more factors such as power reduction factors and system load, where most of the current related works (found in the literature) used the normal equation that used limited factors. Also, it requires to develop a formula to calculate the compliance distances for shared site by multi operators.

- Third, the increase in radiation levels due to the addition of future technologies leads to more restricted compliance distances which constrains the 5G deployment. An enhanced design technique or model is needed to de-concentrate and reduce the accumulated power densities.

1.3. Proposed Solutions

The proposed solutions in this research are based on intensive study and comprehensive investigation of the total accumulated radiation from the muti-technology base station site.

As 5G uses highly massive Multi Input Multi Output (mMIMO) systems, more factors and variables were taken into account in several recent investigations of EMF exposure, such as the actual emitted power, duty cycle, and spatio temporal. In this research, an enhanced equation is proposed by involving the power reduction factor and the system utilization load in the entire used power to calculate the power density and the compliance distance of multi-technology base station.

Also, in this study, a simplified equation is proposed to estimate the compliance distance for the situation of shared sites by a group of Mobile Network Operators (MNO) as multi-operators who are operating with multi-technology and sharing the same tower.

As the main solution in this research, a design model is proposed to de-concentrate and reduce the total exposure from sectorized antennas of the multi-technology base station with no drawback on site performance in term pf coverage level and capacity. The model applies the concept of weighted antenna’s azimuth to spread the total exposure by horizontally separating the installed antennas in the same sector which results in less total exposure ratio and reduces the complaince distance.

1.4. Research Objectives

Under the main aim of investigating the EMF accumulated radiation from the multi-technology base station, the main objectives of this research are:

A. To Enhance the calculation formula that calculate the compliance distance of the multi-technology base station by developing an enhanced equation that considers and involves the power reduction factor and the system utilization load.

B. To develop a mathematical formula to calculate the compliance distance for the site-sharing that includes multi-technology from different operators.

C. To reduce the total exposure ratio and the compliance distance for multi-technology bases station by Developing a design model or technique as a solution to de-concentrate the total exposure ratio and consequently reduce the compliance distance of multi-technology site.

D. To calculate the total exposure ratio of the accumulated radiation from a multi-technology site, quantify the contribution of each technology, and identify the increase in total exposure due to the addition of the 5G technology layers.

1.5. Research Significance

The outcome of this study has scientific significance and importance to the mobile network industry summarized in below points:

A. The analysis of the radiation considering multi-technologies may lead to revisiting and updating the regulation to apply better controls in the base station's deployment.

B. The results provide an enhanced equation that has more accuracy in calculating the compliance distances considering more factors and realistic configuration. This can be used by both mobile operators and the regulatory organizations.

C. The study proposes a new design technique to reduce the radiation level while maintaining the network coverage and capacity. This can be used by the operator's planning team during the design stage of the base station.

D. The results of this research will open the door and pave a way in future for more studies as it drives thinking toward finding and enhancing solutions to control electromagnetic radiation.

1.6. Methodology

The methodology of this study consists of five stages that include a combined approach of mathematical calculations, computational simulation, and field measurements to investigate the EMF exposure levels for multi-technology bases stations with the following details:

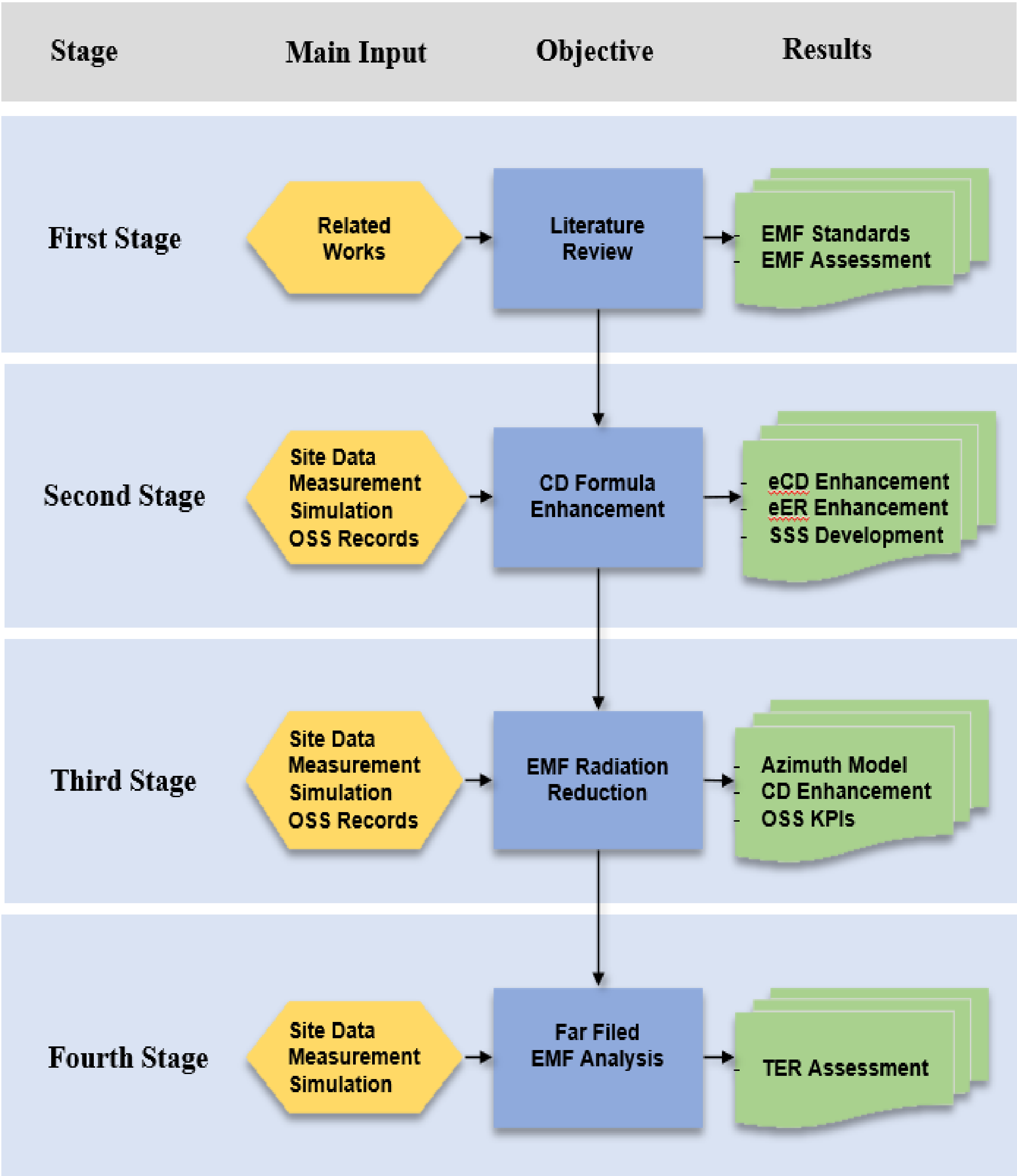

Figure 1.1. Main stages of the research methodology.

First Stage: The Literature Review

- To collect topic literature information and related work data which content of the recent published research and studies in international scientific libraries. Also, this includes studying their research methodologies and analysing their obtained results.

Second Stage: TER and CD Calculation Enhancement

- To use the computational approach (using the total exposure ratio equation) to calculate the compliance distance for multi-technology.
- To develop (to enhance) the compliance distance equation by modifying the formula to consider two factors (power reduction factor, and system load).
- To calculate the compliance distances for multi-technology base stations using the enhanced equation for different types of sites (macro, micro, small cell, and indoor-based solution).

Third Stage: Total Radiation Reduction

- To develop an enhanced technique to design the sectorization model of multi-technology that de-concentrates the radiation in the main direction which reduce the total radiation and resulting a shorter compliance distance.
- To conduct field tests in real-life base stations to evaluate the proposed technique, this should include the collection of field measurements.
- To conduct a computational simulation to evaluate the impact of the new design technique on the site coverage and capacity.

Fourth Stage: EMF analysis At the Far-Field

- To calculate the radiation levels for multi-technology sites using the UM/RM models to simulate and predict the signal strength, and power densities, and convert it to TER for different setup scenarios and worst cases.
- To conduct field measurements to validate and fine-tune the prediction model to reach optimum results and compare the measurement.
- To benchmark the results with the found related work results.

The following are the main tools will be used during the study:

- Narda SRM 3000 radiation meter tool will be used for in site to measure the power densities based on measurement setup and for different site types.
- TEMS (Test of Ericson for Mobile Station) will be sued to perform the road drive tests to measure the signal strength levels for serving and overlapped technologies.
- Huawei WINS cloud & Nokia A9955/Atoll simulation software will be used to perform signal prediction for multi-technology layer (2G, 3G, 4G. and 5G).
- MathWork MATLAB software be used to perform all data processing, modelling, calculation, and generate graphs and charts.

1.7. Thesis Organization

The chapters and corresponding content of this thesis are arranged as follows.

- **CHAPTER 2:** This chapter explores the topic of literature review and related works published recently mainly in the past five years, it summarizes the related studies and their findings results, it provides briefs about used methodologies, and gives comments on their main contributions and gaps.
- **CHAPTER 3:** This chapter discusses the theory of the EMF exposure ratio and the compliance distance calculation for multi-technology base stations, it explains in detail the devolved enhanced equation and proposed in this study to accurately calculate the compliance distance considering more parameters and involving the power reduction factor and system utilization load in the proposed formula. Also, it discusses the compliance distance analysis for multi-technology multi-operator site sharing, it presents the proposed simple formula that is driven to estimate the compliance distance for site-sharing scale up. Additionally, this chapter presents the proposed design technique (or model) for EMF exposure de-concertation as a solution to minimize the total exposure ratio of the multi-technology base station using the concept of weighted antenna's azimuth to spread the total exposure which reduces the compliance distance.

- **CHAPTER 4:** This chapter is the most important part in this thesis, because it includes the research contributions to the science. Its presents and discuss the measurement and simulation results of the proposed enhanced formula for calculating the compliance distance, and also explained the validation results of the formula. Also, this chapter presents the results of the driven equation for site sharing scall up. Further, this section disuses the measurement and results of the proposed de-concertation solution to reduce the total exposure ratio and compliance distance. At last, the chapter provides delated analysis for EMF exposure analysis at the far filed for multi-technology mobile base stations, it explains the methodology applied in the analysis including the simulation and field measurement, and presents the finding results of the total accumulated exposure and the contribution of each technology.

- **CHAPTER 5:** This chapter provided summaries of the thesis's conclusion along with some recommendations for potential further studies.

Chapter Two: Literature Review

2.1. Ionizing and Non-Ionizing Radiation.

Radiation is the emission or transmission of energy in a straight line, similar to a "ray" in geometry, this line propagates outward from the source in all directions when it passes through space or a substance, the term "radiation" can also apply to the energy that is released. Radiation comes in a variety of forms, including thermal, acoustic, electromagnetic, and particle radiation from radioactive sources, such as beta or alpha radiation [4,5,6, and 132], there are two forms of radiation, Iionizing and Non-Ionizing radiation.

2.1.1. Ionizing radiation

Ionizing radiation is a form of electromagnetic radiation or particle radiation that has sufficient energy to ionize atoms and molecules by dislodging tightly bound electrons. This ionization process alters the structure of atoms, leading to potential chemical and biological effects. Ionizing radiation carries high energy, typically greater than 10 eV (electron volts). This high energy is necessary to overcome the binding energy of electrons in atoms. When ionizing radiation passes through matter, it transfers energy to the atoms and molecules it encounters. This energy can knock electrons out of their orbits, creating ions—charged particles. Ionizing radiation is widely used in various fields, including medicine, industry, and scientific research, but requires careful handling and safety protocols to mitigate health risks. As shown in Figure 2.1, the Ionizing As examples, includes radiation emitted from:

- Alpha Particles.
- Beta Particles.
- Gamma Rays (γ):
- X-Rays.
- Neutrons.

2.1.2. Non-Ionizing radiation

Non-ionizing radiation is a type of electromagnetic radiation that does not carry enough energy to ionize atoms or molecules by completely removing electrons from them. Unlike ionizing radiation (such as X-rays and gamma rays), which has high energy and can potentially damage biological tissues and DNA, non-ionizing radiation has lower energy and is generally less harmful. Non-ionizing radiation includes:

- Radio waves: Used for communication, such as in radio, television, and cell phones.
- Microwaves: Used in microwave ovens and some communication technologies.
- Infrared (IR) radiation: Experienced as heat and used in things like remote controls and thermal imaging.
- Visible light: The light we can see, ranging from red to violet.
- Ultraviolet (UV) light: Beyond visible light, but not energetic enough to ionize atoms in most situations. It can cause sunburn and skin damage over prolonged exposure.

In general, non-ionizing radiation is considered less harmful than ionizing radiation, but it's still important to be mindful of exposure, especially in the case of intense or prolonged exposure. For example, excessive UV light can damage skin cells and increase the risk of skin cancer.

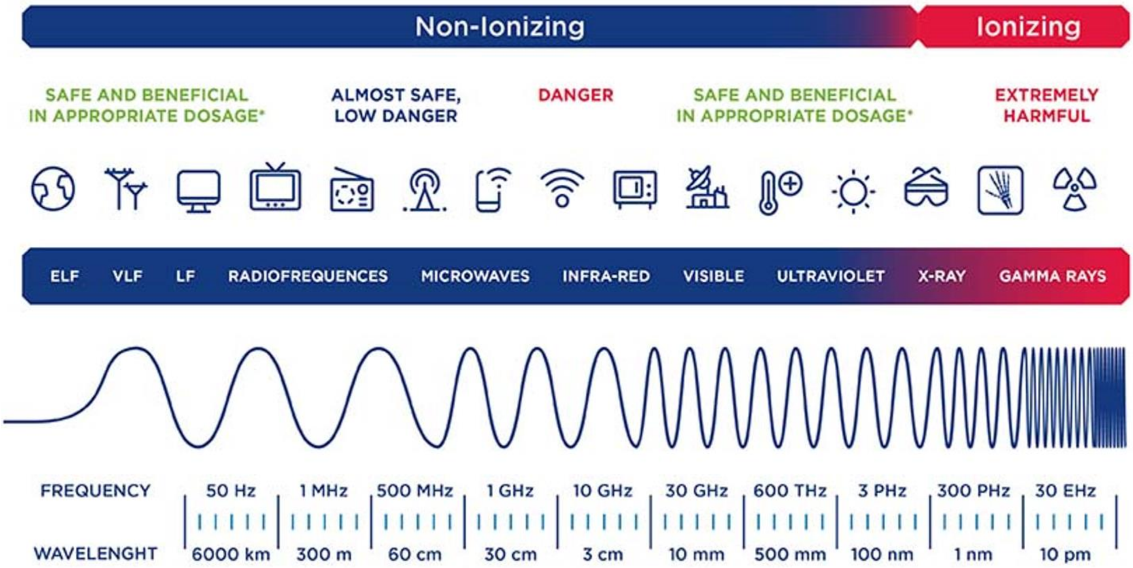

Figure 2.1. Ionizing and Non-Ionizing radiation on the spectrum range.

2.2. EMF Exposure Standrads

2.2.1. Common Adopted Standards

Radio resources emit EMF energy which is classified as Non-Ionizing radiation [4-6], and based on intensive researches conducted over last decades, EMF exposure standards has been set with safety controls on the level of EMF energy that can be absorbed by human bodies, the objective of exposure standards is to set the maximum amount of radio frequency energy level know as Specific Absorption Rate (SAR) measured in watt per kilogram that can be securely absorbed by human bodies. The standards and guidelines are designed to protect public health by limiting exposure to electromagnetic radiation. Several organizations and agencies have established guidelines for EMF exposure. Here are some of the most commonly referenced standards [43]:

1. **International Commission on Non-Ionizing Radiation Protection (ICNIRP)**: ICNIRP provides guidelines on limiting exposure to non-ionizing radiation, their guidelines cover a range of frequencies and are widely used internationally, and they focus on limiting exposure through set of reference limits and total exposure ratio for both occupational workers and general public.
2. **Institute of Electrical and Electronics Engineers (IEEE)**: The IEEE publishes standards related to electromagnetic compatibility (EMC) and safety, their standards are often referenced in various industries, particularly for ensuring safe electromagnetic exposure in occupational settings.
3. **National Council on Radiation Protection and Measurements (NCRP)**: The NCRP provides recommendations for radiation protection and safety, including non-ionizing radiation, and their guidelines are used primarily in the United States.
4. **World Health Organization (WHO)**: The WHO provides information and guidelines on health risks associated with EMF, while it does not set specific exposure limits, it offers guidance based on the assessment of scientific evidence.
5. **Federal Communications Commission (FCC)**: In the United States, the FCC regulates exposure limits for radiofrequency radiation, particularly in relation to telecommunications equipment.

6. **European Union (EU) Standards**: The EU has established limits for EMF exposure through directives such as the European Council Recommendation 1999/519/EC, which provides guidelines on limiting the exposure of the general public to electromagnetic fields.
7. **Canadian Guidelines**: Health Canada provides guidelines for EMF exposure in Canada, based on recommendations from organizations like ICNIRP and research on potential health effects.

Despite differences in scope and specific recommendations of above various standards, they share the following several common features:

1. **Exposure Limits**: All standards set maximum exposure limits to ensure that electromagnetic fields (EMFs) do not exceed levels that could potentially cause harm. These limits are defined for different types of EMF, including radiofrequency, microwave, and magnetic fields.
2. **Frequency-Specific Guidelines**: Guidelines typically provide exposure limits for specific frequency ranges. For instance, ICNIRP and IEEE guidelines address different frequency bands, with specific limits for radiofrequency radiation (e.g., mobile phones) and lower-frequency magnetic fields (e.g., power lines).
3. **Safety Margins**: Standards often incorporate safety margins, setting exposure limits well below levels where health effects have been observed. This approach is intended to account for uncertainties and variations in individual susceptibility.
4. **Health Effect Considerations**: Guidelines are based on scientific research into the potential health effects of EMFs, including both acute and chronic exposure. This includes examining evidence on thermal effects (e.g., heating of tissues) and non-thermal effects.
5. **Public and Occupational Exposure**: Many guidelines distinguish between limits for public (general population) and occupational (workers) exposure, with stricter limits for the general public to account for the lack of control over exposure conditions.
6. **Monitoring and Compliance**: Standards often include recommendations for monitoring and measuring EMF levels to ensure compliance with exposure limits.

This is important for both regulatory enforcement and ensuring safety in environments where EMFs are present.

7. **Periodic Review**: Standards and guidelines are regularly reviewed and updated based on new scientific research and technological developments. This ensures that they reflect the current understanding of potential health risks.
8. **Precautionary Principle**: While standards are based on existing scientific evidence, many guidelines incorporate a precautionary approach, especially in the face of scientific uncertainty. This means adopting protective measures even if the evidence is not conclusive.

This research considers only the ICNIP and FCC when it's required to referrer to exposure limits, because the ICNIRP and FCC are the most common adopted standards in many countries [43].

2.2.2. ICNIRP Standard

The ICNIRP was published in 1998 [22], and the most recent revision was revised in 2020 [4], guidelines for limiting exposure to protect humans exposed to EMF for frequency range between 100 kHz to 300 GH, the guidelines defines exposure limits for two of exposed persons, the occupational person who is exposed to controlled conditions related with his work, he supposed to be trained and aware of the risks of EMF. The general public is normal people who are not aware exposure to EMF radiation, by definition general population has more restricted limits as they are trained to avoid harm of radiation. The ICNIPR defines exposure limits as reference level based on baseline quantities driven form direct relation to adverse health effects caused by electromagnetic radiation. Table 2.1 and figures 2.2/2.3 show the reference levels of ICNIRP for both occupational and general public, and the radiation is considered to comply with guidance limits if shown to be below reference level.

Table 2.1. ICNIRP Exposure Limits for Frequency Range from 0.1 to 300 GHz.

Exposure Scenario	Frequency Range	E-field (V/m)	H-field (A/m)	Power Density (W/m^2)
Occupational	0.1-30 MHz	$660/f_M{}^{0.7}$	$4.9/f_M$	*NA*
	>30-400 MHz	*61*	*0.16*	*10*
	>400-2000 MHz	$3f_M{}^{0.5}$	$0.008f_M{}^{0.5}$	$f_M/40$
	>2-300 GHz	*NA*	*NA*	*50*
General Public	0.1-30 MHz	$300/f_M{}^{0.7}$	$2.2/f_M$	*NA*
	>30-400 MHz	*27.7*	*0.073*	*2*
	>400-2000 MHz	$1.375f_M{}^{0.5}$	$0.0037f_M{}^{0.5}$	$f_M/200$
	>2-300 GHz	*NA*	*NA*	*10*

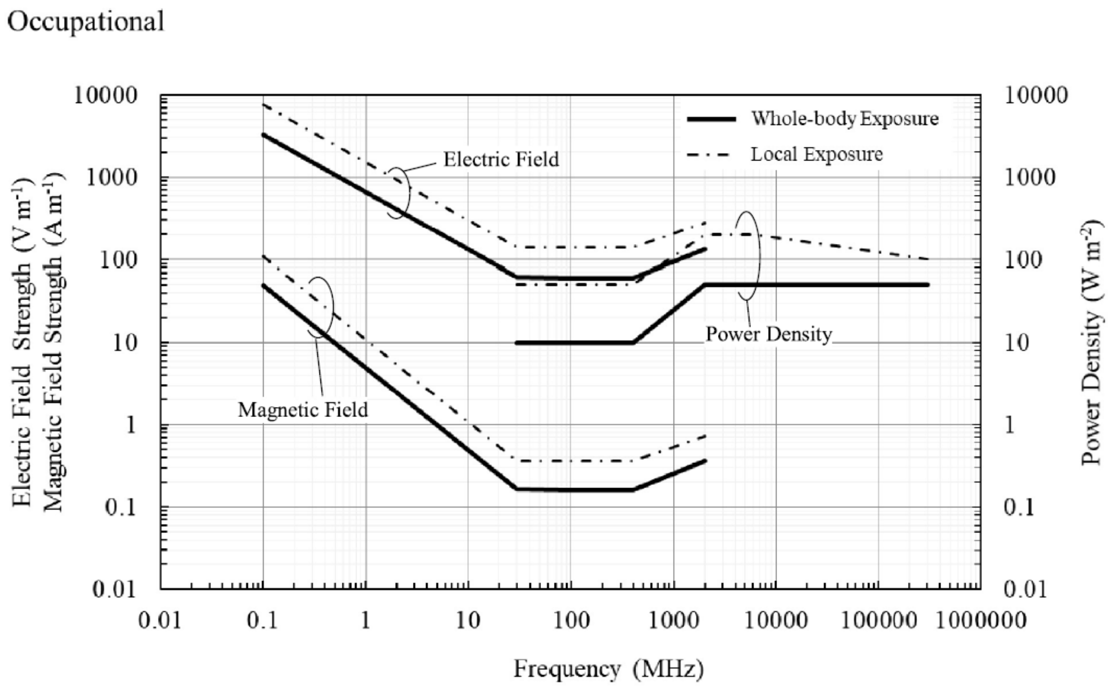

Figure 2.2. ICNIRP exposure limits for occupational frequency range from 0.1 to 300 GHz.

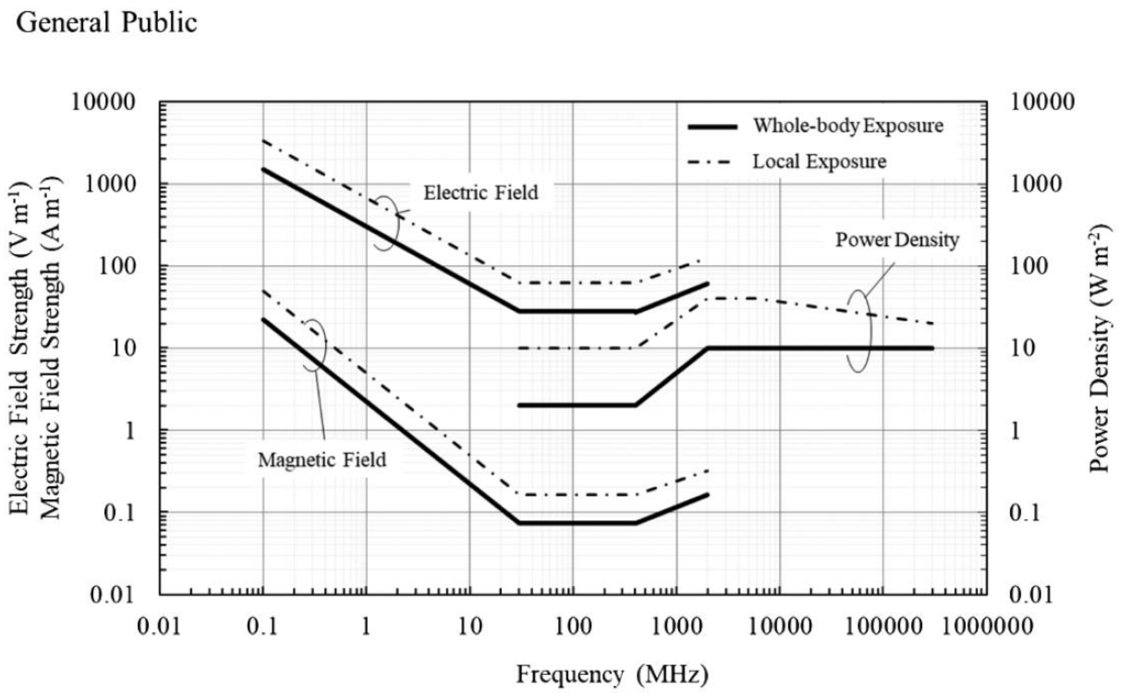

Figure 2.3. ICNIRP exposure limits for general public frequency range from 0.1 to 300 GHz.

In case of instantaneous exposure from different frequencies, ICNIRP states to find whether these exposures are additive in final accumulated effects, in this case, each frequency should be inspected separately against relative limits.

2.2.3. FCC Standard

The FCC exposure guidelines "Evaluating Compliance with FCC Guidelines for Human Exposure to Radiofrequency Electromagnetic Fields" is adopted in 1996 and amended in 1997 [6], The FCC defines exposure limits as Maximum Permissible Exposure (MPE) which are normally grounded on and based on guidelines and recommendations issued by the National Council on Radiation Protection and Measurements (NCRP) in the frequency ranges from 100 MHz to 1500 MHz. The FCC guidelines incorporate MPE limits in terms of electromagnetic power density and field level for those operating transmitters sources at frequency range between 300 kHz and 100 GHz. As with ICNIRP, the FCC guidance differentiates and defines two limits, the occupational (controlled) and general (uncontrolled) exposure limits of the population.

Occupational exposure defines max limits apply to conditions in which persons are exposed to EMF due to their work duties and they are made aware or informed of the potential risk of radiation exposure and can apply control over their conditions, and general population exposure defines limits apply to conditions in which the general. The public may be being exposed to radiation but are not being fully informed or aware of the potential risk due to this exposure or can't apply control over to avoid this exposure, consequently its always considered the general public under these cases they are not related to work employment. Table 2.2 shows the FCC MPE limits for both occupational and general population exposure.

Table 2.2. FCC Maximum Permissible Exposure Levels.

Exposure Scenario	Frequency Range (MHz)	E-filed (V/m)	H-field (A/m)	Power Density (mW/cm^2)
Occupational	0.3-0.3	*614*	*1.63*	*100*
	3.0-30	*1842/f*	*4.89/f*	$900/f^2$
	30-300	*61.4*	*0.163*	*1.0*
	300-1500	-	-	*f/300*
	1,500-100,000	-	-	*5.0*
General Public	0.3-1.34	*614*	*1.63*	*100*
	1.34-30	*824/f*	*2.19/f*	$180/f^2$
	30-300	*27.5*	*0.073*	*0.2*
	300-1500	-	-	*f/1500*
	1,500-100,000	-	-	*1.0*

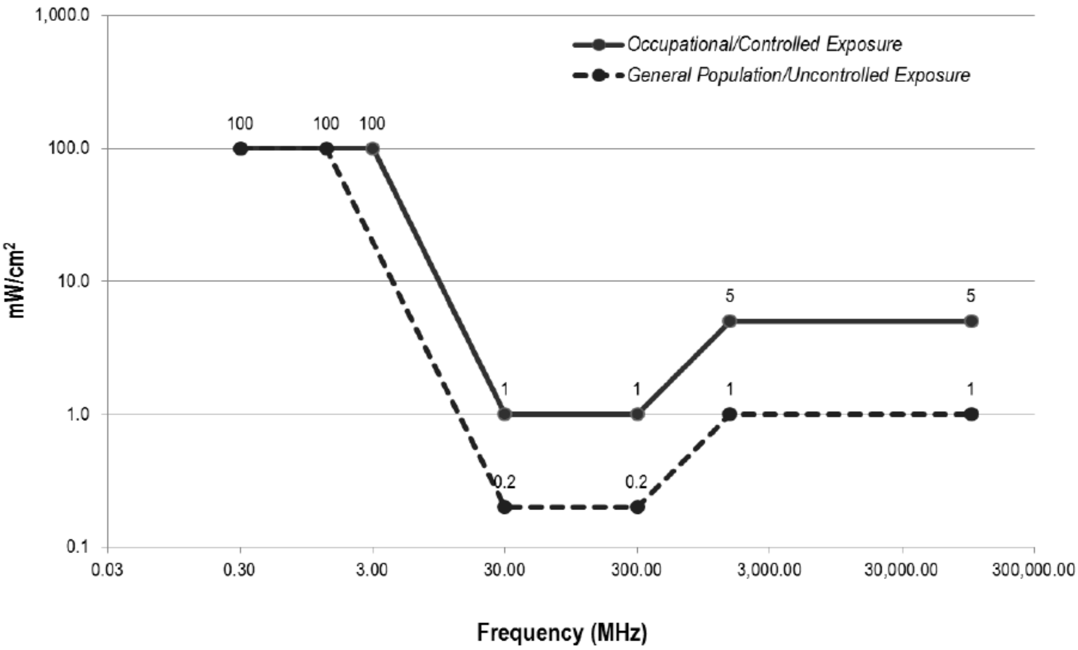

Figure 2.4. FCC limits of maximum permissible exposure for occupational workers and general public.

2.3. Exposure Level Assessment:

Complying with the standards limits for electromagnetic field exposure involves several challenges, which can be technical, regulatory, and societal. Here are some of the key challenges:

- Complex Measurement and Monitoring: The variability in EMF sources, such as mobile phone base stations, Wi-Fi routers, and power lines, emit varying levels of radiation depending on their operation, and monitoring these sources accurately requires sophisticated equipment and methods. Also, the EMF levels can be influenced by environmental factors like building materials, geography, and atmospheric conditions, making consistent measurement difficult.

- Technological Advancements: The rapid development of new technologies, like 5G networks, introduces new sources of EMF that may not have been fully considered when the standard guidelines were established, ensuring compliance with these evolving technologies is challenging. Additionally, with the increasing density of EMF-emitting devices, assessing the cumulative exposure from multiple sources can be complex.

- Regulatory and Policy Issues: Different countries and regions may interpret and implement the standard guidelines differently. Harmonizing these regulations while considering local needs and concerns can be difficult. Also, the governments must balance enforcing ICNIRP limits with other public health concerns, technological progress, and economic development, which may lead to tensions or compromises.

- Public Perception and Acceptance: Despite scientific consensus on the safety of ICNIRP limits, public concern about potential health effects persists, addressing these concerns while ensuring compliance with the limits can be challenging. Also, there is widespread misinformation regarding EMF exposure and its health effects, which can influence public perception and complicate compliance efforts.

- Cost and Infrastructure: Implementing measures to ensure compliance, such as shielding, redesigning infrastructure, or retrofitting existing systems, can be costly. Note that, monitoring and maintaining compliance with ICNIRP limits requires significant resources, including skilled personnel and advanced equipment.

- Interdisciplinary Coordination: Ensuring compliance often requires coordination between various stakeholders, including telecommunication companies, health agencies, and environmental bodies, which can be logistically challenging.

Addressing these challenges requires a coordinated effort involving technological innovation, effective regulation, public communication, and ongoing research into the effects of EMF exposure.

Due to the importance of this topic, huge number of studies are carried, and more are ongoing, we found many results published in international organizations related to this topic, the authors investigated the topic from several angles and from different point of views, however all have common ground to investigate the EMF exposure assessment. In this section, we reviewed some cases recently published and we presented here their work methodologies, findings, and results, and we selected those studies to present two categories, the calculation (predication) based assessment, and measurement-based assessment.

2.3.1. Calculation-Based Assessments

The calculation-based assessment involves estimating the levels of EMF exposure using mathematical models and calculations rather than direct measurements, this approach is particularly useful in scenarios where direct measurement is impractical or when assessing potential exposure in complex environments, here's what it entails:

- Calculation-based assessments start by modelling the EMF sources, this includes identifying the types of sources (e.g., antennas, power lines), their configurations, and their operational characteristics, the model will take into account factors such as frequency, power output, and emission patterns.
- The model incorporates environmental factors that affect EMF propagation, such as the distance from the source, obstacles (e.g., buildings), terrain, and atmospheric conditions, and these factors influence how EMF waves travel and interact with the environment.
- Using the data from the EMF sources and environmental factors, calculations are performed to estimate the electromagnetic field strength at specific locations, this might involve complex algorithms and simulation software to account for various influences and interactions.
- The calculated exposure levels are then compared with established safety guidelines or limits, such as those provided by ICNIRP or local regulations, to determine whether the exposure is within acceptable limits.
- In many cases, calculated estimates are validated by direct measurements to ensure accuracy, this step is crucial to confirm that the models and calculations align with real-world conditions.
- The calculation-based assessments have specific advantages such as they can be faster and more cost-effective than performing extensive direct measurements, especially in large or complex areas. Also, they allow for the assessment of potential exposure in new or modified environments before actual implementation, and useful for assessing scenarios where direct measurements are difficult or impossible, such as underground installations or high-altitude antennas.
- The calculation-based assessments have some limitations, the accuracy of the assessment depends on the quality of the model and the assumptions made.

Incorrect assumptions or incomplete data can lead to inaccurate results. Also, creating accurate models requires a good understanding of EMF propagation principles and access to detailed information about the sources and environment.

In summary, calculation-based assessments provide a useful alternative to direct measurements, particularly for planning and evaluating EMF exposure in various scenarios. However, they must be carefully executed and validated to ensure they provide reliable and accurate results. The next paragraphs summarize some recent related work found during the literature review and all are conducted as calculation-based assessments.

In [23], the authors presented an assessment model for calculating the EMF exposure from 5G BS considering time averaged practically emitted power, this model relays on numerical methodology and assume conservative EMF exposure calculations, the authors claim it is not practically to use the max equipment's power as it is not the real case, therefore the model considers amount of exposure radiation from downlinks which matches with exposure evaluation. This model is presented to calculate the power contribution fraction, the statistically conservative fraction anticipation for contribution of the total TX power to the exposure in the beam direction of broadside can be calculated by Equation (2.1):

$$E\big(P(\rho)\big) = \sum_{n=1}^{n_{conv}} \frac{\rho T_s}{nT} F_{TDD}.\big[k_{BB}(n) + k_{ADJ}(n)\delta_{ADJ} + k_{SL}(n)\delta_{SL}\big](1-\rho)\rho^n \qquad (2.1)$$

Where ρ is 5G system utilization, T_s is scheduling time total average per user (for n users) during EMF averaging time T, F_{TDD} is fractional downlink transmission time form total time (in this work, author used F_{TDD}= 0.75), k_{BB} is users served by broadside beam, k_{ADJ} is users served by adjacent beam waited by factor δ_{ADJ} (author used $\delta_{ADJ} = 0.1$ in this model), k_{SL} is users served by beams outside broadside and adjacent beam waited by factor δ_{SL} (author used $\delta_{SL} = 0.045$ in this model).

The authors, investigated their model accuracy at the far field by calculating the compliance distance considering 8x8 MIMO array, Figure 2.5 summaries the results which shows the actual compliance distances is shorter in the far field.

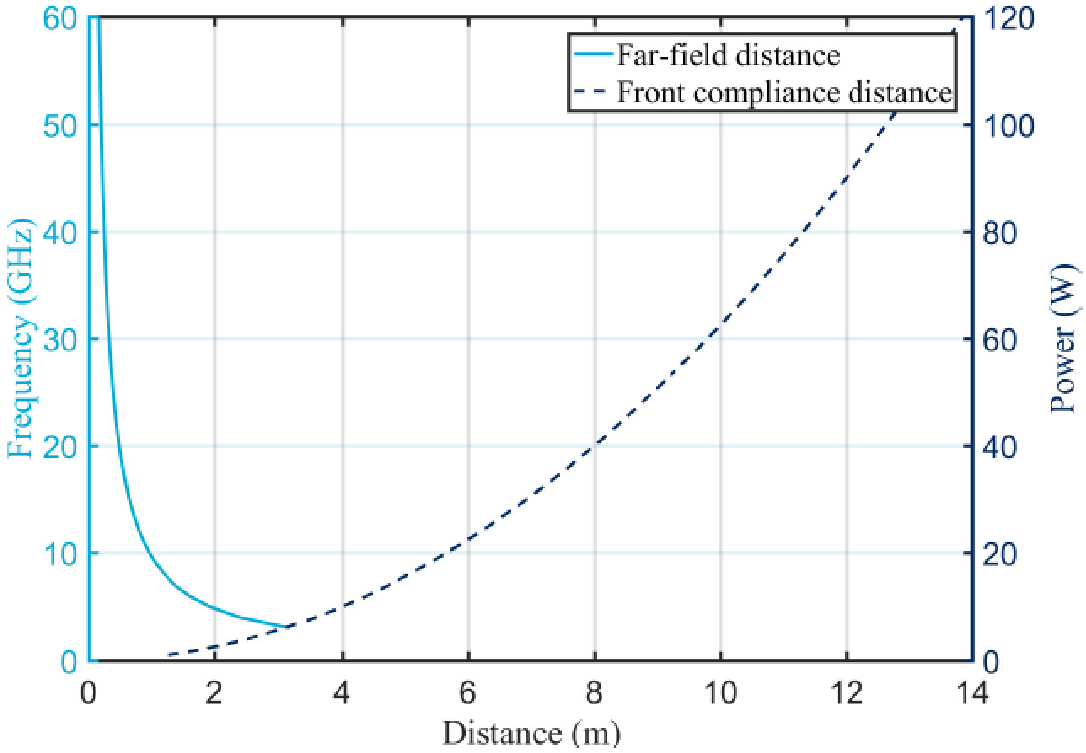

Figure 2.5. The far filed and from compliance distance for 8x8 MIMO array.

The authors evaluated the model for some expected user distribution scenarios (UDS), for different examined scenarios, the results shows that anticipation of statistically conservative fraction to EMF exposure is lower than theoretical max-power values, the max value for a large system utilization in case of users' density is weighted by a cosine function in direction and no elevation scanning is used, the values is about 22% of theoretical max-value, for scenario where user's density is distributed uniformly in direction and no elevation scanning is used, the result shows realistic maximum power value was 15% of the theoretical max-value using system utilization of 94%, for all the examined scenarios, the calculated max-power was lower than the max-theoretical values, even for using large system utilization, the maximum values was between 7% - 22%.

In [14], the authors presented a complete EMF signal level distribution in real public transportation tram car of Bilbao in Spain, they conducted simulation and measurements and used it to assess the exposure levels inside the tram, where signal sources (sideways the tram-ways) come from Mobile BSs providing 2G, 3G, 4G, or 5G.

The author referred to [10] and [14] that radiation for 18 public transport cars in different areas showed uplink connections is not relevant for outdoor. In simulation, the author used simplified human body model that matches low density cases, this to evaluate the effect of inside user density over the electric signal distribution inside the car, specifically the authors considered 101 passengers for high-density scenario and 33 for low density, accordingly the 2G/ 3G/4G/5G level is analysed. The authors use below formal of Equation (2.2) to calculate the E-field exposure level per location from the measurement received power considering the antenna factor:

$$E = P_R - P_{gain} + L_{cable} + AF \qquad (2.2)$$

Where E is the E-field level in V/m, P! is the received power in dBm, P!"#$ is the preamplifier gain, and AF is the antenna factor of the receiving antenna.

The authors used Geometrical Optics (GO) approach and the Uniform Theory of Diffraction (UTD) which electric field E created by GO and the diffracted electric field created by UTD are calculated by Equations (2.3) and (2.4):

$$E_{GO} = \sqrt{\frac{P_{rad} D_t P \eta_0}{2\boldsymbol{\pi}}} \frac{e^{-jBor}}{r} XL \qquad (2.3)$$

$$E_{UTD} = e_0 \frac{e^{-jks_1}}{s_1} D \sqrt{\frac{s_1}{s_2(s_1 + s_2)}} e^{-jks_2} \qquad (2.4)$$

where P_{rad} is the radiated power of the transmitter antenna, D_t is the directivity, X and L are the polarization ratio and path loss coefficients for each polarization, r the distance in the free, s_1 s_2 are the distances from the source to the edge and from the edge to the receiver point.

The highest E levels are measured for the high-density cases and around 1V/m at all frequencies are considered, and vice-versa for all analysed frequencies the E average values are higher for low density cases because impacted area is smaller than the remote area when considered whole vehicle volume. The results show 0.2 V/m approximately as the median for E field, the concluded results for both simulations and measurement show the signal radiation level is far below compare to the international standard of ICNIRP with 1-2% of the limits. Fig. 23 shows the comparison between the simulation and measurement results as a function of location within the tram wagon car. Analyzing the obtained graph, good agreement is achieved between simulation and experimental measurements, with a mean error of 0.019 V/m.

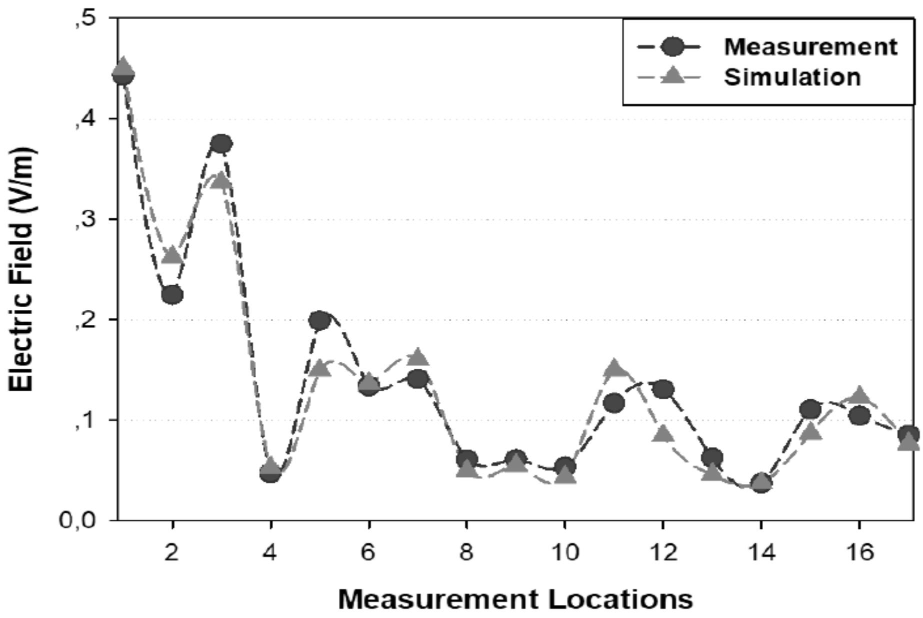

Figure 2.6. Comparison between simulation and measurement results within the tram.

E-field results exhibit slight variations depending on the frequency under analysis, but the maximum E-field levels are obtained for the high-density cases, at all frequencies considered as shown in Figure 2.7

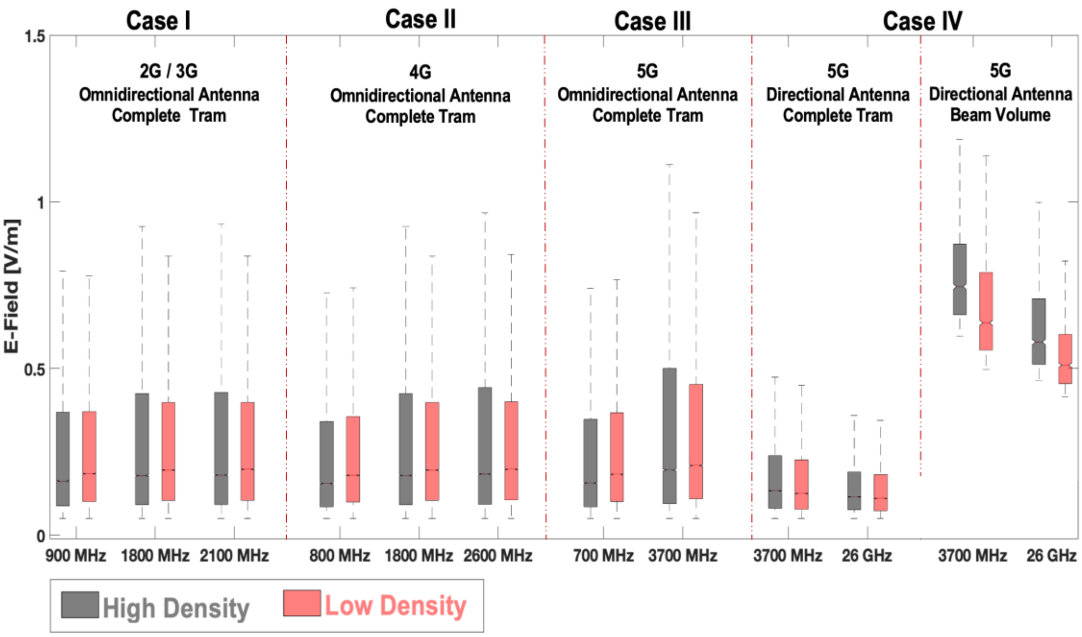

Figure 2.7. Comparison of E-field average exposure for the different systems

In [11], the authors assessed the EMF compliance for 5G through computational method relays on assumption that 5G is not intended to transmit at max equipment power with exception for short periods of times, in their assessment they referred to [17] to use averaged transmitted power significantly lower than max equipment power which leads to overly conservative exposure levels and compliance boundaries that calculated using Equation (2.5).

$$S = \frac{P_{avg} \, . \, G_{\theta,\emptyset}}{4.\pi.r^2} \tag{2.5}$$

Where S is power density, r is from the antenna to the point of calculation, P_{avg} is average transmitted power, G is antenna gain at the direction of r.

The authors used the data input in Table 2.3 for their assessment of 5G rooftop site and they considered the whole transmitted power will be consumed in the beam's traffics, which means no consumption in power for control channels and related signaling.

Table 2.3. Data Inputs for The Assessed 5G Base Station.

Data Input	Value
Technology base station	*5G NR BS*
Frequency band	*3400 MHz to 3600 MHz*
Antenna configuration	*(8x8) array, x-polarized, 128 elements 64(2x1) sub arrays (32/polarization)*
Tx/Rx configuration	*64T / 64R*
Maximum gain	*23.7 dBi*
Horizontal beam-width	$\pm 60^0$
Vertical beam-width	$\pm 20^0$
Down-tilt	3^0
TDD cycle	*75%*
Maximum TX Power	*200 W*
Maximum EIRP	*73.7 dBm*

The result shows for assessing 5G NR massive Multi Input Multi Output (mMIMO) at 50-watt max power for rooftop site to the occupational and the general public, the radiation compliance distance Infront of the antenna for general public is 9.6 meters, this assuming accessible areas and adjacent buildings at distances for public general is larger than calculated compliance distance. Also, the result shows for public general at vertical distance the minimum boundary is 2.8 meters, and is 4.2 meters for occupational workers, which means the radiation is below the limits is both zones are accessible.

Additionally, the results shows that cumulative distribution function value of different factors for rural and urban areas as shown in Figure 2.8.

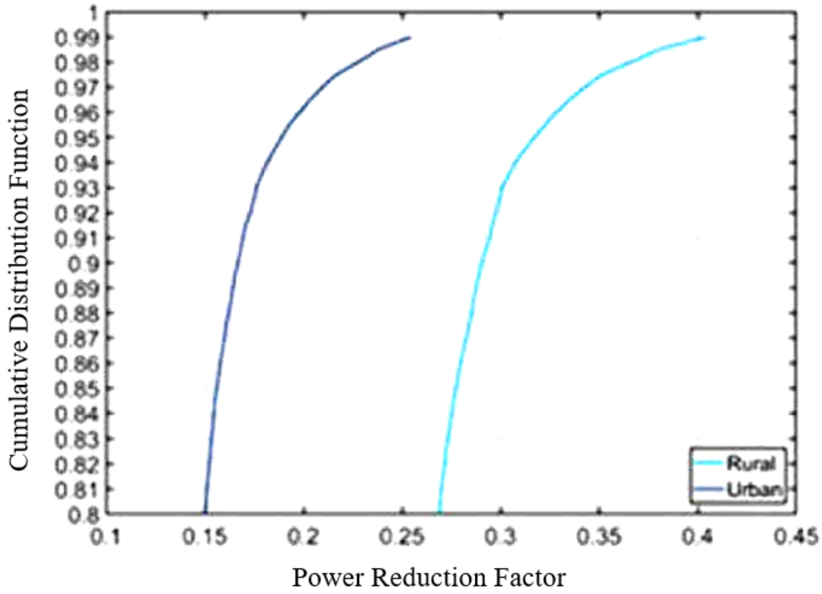

Figure 2.8. Cumulative distribute functions of the power reduction factor for rural and urban.

In [19], the authors conducted filed experimental analysis for verifying the reliability of the extrapolation techniques in overestimating the actual EMF due to LTE systems (Long Term Evaluation) compares to exposure limits, the measurements for two LTE layers at 800 MHz and 1800 MHz of two different operators are collected for a whole week period and analysed for overestimation synthetic indexes; the author used the extrapolation technique for maximal LTE exposure estimation which has been published in [15] and expressed by Equation (2.6)

$$E_{max} = \sqrt{N_{PBCH}} E_{PBCH} \quad (2.6)$$

Where E_{max} is maximum cell power, E_{PBCH} is signal channel power, and N_{PBCH} is scalling facto. The results have shown the overestimation probability index is 0.81 to 0.99, and as example Figure 2.1 shows the measured signal of LTE 1800 MHz for one operator.

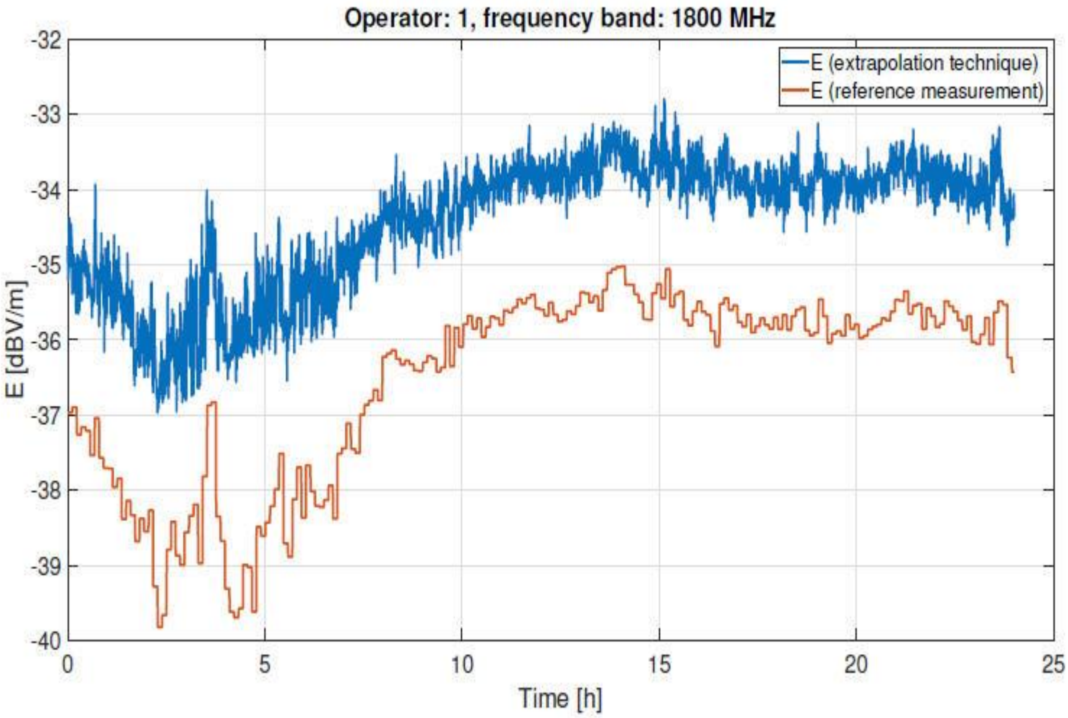

Figure 2.9. Real signal for one Operator for band 1800 MHz.

In [25], the authors provided assessment of the EMF exposure form 5G fixed small cell site compare to other 5G sources, they referred to [8, 20, 21, 26] that new 5G technology systems designed to use frequencies at higher bands than used by earlier mobile generations systems, and EMF radiation from small cells expected to has small exposure to general public as it uses small TX power which cause small energy absorption by human bodies although considering frequencies at higher bands, and in future this decreases may be balance to some degree the massive deployment of small cells compared to current 3G/4G solutions.

In this study, the author evaluated radiation exposures from a 60-watt base station 5G site at frequency 39 GHz installed on a 25 feet pole above ground level, this is typically one-use case for 5G solution deployment as wireless technology and of course other uses may have different scenarios and setup details. Figure 2.2 shows the radiation exposures at different distances from the site which are shown as percent of the maximum limits of FCC permissible exposure on receiving power density of the general public (1 mWatt/cm2).

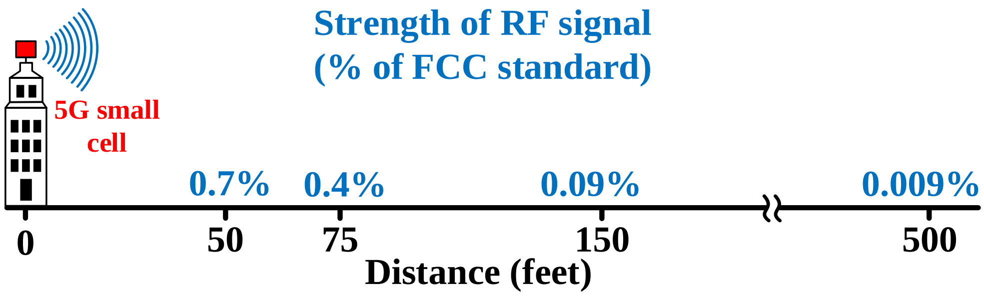

Figure 2.10. Signal level calculated from 5G small cell.

The calculation shows the exposures are very low from this 5G small site cell and decreases rapidly with increase of distance from the cell, and the received signals level from the small cell is measured from inside buildings would be even more smaller, at 50f the calculated radiation level is 0.7% compare to FCC's max limits in the direction facing the antenna, and the exposure is lower at farther distances, and at 150f it becoming smaller than 0.1% and it goes to very small level at 500 feet.

The authors of [20] studied how exposure limits acts as constraints for deploying 5G, they built their work by investigating EMF emissions from pre-5G systems, they referred to measurement done in Serbia [21] which shows 2G and 3G level exceed the limits in 15.6%, also they refereed to similar studies that states currently there is significant level from existing deployed pre 5G networks, the author's stated deploying of 5G sites may be challenging in urban areas because of exposure levels saturation.

In [9], compared the calculated the compliance boundary with measurements using multiple probe sensors. The authors carried measurements of a massive MIMO operating in a 4G LTE TDD (Time Division Duplexing), the probes were placed in the form of the mMIMO transmitter, and they compared the results with conservative simulations considering the same places. Considering 100% BS system load, the results show the peak recorded measurement of the electromagnetic file was 07.3% to 16.1% compare to limits of ICNIRP occupational reference level, and found the calculated figures show 79.3% at 2.3 GHz with TDD ratio 0.75, and compare to the computed values the field measurements represent the far field decrease in the occupational radiation compliance edges between 02.2 and 03.3 times.

In the research study [133], the authors used new statistical model to calculate the real EMF radiated exposure by mMIMo antenna based on average transmitted power over 24-hour period, Equation (2.7) expresses the used model as below:

$$S_{stat} = S_u(b_{max}.N_{max} + b_{adj}.N_{adj} + b_{oth}.N_{oth}) \quad (2.7)$$

Where S_{stat} is the statistical power density, Su is conservative power density, *b* is the beam factors, and *N* is number of users.

The results shown that the average transmitted power over 24 hours from base stations is approximately the 20% of the maximum transmitted power, and the power density *at 20* m evaluation with an antenna Gain of *15 dBi* is in compliance with the standard limits for all possible transmitted power as shown in Figure 2.10.

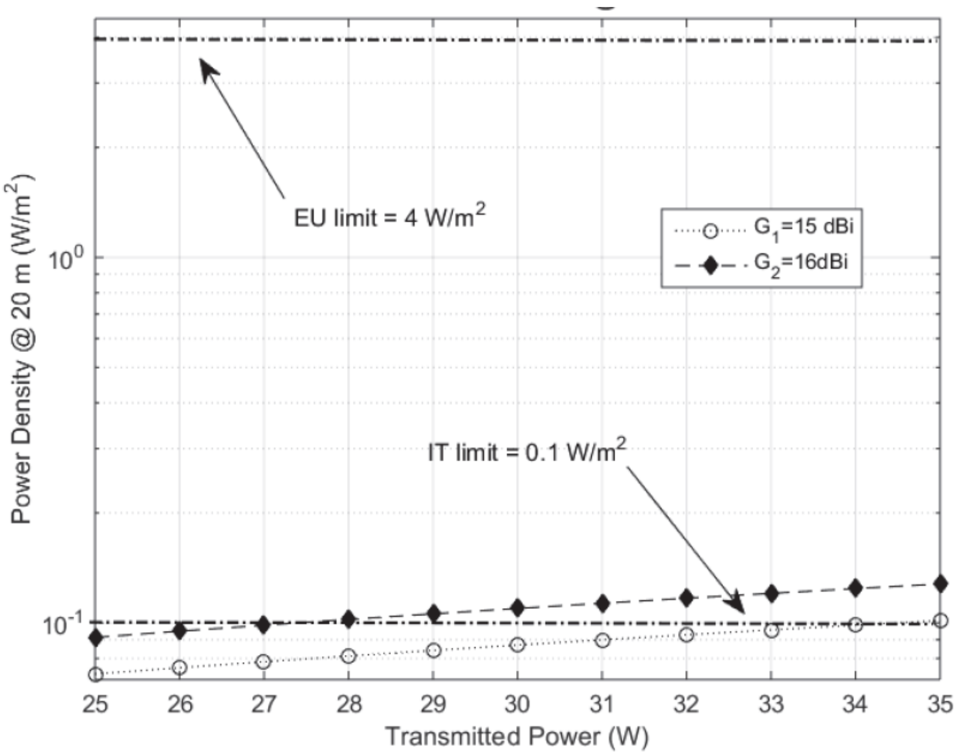

Figure 2.11. Statistical model for mMIMO.

In the research study [164], the authors proposed a calculation-based assessment technique for the spatial-average power density. This proposed technique combines standard near field measurements with the equivalent current method (EQC). The local power density is computed from a direct application of near field transformation from the equivalent currents.

The authors used Equation 2.8 to calculate the spatial-average power density *sPD* over an area A as expressed below:

$$sPD = \frac{1}{2A}\int_{A} Re[E.H].dA \tag{2.8}$$

Ther authors considered that the peak spatial-average power density (*psPD*) is defined as the maximum of *sPD* for all areas at a distance d can be calculated using Equation (2.9):

$$psPD(d) = Max_{all\ areas\ at\ d}\left\{\frac{1}{2A}\int_{A} Re[E.H].dA\right\} \tag{2.9}$$

The comparison of measurement and simulation for the normal component of psPD is shown in Figure 2.1, the blue and green traces are psPD for 1 cm^2 averaging area for measurements and simulations, respectively. The red and black traces are the psPD for 4 cm^2 averaging area for measurements and simulations, respectively. Spatial-average power density results from measured and simulated data shows good accuracy and applicability of the proposed method. The maximum deviation for peak spatial-average power density between measurements and simulations is 0.24dB for both averaging areas.

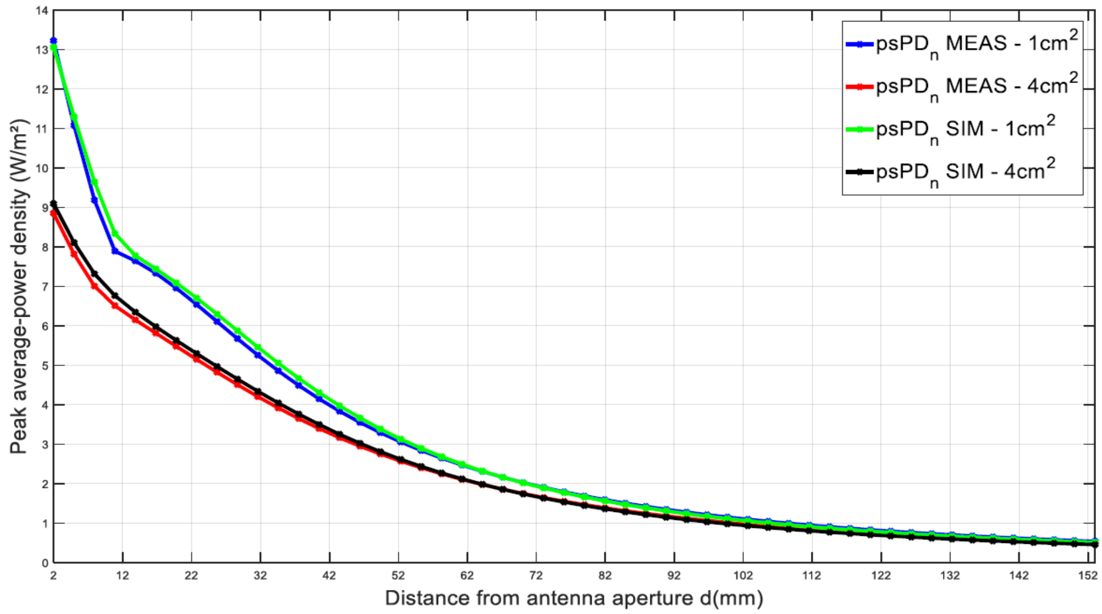

Figure 2.12. psPD comparison between Measured and Simulated data.

In [150], researchers from Ericsson proposed an average power feedback controller that mathematically guarantees that the average power transmitted over a specified time window by a single radio base station stays below a determined value defining the exclusion zone. The developed average power controller uses a combination of controllers to regulate the rate of change of a momentary fractional frequency resource limit in the scheduler. This restricts the momentary total transmit power since the transmit power is proportional to the scheduled frequency resources.

The proposed power control includes combination of proportional-differentiating control (PDC) and low complexity variant of model predictive control (MPC). The PDC controller provides smooth average power regulation during normal operating conditions such as for regular traffic, while the MPC acts as a safety net that guarantees that the selected average power threshold cannot be exceeded at any given time for any traffc type. This enables further reductions of the exclusion zone and/or reduces the inevitable throughput impact that follows from the use of an average power threshold, selected below the maximum power of the radio base station.

The authors use below Equation (2.10) to calculate the total power P_{tot} as:

$$P_{tot} = \frac{P_{max} + P_{max}T_D C}{s^2\left(\frac{1}{T} + P_{max}T_D C\right) + P_{max}C} {P_{tot}}^{ref} \tag{2.10}$$

Where P_{max} is the maximum power, C is proportional gain, T_D is the differentiation time, and P_{to}^{tref} is the control reference power.

Figure 2.13 shows the measured power density with the power control feature inactive and active. The green dashed line represents 0.84 W/m^2 which corresponds to 25 % of the power density at peak power, and the dashed black line represents 0.78 W/m^2 which is the maximum time-averaged power density measured with the power control feature activated.

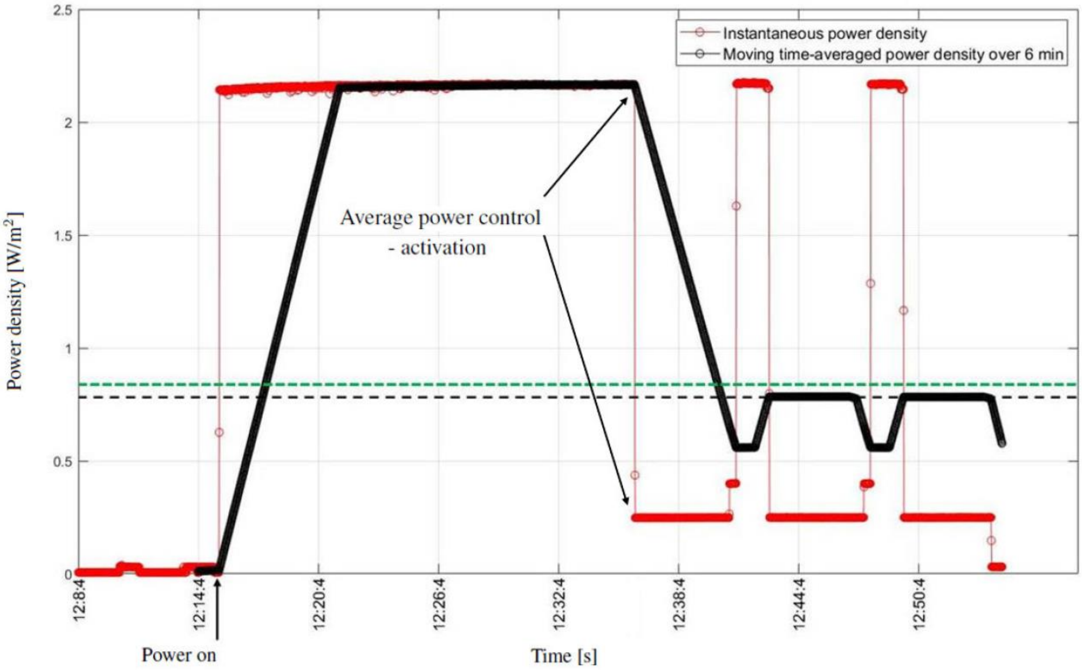

Figure 2.13. The power density with the power control feature inactive and active.

2.3.2. Measurement-Based Assessments

The measurement-based assessments for electromagnetic field exposure involves directly measuring the actual levels of electromagnetic fields in an environment rather than estimating them through calculations or models, this method provides real-world data on EMF exposure and is often used to ensure compliance with safety standards or guidelines, here's a detailed look at what it entails:

- Specialized measurement equipment and instruments are used to measure the strength and characteristics of electromagnetic fields, these include field meters and devices that measure the electric and magnetic field strengths, the spectrum analyzer tools used to assess the frequency and intensity of EMF across a range of frequencies, and the Dosimeter **i**nstruments that can measure accumulated exposure over time.

- The measurement-based assessments require to follow specifics measurement procedures include site assessment where the area of interest is surveyed to identify potential sources of EMF and determine the locations where measurements will be taken, data collection are taken at various points and heights to capture the spatial distribution of EMF for both indoors and outdoors, if applicable, and measurement should cover a range of frequencies, depending on the sources being assessed (e.g., radio, microwave, or power frequencies).

- The measurement-based assessments require analysis the collected data to determine the field strength and compare it with established safety limits, and evaluating how the measured EMF levels translate into potential exposure for people in the area.

- As advantage, the measurement-based assessments provide provides direct real-world measurements of EMF levels, which can offer a more accurate assessment of actual exposure compared to theoretical calculations. And, allows for the identification of specific sources and patterns of EMF exposure, which can be useful for addressing concerns or making improvements.

- measurement-based assessments have some limitation such as be time-consuming and costly, requiring specialized equipment and trained personnel. Also, it provides data for specific points in time, and exposure levels may vary due to changes in equipment operation or environmental conditions. In large or complex environments, it may be impractical to measure every possible exposure scenario, potentially leading to incomplete assessments.

In summary, measurement-based assessments provide concrete data on EMF exposure by directly measuring field strengths in the environment. This method is crucial for accurately assessing exposure and ensuring compliance with safety standards but requires careful planning and resources. The next paragraphs summarize some recent related work found during the literature review and all are conducted as measurement-based assessments.

In [18], the authors measured and investigated exposure levels at School in Spain, they conducted measurement in selected places around and inside the school building, Table 2.4 shows the downlink measured exposure level from mobile bands of GSM, UMTS, and DCS (Digital Cellular System).

Table 2.4. Personal Exposure Level from Mobile Phone.

Mobile Bands	Frequency (MHz)	Personal Exposure ($\mu W/m^2$)	
		Weekend	Week
GSM DL	*925-960*	*89.9*	*300*
DCS DL	*1805-1880*	*63.4*	*96.2*
UMTS DL	*2110-2170*	*99.2*	*214*

The results show the highest value during weekend was 99.2 $\mu W/m^2$ from 3G Downlink, and during the week was 300 $\mu W/m^2$ from 2G downlink, this is mainly due to the usage of handset and connections is more during week compare to weekend.

In [13], the author assessed the EMF exposure for frequencies 75 MHz to 3 GHz through indoor measurement, and compared the results to standard limits, the measurement covered the entire corporate building including various floors and offices. The authors mounted the measuring devices (isotropic probes) at different three heights 1.1m/1.5m/1.7m and all were above the floor level, and the time averaged is recorded for the signal level at every 2 minutes period with 6 minutes total for each height. Then, the E filed level is processed using the spatially average for each height matching to the measurement. Using Equation (2.11) they calculated the Total Exposure Ratio considering the total radiation level from different sources at each measured location.

$$\mathrm{TER} = \sum_{i>75\ \mathrm{MHz}}^{300\ \mathrm{MHz}} \left(\frac{E_i}{E_{lim,i}}\right)^2 \leq 1\,, \qquad f \geq 100\ kHz \tag{2.11}$$

where $E_{lim,i}$ is the exposure limit for the I sub band, according to the radiation regulation, and according to ICNIRP guidelines, if the TER is below 1 then the total radiation level is below the limits, and if the TER is above 1 then the total radiation level is above the limits. The results show that total the EMF signal was between 0.29V/m and 0.75 V/m, and TER was 0.000335 ± 0.000141 which clearly comes below the adopted Greek limits. The result found radiation for indoor is strongly related to the level of the floor, this because of the penetration and diffraction. The mobile network and broadcast radiation found more than 57 percent of the total radiation level, and it’s found to be more (reached 80 percent) at higher floors, In the areas of the indoor offices found has radiation level lower than limits.

In [16], the authors assessed the EMF exposure through filed measurements for frequency between 4 MHz to 6 MHz and compared the measured values with standard limits, the measurements were conducted in 4 different locations in educational institute in India where there are 3 BTS towers (Base Transceiver Station) and several WiFi hotspots (Wireless Fidelity) in the institute buildings. The results show the highest values are recorded respectively for 4G TDD, 2G 900, WLAN (Wireless Local Area Networks), and GSMR bands, the highest radiation exposure values are 547.8 mV/m, 1471 µA/m and 811.2 µW/m2 for 4G TDD at location L1, and the measured radiation at all 4 locations found far lower compare to standard limits, Table 2.5 shows the highest measurement as ratio compare to ICNIRP limits for different locations.

Table 2.5. Ratios of the Measurement Compare To ICNIRP.

EMR (Max)	Ratio (Measured / ICNIRP)			
	L1 (LTE-TD)	L2 (GSM900)	L3 (WLAN)	L4 (GSMR)
E_{avg} (mV/m)	*0.0089803*	*0.0092324*	*0.0022869*	*0.0021087*
H_{avg} $(\mu A/m)$	*0.0091937*	*0.0085036*	*0.0022594*	*0.0020881*
S_{avg} $(\mu V/m)$	*0.0000811*	*0.0000702*	*0.0000049*	*0.000044*

In [12], the authors assessed the EMF exposure through measurement form 5G uplink signal at frequency 3.5 GHz for three operators in Seoul city in South Korea, the measured traffics were obtained for period over approximately 270 hours, Figure 2.12 shows the RX power in dBm, and Table 2.6 shows the summary of measured mean liner RX power and the mean power density for the three operators.

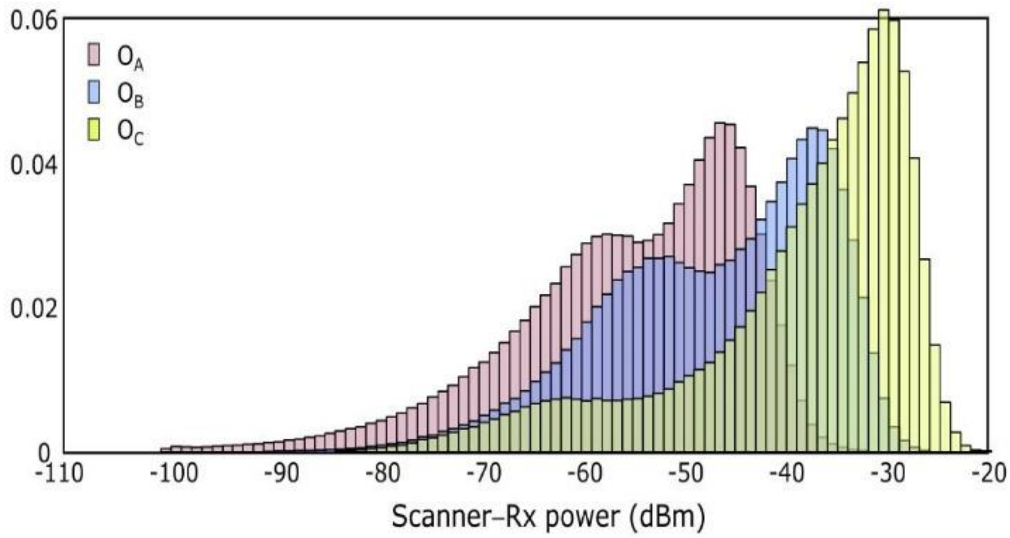

Figure 2.14. Measured RX power of the three operators.

Table 2.6. The Measured Mean Rx Power and Power Density.

Operator	Mean Rx Power (nW)	Mean PD μW/m^2
O_A	20.55	19.12
O_B	134.03	117.92
O_C	640.32	535.16

The results show the mean power density is lower than standard limits, and the authors concluded at the EMF level at receiver could be the level for human near an active handset, and it was no way to quantify the amount of exposure level contributed by only the traffic beam, and the total mean power density owing to the traffic beam, SSB beams, and transmitted power of the UE for each operator was less than 1 *m*W/m^2.

In the research study [159], the authors investigated the RF-EMF exposure for 5G bases-station with MIMO antenna through measurements. The study elaborated on how to take the measurement, sort, extract, and calculate the data, besides the effect of time duration on the amount of exposure. Various antenna directions, and using UE devices on six different test's location were uses in the experimental measurement. For all the tests, the distance between the 5G base station and the receiver was the same, and the locations were chosen based on getting the maximum power. The investigation was based on a code selective method due to the radiated power fluctuations over time with data traffic. The results shows that the maximum exposure from the base station is found to be 5.71 V/m, and the highest amount of average exposure is 2.02V/m.
The authors provide interesting details about the relation between the exposure and the UE applications during the measurements condensing various time duration as shows in Figure 2.15 and Figure 2.16.

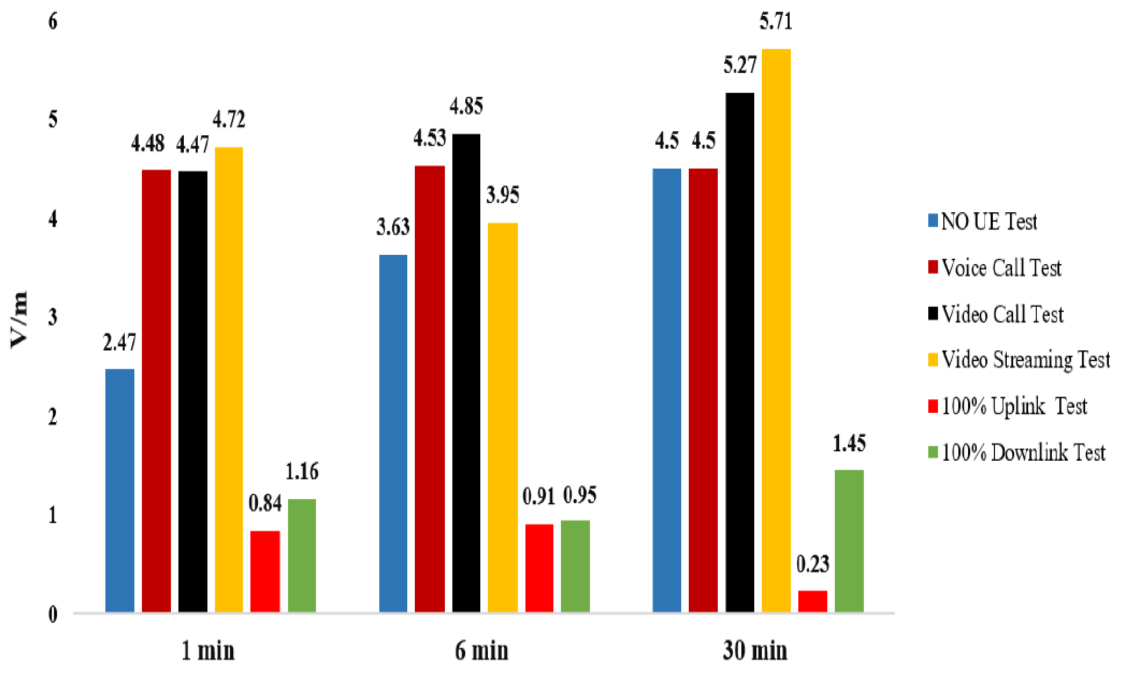

Figure 2.15. The maximum measured exposure level for various duration.

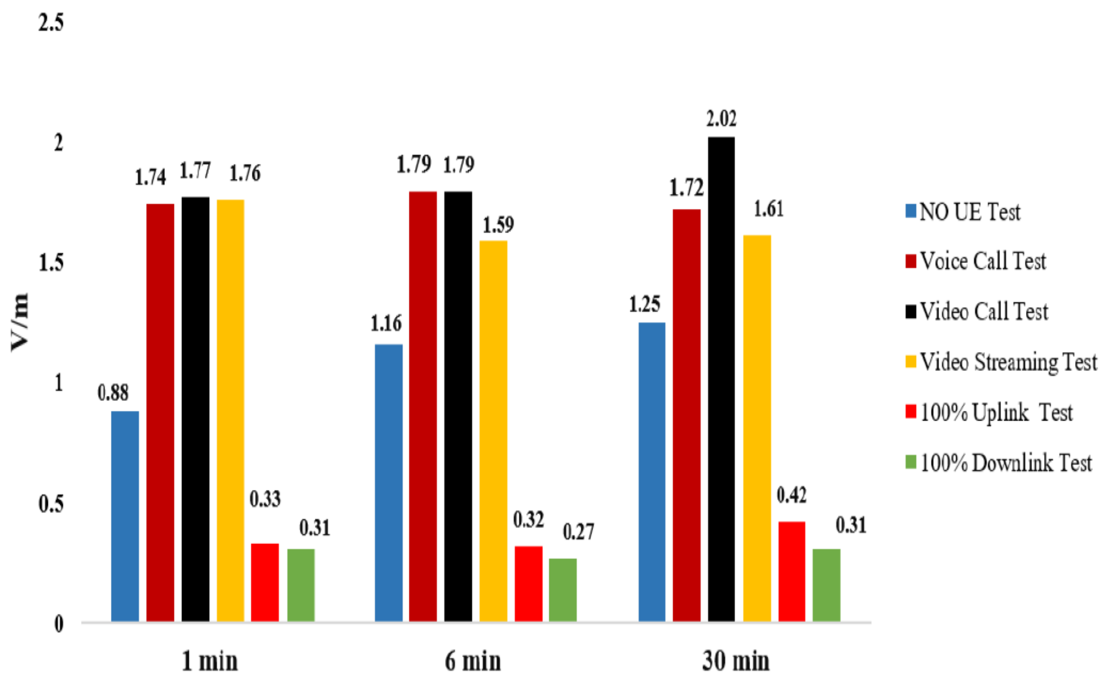

Figure 2.16. The maximum measured exposure level for various duration.

Chapter Three: Theory and Proposed Solutions

3.1. Total Exposure Ratio and Compliance Distance

3.1.1. Total Exposure Ratio for Multi-Technology

Based on massive biological studies, the ICNIRP has defined basic restrictions in terms of the specific absorption rate (SAR) to protect humans from RF adverse health effects. Because the ICNIRP is the most adopted standard in many countries [43], especially in Europe and the Middle East, in this study, the general public limits are used as a reference for total exposure levels. From the basic restrictions, a set of reference limits is defined by ICNIRP to translate the radiation restrictions into figures that can be practically measured and applied. In addition, ICNIRP has a defined limit for accumulative exposure of different sources instantaneously radiating, and the total exposure ratio (TER) should be accumulated according to Equation (3.1):

$$TER = \sum_{f=100\text{ kHz}}^{30\text{ MHz}} \left\{ \left(\frac{E_{inc,f}}{E_{inc,RL,f}} \right)^2 + \left(\frac{H_{inc,f}}{H_{inc,RL,f}} \right)^2 \right\}$$

$$+ \sum_{f>30\text{ MHz}}^{2\text{ GHz}} \text{MAX} \left\{ \left(\frac{E_{inc,f}}{E_{inc,RL,f}} \right)^2, \left(\frac{H_{inc,f}}{H_{inc,RL,f}} \right)^2, \left(\frac{S_{inc,f}}{S_{inc,RL,f}} \right) \right\} \qquad (3.1)$$

$$+ \sum_{f>2\text{ GHz}}^{300\text{ GHz}} \left(\frac{S_{inc,f}}{S_{inc,RL,f}} \right) \leq 1$$

where $E_{inc,f}$ incident E-field, $H_{inc,i}$ incident H-field, and $S_{inc,f}$ incident power density at frequency f. And, $E_{inc,RL,f}$, $H_{inc,RL,f}$ and $S_{inc,RL,f}$ are incident reference levels of F-field, H-field, and power density at frequency f.

The E_{inc} and H_{inc} terms have approximately the same ratio to Sinc outside the reactive antennas. Therefore, Equation (3.1) is modified to Equation (3.2), which means the *TER* depends on power density S_{inc}. Accordingly, below Equation (3.2) has been used for all TER calculations.

$$TER = \sum_{f>30\ \text{MHz}}^{300\ \text{GHz}} \left(\frac{S_{\text{inc,f}}}{S_{\text{inc,RL,f}}} \right) \leq 1 \qquad (3.2)$$

3.1.2. Compliance Distance for Multi-Technology

Both standards, the ICNIRP [5], and FCC [6], has defined the compliance distance (CD) or compliance boundaries form EMF exposure source is the minimum distance required to ensure that the levels of EMF exposure are within the safety limits and doesn't exceed maximum permitted power density set by regulatory bodies, and these limits are designed to protect human health by preventing excessive exposure to EMF, which can have biological effects. Simply, the compliance boundaries are distance where the TER equal one, therefore Equation 3.2 goes to Equation (3.3) at the compliance boundaries.

$$TER = \sum_{f>30\ \text{MHz}}^{300\ \text{GHz}} \left(\frac{S_{\text{inc,f}}}{S_{\text{inc,RL,f}}} \right) = 1 \qquad (3.3)$$

In [57], the International Electrotechnical Commission (IEC) has specified in their standard IEC62232 that the most accurate compliance boundary is obtained as an iso-surface shape that may be enclosed in simpler shaped volumes to define more conservative boundaries, such as the box shape (horizontal, vertical, and side) that is suitable for the sector coverage antenna with the described boundary in the horizontal, side, and vertical directions. In this study, the box-shape compliance boundary is considered to examine the exposure in the main two directions facing the antenna's horizontal and vertical beams. Following some related work and studies [58, 59, 89-130], we used the compliance distance (R_{CD}) to refer to the distance from the transmitter in which the total exposure ratio equals one as shown in Figure 3.1 .

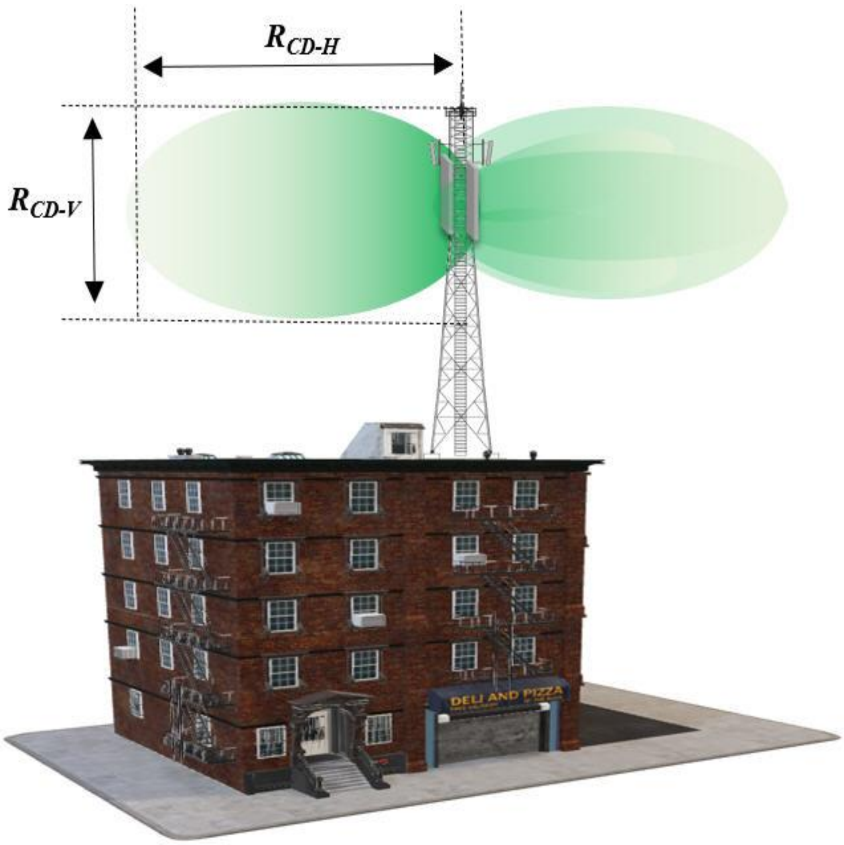

Figure 3.1. The Horizontal and Vertical Compliance Distances.

For the near field distance (R), the power density ($S_{inc,f}$) can be calculated using the free space model [57], as expressed in Equation (3.4):

$$S_{inc} = \frac{P_{T,f} \,.\, G_{A,f\ (\theta,\emptyset)}}{4.\pi.R^2} \tag{3.4}$$

Where P_T is the transmitted power in watt, and G_A is the transmitter antenna gain at the direction R. By substituting Equation (3.4) into the numerator of Equation (3.3), TER can be expressed as:

$$TER = \sum_{f > 30\ MHz}^{300\ GHz} \left(\frac{P_{T,f} \,.\, G_{A,f\ (\theta,\emptyset)}}{4.\pi.R^2.S_{inc,RL,f}} \right) \tag{3.5}$$

At the compliance distance R_{CD}, TER =1, then:

$$R_{CD} = \left(\frac{1}{4\pi} \sum_{f > 30\ \mathrm{MHz}}^{300\ \mathrm{GHz}} \frac{P_{T,\mathrm{f}} \cdot G_{A,\mathrm{f}\,(\theta,\emptyset)}}{\mathrm{S}_{\mathrm{inc,RL,f}}} \right)^{1/2} \tag{3.6}$$

3.1.3. An Enhanced Compliance Distance Formula

One of the crucial concerns is determining the compliance boundaries based on calculations that consider the accumulated power density from the multi-technology, using typical operating configuration, and involve the actual power reduction factor and system utilization load. The power reduction factor [57] is the factor applied to the maximum transmitted power to obtain the actual maximum transmitted power, and the system load is the actual system load due to the carrying traffic.

Equation (3.6) calculates the compliance distance based on the total maximum transmitted power, which is very conservative and doesn't reflect the actual practical power rating. Therefore, in this study an enhanced formula is investigated and proposed based to enhance the accuracy of compliance distances calculation.

There are three main aspects affect the actual maximum power that results in a realistic time-averaged transmitted exposure from mMIMO: 1-the TDD duty cycle, 2-the spatial distribution and scheduling time for connected users, and 3-the traffic load (system utilization). In the network where the test is done, the TDD duty cycle setting is 0.8 for all sites. The first and second factors are reflected and included in the power reduction value. Thus, using the power reduction factor and system utilization load provides an accurate result based on realistic average-time transmitted power. The 5G NR is designed based on mMIMO TDD or mMIMIO FDD, note that the main characteristic of the mMIMO is the beamforming, which targets transmitting power in the required directions rather than continuous power in a wide angular direction. The traditional approach to EMF calculations would consider the theoretical maximum power in each possible direction, this is inaccurate and would lead to bigger compliance distances consistent with all possible beams each transmitting at the maximum power.

With the growth of 5G using high grade of mMIMO systems, some recent studies investigated EMF exposure considering more parameters and methods such as the actual averaged radiated power, system utilization load, spatio-temporal, and spatial/time duty cycle [60, 61]. Additionally, in [57] IEC 62232 stated that EMF radiation assessments for human exposure can be conducted for actual maximum situations. In [62, 48], researchers from Ghent University and Ericsson conducted an investigation of the time-averaged instantaneous radiation and the theoretical maximum exposure from 5G NR. Their results found that the actual maximum exposure is very low compared to the theoretical maximum exposure for NR mMIMO. Accordingly, In this study, we added the power reduction factor ρ_r and the system load factor a_b as a reduction in the TX total power [63], which is used to compute the power density based on realistic condition, so Equation (3.5) expands to Equation (3.6), and Equation (3.7) transforms to Equation (3.8).

$$TER = \sum_{\mathrm{f} > 30\,\mathrm{MHz}}^{300\,\mathrm{GHz}} \left(\frac{\rho_{r,f} . a_{b,f} . P_{T,\mathrm{f}} . G_{A,\mathrm{f}\,(\theta,\emptyset)}}{4. \pi. R^2. \mathrm{S}_{\mathrm{inc,RL,f}}} \right) \tag{3.7}$$

$$R_{CD} = \left(\frac{1}{4\pi} \sum_{f > 30\,MHz}^{300\,GHz} \frac{\rho_{r,f} . a_{b,f} . P_{T,\mathrm{f}} . G_{A,\mathrm{f}\,(\theta,\emptyset)}}{S_{inc,RL,f}} \right)^{1/2} \tag{3.8}$$

The value of power reduction factor ρ_r and the system load factor a_b as vary from network to network, and from site to site, its mainly depend of the carried traffic and used technology. Chapter 4 diseuses and explained in details the used value of these two parameters in calculation.

Above Equation (3.8) represents the enhanced formula which is useful for network engineers to predict the EMF level and CD during the design stage before moving on to the installation stage. Also, this enhanced equation can be employed in EMF tools to determine the EMF CD through calculations.

3.2. Multi-Technology Site Sharing

3.2.1. Site Sharing Setup

The group of solutions and technologies operating at one site causes an increase in EMF exposure, and investigation is needed to evaluate the total accumulated radiation and assess it versus the standard limits [14, 29, 30].

In many countries, the MNOs have started to share mobile sites to expand their network services in terms of coverage footprint and capacity resources [81]. Site sharing has become a good alternative and a key approach because of the following main reasons [80]:

- It is less expensive to share a site than to build a new one. According to [76], infrastructure sharing can result in significant cost savings—up to 40% of assets can be saved by site sharing, and cash flow can improve by 31% as a result.
- The densification of the existing sites increases the difficulty of acquiring more physical sites within the required nominal locations and leads to fewer options.
- Site sharing enables the rationalization of the legacy 2G and 3G networks, taking into account the declining revenues from 2G and 3G networks and the higher spectral efficiency of the next generation of 4G and 5G technologies.
- Site sharing enables diverting the investment to other important innovations, such as the deployment of more 5G sites.
- Site sharing has some social benefits because it lowers network costs, which lowers the customer's service fee.
- Tower sharing benefits the environment by reducing the number of sites with better looks and views.

Network sharing can proceed in many ways, starting from a small part of the infrastructure up to full sharing, including core parts [82]. Sharing can be classified into two groups. The first is passive sharing, which mainly involves sharing parts of the tower site, antennas, and/or the backhaul part (MW, transport, fiber, etc.), as illustrated in Figure 3.2.

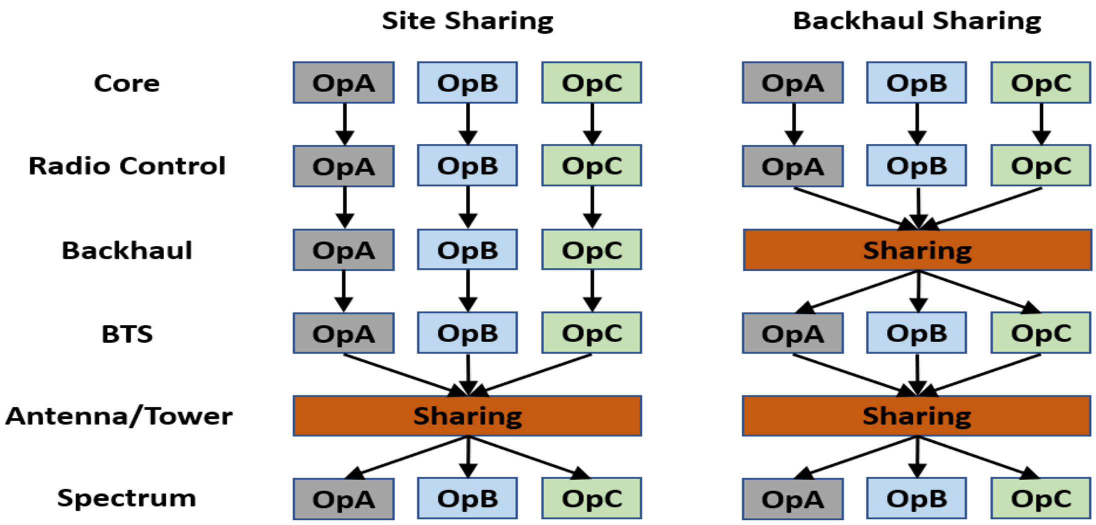

Figure 3.2. RAN passive sharing for 3 operators.

The second group is active sharing, which consists primarily of sharing the Radio Access Network (RAN) component with a dedicated frequency spectrum for each operator as the Multi-Operator RAN (MORAN) and a shared frequency spectrum as the Multi-Operator Core Network (MOCN), as shown in Figure 3.3.

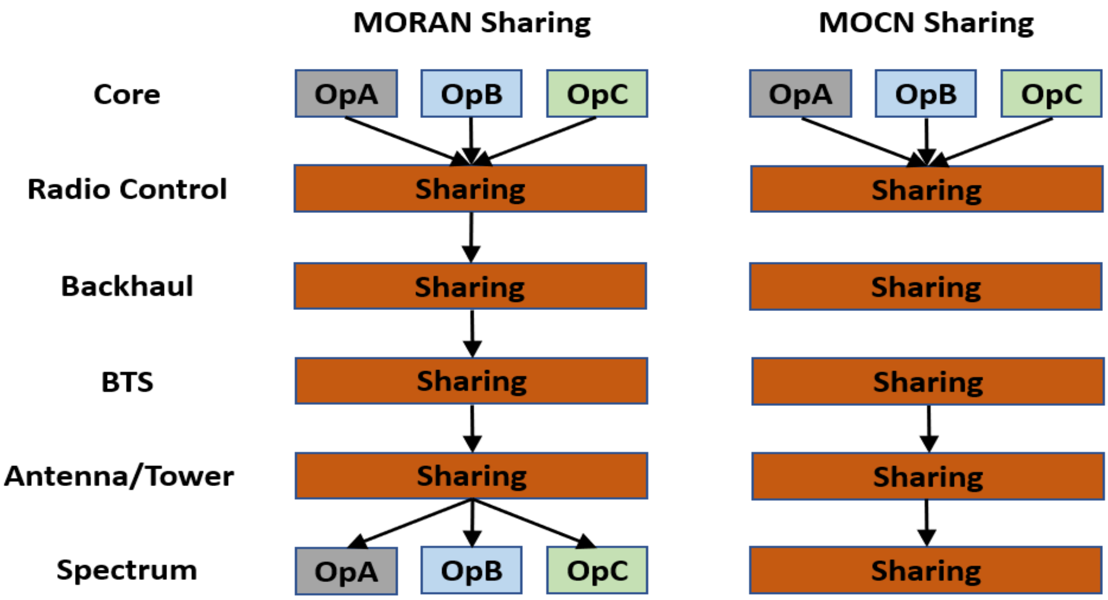

Figure 3.3. MORAN and MOCN active sharing for three operators.

Passive site sharing raises concerns about the total EMF exposure radiated from the antennae because each operator has separate radio equipment and all of them transmit from the same location. In this study, we determined the total accumulated exposure by calculating and analysing the CDs for the two types of sites sharing at the macro site and the indoor IBS site.

The merit of this analysis is in the calculations that consider the real operating setup (typical configurations) and involve the actual realistic transmitted power. Additionally, the goal was not to compare the levels of exposure to different technologies. Instead, it was to find out what the CDs are when different technologies and operators all transmit in the same place.

3.2.2. Total Exposure and Compliance Distance for Site Sharing

In the situation of the site sharing, the co-exist of many transmitters forms a multi-technology source of EMF radiation. In this case the total exposure ratio can be determined by enhanced Equation (3.7) which re-written here as Equation (3.9) considering all sources from all operators who transmit from the same site

$$\boldsymbol{TER\ (site\ sharing)} = \sum_{f > 30\ MHz}^{300\ GHz} \left(\frac{\rho_{r,f} . a_{b,f} . P_{T,f} . G_{A,f\ (\theta,\emptyset)}}{4 . \pi . R^2 . S_{inc,RL,f}} \right) \tag{3.9}$$

Furthermore, considering the enhanced formula the accurate R_{CD} for site sharing muti source can be determined by Equation (3.10):

$$R_{CD}(site\ sharing) = \left(\frac{1}{4\pi} \sum_{f > 30\ MHz}^{300\ GHz} \frac{\rho_{r,f} . a_{b,f} . P_{T,\mathrm{f}} . G_{A,\mathrm{f}\ (\theta,\emptyset)}}{S_{inc,RL,f}} \right)^{1/2} \tag{3.10}$$

3.2.3. Site Sharing Scale up Equation

The compliance distance calculation in Equation (3.10) fir site sharing can be scaled up to any number N of MNO operators sharing the same site, assuming all operators use the same configuration and technologies. For one MNO operator, Equation (3.10) and can be written as:

$$\mathbf{CD_1} = \left(\frac{\mathbf{1}}{\mathbf{4\pi}} \sum_{\mathbf{f > 30\,MHz}}^{\mathbf{300\,GHz}} \frac{\boldsymbol{\rho}_{\mathbf{r,f}} .\, \mathbf{a_{b,f}} .\, \mathbf{P_{T,f}} .\, \mathbf{G_{A,f\,(\theta,\emptyset)}}}{\mathbf{S_{inc,RL,f}}} \right)^{\mathbf{1/2}} \tag{3.11}$$

For N number of MNOs, Equation (3.11) becomes Equation (3.12):

$$\boldsymbol{CD_N} = \left(\frac{\mathbf{1}}{\boldsymbol{4\pi}} \sum_{\boldsymbol{f > 30\,MHz}}^{\boldsymbol{300\,GHz}} \boldsymbol{N}.\frac{\boldsymbol{\rho_{r,f}} .\, \boldsymbol{a_{b,f}} .\, \boldsymbol{P_{T,f}} .\, \boldsymbol{G_{A,f\,(\theta,\emptyset)}}}{\boldsymbol{S_{inc,RL,f}}} \right)^{\mathbf{1/2}}$$

$$\boldsymbol{CD_N} = (\,\boldsymbol{N})^{\mathbf{1/2}}.\left(\frac{\mathbf{1}}{\boldsymbol{4\pi}} \sum_{\boldsymbol{f > 30\,MHz}}^{\boldsymbol{300\,GHz}} \frac{\boldsymbol{\rho_{r,f}} .\, \boldsymbol{a_{b,f}} .\, \boldsymbol{P_{T,f}} .\, \boldsymbol{G_{A,f\,(\theta,\emptyset)}}}{\boldsymbol{S_{inc,RL,f}}} \right)^{\mathbf{1/2}} \tag{3.12}$$

As results, Equation (3.13) is driven form Equation (3.11) as below:

$$\boldsymbol{CD_N} = \boldsymbol{N}^{\mathbf{1/2}}.\boldsymbol{CD_1} \tag{3.13}$$

Equation (3.13) represents a simplified formula that gives the compliance distance based on the EMF Site-Sharing Scale (EMF-SSS formula). In reality, it is very hard to find a group of MNO operators that use the same configuration for multi-technology, including the power rating and system load. However, EMF-SSS formula is useful for predicting the CD and indicating the expected increase in the CD when accommodating more than one MNO at the same site

3.3. Total Exposure Reduction

3.3.1. Challenge for Reducing the TER

A set of technologies and solutions at one location necessitates an analysis to determine the exposure level in relation to standard limits and to analyse the total accumulated radiation [14, 29, 30], and many studies indicate this evaluation even should take place during the design stage of the network prior to deployment as EMF is a constrain in network planning especially for 5G [20, 84].

Almost, all cellular network operators use sectorized BSs with directional antennas, especially the three-sector model that helps to maximize the outdoor and indoor coverage**,** load balancing, capacity resources management, and interference optimization. Furthermore, the same sectors carry different technologies radiating in the same directions as co-located. Depending on the design strategy of the operator, the group of technologies either be connected to one multi-band antenna, or might be installed into separate antennas, but all antennas of one sector are directed in the same.

The investigation of EMF for multiple technologies is a crucial topic that aims to enhance the assessment of the compliance distance and to introduce models to minimize it, especially since it requires the operators to identify the compliance distances and mark them as exclusive zones and should be not accessible for the general public. This work's originality lies in providing a simple model (design technique) to de-concentrate the total exposure emitting from sectorized antennas of the multi-technology BS, while maintaining the network performance with no impact on the coverage signal levels and main KPIs. And, this model can be practically applied to the widely commonly used antennas that are currently installed for multi-technology BS.

3.3.2. TER for Sectorized BS

More effective coverage planning is possible when the cell site coverage is divided into sectors, which means dividing the coverage area into smaller sectors served by individual antennas. RF engineers adjust the signal propagation to reflect the geographic distribution of mobile users by concentrating the coverage in particular directions as shown in Figure 3.4 which represents (as an example) the three-sector model with 0/120/240 degrees as antennas' azimuth for the horizontal directions. Within the same cell site, the available frequency spectrum can be utilized numerous times with sectors remaining unaffected. This expands the cell site's total capacity and enables the simultaneous service of additional customers [85]. Also, improved load distribution throughout the cell site is made possible by antenna sectorization. Traffic can be dynamically forwarded across sectors during high usage periods to reduce congestion and guarantee that all users receive sufficient service quality. The RF engineers may simplify their planning and deployment process according to the area's nature, and they focus on improving every region separately, accounting for variables like topography, population density, and anticipated traffic patterns. Generally, sectorization is a commonly used technique in the construction and optimization of mobile cellular networks because it offers a balance between coverage, capacity, and interference control overall [86].

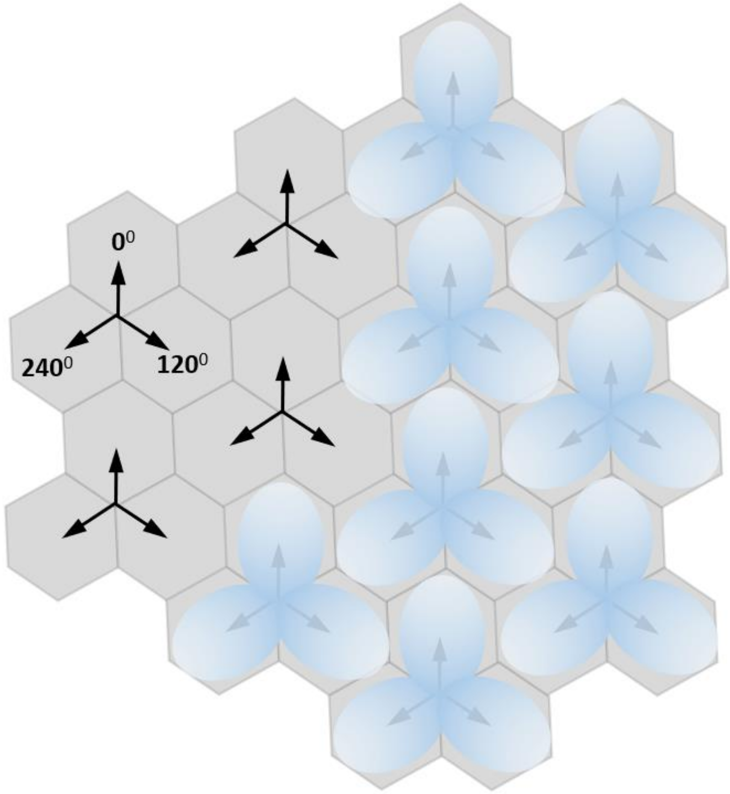

Figure 3.4. The three-sector model used in mobile networks.

While sectorization can enhance network performance and capacity, it increases the EMF radiation by concentrating the transmitting signals from all technologies in the antenna's directions. Upon the guiltiness of ICNIRP and FCC, the total exposure should be calculated considering the accumulated power density from the transmitting multi-technology sources.

3.3.3. Proposed Exposure Reduction Model

Figure 3.5 shows a sectorized cell with n number of antennas in one sector. From [4-6] the exposure ratio for each transmitter can be calculated using Equation (3.14).

$$\boldsymbol{ER_f}(\mathbf{sector}) = \frac{\boldsymbol{S_{inc,f}}}{\boldsymbol{S_{inc,RL,f}}} \tag{3.14}$$

Where ER_f is the Exposure of the antenna transmitting at frequency *f*. $S_{inc,f}$ and $S_{inc,RL,f}$ are the incident local power densities and their reference level at frequency *f*.

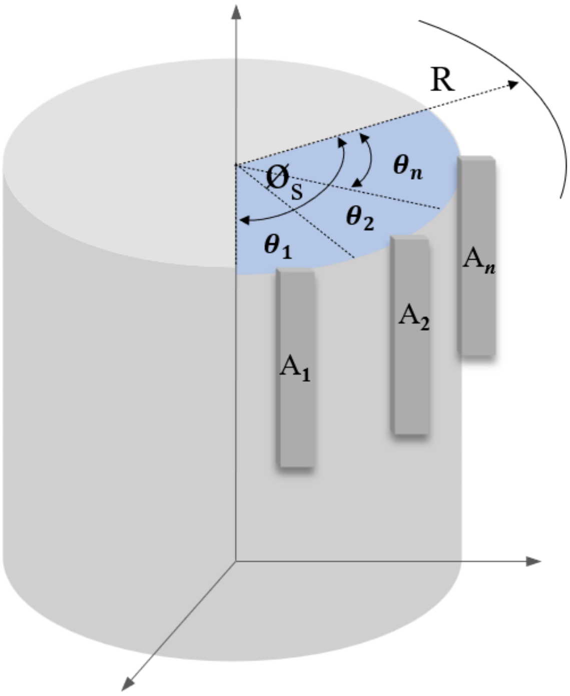

Figure 3.5. One sector in sectorized cells with i number of antennas.

With one sector, the exposure ration of one antenna that transmit at frequency f can be calculated by Equation (3.15)

$$ER_f = \frac{P_{T,f} \cdot G_{A,f\ (\theta,\phi)}}{4.\pi.R^2.S_{inc,RL,f}} \quad (3.15)$$

As per [29, 30, 83] The total exposure ratio of n number of transmitters in one sector TER_n can be calculated using Equation (3.16) as:

$$TER_n = \sum_{n,f} ER_f \quad (3.16)$$

Furthermore, the total exposure ratio of N sectors in one site TER_N can be calculated using Equation (3.17) as:

$$\boldsymbol{TER_N} = \sum_{\boldsymbol{n=1}}^{\boldsymbol{N}} \boldsymbol{TER_n} \tag{3.17}$$

Thus, by substituting Equation (3.16) in Equation (3.17), the TER_N can be calculated using Equation (3.18) as:

$$\boldsymbol{TER_N} = \sum_{\boldsymbol{n=1}}^{\boldsymbol{N}} \sum_{\boldsymbol{n,f}} \boldsymbol{ER_f} \tag{3.18}$$

Although the three-sector model is commonly used for cell sectorization, in this study we consider the general case of Ns number of sectors of one BS in the proposed model. Assuming each sector contributes equally in the *TER* of one BS, thus, the total exposure of one sector comes through angle width $\emptyset_{\boldsymbol{s}}$ which can be calculated simply using Equation (3.19)

$$\emptyset_{\boldsymbol{s}} = \frac{\boldsymbol{360}}{\boldsymbol{N_s}} \tag{3.19}$$

Within one sector, the total exposure TER_N can be distributed among the whole $\emptyset_{\boldsymbol{s}}$ by azimuth shifting the direction of each antenna towered separate sub-angle, each sub-angle has an angle width $\boldsymbol{\theta_n}$ where n is the number of antennas in one sector. Each $\boldsymbol{\theta_n}$ to have an angle width based on the TER_n weight out of the TER_N, which means the $\boldsymbol{\theta_n}$ is the weighted angle proportional to TER_n. Of course, this manner is to be applied for other sectors in the same site to have repeated antennas azimuth arrangement in the way for one technology to have the same antenna angle separation between all sectors. Thus, this approach gives a model to deconcentrate the total exposure (as spreading) in sub-directions rather than having all antennas transmitting toward one direction. So, the $\boldsymbol{\theta_n}$ can be calculated using Equation (3.20).

$$\boldsymbol{\theta_n} = \emptyset_s * \frac{\boldsymbol{ER_n}}{\boldsymbol{TER}} = \frac{\boldsymbol{360}}{\boldsymbol{N_s}} * \frac{\boldsymbol{TER_n}}{\boldsymbol{TER_N}} \tag{3.20}$$

Finally, by substituting Equations (3.15, 3.16, 3.18) into Equation (3.20), it gives Equation (3.21) to calculate the θ_n .

$$\boldsymbol{\theta_n} = \frac{\mathbf{360}}{\boldsymbol{N_s}} * \sum_{n,f} \frac{\boldsymbol{P_{T,f}} \cdot \boldsymbol{G_{A,f(\theta,\emptyset)}}}{\mathbf{S}_{\mathbf{inc,RL},f}} \Bigg/ \left(\sum_{n=1}^{N} \sum_{n,f} \frac{\boldsymbol{P_{T,f}} \cdot \boldsymbol{G_{A,f(\theta,\emptyset)}}}{\mathbf{S}_{\mathbf{inc,RL},f}} \right) \quad (3.21)$$

In the validation and results (section 4.3), will discuss in detail the results that show this model doesn't affect the base station performance in terms of coverage level and capacity. However, it is important to mention this model is applicable for macro sites that serve in areas where continuous coverage is required around the whole site area, and it's not applicable for below such cases:

- For sites that have sector's azimuths intentionally are directed toward certain locations for special coverage and capacity requirements such as highway road sites.
- For sites that use one antenna for all technologies such as penta-band and hexa-band antennas.

3.3.4. Complaince Distance Reduction

Consequentially, applying the proposed design model using Equation (3.21) as separation angles between antennas, this will result in reducing the compliance distances as well. This reduction in only the horizontal direction which the most critical as it's the direction of the main antenna's main beam.

In [43, 71], the IEC62232 has stated in their guidelines the most precise compliance border possible as an iso surface pattern that may be contained in simpler shaped volume to create more restricting parameters, such as the box-shape (horizontal, vertical, and side) that is appropriate for the sectorized site with the vertical and horizontal boundaries of the coverage antenna. The side CD ($R_{CD\text{-}S}$) can reach maximum value equal to horizontal CD when rotate the antenna's main beams horizontally toward the side direction note that horizontal azimuth can be from 0 to 360 degrees. In this work, the two primary directions facing the horizontal and vertical beams of the antenna are considered similar to related studies found in the literature [58, 59, 77-79] assuming the $R_{CD\text{-}H}$ is maximum boundary for all horizonal directions including side direction as shown in Figures 3.6, 3.7, and 3.8, where the R_{CD} is the compliance distance in the two directions ($R_{CD\text{-}H}$ at the horizontal, and $R_{CD\text{-}V}$ at vertical) from the transmitter at which the entire *TER* equals one as per ICNIRP and FCC guidelines [4-6].

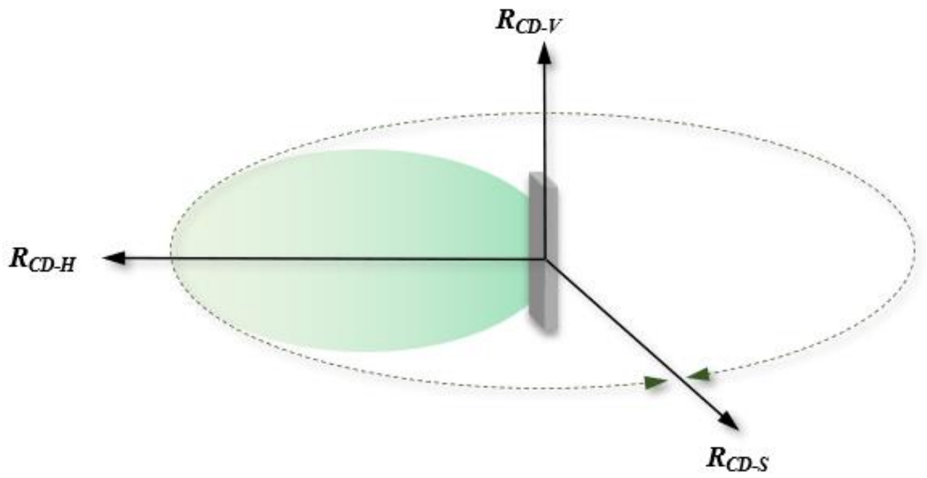

Figure 3.6. Horizontal, vertical, and side boundaries of sectorized site.

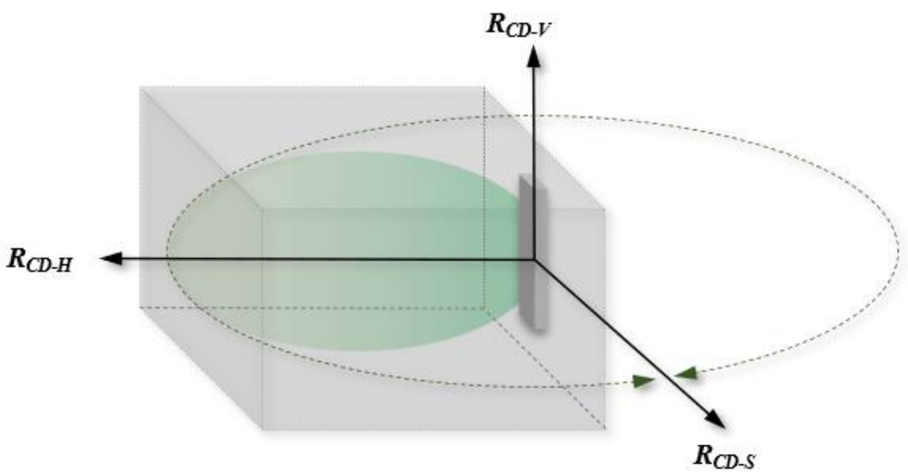

Figure 3.7. Box-shape CD boundaries of the sectorized site.

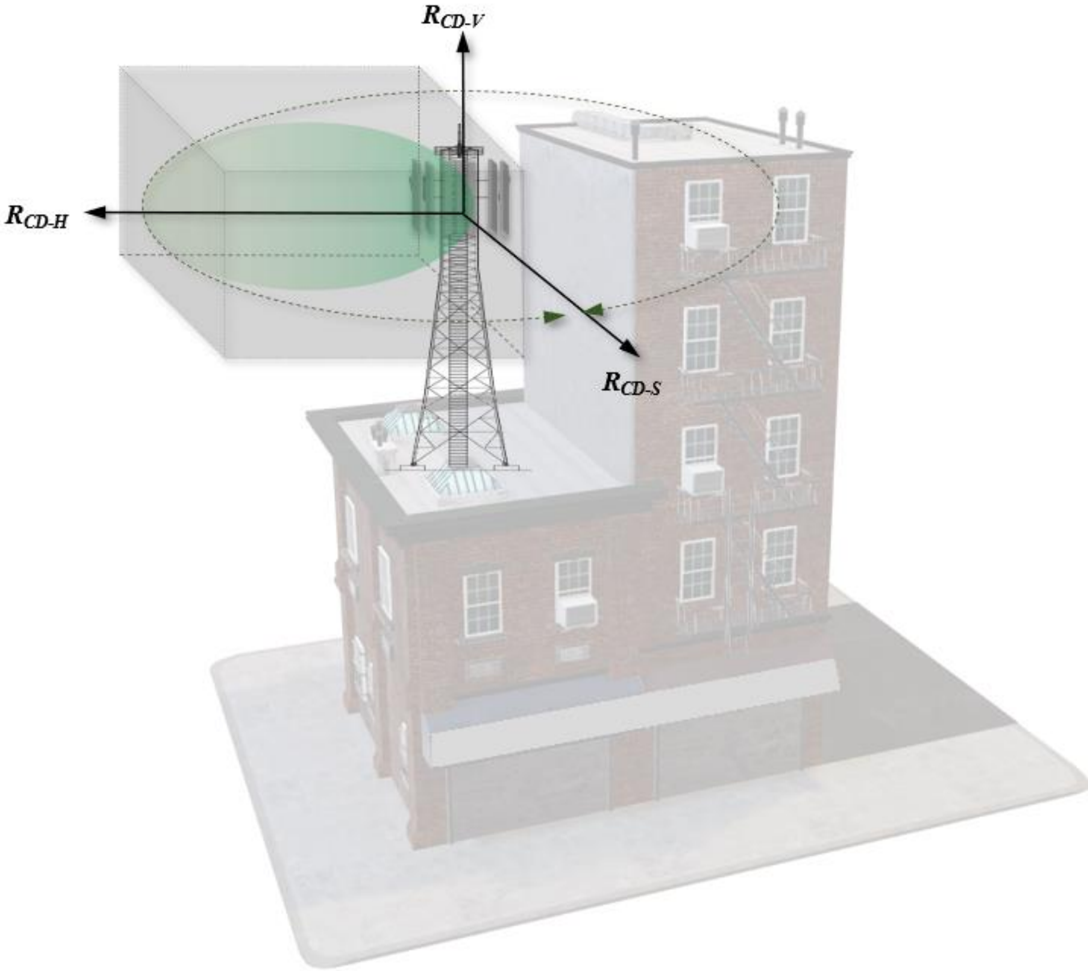

Figure 3.8. Horizontal and vertical compliance distances for Macro site.

Using the basic Equation (3.6), the R_{CD}, where *TER =1*, can be calculated using Equation (3.22) as:

$$\boldsymbol{R_{CD}} = \left(\frac{\mathbf{1}}{\mathbf{4\pi}} \sum_{n=1}^{N} \sum_{f>30\,MHz}^{300\,GHz} \frac{\boldsymbol{P_{T,f}} . \boldsymbol{G_{A,f\,(\theta,\emptyset)}}}{\boldsymbol{S_{inc,RL,f}}} \right)^{1/2} \tag{3.22}$$

Furthermore, by applying the enhanced formula of Equation (3.8), thus Equation (3.23) changed to Equation. (3.23) which presents the enhanced compliance distances R_{CD}.

$$\boldsymbol{R_{CD}} = \left(\frac{\mathbf{1}}{\mathbf{4\pi}} \sum_{n=1}^{N} \sum_{f>30\,MHz}^{300\,GHz} \frac{\boldsymbol{\rho_{r,f}} . \boldsymbol{a_{b,f}} . \boldsymbol{P_{T,f}} . \boldsymbol{G_{A,f\,(\theta,\emptyset)}}}{\boldsymbol{S_{inc,RL,f}}} \right)^{1/2} \tag{3.23}$$

If look at each technology separately, the proposed solution just rotates the sectors while keeping the manner of the sectorization as one group, which maintains the overall site coverage at the same level for this technology as shown in Figures 3.9 and 3.10.

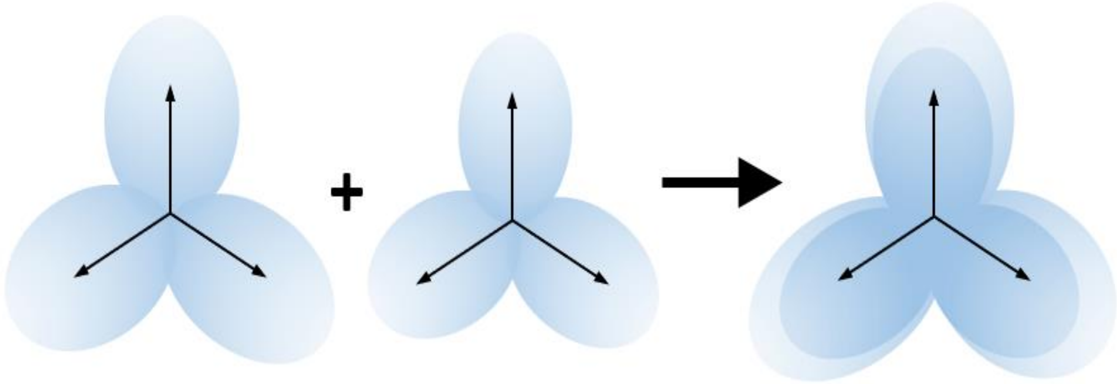

Figure 3.9. The current classic way for implementing 3 sectors directions

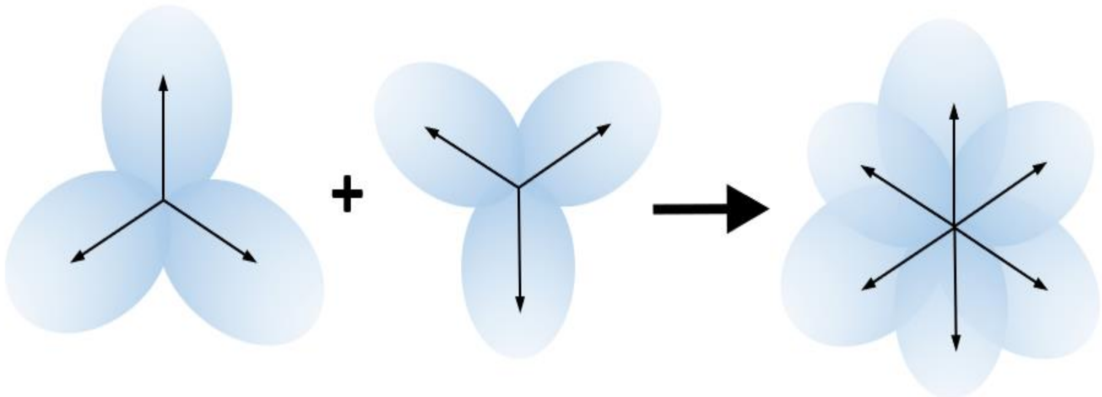

Figure 3.10. The proposed solution for sectors separation.

The different technologies have different signal levels in the same direction, so, in any place, some technologies will be stronger than others especially in null areas between sectors, but this also exists before applying the solution as shown in Figure 3.11 that shows the ideas of the proposed solution.

In the situation of having continuous coverage for each technology, the network pushes the users to camp on specific technology based on the certain parameter's setting controlled by MNO' engineers fundamentally based on MNO strategy for the cell selection and reselection. Also, the user can force and lock his handset (from the handset setting) to camp on the desired technology.

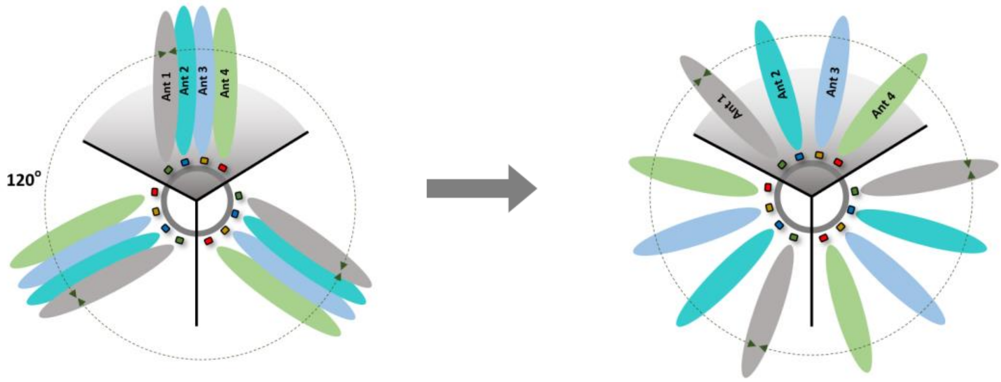

Figure 3.11. The proposed solution for sectors separation considering multi-technology

3.4. Far Field Exposure Assessement

3.4.1. Overview for the Far-Field Expsoure

The far field refers to a region far enough from the source where the EMF behaves as a plane wave and the spatial variation of the field is minimal, and practically these are all areas and regions far from the antennas and the signal reach in outdoor and indoor where people leave. Most national regulators in most of the countries requires from MNOs to assess the overall EMF exposure for general public everywhere they exist. To assess electromagnetic field (EMF) exposure in the far field, several techniques and methods are commonly used such as using field prop meters, exposure simulation-based tools. In this assessment, the coverage signal levels are employed to predict the far-field total exposure ratio of multi-technology site, the coverage levels itself require to employ the suitable propagation models to predict it.

Mobile wireless networks require proper radio planning and design for the required capacity and coverage [20]. This should be performed before implementation to ensure that the planned signal levels reach and cover the targeted areas well. A wide variety of approaches have been developed to predict the coverage level using propagation models that calculate the transfer of signals from the transmitter to the receiver. Predication software-based tools were developed to run the predicted computational operations using a suitable propagation model equation according to the site and location data input.

3.4.2. Employing the Rx Level in Exposure Simulation

In this simulation, for the 2G 900 MHz and 3G UMTS 900 MHz calculations, the COST231-Hata is used, which was developed by European Cooperation in Science and Technology (COST) based on the Okumura-Hata model [35, 36]. This model is suitable for the urban environment and can be used for distances up to 30km between the BS and receiver. The path loss is presented by Equation (3.24), which expresses the path loss in dB as:

$$L_{COST231\,Hata} = 33.9\log f_c - 13.82 h_{tr} - ah_{re} + (44.9 - 6.55\log h_{tr})\log d + C_m + 46.3 \quad (3.24)$$

where Cm is a constant and ah_{re} is the correction factor, and both depend on the environment type.

For the 4G LTE FDD (800, 1800, and 2100 MHz), the urban macro cellular model (UMa) is used, its developed by 3GPP for frequencies from 450 MHz to 6 GHz [37]. It is suitable for Macro sites where the BS height is assumed to be higher than that of the surrounding rooftops. This model has two modes, non-line of sight (NLOS) and LOS path loss, and Equations (3.25 and 3.26) represent the UMa-LOS.

$$L_{4G\,UMa} = 22\log(d) + 28 + 20\log(f) \qquad 10m \le d \le d_b \tag{3.25}$$

$$L_{4G\,UMa} = 40\log(d) - 28 + 20\log(f) - 9[(d_b)^2 + (h_t - h_r)^2] \qquad d_b \le d \le 5000m \tag{3.26}$$

where d is the distance from the BS, d_b is the break point distance, which depends on the height of the antennas ($d_b = 4h_t h_r/\lambda$), and the model assumes an MS height between 1.5 m and 22.5 m.

With the introduction of 5G New Radio (NR), 3GPP has standardized the UMa model for 5G and covers a wider range of frequencies up to 100 GHz, because there is high expectation that 5G NR will also operate at higher frequencies [38]. The 3GPP UMa 5G model [39] has parameters similar to 4G Uma, with more frequency modules to support a higher frequency range, especially for NLOS MUa modes. This model effectively supersedes all previous models [40]. Equations (3.27, 3.28, and 3.29) represent the line of sight (LOS) path loss for 5G UMa used in this study to calculate the 5G Rx level.

$$L_{5G\,UMa} = \begin{cases} PL_1, & 10m \le d \le d_b \\ PL_2, & d_b \le d \le 5000m \end{cases} \tag{3.27}$$

$$PL_1 = 28 + 22\log(d) + 20\log(f) \tag{3.28}$$

$$PL_2 = 28 + 40\log(d) + 20\log(f) - 9[(d_b)^2 + (h_t - h_r)^2] \tag{3.29}$$

where d is the distance from the BS, and d_b is the break point distance depending on the height of the antennas ($d_b = 4h_t h_r/\lambda$). This 5G-UMa model also assumes a UE height between 1.5 m and 22.5 m.

Chapter Four: Validation and Results Anlaysis

4.1. Validation of the Proposed Enhanced Compliance Distance

4.1.1. Validation Methodology Steps

The proposed enhanced formula in Equation (3.8) for calculation the accurate compliance distance is valided to figure out the accuracy and delta compare the original calculations, the validation involved in-situ measurement and calculation-based assessment.

Figure 4.1 summarizes the steps that are followed in this assessment, first the measurements are conducted, and then the measurement results and OSS system data (Operation Support System) are used to validate proposed formula of the the power density calculation. In the last step, the proposed formula is used to determine the CDs using different data sets considering the maximum system load as a worst-case scenario of the maximum traffic that cause maximum power density emission.

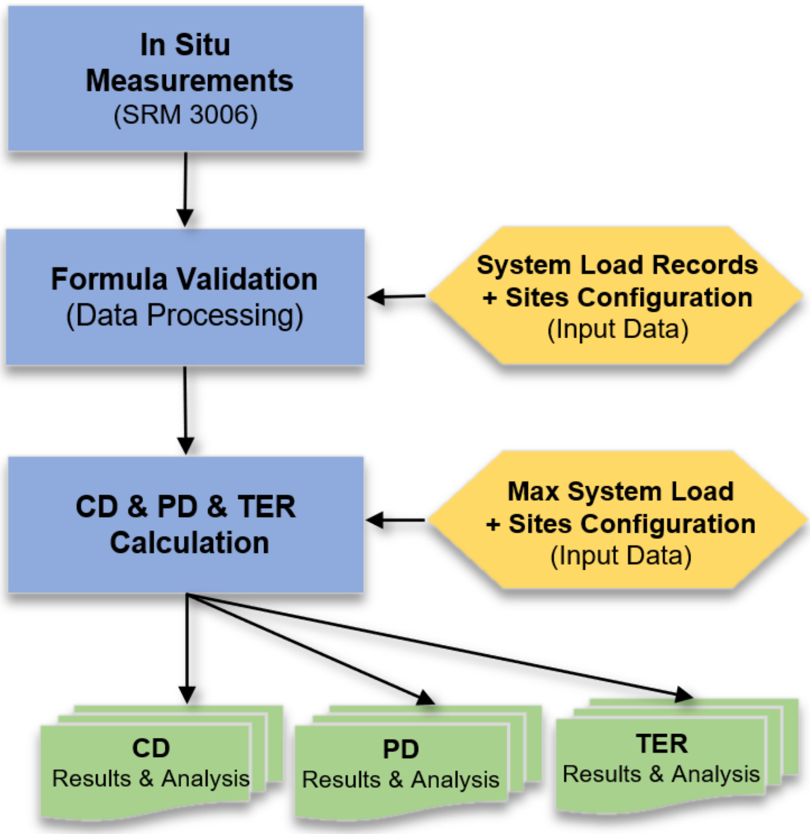

Figure 4.1. The methodology steps to validate the proposed formula.

4.1.2. In-Situ Measurement and Validation

In-situ measurements are conducted to achieve the power density for the site under test as shown in Figure (4.5). A physical macro site is selected in the Kingdom of Saudi Arabia, located in a dense residential area at Khubar city. The site is operating with six technologies 2G GSM at 900 MHz (G900), 3G UMTS at 900 MHz (U900), 4G LTE at 800 MHz (L800), 4G LTE at 1,800 MHz (L1800), 4G LTE at 2,100 MHz (L2100), and 5G NR at 3,500 (N3500).

The hourly traffic and utilization are obtained using the system row counters and statistics of the OSS. Accordingly, the highest hours of traffic and system load (busy hours) are identified (from 8:00 pm to 00:00 am) and these hours are chosen to conduct the field measurement. Figure 4.2 shows the hourly data traffic over one week for the 5G N3500 sector of the measurement. It also shows the system load percentage, which is recorded based on the PRB utilization, it reaches up to 67%. Figure 4.3 shows the same for 4G L2100 which reaches up to 85%, and Figure 4.4 shows the same for 3G U900, which reaches up to 50%. However, for 3G, the OSS records the system load based on the power utilization counters.

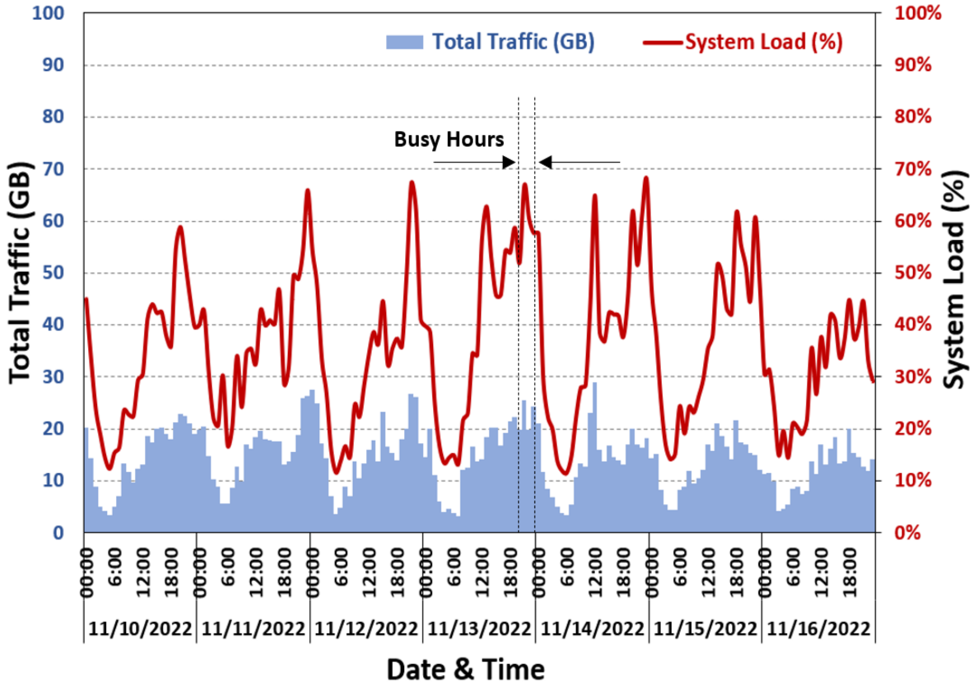

Figure 4.2. The 5G N3500 hourly traffic and system load of the site.

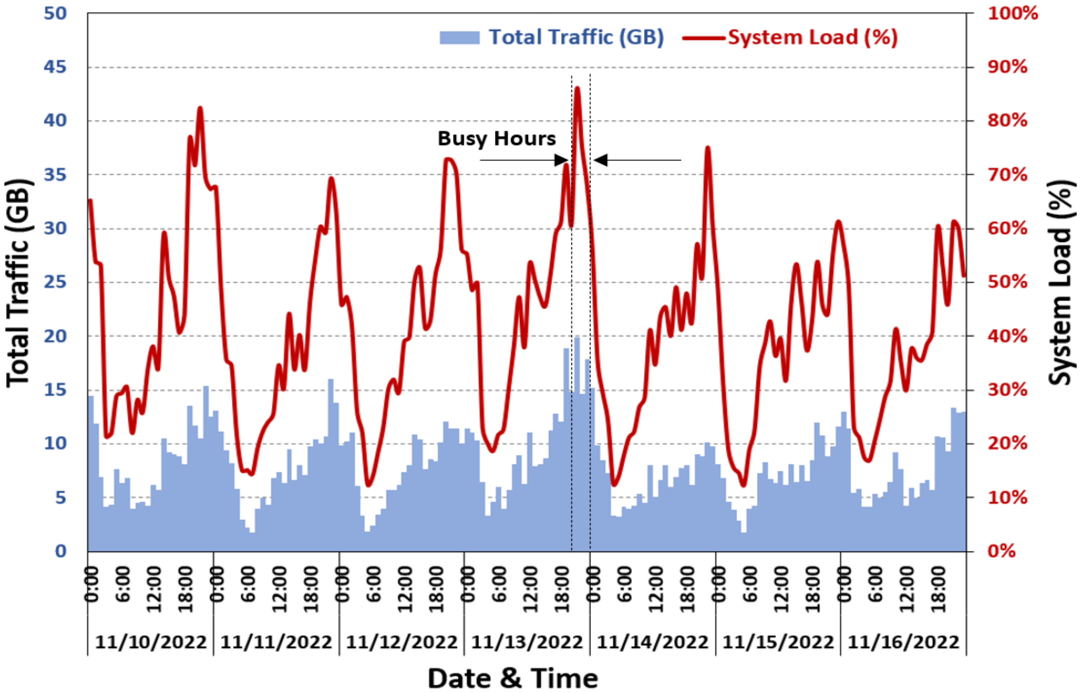

Figure 4.3. The 4G L2100 hourly traffic and system load of the site.

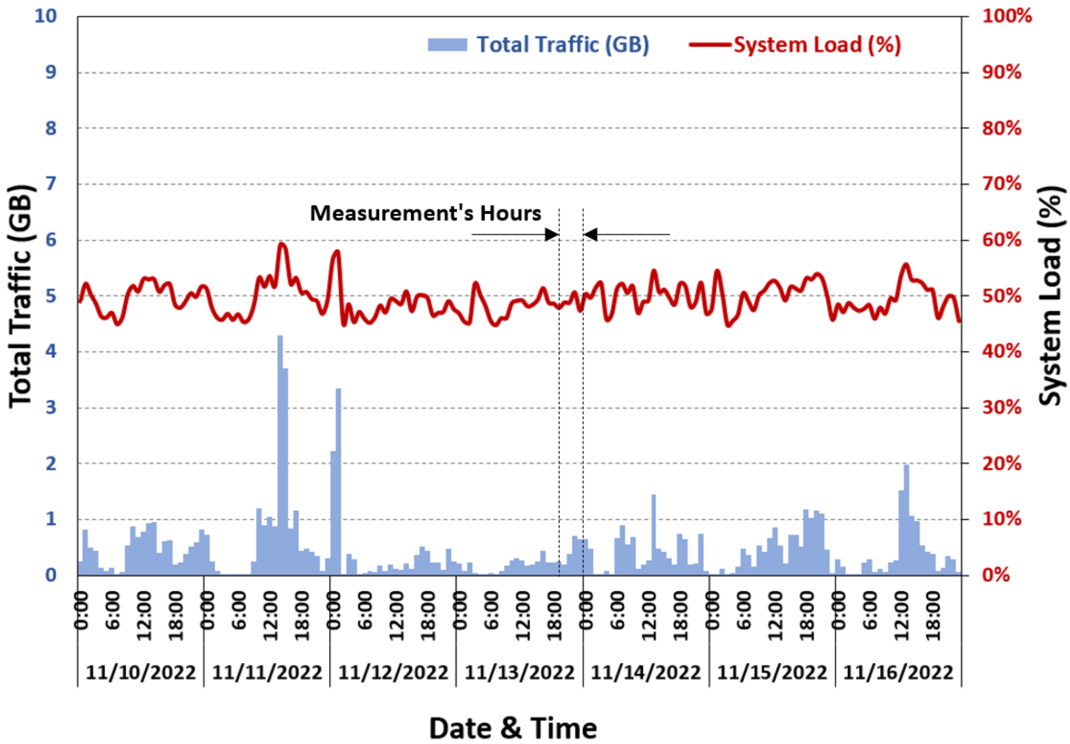

Figure 4.4. The 3G U900 hourly traffic and system load of the site.

A Narda SRM-3006 [64] EMF selective radiation meter is used for the measurements, which supports a frequency range from 9 kHz to 6 GHz, and has a three-axis isotropic antenna (E-field). Figure 4.5 shows the site and the meter position during the field test at the selected site, which is installed on rooftop with a 12 m height from the same floor level.

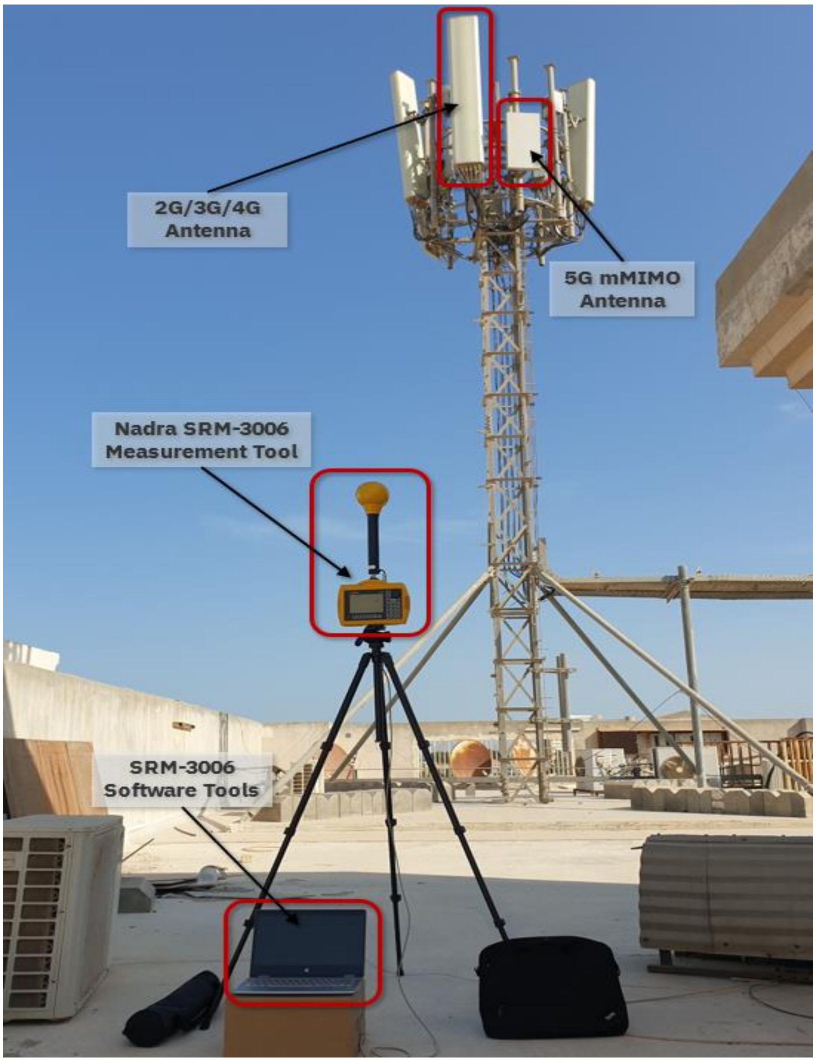

Figure 4.5. The radiation meter position in the site.

The meter was standing on a tripod with an antenna height of 2 m facing the antenna's main beam direction. The measurements were collected for two points at horizontal distance D_H as illustrated in Figure 4.6. Initially the D_H was 10 m, D_{3D} was 14.14 m and facing vertical angle Ø was 45^o. At the second point, the D_H was 20 m, D_{3D} was 22.36 m, and facing vertical angle Ø was 26^o.

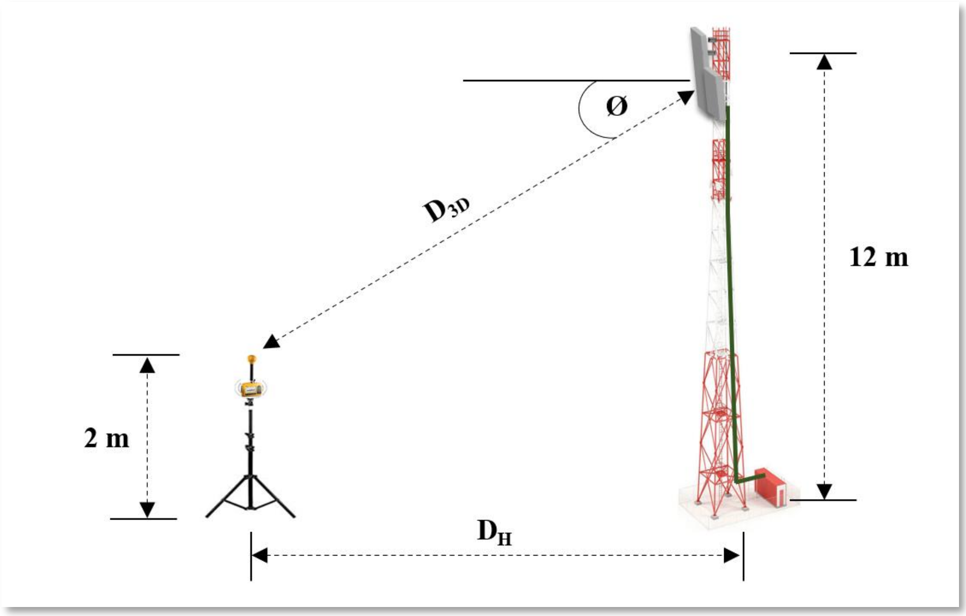

Figure 4.6. Measurement setup for the radiation meter in the site.

The SRM meter was set to measure the downlink (DL) frequency ranges. A total 9,600 measurement samples are recorded for each technology with a scan rate of 0.67 samples/second. The recorded samples were post-processed, the processing includes importing the measurement data (S_{inc}, H_{inc}, and E_{inc}) from the radiation meter, converting it to the desired units, sorting the measured samples for each technology, and then calculating the average power density PD for all collected samples per technology. Finally, the average PD is divided by reference levels to calculate the exposure ratio. Table 4.1 lists the average measured S_{inc}, E_{inc}, and H_{inc}, and the exposure ratios are calculated based on the corresponding ICNIRP reference level for the GP at the first point (10m from the site).

Table 4.1. The measurement results vs calculated ICNIRP at 10m distance.

Techn.	Measurements			Reference Levels			Exposure Ratio		
	S_{inc} mW/m^2	H_{inc} mA/m	E_{inc} V/m	S_{incRL} mW/m^2	H_{incRL} mA/m	E_{incRL} V/m	S_{inc}/S_{incRL} x10^{-3}	H_{inc}/H_{incRL} x10^{-3}	E_{inc}/E_{incRL} x10^{-3}
2G G900	0.302	0.895	0.338	4,500	111	41	0.07	0.07	0.07
3G U900	0.161	0.653	0.246	4,500	111	41	0.04	0.03	0.04
4G L800	0.463	1.108	0.418	4,000	105	39	0.12	0.11	0.12
4G L1800	1.299	1.865	0.700	9,000	157	58	0.14	0.14	0.14
4G L2100	2.076	2.347	0.885	10,000	N/A	N/A	0.21	N/A	N/A
5G N3500	6.366	4.109	1.549	10,000	N/A	N/A	0.64	N/A	N/A

The power density was validated by comparing the measurements with the calculation using Equations 3.7 for $S_{inc,PF}$ with ρ_r = 0.22, compared to S_{inc} with ρ_r = 1 (without power reduction). The value of ρ_r = 0.22 is used based on the work [23] who reported that actual power varies between 7% and 22% of the maximum possible output power depending upon different user distributions and exposure scenarios, and also based on the work [65] who reported the actual power is 22% for mMIMO in the Urban site.

Table 4.2 shows the validation results in terms of S_{inc} mean error (ME) and the differences compared to the measurements at point 10 m. For 5G N3500 mMIMO, the results show that $S_{inc,PF}$ is 7.12 mW/m^2, and S_{inc} is 26.02 mW/m^2. $S_{inc,PF}$ has less difference that reaches up to 10.6% compared to the difference of the basic S_{inc}, which reaches a maximum 80.3%.

Table 4.2. The power density validation at 10m distance.

Techn.	S_{inc} Measured	S_{inc} Calculation					
		With ρ_r $S_{inc,PF}$			No ρ_r S_{inc}		
	mW/m^2	mW/m^2	ME mW/m^2	Difference	mW/m^2	ME mW/m^2	Difference
2G G900	0.302	0.339	0.04	10.8%	0.339	0.04	10.8%
3G U900	0.161	0.178	0.02	9.8%	0.178	0.02	9.8%
4G L800	0.463	0.528	0.06	12.3%	0.528	0.06	12.3%
4G L1800	1.299	1.455	0.16	10.7%	1.455	0.16	10.7%
4G L2100	1.246	1.405	0.16	11.3%	1.405	0.16	11.0%
5G N3500	6.366	7.124	0.76	10.6%	32.38	26.02	80.3%

Similar results were obtained for the measurements at the 20 m distance far from the site, as listed in Table 4.3. where it shows that the $S_{inc,PF}$ is 07.24 mW/m^2 and for S_{inc} is 26.36 mW/m^2. $S_{inc,PF}$ has difference reaches of 9.5% compared to the basic S_{inc}, which was 80.1%.

Table 4.3. The power density validation at 20m distance.

Techn.	**Measured**	**S_{inc} Calculation**					
		With ρ_r $S_{inc,PF}$			**No ρ_r S_{inc}**		
	mW/m^2	mW/m^2	ME	Difference	mW/m^2	ME	Difference
2G G900	0.270	0.310	0.04	13.0%	0.310	0.04	13.0%
3G U900	0.195	0.220	0.03	11.4%	0.220	0.03	11.4%
4G L800	0.465	0.530	0.07	12.3%	0.530	0.07	12.3%
4G L1800	1.580	1.798	0.22	12.1%	1.798	0.22	12.1%
4G L2100	1.609	1.777	0.17	9.4%	1.777	0.17	9.4%
5G N3500	6.549	7.239	0.69	9.5%	32.90	26.36	80.1%

4.1.3. Power Density and Compliance Distance Analysis

Most mobile wireless networks comprise a combination of different site types and different access technologies, interworking as a heterogeneous network. In a real network, the radio planning teams design and select the sites based on many factors, such as the required coverage range, number of users, traffic growth, total cost, and the nature of the area (rural, urban, suburban, dense, indoor building, etc..). This study investigated the CDs for four site types, the macro, micro, small cell, and the Indoor based solution (IBS), which all are used as a combination in the typical mobile network as illustrated in Figure 4.7.

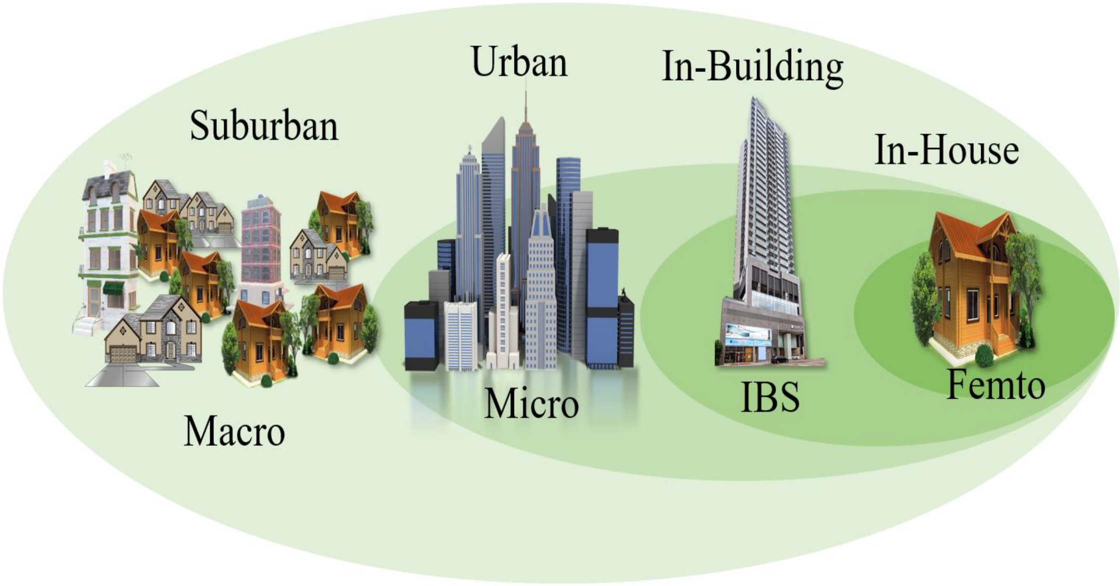

Figure 4.7. Site types of base stations according to coverage type.

4.1.3.1. The Macro Site

Macro site is a general and most common solution used by all operators to provide coverage in populated areas [66]. The macro has radio equipment with higher BS power compared to other types of sites (micro/femto/IBS), and the coverage range reaches further distances depending on the antenna height and the site configurations. The macros can be installed in different civil models, such as on a monopole, self-based towers, cells on the wheel (COW), wall-mounted antennae, or rooftop sites, as illustrated in Figure 4.8.

Typical configurations of a single BS macro site equipped with multi-technology solutions are used as input data for the calculation in this study, and the configuration data were obtained from two mobile network operators in the Kingdom of Saudi Arabia from the operation team. The input data for each technology, including the number of Tx/Rx, antenna gain, frequency bandwidth, system load, technology types, and transmitting power are listed in Table 4.4. For N3500 which has high-grade mMIMO (64T/64R). The measurement results reflected the EMF levels during the measurement time which was not reaching the maximum EMF level, and the authors have no facilities to generate maximum traffic on the site causing maximum power density emission. In the validation stage, the system load was recorded during the measurement time and used for validating Equations (3.7 and 3.8). But, considering the purpose of the simulation is to investigate the power densities and CDs using Equations (3.7 and 3.8) under maximum radiation, the system utilization load is used (95%) for all technologies in to determine the EMF compliance boundaries as a worst-case scenario.

Table 4.4. The configuration Setup for the macro site.

Configuration	**2G G900**	**3G U900**	**4G L800**	**4G L1800**	**4G L2100**	**5G N3500**
Freq. (MHz)	900	900	800	1800	2100	3500
Freq. BW (MHz)	5	5	10	20	20	100
Total TXs	2	1	2	2	4	64
Total RXs	2	1	2	2	4	64
Power TX	40W	40W	80W	60W	60W	160W
Power ρ_r	1.0	1.0	1.0	1.0	1.0	0.22
System Load	95%	95%	95%	95%	95%	95%
Ant. Gain	17dBi	17dBi	16.7dBi	16.6dBi	17dBi	24.8dBi

The site configuration data are utilized in Equations (3.8) to compute the vertical and horizontal CD (R_{DC-H} & R_{DC-V}) as illustrated in Figure 4.7. The outcome expresses that all horizontal R_{DC-H} distances are longer than the vertical R_{DC-V} distances, and the ICNIRP has a slightly more restricted R_{CD} compared to the FCC. The R_{CD-H} general public for ICNIRP is 14.81 m compared to 6.51 m R_{CD-v}, and the R_{CD-H} FCC general public is 13.84 m compared to 5.89 m R_{CD-v}. Figure 4.8 summarizes the compliance distances R_{CD} in both directions, and the results are in line with the results found in [47, 59].

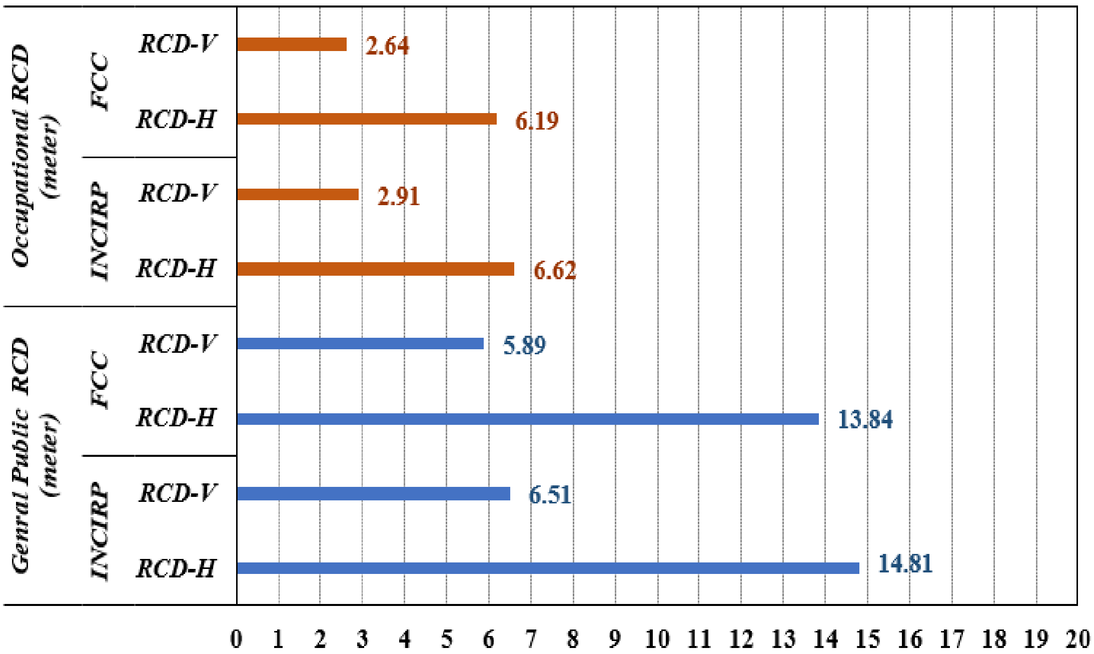

Figure 4.8. The CD for Macro site referenced ICNIRP and FCC limits.

The emitted power density was then processed to look at it per technology. Figure 4.9 presents the P_D (W/m^2) calculated at a distance (m) from the antennae, which shows that 5G N3500 has the highest PD compared to the other technologies, and all technologies reach high levels at distances very close to the macro site antenna (less than 3 m).

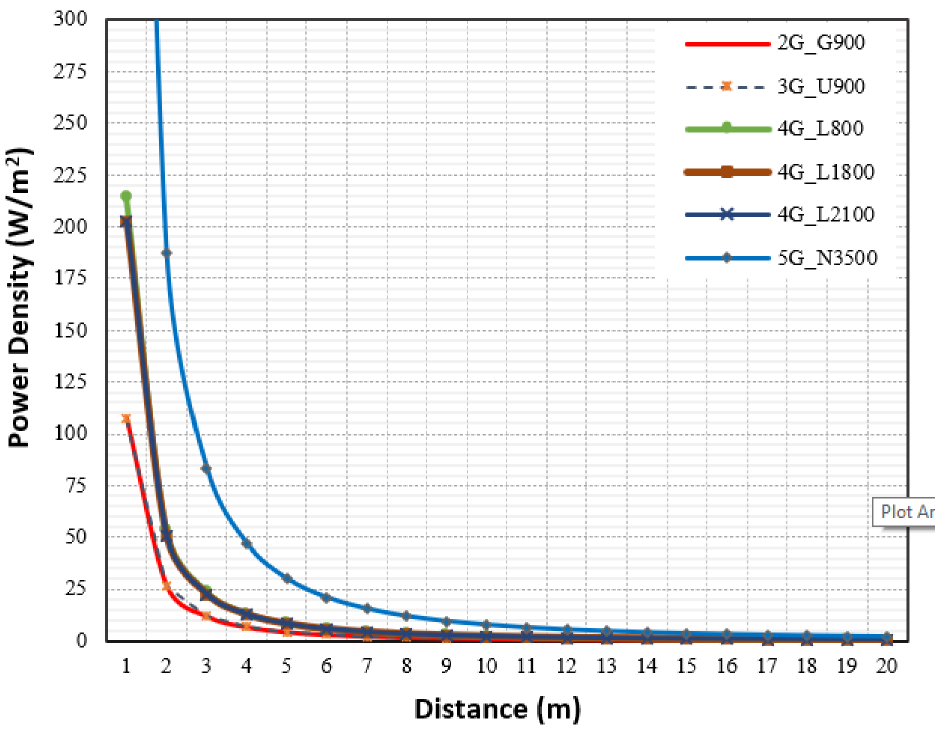

Figure 4.9. The PD at the main directions for the Macro site antenna.

Referring to the standard limits for GP, Figures 4.10 and 4.11 display the exposure ratio calculated in the horizontal directions and the total TER. For both the ICNIRP and FCC, the results demonstrate that 5G N3500 has the highest contribution to the TER at the compliance distances.

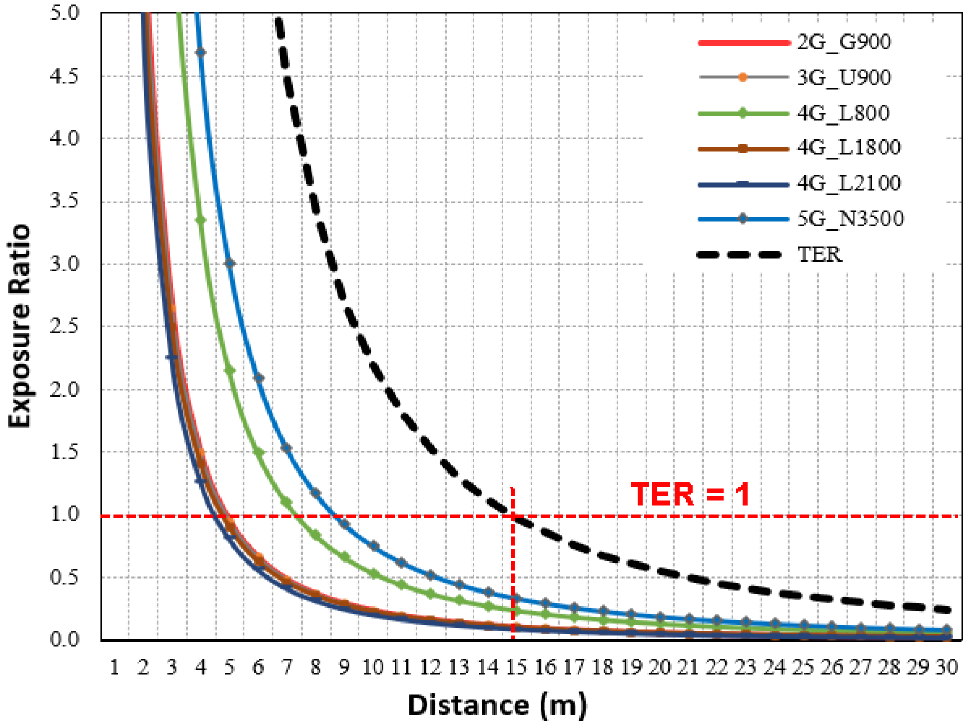

Figure 4.10. The exposure ratio for macro site reference to ICNIRP limits.

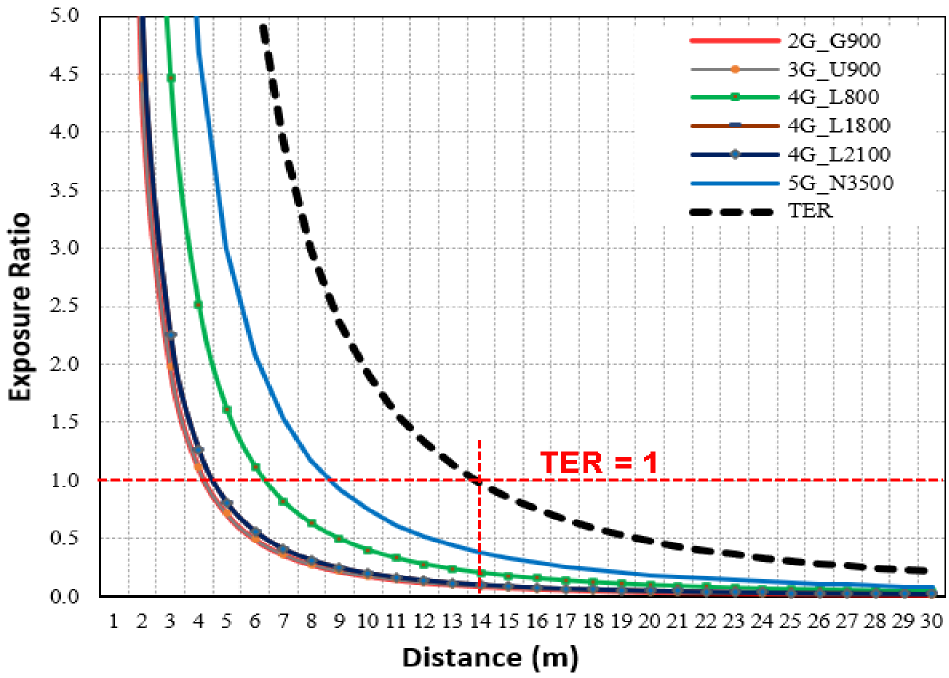

Figure 4.11. The exposure ratio for Macro site references to FCC limits for GP.

At the R_{CD}, the 5G N3500 contributes 34%, then the 4G L800 contributes 24%, the 4G L1800 and L2100 contributes 9-10% each, and the 2G G900 and 3G U900 contributes 11% each. Additionally, for FCC, the highest is N3500 which contributes 39%, followed by 4G L800 with 21%, 4G L1800 and L2100 with 11% each, the lowest being 2G G900 and 3G U900 with 9% each. Figure 4.12 summarizes the contributions of each technology which is in line with the results of our previous study for the far field done by the same research team and published in [67].

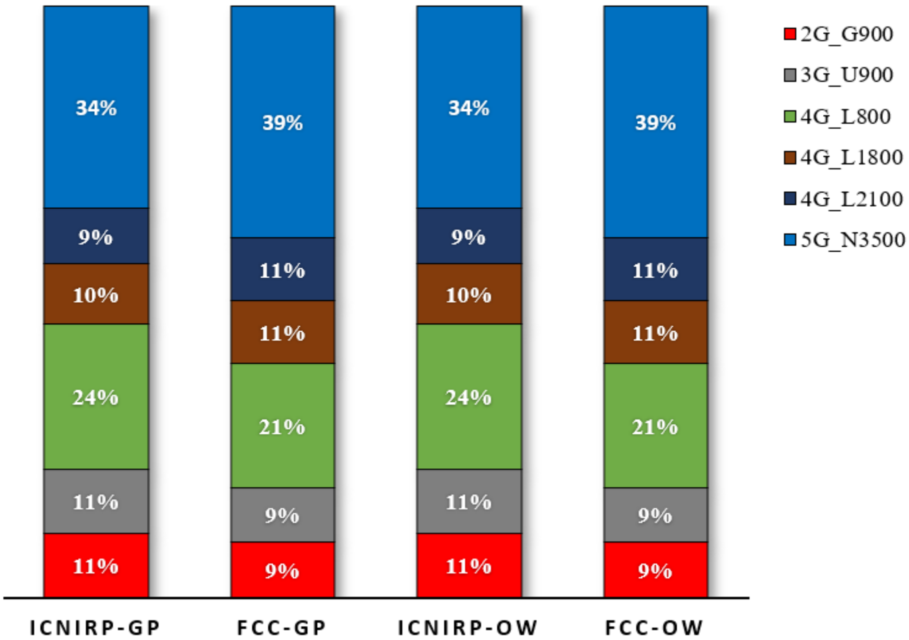

Figure 4.12. The PD contribution at the CD per technology.

The results computed using the proposed enhanced formula give shorter compliance distances compared to calculations done using the basic frmula. These are expected results because the ρ_r gives more accurate distances based on realistic rated power for the mMIMO equipped in the 5G rather than the conservative power levels used in proposed equation. Table 4.5 summarizes the comparison results which show that $R_{CD\text{-}PF}$ distances are less than R_{CD} by 34.5%-36.9% in the horizontal direction, and $R_{CD\text{-}PF}$ distances are less than R_{CD} by 16.2%-18.5% in the vertical direction for the GP and OW respectively.

Table 4.5. The CDs for Macro site referenced to ICNIRP and FCC limits.

Calculation Method			R_{CD} (m)	R_{CD-PF} (m)	Delta (m)	Delta %
R_{CD-H}	GP	INCIRP	22.6	14.8	-7.8	-34.5%
		FCC	21.9	13.8	-8.1	-36.9%
	OW	INCIRP	10.1	6.6	-3.5	-34.5%
		FCC	9.8	6.2	-3.6	-36.9%
R_{CD-V}	GP	INCIRP	7.8	6.5	-1.3	-16.2%
		FCC	7.2	5.9	-1.3	-18.5%
	OW	INCIRP	3.5	2.9	-0.6	-16.2%
		FCC	3.2	2.6	-0.6	-18.5%

It's not easy to compare the above results directly with related works found during the literature review, because many related studies investigated the EMF exposure topic from different angles, for these works who focused on determining the compliance boundaries similar to our study, below are some summaries:

- In [58], the authors proposed conservative formulas to estimate the localized and whole-body SAR for the exposure of the main beam from the BS. The proposed formulas have a heuristic nature, are applicable to a class of typical base station antennas, were created based on a number of physical observations, and are supported by the findings of a thorough literature review, measurements, and numerical simulations of typical exposure scenarios.
- in [59], the authors conducted field measurements inside the university (Symbiosis International University campus Pune, India) in different locations, and calculated the compliance distance for 2G GSM operating at 1800 MHz, the result shows the calculated compliance distance is 8.4 meter.
- In [52] the authors proposed a new protocol for the measurement assessing the 5G NR exposure based on user activities including the assessment of auto included exposure of both the base stations and user handsets. Their work is based on knowledge of some studies simulating NR base stations and measurements near test sites, and from prior RF-EMF exposure research.
- In [68] the authors conducted in situ measurement for the 4G LTE TDD mMIMO considering maximum system utilization and 100% traffic load, the results show that

EMF level was 7.3-16.1% of the ICNIRP occupational reference level compared to 79.3% based on traditional conservative calculation, and there is a reduction in the actual compliance boundaries 2.2-3.3 times the conservative's calculated boundaries. The authors justify this decrease can be attributed to mMIMO beamforming's sporadic and erratic behavior, and they mentioned due to the fact that actual RBS traffic loading is frequently much lower than 100%, a further reduction in the compliance boundary is expected.

- In [69], Pinchera et al. analyzed the power levels around the 5G antenna array to reasonably assess the exposure level and calculate the compliance boundary. The authors introduced a metric for calculating of the average power density around the antenna as a normalized average power pattern (NAPP) through a statistical approach. Their results show the calculated compliance distances results using different values for the power reduction factor.
- In [70], Thielens et al. (at Ghent University) determined the EMF exposure compliance boundaries using finite-difference time-domain (FDTD) simulations for a 4G LTE base station antenna at 2,600 MHz. Their results show for the various basic restriction and reference levels, the reference levels are not conservative when the antenna is only partially radiating. Also, their results show that the 10g averaged SAR in the head and trunk of the body gives the compliance boundaries for basic restriction at lower antenna powers.
- In [71], Heliot et al. investigated the nature of mMIMO exposure and its impact on the compliance boundary using mMIMO configurable testbed (at 2.6 GHz) and commercial 5G BS (at 3.6 GHz). Their results for defining the exclusive zones based on statistical exposure are interesting. Their analysis indicates that the significant exposure variations occur according to the beam directions, and for a constant traffic load, the variance of the exposure tends to decline as the number of users rise. Also, contrarily, the exposure increases sub-linearly with traffic load, irrespective of the user count.

With a review of the above-mentioned related works, this study mainly differs by determining the compliance distances for the entire accumulated EMF from multi-technology colocated at one site.

4.1.3.2. Micro Site

For the operators in crowded locations with good coverage, capacity is a concern. Micro sites are a good option with low power to expand capacity in highly utilized areas [72, 73]. It has a small hardware size that is easy and quick to install (e.g., on the rooftop, light pole, or as wall-mounted) at relatively low heights as illustrated in Figure 4.13. Additionally, it has lower costs than macro sites.

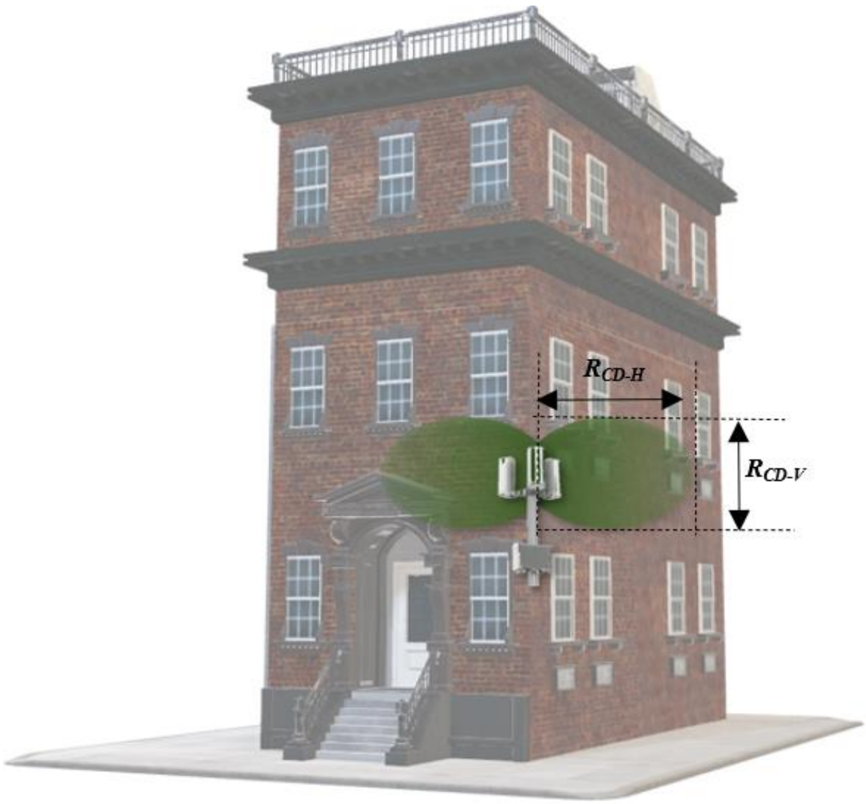

Figure 4.13. Horizontal and Vertical compliance distances for micro site.

A high configuration of a single micro site equipped with multi-technology solutions is considered in this study. The site is operating with six technologies; G900, U900, L800, L1800, L2100, and N3500. The input data for each technology are listed in Table 4.6. This is like the macro site but has less TXs power, lower antenna gain, and no mMIMO in the 5G NR.

Table 4.6. The configuration setup for the micro site.

Configuration	2G G900	3G U900	4G L800	4G L1800	4G L2100	5G N3600
Freq. (MHz)	900	900	800	1800	2100	3500
Freq. BW (MHz)	5	5	10	20	20	100
Total TXs	2	1	2	2	2	4
Total RXs	2	1	2	2	2	4
Power TX	10W	10W	10W	5W	5W	40W
Power ρ_r	1.0	1.0	1.0	1.0	1.0	1.0
System Load	95%	95%	95%	95%	95%	95%
Ant. Gain	8dBi	8dBi	8dBi	10dBi	10dBi	11.1dBi

The calculations show that all horizontal $R_{CD\text{-}H}$ distances are longer than the vertical $R_{CD\text{-}V}$ distances. For the ICNIRP general public, $R_{CD\text{-}H}$ is 2.83 m compared to 1.17 m for $R_{CD\text{-}v}$. For the FCC general public, $R_{CD\text{-}H}$ is 2.67 m compared to 1.08 m for $R_{CD\text{-}v}$. Figure 4.14 summarizes the calculation results.

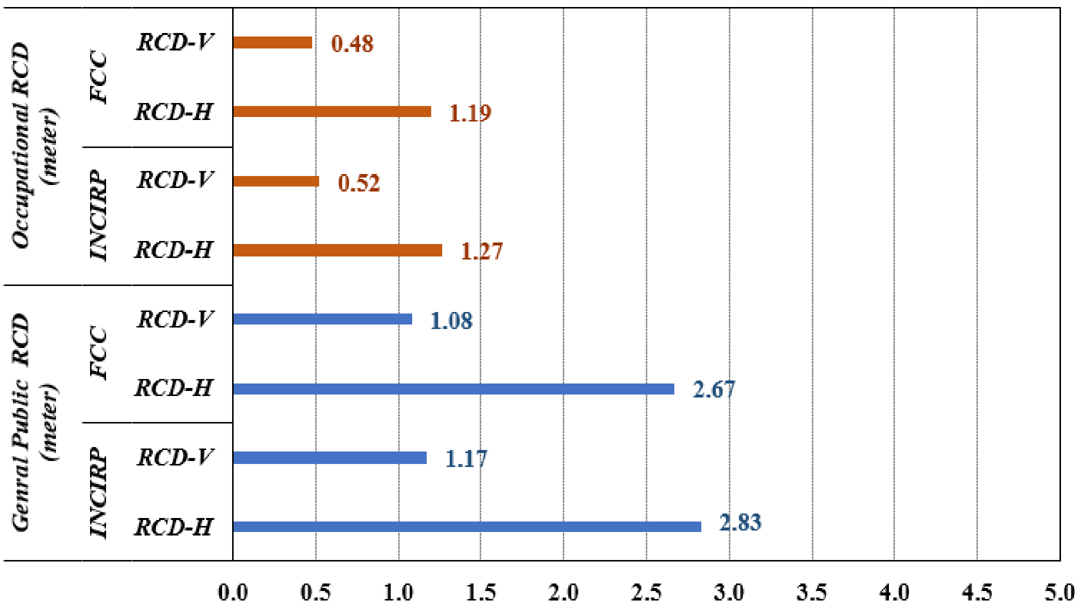

Figure 4.14. The CD for Micro site referenced to ICNIRP and FCC limits.

Figure 4.15 presents the calculated P_D per technology, like the macro, the micro results show that 5G N3500 has the highest P_D compared to the other technologies, and all technologies reach high levels at distances very close to the antenna (less than 2 m).

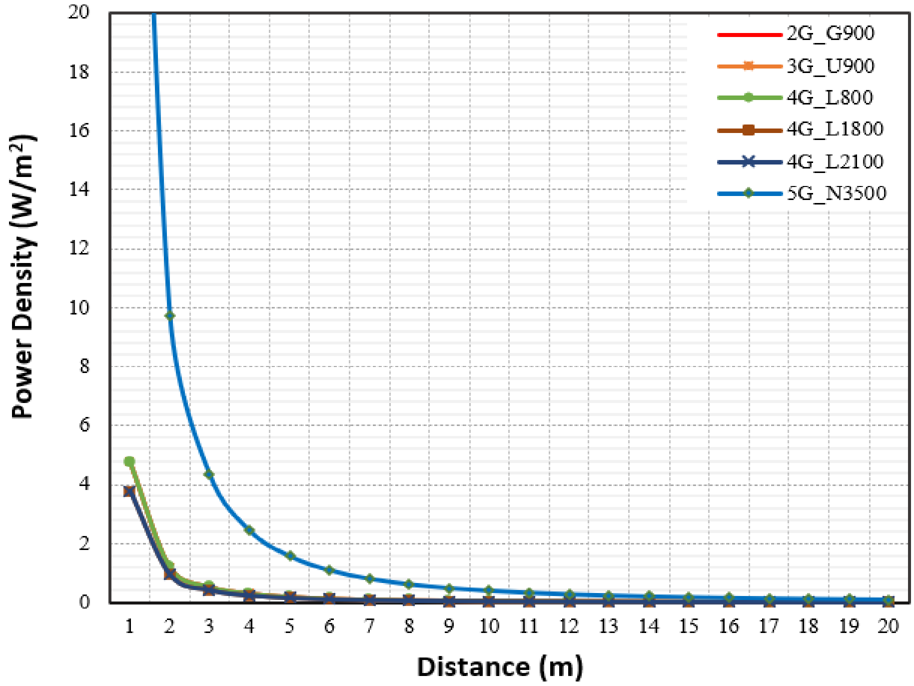

Figure 4.15. The power densities in main direction of the micro site antenna.

Referring to ICNIP and FCC limits for the GP, Figures 4.16 and 4.17 present the exposure ratio for each technology calculated in the horizontal directions, and the total TER for the micro site.

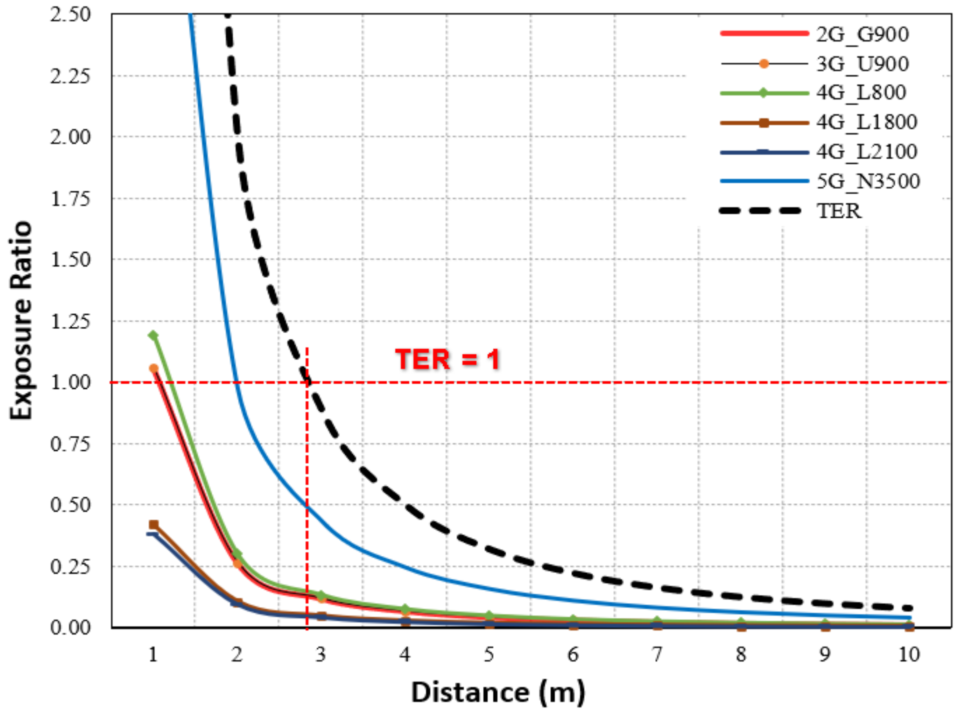

Figure 4.16. The exposure ratio for the micro site is based on the ICNIRP limits.

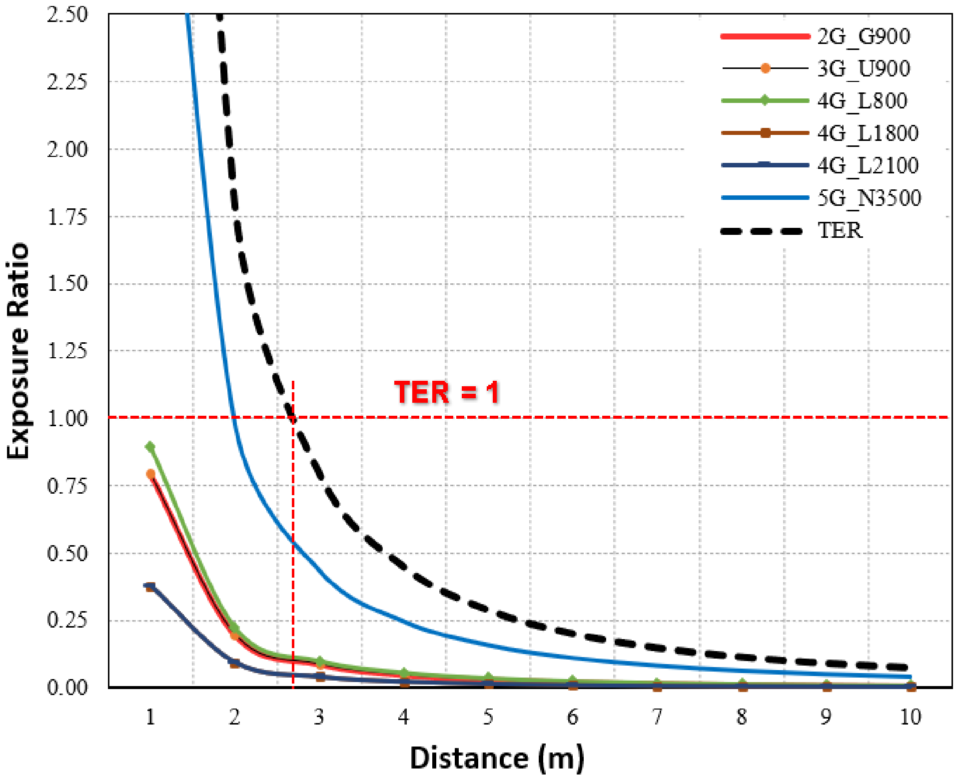

Figure 4.17. The exposure ratio for the micro site reference to FCC limits.

Additionally, the results show that 5G N3500 has the highest contribution at ICNIRP compliance distances with 49%, followed by 4G L800 with 15%, 4G L1800 and L2100 with 5% each, and 2G G900 and 3G U900 with 13% each. For the FCC standard, N3500 is the highest contributor with 55%, followed by 4G L800 with 13%, 4G L1800 and L2100 with 5% each, and 2G G900 and 3G U900 with 11% each. Figure 4.18 shows the summarized contributions, and this comparison to the results in Figure 4.13 (macro site) demonstrates that the 5G contribution at the micro site is higher than that at the macro site because the macro uses a higher grade of mMIMO (64T/64R). Hence, we used a lower power rating factor (0.22) in the calculations.

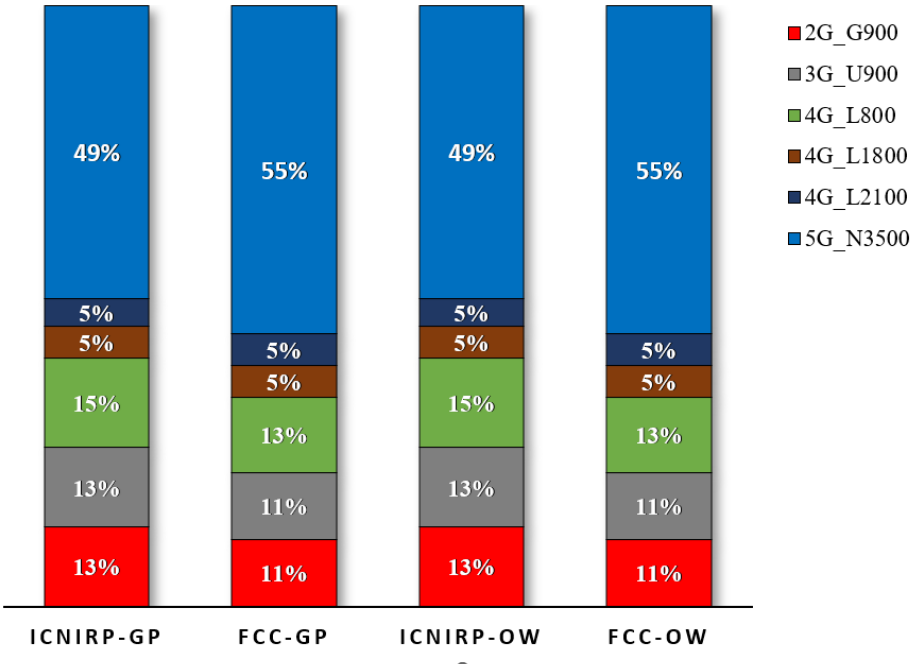

Figure 4.18. The PD contribution per technology at the CD for the micro site.

The micro site boundary calculation using Equation 3.8 ($R_{CD\text{-}PF}$) provides similar distances with slight differences compared to calculations done without power factor. These are expected results because the micro has no mMIMO and uses normal TX power here. Table 4.7 summarizes the comparison results which show that the $R_{CD\text{-}PF}$ distances are much less than 2.5% in all directions compared to the R_{CD}.

Table 4.7. The CDs for micro site referenced to ICNIRP and FCC limits.

Calculation Method			R_{CD} (m)	$R_{CD\text{-}PF}$ (m)	Delta (m)	Delta %
$R_{CD\text{-}H}$	GP	INCIRP	2.9	2.8	-0.1	-2.5%
		FCC	2.7	2.7	-0.1	-2.5%
	OW	INCIRP	1.3	1.3	0.0	-2.5%
		FCC	1.2	1.2	0.0	-2.5%
$R_{CD\text{-}V}$	GP	INCIRP	1.2	1.2	0.0	-2.5%
		FCC	1.1	1.1	0.0	-2.5%
	OW	INCIRP	0.5	0.5	0.0	-2.5%
		FCC	0.5	0.5	0.0	-2.5%

4.1.3.3. 4.4.C. Small Cell Site

For coverage in homes and small offices, the small cell (or femto) is a practical choice as illustrated in Figure 4.19, it provides limited indoor coverage and capacity where the network signal is weak [74]. It has very tiny hardware dimensions, simple and quick to mount on the ceiling or wall-mounted like the WiFi hotspot. Additionally, it has a lower cost compared to the macro/micro/IBS sites, but it has a very small capacity and coverage with very low power. Therefore, 4G/5G small cells are a cost-effective way to extend the availability of 4G/5G in urban and suburban areas.

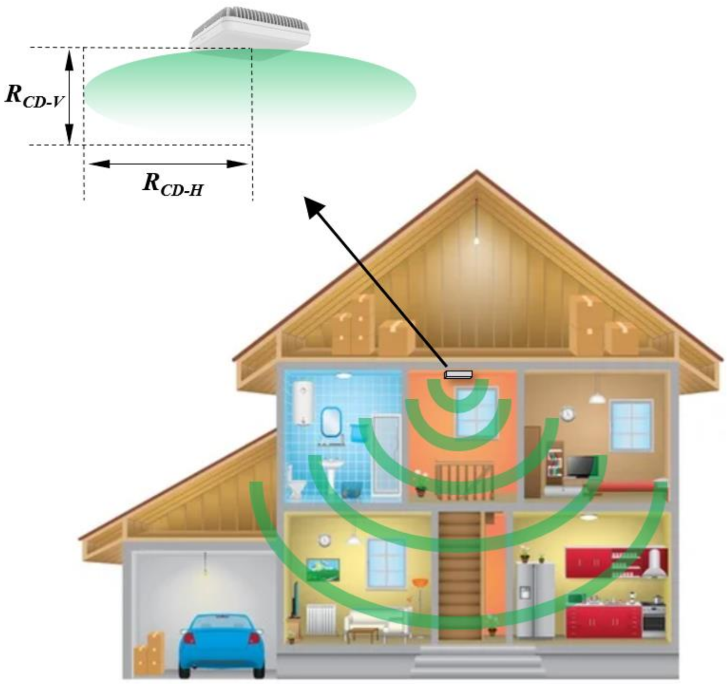

Figure 4.19. The compliance distances for small cell installed on the ceiling.

We considered five small cells installed in the same location to examine the maximum total radiation as a worst-case situation. Although so many operators have started the 5G small cell deployment on 6 GHz, in this study, we used 3.5 GHz because it was the frequency used by the operators who provided the configuration for this study. Table 4.8 presents the typical small cell configurations used in the calculations for PD and CD.

Table 4.8. The configuration setup for small cell.

Site Setting	**2G G900**	**3G U900**	**4G L800**	**4G L1800**	**4G L2100**	**5G N3600**
Freq. (MHz)	900	900	800	1800	2100	3500
Freq. BW (MHz)	5	5	10	20	20	100
Total TXs	2	1	2	2	2	4
Total RXs	2	1	2	2	2	4
Power TX	0.4W	0.4W	0.4W	0.4W	0.4W	1W
Power ρ_r	1.0	1.0	1.0	1.0	1.0	1.0
System Load	95%	95%	95%	95%	95%	95%
Ant. Gain	4dBi	4dBi	4dBi	4dBi	4dBi	11.1dBi

Figure 4.20 presents the summarized compliance boundaries for the small cell, which shows that all horizontal $R_{CD\text{-}H}$ distances are longer than the vertical $R_{CD\text{-}V}$ distances. For the ICNIRP GP, the $R_{CD\text{-}H}$ is 0.52 m compared to 0.34 m for the $R_{CD\text{-}V}$. Additionally, the FCC $R_{CD\text{-}H}$ is 0.48 m compared to 0.30 m for $R_{CD\text{-}V}$.

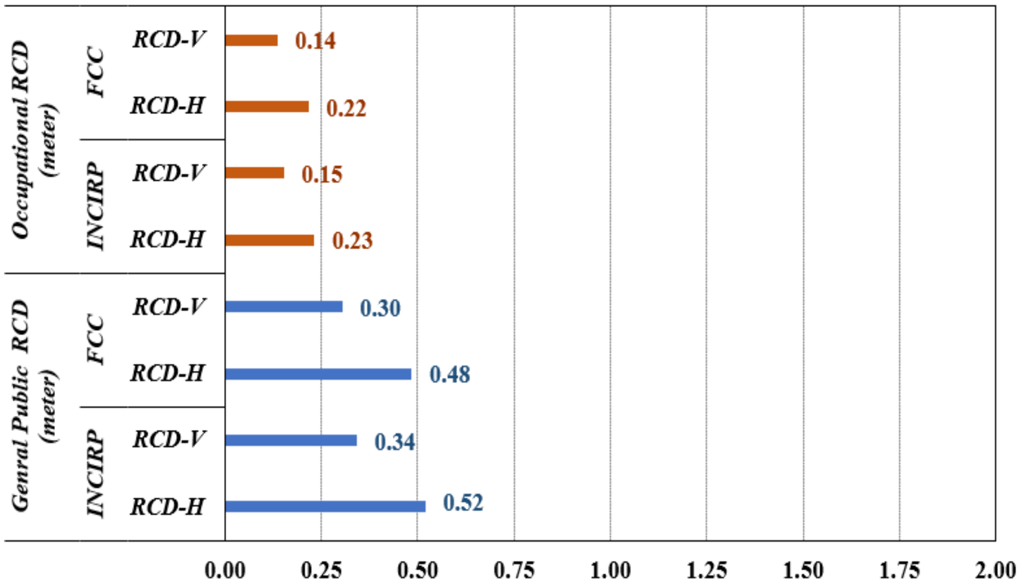

Figure 4.20. The CDs for small cell referenced to ICNIRP and FCC limits.

Analyzing the PD and its contribution to the total exposure ratio underwent additional processing. Figure 4.21 shows that 5G N3500 has the highest P_D compared to the other technologies, and all technologies reach high levels at distances very close to the antenna of the small cell (less than 0.3 m).

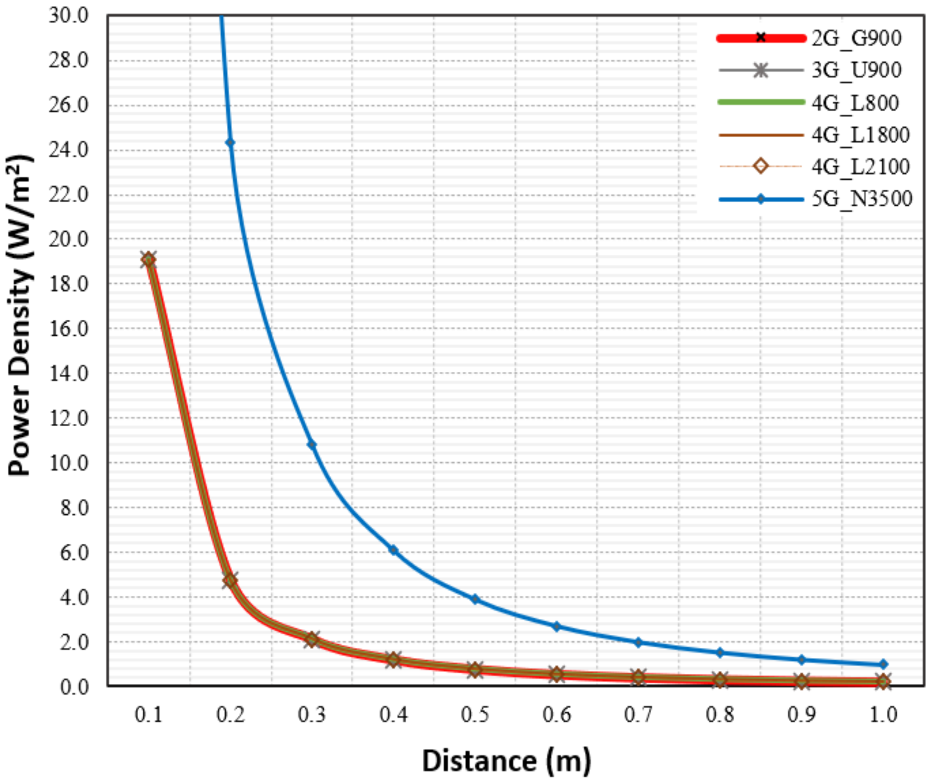

Figure 4.21. The power densities from the small cell antenna.

In reference to ICNIP and FCC limits for the GP, Figures 4.22 and 4.23 show the exposure ratios in the horizontal direction. It is clear that TER reaches 1 at very close distances and is very low at distances below 1 m, which is expected because the small cell transmits very low power. The results are very much in line with findings in [25] in which the authors studied EMF radiation from a 5G small cell at a frequency of 39 GHz and installed on a 25 feet pole above ground level. Their results show that the PD rapidly decreases with increasing, reaching 0.7% at a distance of approximately 15 m.

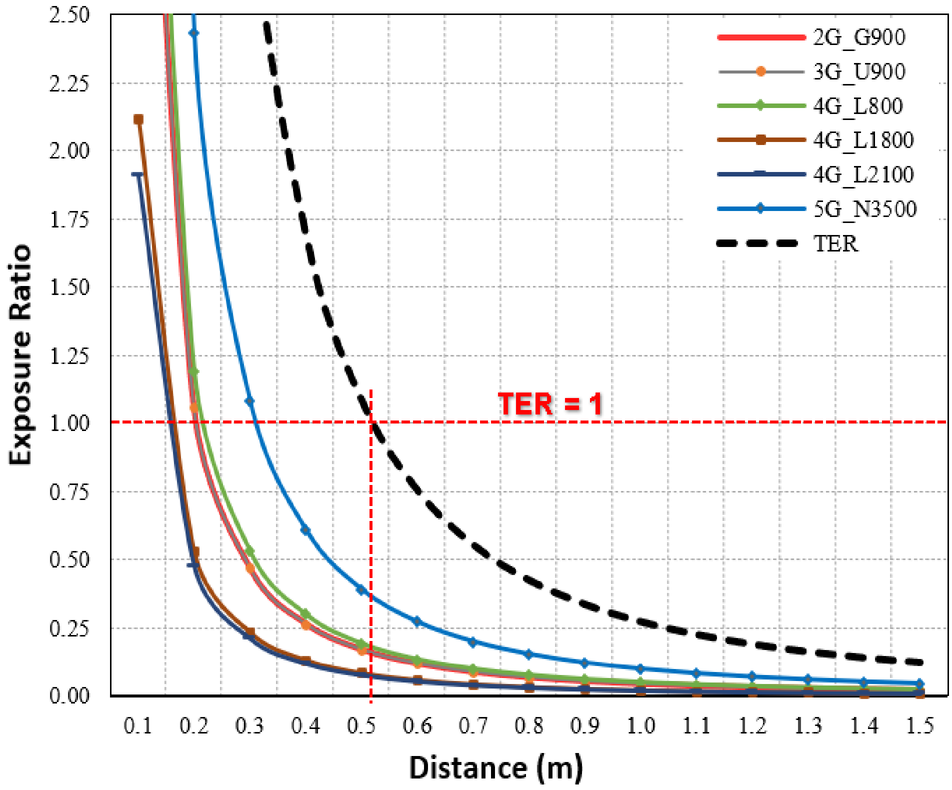

Figure 4.22. The exposure ratio for small cell reference to ICNIRP limits.

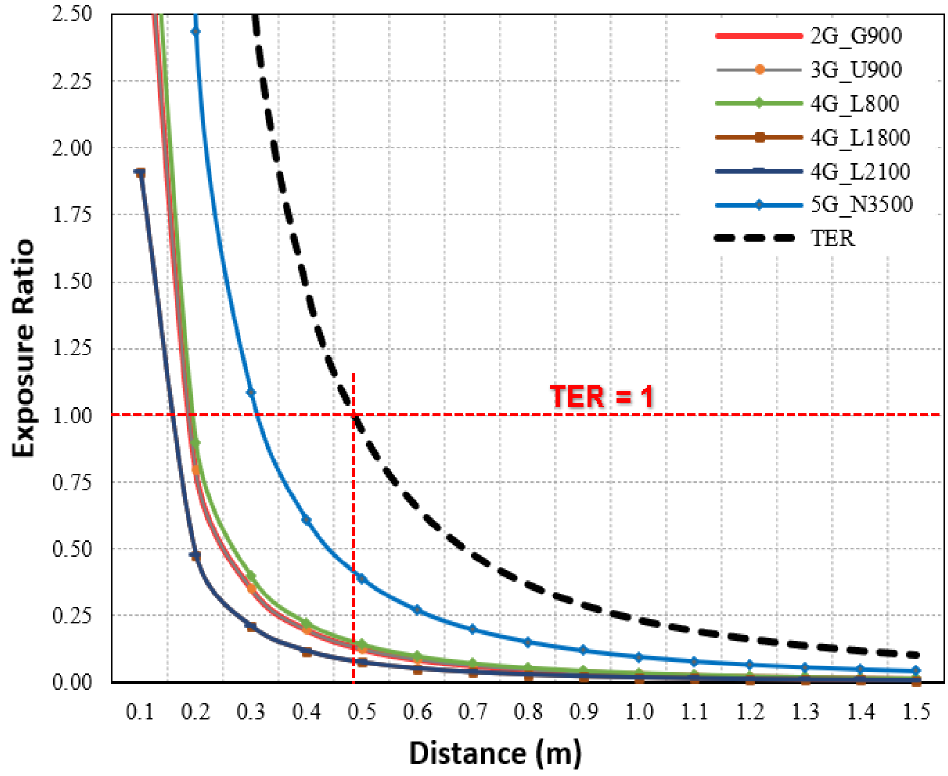

Figure 4.23. The exposure ratio small cell reference to FCC limits.

Similar to the outcomes on macro and micro, the small cell 5G has the highest contribution in the TER with 49%, followed by 4G L800 with 15%, the 4G L1800 and L2100 with 5% each, and the 2G G900 and 3G U900 with 13% each. Additionally, based on FCC limits, the highest is N3500 with a contribution of 55%, followed by 4G L800 with 13%, 4G L1800 and L2100 with 5% each, and 2G G900 and 3G U900 with 11% each. Figure 4.24 summarizes the exposure contributions of each technology at the R_{CD}.

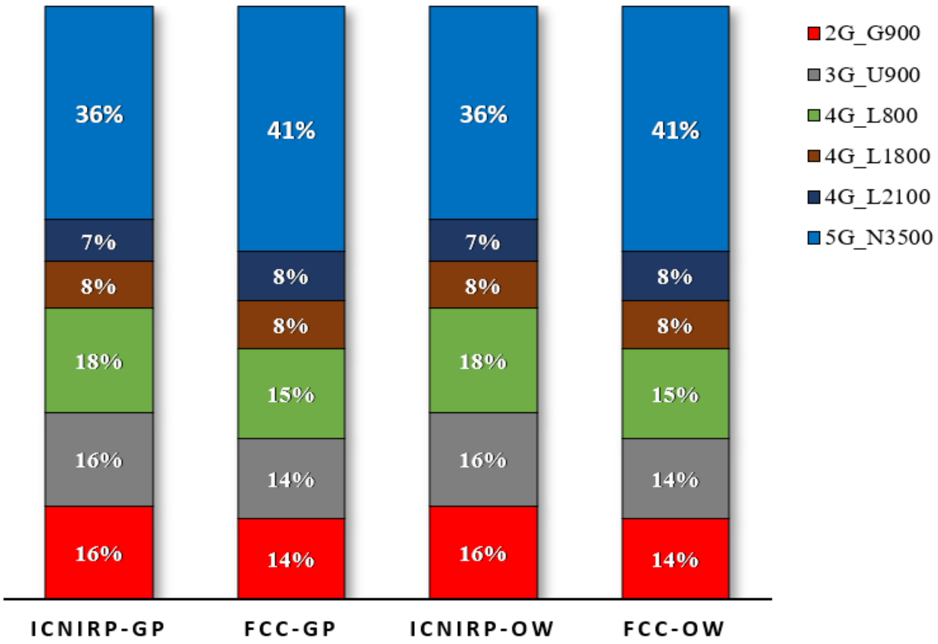

Figure 4.24. The PD contribution per technology for small.

The boundary results using the proposed enhanced Equation (3.8) gives similar distances with slight differences compared to calculations done without power factor. Table 4.9 summarizes the comparison results, which show that $R_{CD\text{-}PF}$ distances are less than 2.5% in all directions compared to the R_{CD} and this is due that the IBS configuration is not equipped with mMIMO technologies.

Table 4.9. The CDs for small cell referenced to ICNIRP and FCC limits.

Calculation Method			R_{CD} (m)	R_{CD-PF} (m)	Delta (m)	Delta %
R_{CD-H}	GP	INCIRP	0.533	0.520	-0.014	-2.5%
		FCC	0.497	0.485	-0.013	-2.5%
	OW	INCIRP	0.239	0.233	-0.006	-2.5%
		FCC	0.222	0.217	-0.006	-2.5%
R_{CD-V}	GP	INCIRP	0.351	0.342	-0.009	-2.5%
		FCC	0.312	0.304	-0.008	-2.5%
	OW	INCIRP	0.157	0.153	-0.004	-2.5%
		FCC	0.140	0.136	-0.004	-2.5%

4.1.3.4. Indoor Based Solution (IBS) Site

In-building solution (or indoor-based solution) provides indoor coverage using a series of hub (splitter) equipment distributing the signal to several antennae, as illustrated in Figure 4.25. The IBS provides extra leverage to boost the strength of wireless signals, ensuring seamless wireless connection for mobile network users. Due to construction penetration losses, the operators install the IBS within huge buildings and high-rise towers where coverage from outdoor macro sites is challenging. The typical deployment of IBSs combines all the technologies in one distributed antenna system (DAS) in which each antenna provides coverage for a certain zone as a hotspot [75, 76].

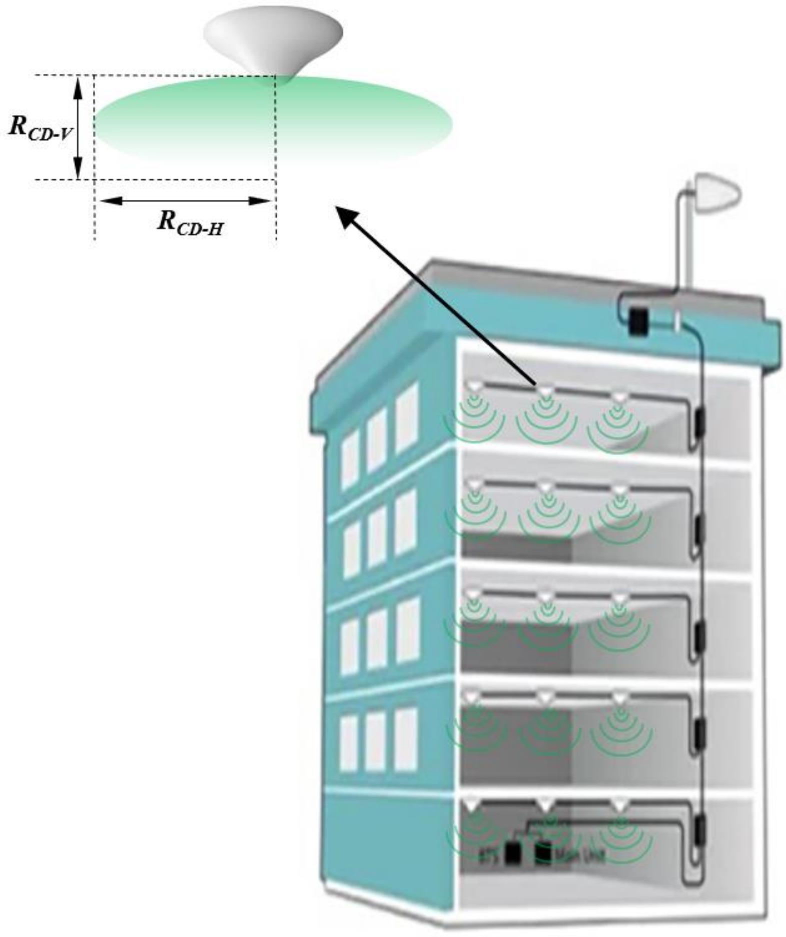

Figure 4.25. The CD for one IBS antenna installed on the roof ceiling.

The IBS includes DAS (IBS-DAS) consists of many connected antennae that are shared and energized from the same radio transmitters in the splitting system. In this study, we consider the radiation from one antenna (one zone). Table 4.10 lists the typical configurations used in the calculations for the IBS site at one antenna. We consider high configurations of IBS-DAS with six technologies G900, U900, L800, L1800, L2100, and N3500.

Table 4.10. The configuration setup for IBS DAS.

Configuration	2G G900	3G U900	4G L800	4G L1800	4G L2100	5G N3500
Freq. (MHz)	900	900	800	1800	2100	3500
Freq. BW (MHz)	5	5	10	20	20	100
Total TXs	2	1	2	2	2	4
Total RXs	2	1	2	2	2	4
Power TX	1.3W	1.3W	1.3W	1.3W	1.3W	2W
Power ρ_r	1.0	1.0	1.0	1.0	1.0	1.0
System Load	95%	95%	95%	95%	95%	95%
Ant. Gain	8dBi	8dBi	8dBi	10dBi	10dBi	11.1dBi

The calculations show that all horizontal $R_{CD\text{-}H}$ distances are longer than vertical $R_{CD\text{-}V}$ distances. For the ICNIRP GP, the $R_{CD\text{-}H}$ is 0.87 m compared to 0.40 m for the $R_{CD\text{-}V}$. For the FCC, the $R_{CD\text{-}H}$ is 0.80 m compared to 0.36 m for the $R_{CD\text{-}v}$. Figure 4.26 presents the summarized distances.

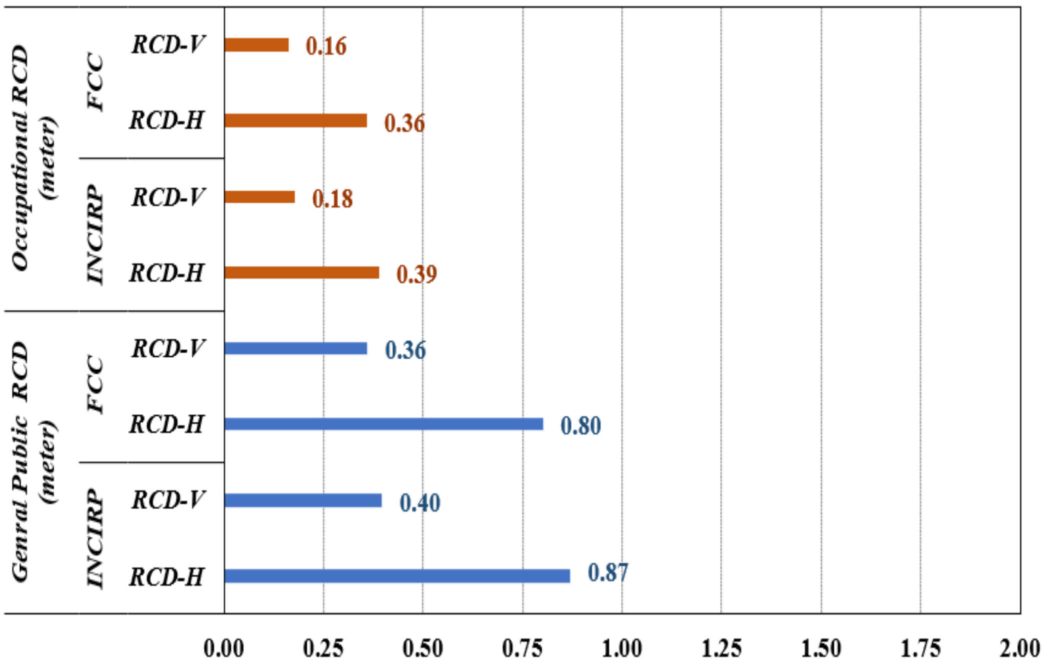

Figure 4.26. The CDs for IBS referenced to the ICNIRP and FCC limits.

In [6], the FCC mentioned set 20 cm as the minimum compliance distance that should be maintained between the users and the portable devices, and hotspots. However, the CD distances in Figures 4.20 and 4.26 represent the distances at which the power density reaches the limits regardless there is another minimum distance that should be considered (20 cm). Additionally, the results in Figure 20 show the simulated CDs for the general public are 48 cm and 30 cm horizontally and vertically, and in Figure 4.26 its 80cm and 60cm, which means all are less than 20 cm.

Figure 4.27 presents the power density P_D (W/m^2) calculated at a distance (m) from the DAS antenna, the results show that 5G N3500 has the highest P_D compared to the other technologies, and it reaches high levels at distances very close to the antenna (at less than 0.45 m).

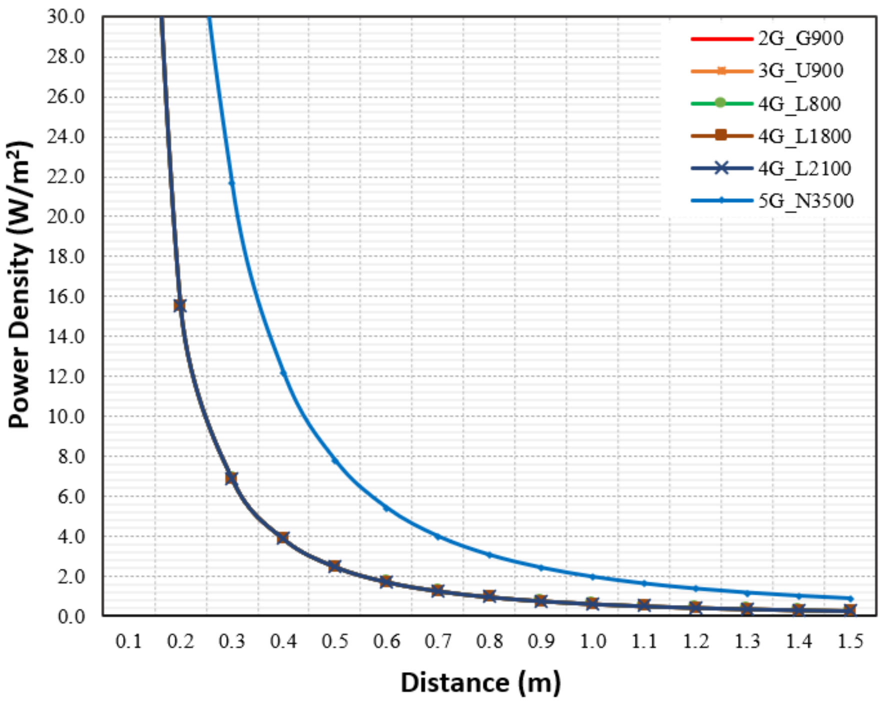

Figure 4.27. The PD from multi-technology IBS antenna.

Referring to the ICNIP and FCC limits for the GP, Figures 4.28 and 4.29 show the exposure ratio for each technology calculated at a distance (m) from the DAS antenna. The results show that 5G N3500 has the highest contribution in the TER at the CD.

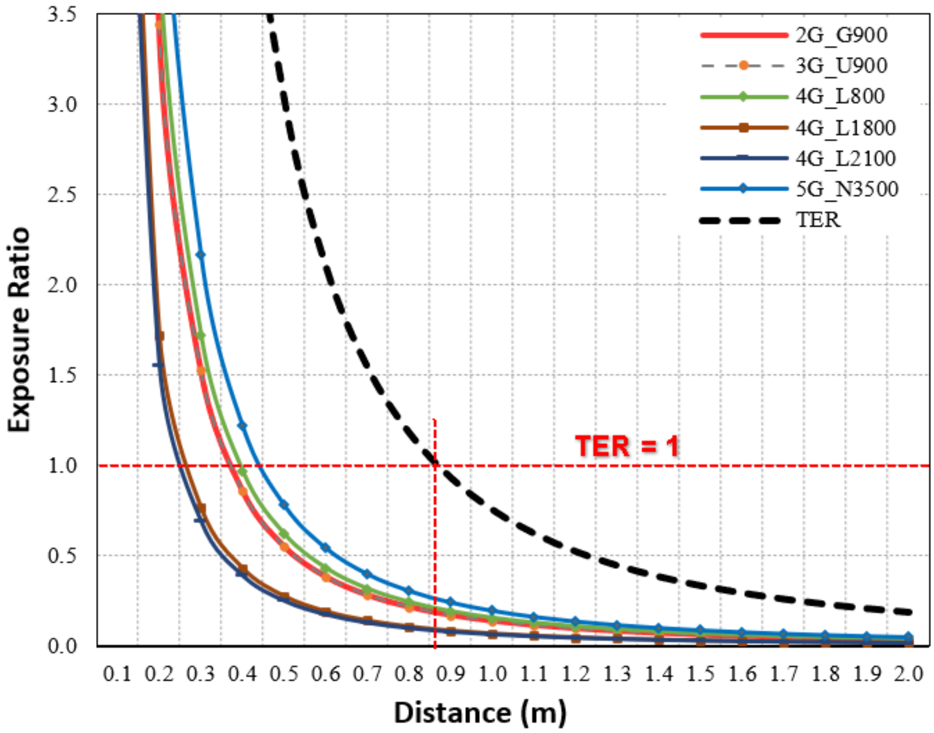

Figure 4.28. The exposure ratio for IBS site reference ICNIRP limits.

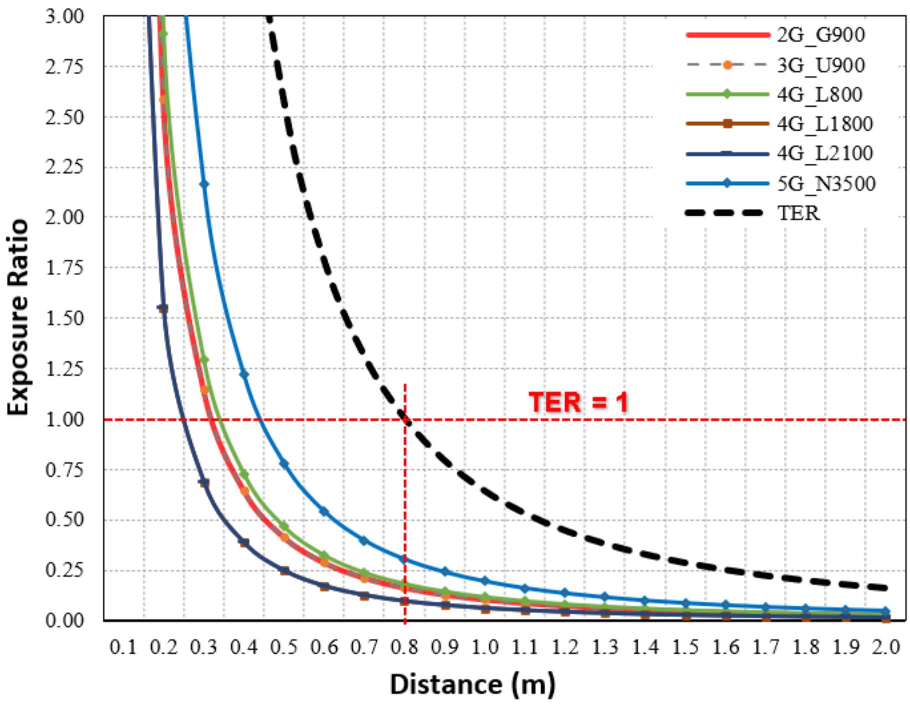

Figure 4.29. The exposure ratio for IBS reference FCC limits.

Figure 4.30 shows the summarized contributions of each technology at the compliance boundary R_{CD}. For the ICNIRP, 5G N3500 contributes 26%, followed by 4G L800 with 20%, G900 and U900 at 18%, and L1800 and L2100 at 9% and 8% respectively. For the FCC, 5G N3500 contributes 30%, the 4G L800 with 18%, G900 and U900 with 16% each, and L2100 and L1800 with 10% each.

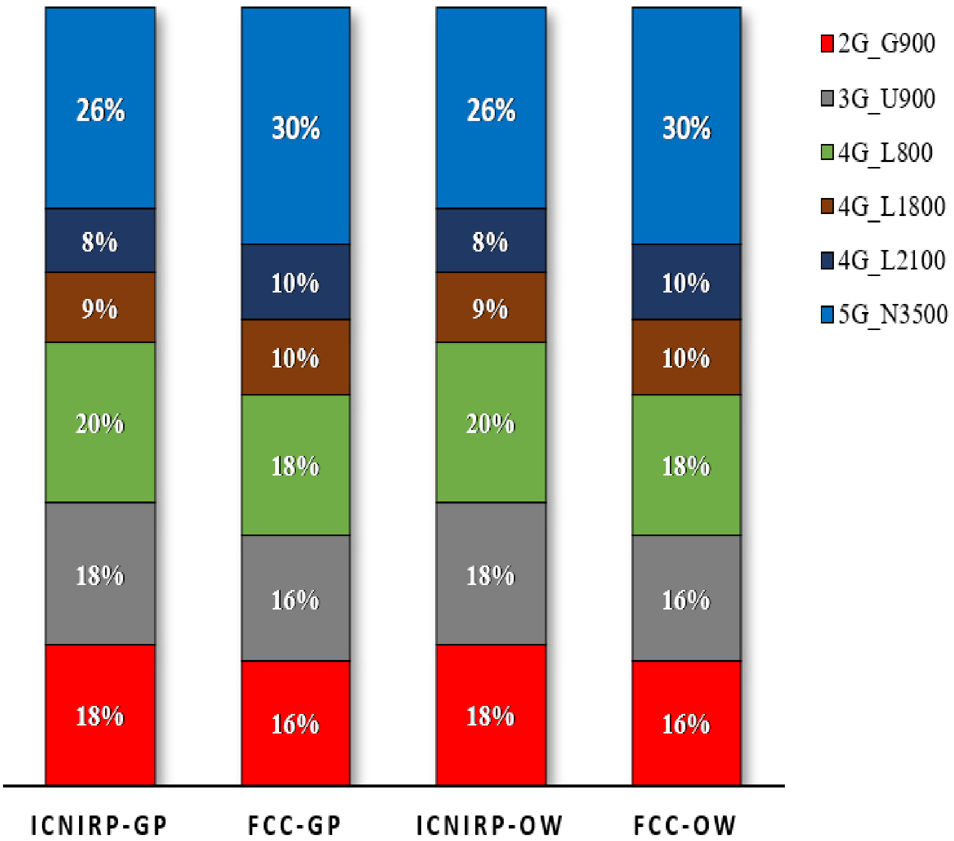

Figure 4.30. The PD contribution per technology for IBS-DAS.

The boundary calculation using Equation (3.8) provides similar distances with slight differences compared to calculations done without power factor. Table 4.11 summarizes the comparison results, which show that the R_{CD-PF} distances are less than 2.5% in all directions compared to the basic R_{CD}.

Table 4.11. The CDs for IBS referenced to the ICNIRP and FCC limits.

Calculation Method			R_{CD} (m)	$R_{CD\text{-}PF}$ (m)	Delta (m)	Delta %
$R_{CD\text{-}H}$	GP	INCIRP	0.89	0.87	-0.02	-2.5%
		FCC	0.82	0.80	-0.02	-2.5%
	OW	INCIRP	0.40	0.39	-0.01	-2.5%
		FCC	0.37	0.36	-0.01	-2.5%
$R_{CD\text{-}V}$	GP	INCIRP	0.41	0.40	-0.01	-2.5%
		FCC	0.37	0.36	-0.01	-2.5%
	OW	INCIRP	0.18	0.18	0.00	-2.5%
		FCC	0.17	0.16	0.00	-2.5%

4.1.4. Summary of Compliance Distance Results

An enhanced formula is proposed to calculate the CD considering more factors to give an accurate result. The study covered four main types of sites; macro, micro, small cell, and indoor IBS site. For a typical site operating with 2G/3G/4G/5G, the compliance distance results for the OW zone were less than the GP zone. The ICNIRP limits have slightly more restricted boundaries compared to the FCC limits. For the macro site, the GP horizontal CDs were 14.8 m and 13.8 m according to ICNIRP and FCC respectively. Additionally, the 5G NR 3,600 MHz has the highest contribution with 34% and 39% from the TER at the horizontal compliance distances. For typical configurations, the results show that the ICNIRP horizontal CDs were 2.9, 0.53, 0.89 m for the micro, small cell, and IBS sites respectively. For the macro site, the calculation involving the power reduction factor (ρ_r) gives ICNIRP horizontal CDs less by -34.5% compared to the original equation, and less by -16.2% for vertical CDs. In the future, the research team will investigate the CDs in the multi-operator with multi-technology colocated in a shared tower scenario and the accumulated radiation contribution from neighboring sites.

4.2. Complaince Distance of Site Sharing

4.2.1. Macro Site Sharing

The macro site is most type shared between MNO operators, because it commonly has a bigger civil structure (towers, monopoles, rooftop, etc…), this study considered passive sharing Macro site, as illustrated in Figure 4.31., to determine the total exposure and the compliance distance using the proposed enhance equations (3.9) and (3.10).

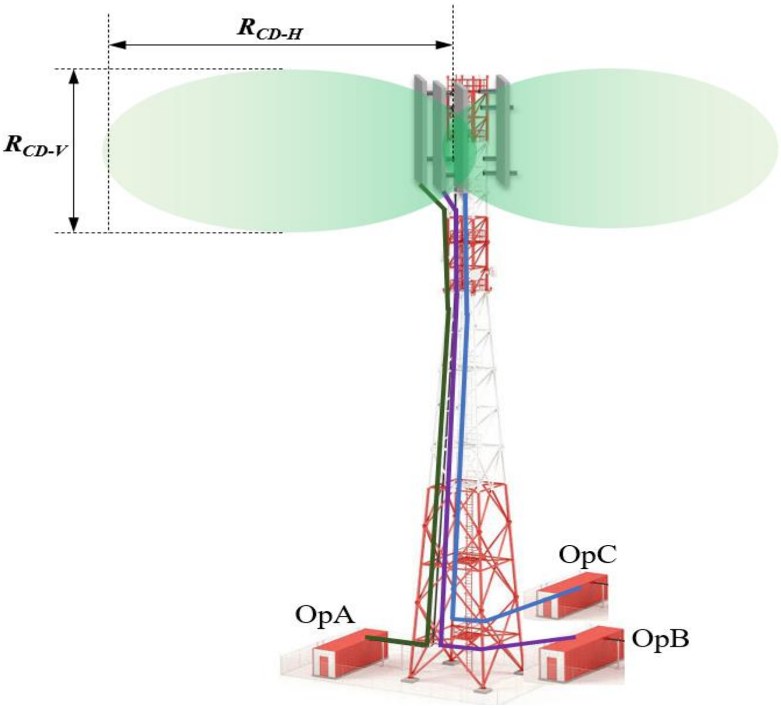

Figure 4.31. The CDs for macro sharing in tower site.

Typical configurations of macro sites equipped with multi-technology solutions were used as input data for the calculations. The site was operated with six technologies: 2G GSM at 900 MHz (G900), 3G UMTS at 900 MHz (U900), 4G LTE at 800 MHz (L800), 4G LTE at 1800 MHz (L1800), 4G LTE at 2100 MHz (L2100), and 5G NR at 3500 MHz (N3500). The input data for each technology, including Tx/Rx, antenna gain, frequency bandwidth, system load, and transmitting power, are listed in Table 5.1. For N3500, which has a high grade of mMIMO (64T/64R), we used 0.22 as a realistic power factor. This was taken from the interesting results and findings of the studies [9, 52, 53]; it indicates that the realistic transmitted power of mMIMO reaches 16–22% of the maximum equipment power when it operates at a full system load.

Table 4.12. Configuration setup for macro site.

Site Setting	2G G900	3G U900	4G L800	4G L1800	4G L2100	5G N3500
Freq. Band (MHz)	900	900	800	1800	2100	3500
Freq. BW (MHz)	5	5	10	20	20	100
Total Tx	2	1	2	2	4	64
Total Rx	2	1	2	2	4	64
Power Tx	40 W	40 W	80 W	80 W	80 W	160 W
System Load	95%	95%	95%	95%	95%	95%
Ant. Gain	17 dBi	17 dBi	16.7 dBi	16.6 dBi	17 dBi	24.8 dBi

The site configuration data were utilized in Equation (3.9) to compute the vertical and horizontal R_{CD} ($R_{DC\text{-}H}$ and $R_{DC\text{-}V}$), as displayed in Figure 5. The calculation outcome expressed that all horizontal $R_{DC\text{-}H}$ distances were longer than the vertical $R_{DC\text{-}V}$ distances, and the ICNIRP has a little more restricted R_{CD} compared with the FCC. In the main antenna horizontal direction, the general public ICNIRP $R_{CD\text{-}H}$ was 14.81 m when there was a single MNO, while it increased to 29.6 m when 4 MNOs shared the macro site. The general public FCC $R_{CD\text{-}H}$ was 13.8 m when there was a single MNO, and it increased to 27.7 m for 4 MNOs. Figure 4.32 summarizes the R_{CD} in both the vertical and horizontal directions for the GP.

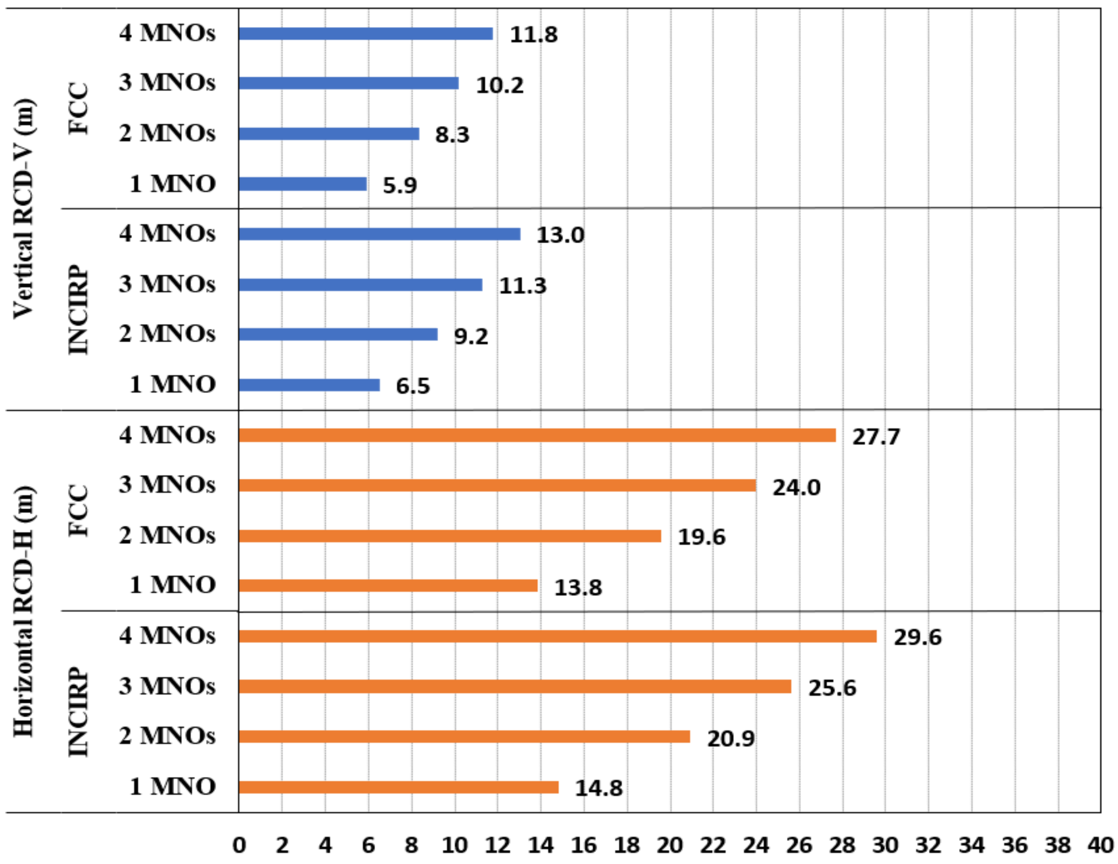

Figure 4.31. CD for multi-operator sharing a macro site.

Further processing was carried out to analyze the total emitted power density and related contribution to the total exposure ratio. Figure 4.33 depicts the power density PD (W/m2) calculated at distance (m) from the antennae in the presence of four MNOs, and the analysis showed that 5G N3500 had the highest PD among the technologies, and all technologies reached high levels at distances very close to the macro site's antenna (less than 3 m).

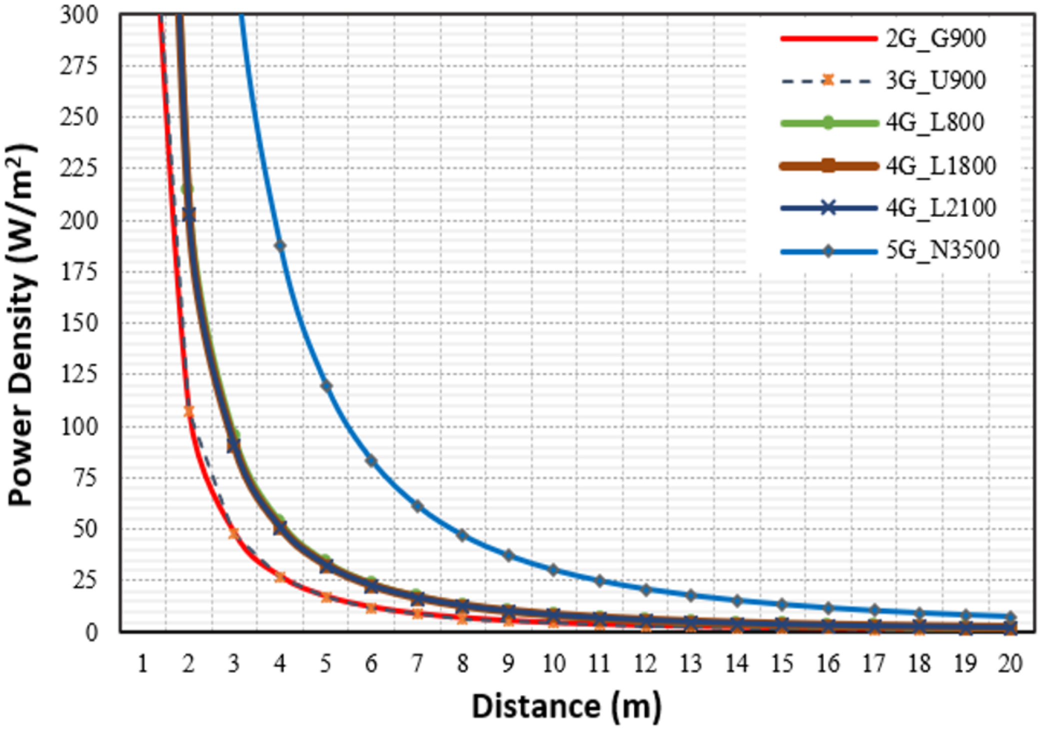

Figure 4.32. The power densities for the macro site shared by 4 MNOs.

With reference to the ICNIP for the GP, Figure 4.34 displays the exposure ratio for each technology calculated by Equation (3.9) in the horizontal direction and TER for the macro site shared by a single MNO, two MNOs, three MNOs, and four MNOs.

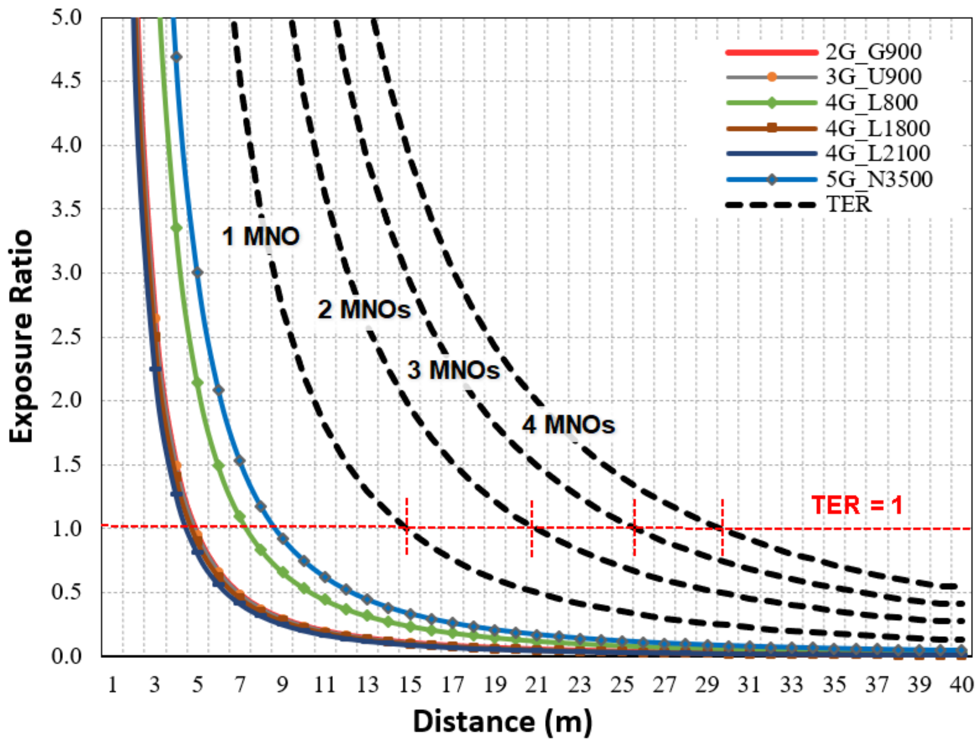

Figure 4.33. The ER for macro sharing site with reference to ICNIRP limits.

The results showed that 5G N3500 had the highest contribution at the R_{CD} with 34%, followed by 4G L800 with 24%, 4G L1800 and L2100 with 9–10% each, and 2G G900 and 3G U900 with 11% each. Similarly, at the R_{CD} based on FCC limits, the highest contributor was N3500 (39%), followed by L800 (21%), L1800 and L2100 (11% each), and G900 and U900 (9% each). Figure 4.35 summarizes the exposure contributions of each technology at the R_{CD}, and these were in line with the results found in [66] for the power density.

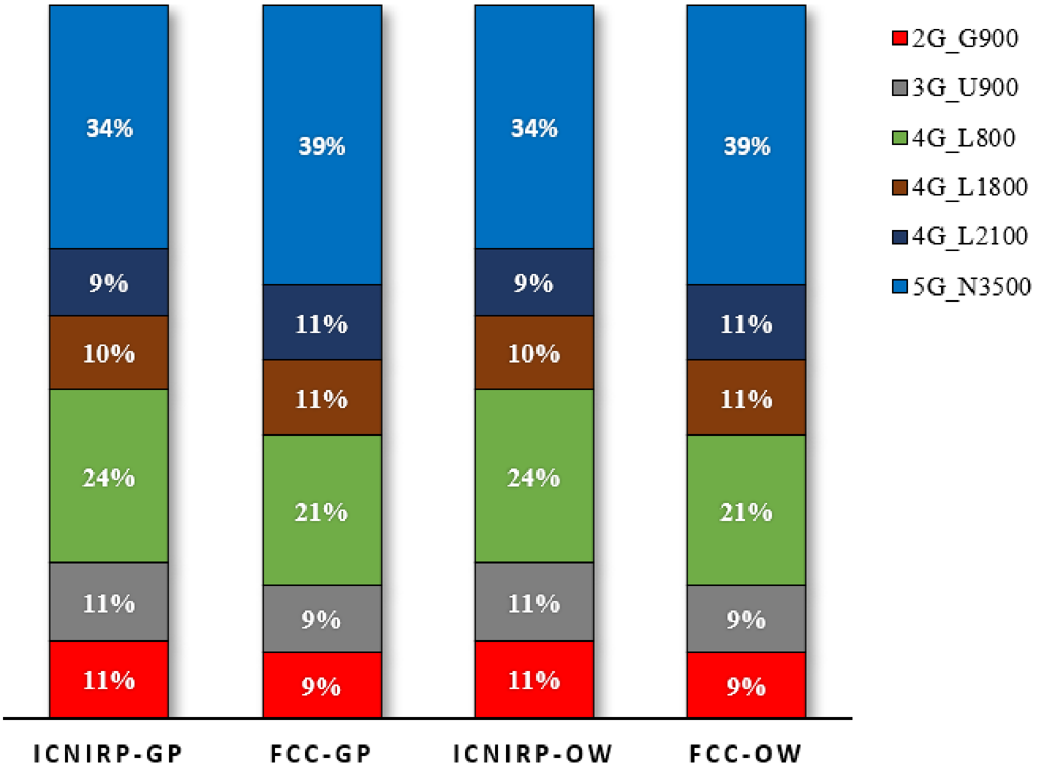

Figure 4.34. TER contribution per technology for Macro shared by 4 MNOs.

Equation (3.10) gives shorter compliance distances compared with the calculations performed using Equation (3.6) because it is based on realistic rated power for the mMIMO rather than the conservative power levels used in Equation (3.6). The R_{CD} increased with the increase in the number of MNOs sharing the same location, Table 4.13 summarizes the percentage of the distance increase compared with a single MNO with reference to the ICNIRP and FCC limits. It shows a +41% increase for 2 MNOs for all standard limits, +73% for 3 MNOs, and +100 for 4 MNOs.

Table 4.13. CDs for macro site shared by up to 4 MNOs.

Limits	Compliance Distance R_{CD} (m)						
	1MNO	2xMNO	%	3xMNO	%	4xMNO	%
INCIRP	14.8	20.9	+41%	25.6	+73%	29.6	+100%
FCC	13.8	19.6	+41%	24.0	+73%	27.7	+100%
INCIRP	6.6	9.4	+41%	11.5	+73%	13.2	+100%
FCC	6.2	8.8	+41%	10.7	+73%	12.4	+100%
INCIRP	6.5	9.2	+41%	11.3	+73%	13.0	+100%
FCC	5.9	8.3	+41%	10.2	+73%	11.8	+100%
INCIRP	2.9	4.1	+41%	5.0	+73%	5.8	+100%
FCC	2.6	3.7	41%	4.6	73%	5.3	100%

Using the data in Table 4.12 as input for input for the site sharing formula Equation (3.13) was used to scale up the increase in CD with the increased N of MNOs sharing the Macro site, the results as shown in Figure 4.37.

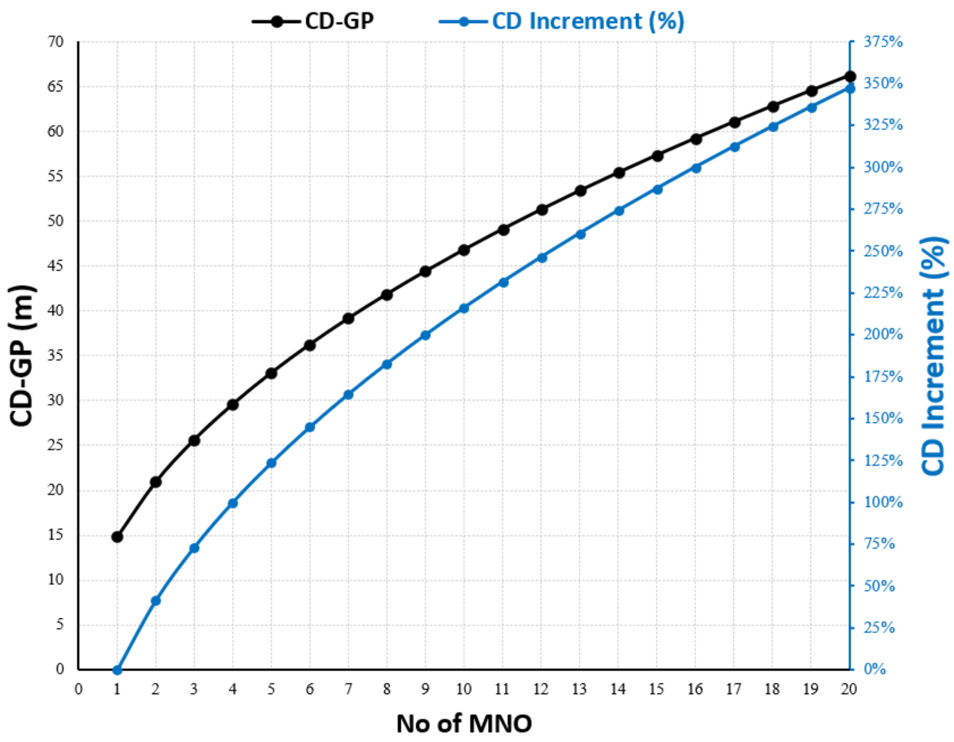

Figure 4.35. CD increment at Macro site shared by N number of MNOs.

4.2.2. IBS Indoor Site Sharing

Most of the traffic in mobile networks is generated from indoor houses and buildings [73], and in some dense areas, huge buildings suffer from weak indoor single strength due to construction loss [72], especially in public places such as airports, commercial malls, cinemas, hospitals, hotels, universities, and commercial buildings. The in-building solution (or indoor-based solution) provides indoor coverage by distributing the signal to several antennae via a series of hubs (splitters), as shown in Figure 4.37. The IBS gives additional leverage to strengthen the level and quality of wireless signals, thereby ensuring smooth wireless communication for mobile network users. The operators install the IBS inside massive buildings and high-rise towers, where the received coverage from outdoor macro sites is weak due to the construction penetration losses. The IBS combines all the technologies into one DAS in which each antenna provides coverage for a certain zone as a hotspot [75, 76].

Figure 4.36. The shared IBS Indoor DAS site by 4 MNOs.

The IBS-DAS consists of many connected antennae that are shared and energized from the same radio transmitters in the splitting system. In this study, we looked at radiation from a single antenna (one zone) using high-density configurations of a single IBS site outfitted with multi-technology as shown in Figure 4.37.

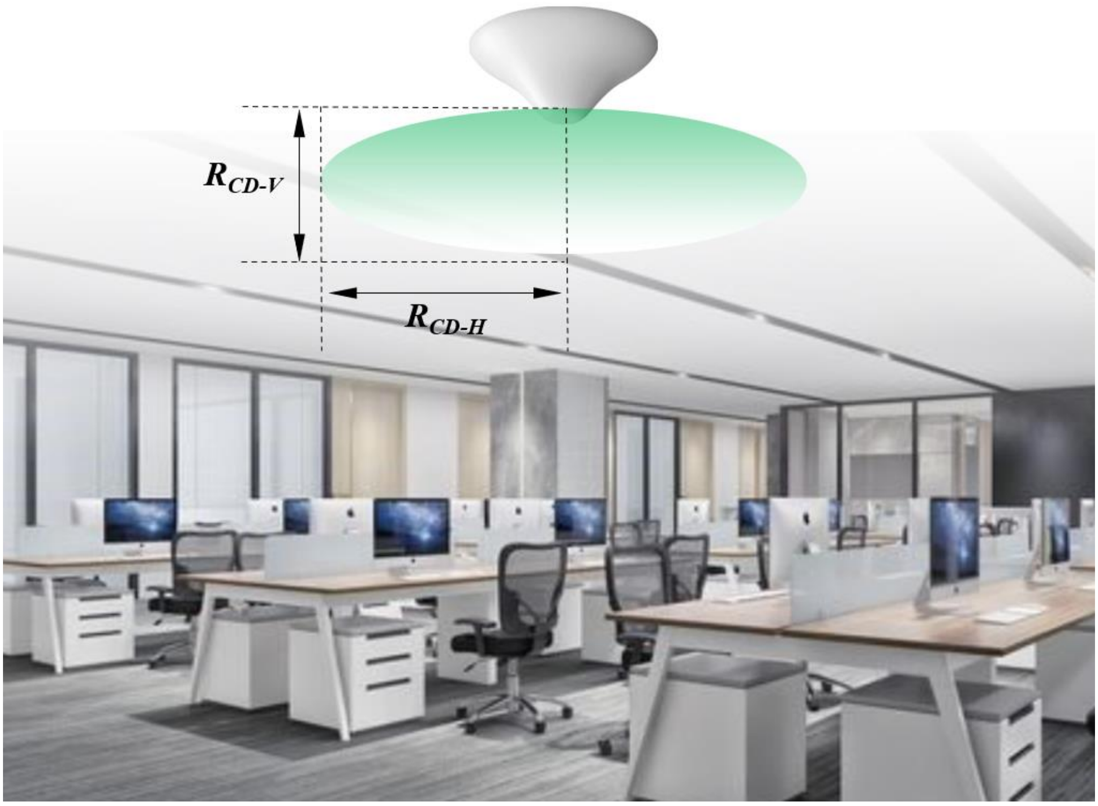

Figure 4.37. The compliance distances for one IBS antenna.

The IBS was operated with six technologies: G900, U900, L800, L1800, L2100, and N3500. The input data for each technology are listed in Table 4.14. They are similar to those of the macro site but have less Tx power, lower antenna gains, and no mMIMO in 5G.

Table 4.14. Configuration setup for shared indoor IBS.

Site Setting	2G G900	3G U900	4G L800	4G L1800	4G L2100	5G N3600
Freq. Band (MHz)	900	900	800	1800	2100	3500
Freq. BW (MHz)	5	5	10	20	20	100
Total Tx	2	1	2	2	2	4
Total Rx	2	1	2	2	2	4
Power Tx	1.3 W	1.3 W	1.3 W	1.3 W	1.3 W	2 W
System Load	95%	95%	95%	95%	95%	95%
Ant. Gain	8 dBi	8 dBi	8 dBi	10 dBi	10 dBi	11.1 dBi

Similar to the macro results, the IBS results expressed that all $R_{DC\text{-}H}$ distances were longer than the vertical $R_{DC\text{-}V}$ distances, and the ICNIRP had a slightly more restricted R_{CD} compared with the FCC. The general public ICNIRP $R_{CD\text{-}H}$ was 0.89 m when there was a single MNO, but it increased to 1.74 m for four MNOs. Additionally, for the general public, $R_{CD\text{-}H}$ was 0.4 m when there was a single MNO, while it increased to 0.79 m for four MNOs. Figure 4.38 shows the R_{CD} for the general public in both the vertical and the horizontal direction.

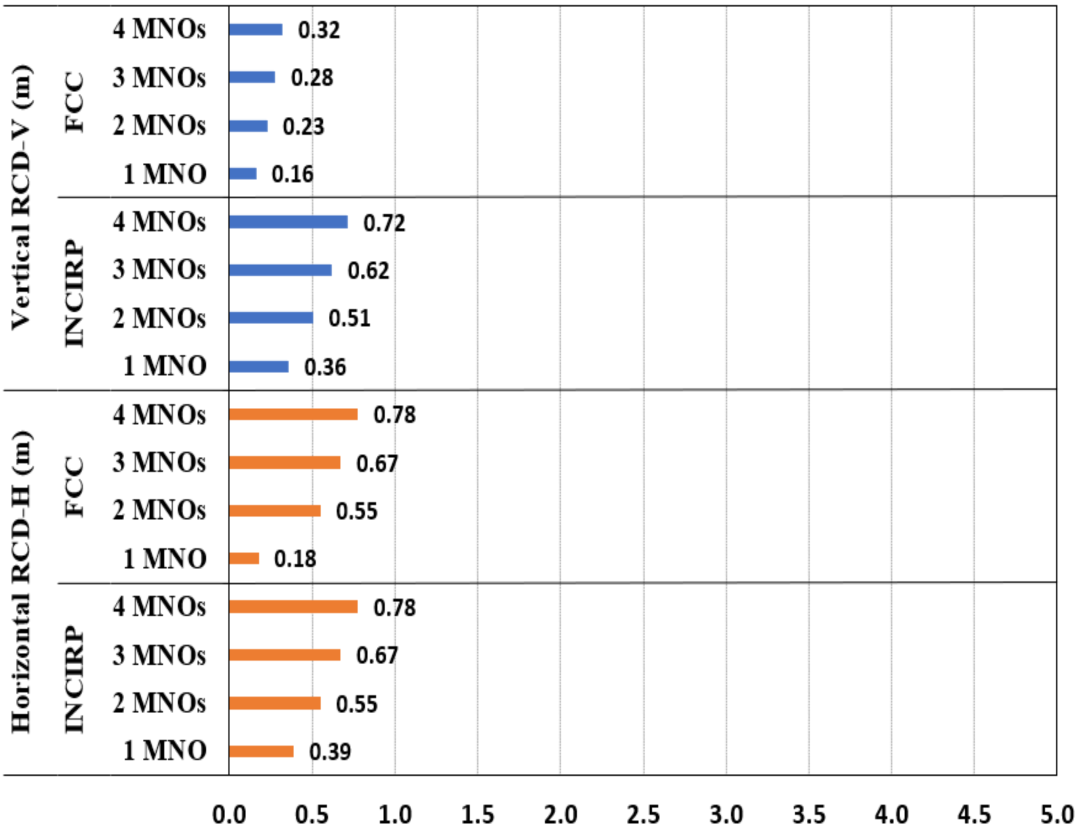

Figure 4.38. CDs for shared IBS reference to ICNIRP and FCC limits.

In addition, further processing was carried out to analyze the power density and its related contribution to the total exposure ratio. Figure 4.39 presents the power density PD (W/m2) calculated at a distance (m) from the antennae, and the analysis showed that 5G N3500 had the highest PD compared with the other technologies; it reached high levels at distances very close to the DAS antenna.

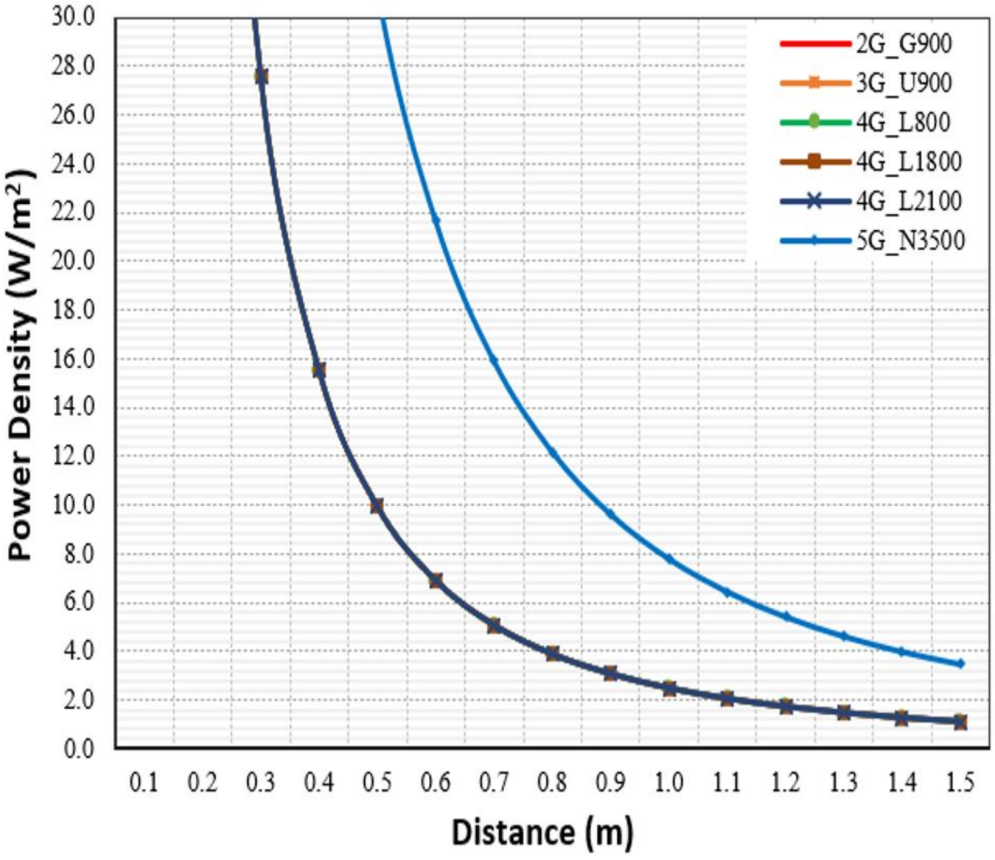

Figure 4.39. The PD from the antenna for the shared IBS site.

With reference to the ICNIP for the GP, Figure 4.40 displays the exposure ratio for each technology calculated using Equation (3.9) in the horizontal direction and the total TER for the IBS site shared by a single MNO, two MNOs, three MNOs, and four MNOs.

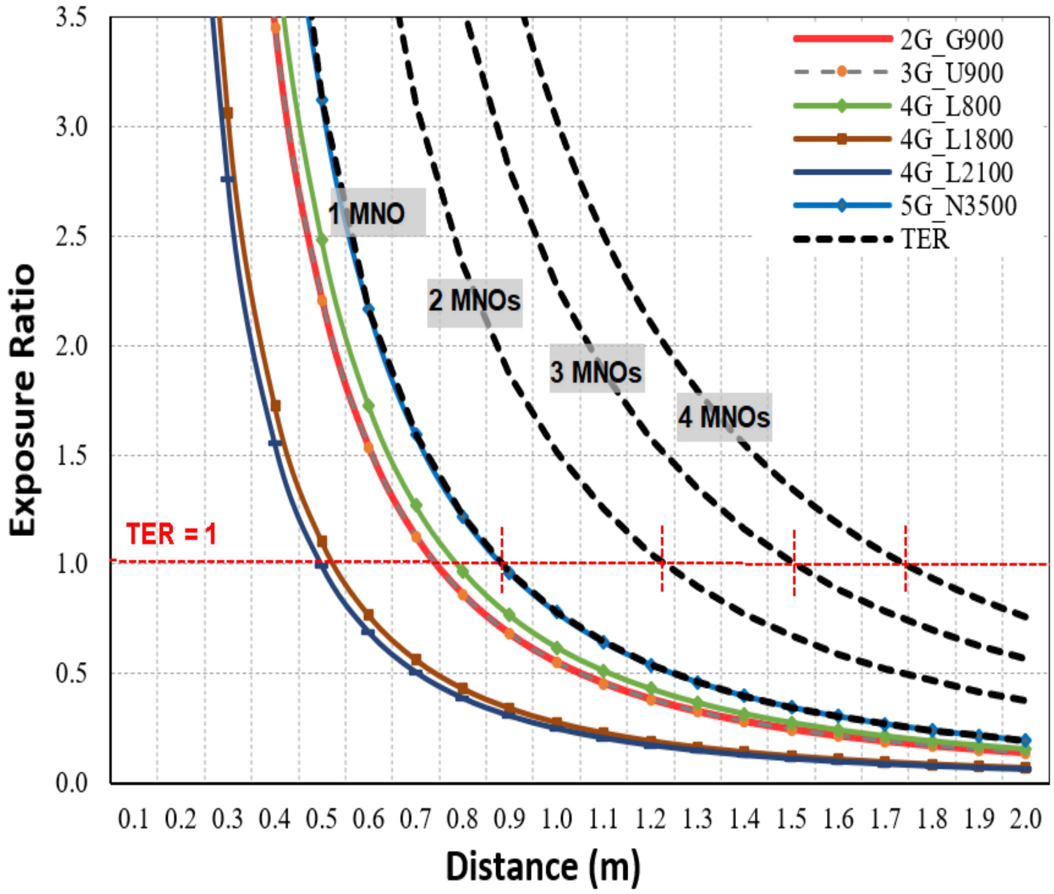

Figure 4.40. The ER shared IBS site referencing ICNIRP limits.

The results showed that 5G N3500 MHz had the highest contribution to the TER at the compliance distances for the ICNIRP with a contribution of 26%, followed by 4G L800 with 20%, 2G G900 and 3G U900 with 18% each, 4G L1800 with 9%, and 4G L2100 with 8%. Similarly, the N3500 had the highest contribution (30%), followed by 4G L800 (18%), 2G G900 and 3G U900 (16% each), and 4G L1800 and 4G L2100 (both with 10%). Figure 4.41 summarizes the exposure contributions of each technology at the R_{CD}, and these were the expected results because the IBS site does not use a high grade of mMIMO.

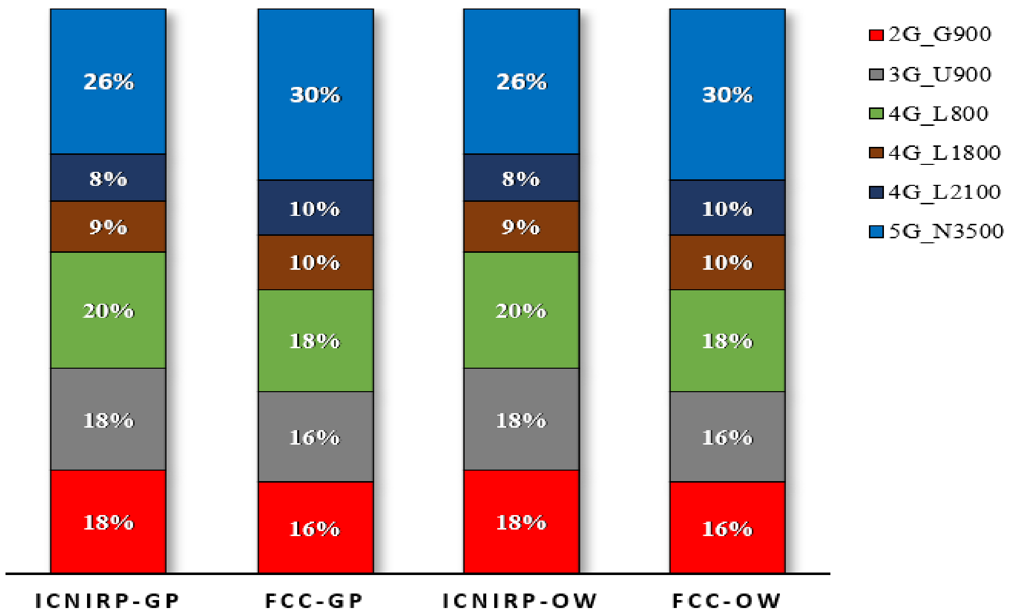

Figure 4.41. TER contribution per technology for shared IBS site.

Similar to that of the shared macro site, with an increase in the number of MNOs, the R_{CD} of the IBS increased with the same percentage for all references. Table 4.15 summarizes the percentage of the distance increase compared with a single MNO with reference to the ICNIRP and FCC limits. It shows an increase of +41% for two MNOs, +73% for three MNOs, and 100% for four MNOs.

Table 4.15. The compliance distances for shared IBS by up to 4 MNOs.

Limits	Compliance Distance R_{CD} (m)						
	1MNO	**2xMNO**	**%**	**3xMNO**	**%**	**4xMNO**	**%**
INCIRP	0.9	1.2	+41%	1.5	+73%	1.7	+100%
FCC	0.8	1.1	+41%	1.4	+73%	1.6	+100%
INCIRP	0.4	0.6	+41%	0.7	+73%	0.8	+100%
FCC	0.4	0.5	+41%	0.6	+73%	0.7	+100%
INCIRP	0.4	0.6	+41%	0.7	+73%	0.8	+100%
FCC	0.4	0.5	+41%	0.6	+73%	0.7	+100%
INCIRP	0.2	0.3	+41%	0.3	+73%	0.4	+100%
FCC	0.2	0.2	+41%	0.3	+73%	0.3	+100%

Additionally, in practice, it is difficult to find groups of MNO operators that share IBS sites with the same configurations. However, using similar configuration as the input for the site sharing formula Equation (3.13) was used to scale up the increase in R_{CD} with the increased N of MNOs sharing the IBS, as shown in Figure 4.42.

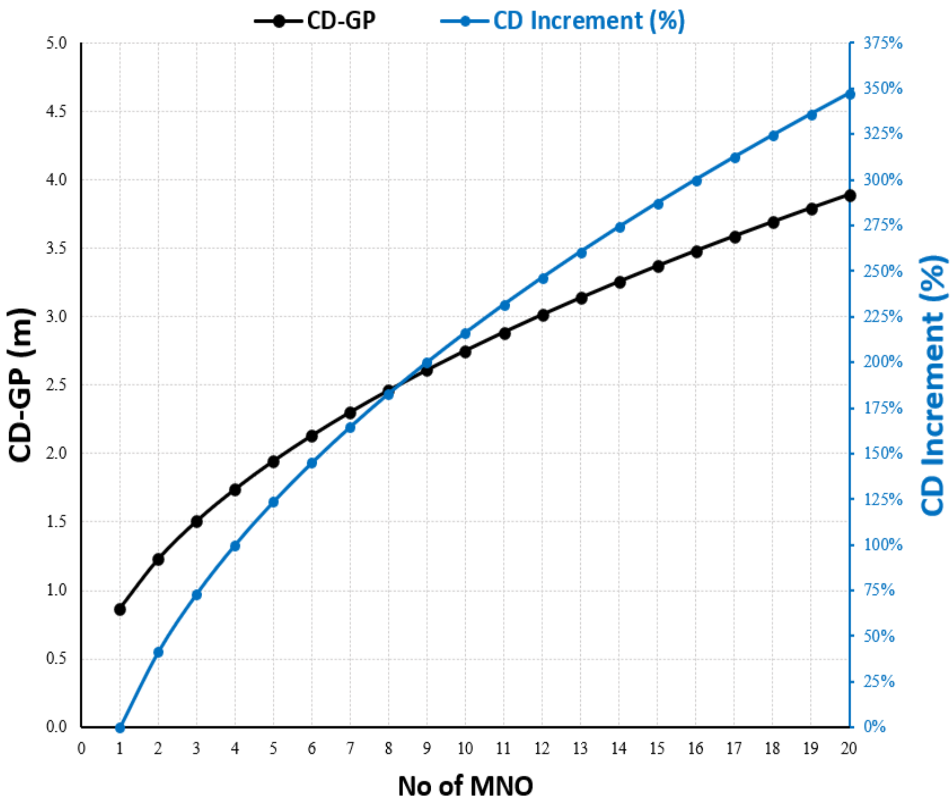

Figure 4.42. CD increment at IBS site shared by N number of MNOs.

4.2.3. Summary of Site Sharing Results

The EMF exposure compliance boundary for multi-technology, multi-operator site sharing was discussed and analyzed using calculations that considered realistic configurations, and the study covered two types of site sharing: macro and indoor IBS sites. For a typical site operating with 2G/3G/4G/5G, the compliance distance results for the general public zone were less than those for the occupational zone. The ICNIRP limits were slightly more restricted than the FCC limits. For a macro site with a single MNO, the general public's horizontal R_{CD} distances were 14.8 m and 13.8 m according to the ICNIRP and FCC, respectively. Furthermore, for a macro site shared by four MNOs, the R_{CD} distances were 29.61 m and 27.69 m according to the ICNIRP and FCC, respectively. In addition, for all shared macro site scenarios, the 5G N3500 MHz had the highest contributions to the TER of 34% and 39% at the horizontal R_{CD} according to the ICNIRP and the FCC, respectively. For the indoor IBS site with a single MNO, the general public's horizontal R_{CD} distances were 0.87 m and 0.8 m according to the ICNIRP and FCC, respectively. In addition, for an IBS shared by four MNOs, the R_{CD} distances were 1.74 m and 1.6 m according to the ICNIRP and FCC, respectively. Moreover, for all shared IBS site scenarios, the 5G N3600 MHz had the highest contributions to the TER of 26% and 30% at the horizontal compliance distances according to the ICNIRP and FCC, respectively. In the future, the research team will investigate the R_{CD} for the accumulated radiation considering the neighboring sites**.**

4.3. Validation of the Proposed Expsoure Reduction

This section discusses in details the validation and the result of using the proposed solution (design model) in section 3.3 to deconcentrate the total exposure ratio and reduce the compliance distance for multi-technology site.

4.3.1. TER and CD Simulation for 3-Sectors BS

In the three-sector model, the sector's directions are horizontally separated by 120-degree, so in this study, the model uses 0/120/240 degrees for sectors 1/2/3. The theoretical TER and CD figures are calculated for different scenarios of BSs that use a three-sector and examines the de-concentration options by using different azimuths for antenna directions using Equation (3.21).

Table 4.16 lists a typical configuration for a three-sector site used for the TER and CD calculations. The BS is equipped with 6 technologies that transmit at the same time (GSM at 900 MHz, UMTS at 900 MHz, LTE at 800/1800/2100 MHz, and NR at 2600 MHz). In many countries, some operators run the 5G NR at higher frequencies such as 3.5GHz, or millimetre waves (mM) 28/39 GHz, but here the 5G NR is taken at 2.6 GHz because the calculations are validated in real-life sites operating with the same frequencies

Table 4.16. The technology configurations of 3-Sector site.

Site Setting	2G 900	3G 900	4G 800	4G 1800	4G 2100	5G 2600
Freq. Band (MHz)	900	900	800	1800	2100	2600
Freq. BW (MHz)	4	4.2	10	10	20	60
Number of Tx	2T	1T	2T	2T	4T	64T
Number of Rx	2R	2R	2R	4R	4R	64R
Tx Power (Watt)	40	40	40	60	60	200
System Load	95%	95%	95%	95%	95%	95%
Ant. Gain (dBi)	16.6	16.6	16.2	16.5	17	24.8
Horizontal BW	60	60	65	65	65	65
Vertical BW	7.5	7.5	7.8	6	6o	6.5
Ant. Tilt Angle	-6	-6	-6	-6	-6	-6
Ant. Height	35 m	35 m	35 m	35 m	35 m	35 m

Mathematical simulations are carried out to determine the TER and CD results for the proposed model using Equation (3.21) for the antenna's azimuths compared to the normal default azimuths where all antennas have the same direction. In this simulation, The TER & CD are calculated for two types of scenarios as follows:

- **Scenario A:** Applying the default azimuth, where all the antennas (of one sector) are directed in the same azimuth angle, this includes all technologies that transmit toward one direction. This design is commonly deployed in life networks where all technologies in one sector are connected to one multi-band antenna, or separate antennas but directed in one direction. For both, all transmitters radiate in the same sector direction as illustrated in Figure 4.43.
- **Scenarios B, C, D, E, F:** Applying the proposed model by using different azimuths, the angle separation for each technology is calculated using Equation (3.21). In B, two antennas are used per sector, the first antenna transmits the 900/800/1800/2100 MHz, and the second antenna transmits the 2600 MHz. In C, three antennas are used per sector (1: G900/U900/L800, 2: L1800/L2100, 3:

N2600). In D, four antennas are used (1: G900/U900, 2: L800, 3: L1800/L2100, 4: N2600). In E, five antennas are used (1: G900/U900, 2: L800, 3: L1800, 4: L2100, 5: N2600). In F, six antennas are used (1: G900, 2: U900, 3: L800, 4: L1800, 5: L2100, 6: N2600). Practically, the RF engineers design the antennas according to the site requirements and of course consider the company's strategy for deploying the technologies as most of the networks start with the classic system (2G, and 3G), then grow to advanced solutions including 4G and 5G.

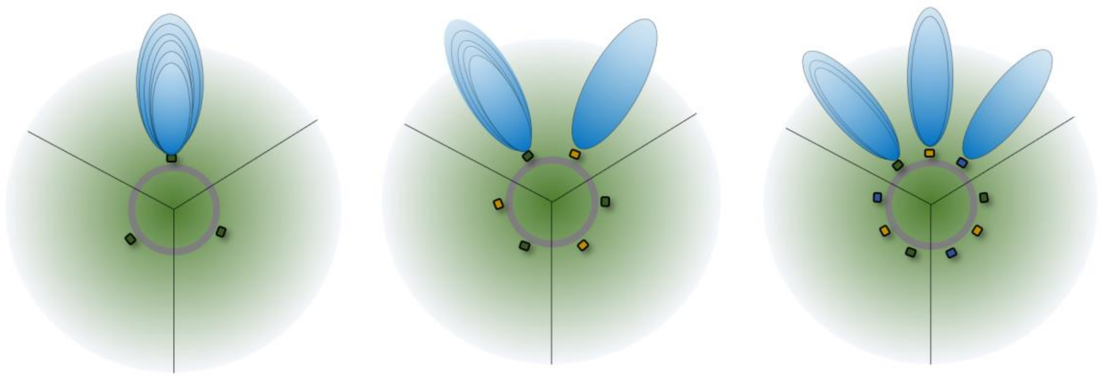

A: One azimuth   B: Two different azimuths   C: Three different azimuths

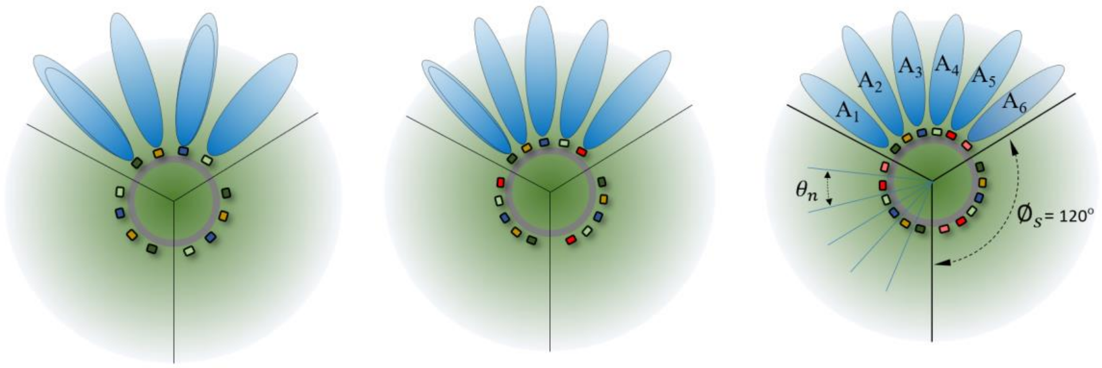

D: Four different azimuths   E: Five different azimuths   F: Six different azimuths

Figure 4.43. Scenarios A-F of different number of antennas in one sector.

The simulation results are concluded in Table 4.17 listed the θ_n values for each technology (antenna) calculated for the corresponding scenario. Also, it shows the CD distances (in meter) reference to ICNIRP for general public [47, 59], also it lists the reduction percent compared to the default setup using one direction for all technologies of serio A. the results show that using 2 azimuths in scenario B gives less compliance distance by 23.3% compared to scenario A of having one direction. The 3 azimuths in scenario C gives

35.9% less CD, the 4 azimuths in scenario D gives 39.8% less CD, the 5 azimuths in scenario E gives 41.3% less CD, and the 6 azimuths in scenario F gives 43.4% less CD compared to scenario A. Furthermore, Table 4.18 lists more detailed results of the horizontal and vertical compliance distances for the mentioned six scenarios references to both standards ICNIRP and FCC limits.

Table 4.17. The configurations and antenna azimuths of 3-Sector site.

Antenna's Sector Configuration Azimuths (Multi-Technologies)	Separation Angles (Degree)						CD (m)	CD Reduction (%)
	G9	U9	L8	L18	L21	N26		
1 Azimuth (G9/U9/L8/L18/L21/N26)	120.0						15.58	0.00%
2 Azimuths (G9/U9/L8/L18/L21), (N26)	70.3					49.7	12.63	-23.3%
3 Azimuths (G9/U9/L8), (L18/L21), (N26)	47.9			22.4		49.7	11.45	-35.9%
4 Azimuths (G9/U9), (L8), (L18/L21), (N26)	30.4		17.5	22.4		49.7	11.13	-39.8%
5 Azimuths (G9/U9), (L8), (L18), (L21), (N26)	30.4		17.5	11.2	11.3	49.7	11.02	-41.3%
6 Azimuths (G9), (U9), (L8), (L18), (L21), (N26)	15.2	15.2	17.5	11.2	11.3	49.7	10.85	-43.4%

Table 4.18. The horizontal and vertical compliance distances for the general public and occupational workers reference to ICNIP and FCC reference limits.

Antenna's Sector Configuration Azimuths (Multi-Technologies)	ICNIRP GP (m)		ICNIRP OW (m)		FCC GP (m)		FCC OW (m)	
	CD_H	CD_V	CD_H	CD_V	CD_H	CD_V	CD_H	CD_V
1 Azimuth (G9/U9/L8/L18/L21/N26)	15.58	2.51	6.97	1.12	14.70	2.29	6.57	1.02
2 Azimuths (G9/U9/L8/L18/L21), (N26)	12.63	1.92	5.34	0.86	11.27	1.76	5.04	0.79
3 Azimuths (G9/U9/L8), (L18/L21), (N26)	11.45	1.60	4.46	0.72	9.41	1.47	4.21	0.66
4 Azimuths (G9/U9), (L8), (L18/L21), (N26)	11.13	1.51	4.19	0.67	8.84	1.38	3.95	0.62
5 Azimuths (G9/U9), (L8), (L18), (L21), (N26)	11.02	1.47	4.09	0.66	8.63	1.34	3.86	0.60
6 Azimuths (G9), (U9), (L8), (L18), (L21), (N26)	10.85	1.42	3.94	0.63	8.31	1.30	3.72	0.58

4.3.2. In Situ Assessment for TER Reduction

A field experiment is done in a life network to examine the results of the proposed model by applying the antenna's azimuths with angles calculated using Equation (3.21). To have an accurate result, the experiment is done for 4 Macro BS sites (one cluster) that service a residential populated district at Khubar city in the Kingdom of Saudi Arabia as shown in Figure 4.44. The 4 sites belong to one public land mobile network operator (PLMN), all sites have the same configuration of three-sector, and each is equipped with 6 systems that transit as co-located in a multi-technology site.

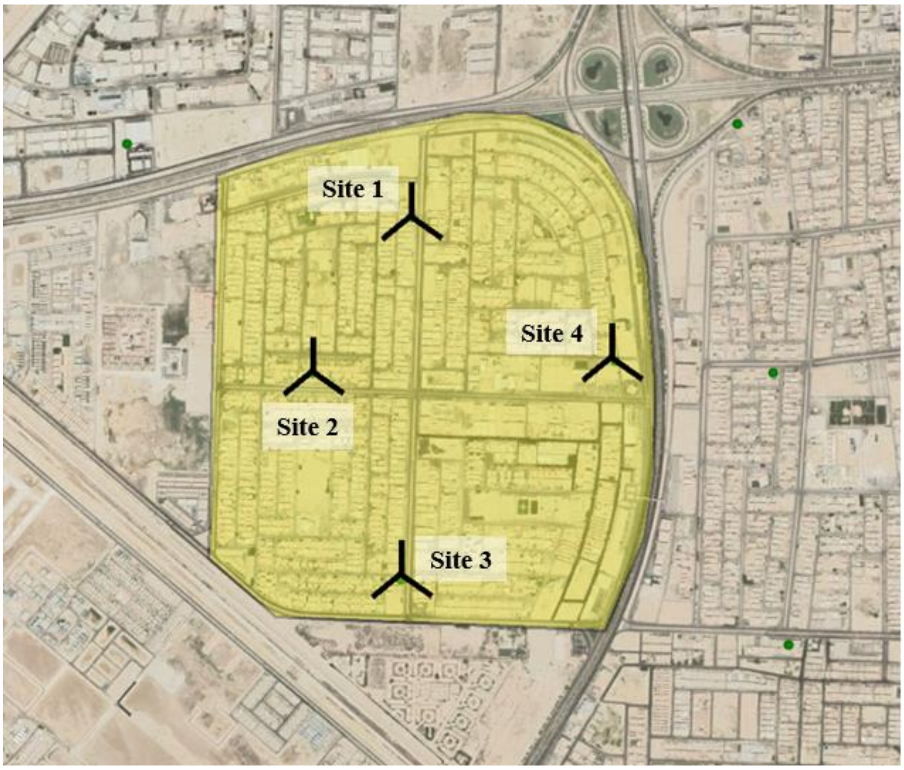

Figure 4.44. Location of 4 sites where the field experiment is done.

The 4 sites use 0/120/240 degrees for the sector's azimuths, where the 0 degree starts from the north geographical direction and increases clockwise. All the sites were deployed with scenario B using two antennas, one for G9/U9/L8/L18/L21, and the second antenna for N26. Initially, all antennas were directed toward the same azimuth and were transmitted in the same direction. Then, the 2nd antennas of all sectors are redirected (rotated) to new directions with azimuths 60/180/300 degrees which gives 60 degree as horizontal separation angles between the two antennas in each sector.

Two types of data are collected to assess the total exposure before and after applying the antenna azimuth changes, and also to evaluate the effects (impact) on the coverage signal level and capacity, as follows:

A. Power density field measurement (radiation meter).
B. TER from Geo-location data (system records).
C. Signal level field measurements (drive test).
D. Network's OSS KPIs data (system records).

4.3.2.1. Power Density Field Measurement

Field measurements are conducted to measure the power density from two points in Site 1 (P1 and P2) as shown in Figure 4.45, and also from two points in Site 2 (P3 and P4) as shown in Figure 4.46. The locations P1 and P3 are intentionally selected facing the initial direction of the antennas at 0/120/240 degrees, and locations P2 and P4 are selected facing 60/180/300 degrees.

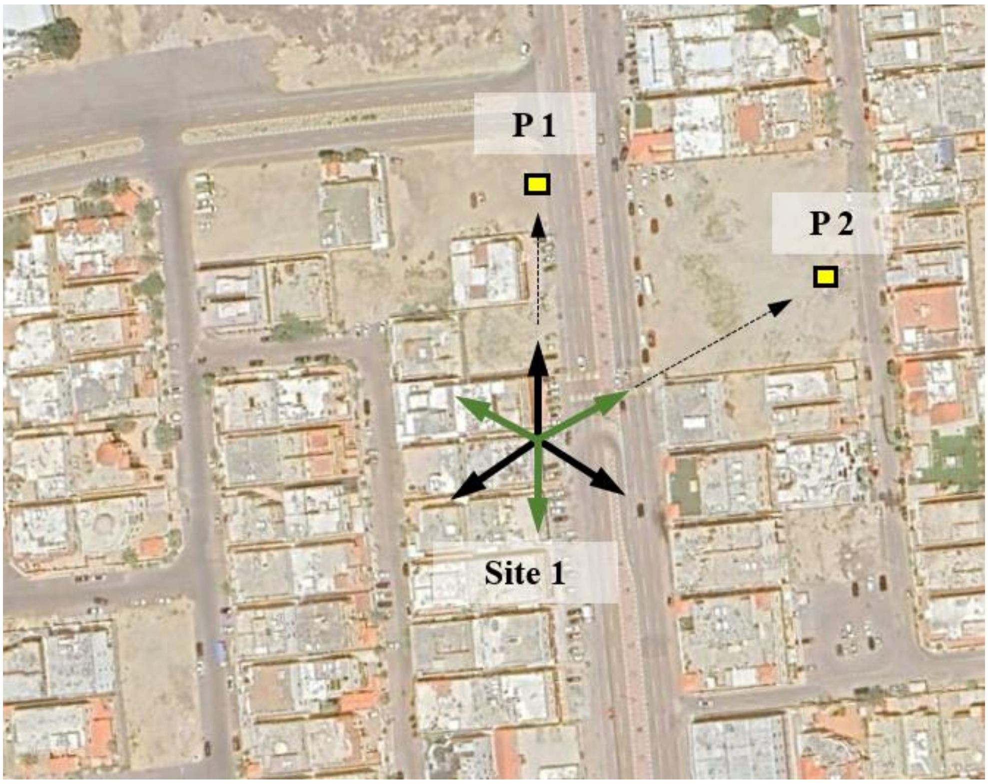

Figure 4.45. Site 1, location of P1 and P2 measurements.

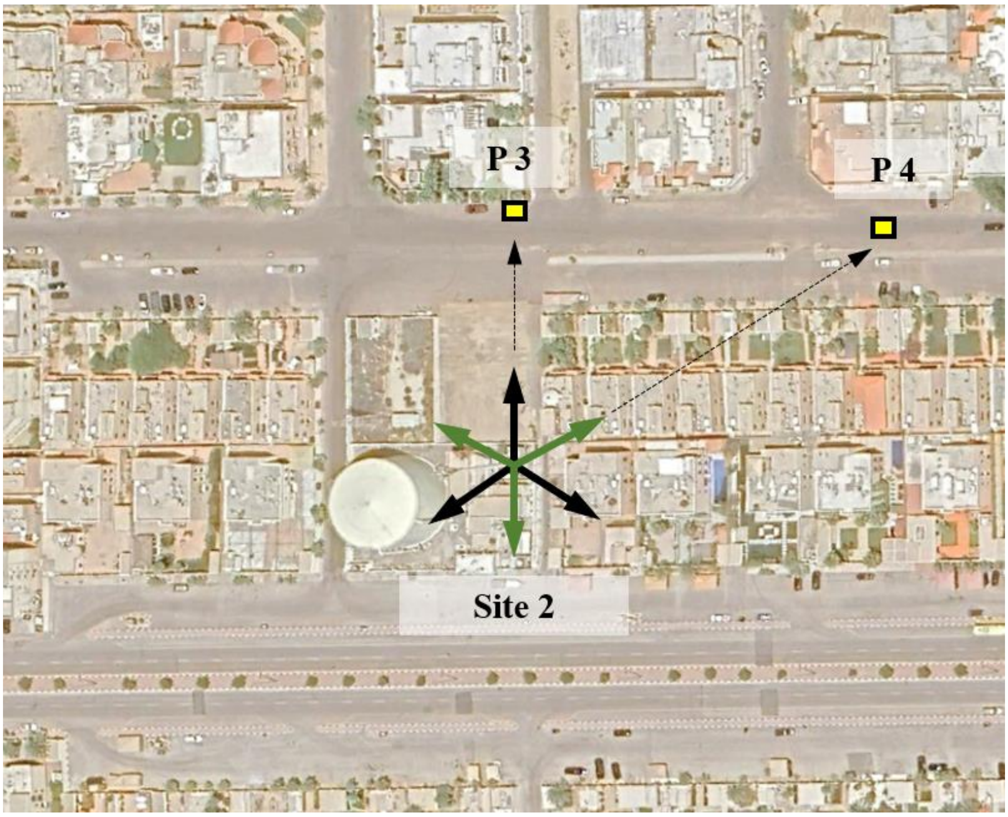

Figure 4.46. Site 2, locations of P3 and P4 measurements.

The SRM-3006 Narda [64] radio selective radiation meter is used for the measurements, this tool supports a frequency range from 9.0 kHz to 6.0 GHz, and has a three-axis isotropic antenna (E-field). Figure 4.47 shows the site and the meter position during the field test at the selected site, and the meter was positioned facing the primary beam direction of the antenna at a height of 2 meters on a tripod.

Figure 4.47. The location the SRM radiation meter measurement.

The SRM-3006 was configured to scan the downlink (DL) frequency ranges, the team collected approximately 7,200 measurement samples for each system technology at each point with a scan rate of 0.67 sample/second. To have an accurate evaluation, all measurements are conducted during the same time during the highest hours of traffic (from 07:00 to 10:00 pm). For each point, the measurements are done twice, before the antenna's azimuth changes (Pre), and after the azimuth change (Post).

Table 4.19 lists the results of the measured power density and TER at each point (for both Pre-and-Post measurements). The results from site 1 show that TER decreased at point 1 by -5.41% while it increased at P2 by 5.95% with reference to the ICNIRP limit. Also, the results for site 2 show that TER decreased at point 1 by -5.52% while it increased at P2 by +5.05% with reference to the ICNIRP limit. Furthermore, Table 4.19 listed the TER increase/decrease for sites 1 and 2 in reference to FCC limits.

Table 4.19. The Pre and Post measured PD and TER.

Measurement	Site	Site 1: PD (mW/m2)				Site 2: PD (mW/m2)			
	Location	P1		P2		P3		P4	
		Pre	Post	Pre	Post	Pre	Post	Pre	Post
Power Density (mW/m2)	G900	0.26	0.26	0.21	0.21	0.23	0.23	0.21	0.21
	U900	0.91	0.91	0.80	0.80	0.15	0.15	0.13	0.13
	L800	0.43	0.43	0.33	0.33	0.49	0.49	0.39	0.39
	L1800	1.12	1.12	1.02	1.02	1.15	1.15	1.05	1.05
	L2100	2.04	2.04	2.00	2.00	2.02	2.02	1.82	1.82
	N2600	5.85	5.15	4.86	5.52	6.39	5.74	5.59	6.11
ICNIRP GP	TER	0.0013	0.0012	0.0011	0.0012	0.0012	0.0011	0.0010	0.0011
	TER (%)		-5.41%		5.95%		-5.52%		5.09%
FCC GP	TER	0.0012	0.0011	0.0010	0.0011	0.0017	0.0016	0.0015	0.0016
	TER (%)		-5.89%		6.47%		-6.23%		5.71%
ICNIRP OW	TER	0.0003	0.0002	0.0002	0.0002	0.0002	0.0002	0.0002	0.0002
	TER (%)		-5.41%		5.95%		-5.52%		5.09%
FCC OW	TER	0.0002	0.0002	0.0002	0.0002	0.0002	0.0002	0.0002	0.0002
	TER (%)		-5.89%		6.47%		-5.84%		5.37%

4.3.2.2. TER Evaluation form Geo-Location Data

The TER is evaluated for the whole cluster before and after the antenna changes (Pre-and-Post) using the geo-location data recorded in the OSS system. The network OSS archives the daily (and hourly) statistics and information about network traffic and performance, this includes counters and key performance indicators. It also includes geo-location data that contains the information associated with handset devices connected to the network such as the radio conditions (received signal level, channel quality, etc..) with the associated coordinates.

The received levels of all technologies from all devices in the cluster (within the polygon of the test area) are recorded before and after the azimuth changes, and it's used to calculate the TER [41]. The geo-location system gives the data as average for pixels of 50x50 meters each, the area under this test consists of 954 pixels within the cluster polygon of 2.3 Km^2.

The geolocation data is collected and calculated for two weeks period, one week before and one week after the antenna azimuth change. Figure 4.48 summarizes the results which show the average Pre TER is 23.4x10-6, and it decreased to 18.91x0-6 after antenna azimuth is changed, this reduction is an improvement of -19.23% in average TER.

Pre (before azimuth changes) Post (after azimuth changes)

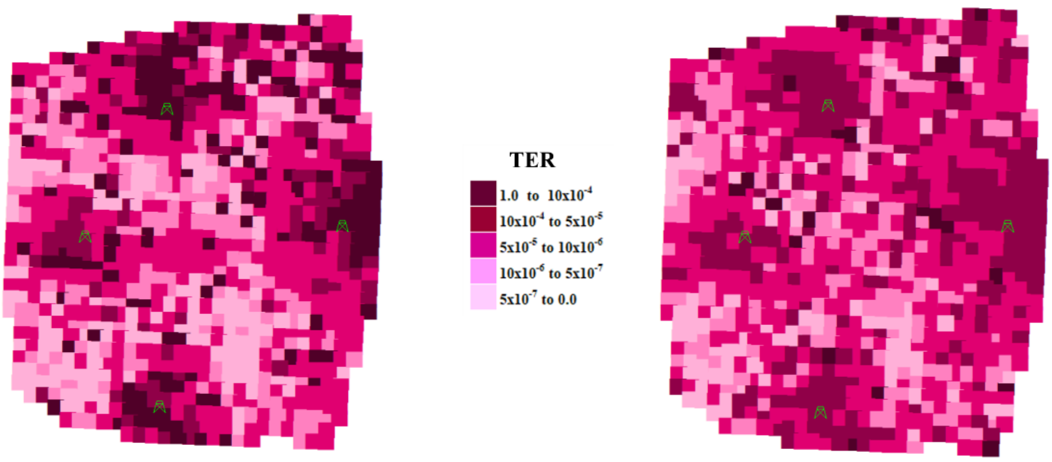

Average TER = 23.4×10^{-6} Average TER = 18.9×10^{-6} (-19.23%)

Figure 4.48. The Pre and Post TER form Geo-location records.

Also, the TER distribution is evaluated and the results show that the higher range of TER (1.0 to 10x10-4) was counted for 17.0% on total pixels pre the antenna changes, and it decreased to 2.7% after antenna azimuth is changed as listed in Table 4.20. As a consequence, results, the lower range of TER (5x10-7 to 0.0) is increased from 16.7% to 10.2%. These results state that the total exposure is deconcentrated when separate directions are used for antennas azimuths.

Table 4.20. The TER distribution (Pre and Post) for the test cluster.

TER	Pre		Post	
	Pixel Count	**Pre %**	**Pixel Count**	**Post %**
1.0 to 10x10-4	162	17.0%	26	2.7%
10x10-4 to 5x10-5	98	10.3%	269	28.2%
5x10-5 to 10x10-6	368	38.6%	399	41.8%
10x10-6 to 5x10-7	167	17.5%	163	17.1%
5x10-7 to 0.0	159	16.7%	97	10.2%
Total Pixel	954		954	

4.3.2.3. Signal Level Field Measurement

Drive test field measurements were conducted to evaluate the effect of azimuth rotation on the network received signal levels from all technologies. The team used Test of Mobile System (TEMS) Investigation v20 [33] which was installed on a laptop PC and connected to GPS and three mobile user equipment (UE), as seen in Figure 4.49. The UEs were mounted inside a vehicle in front of the dashboard at a height of 1.3 to 1.5 meters from the ground, and each UE was locked to measure single technology Rx signal level. The measured samples were taken every 0.5 seconds for each UE, with over 3,290 measurement samples for each technology. The measurements are stored in log files together with the relevant time and GPS coordinates. The collected measurements include Rx signal level in dBm of the Broadcast Common Control Channel (BCCH) for 2G, the Received Signal Code Power (RSCP) for 3G, the Reference Signal Received Power (RSRP) for 4G, and the Secondary Synchronization Reference Signal Received Power (SS-RSRP) for 5G.

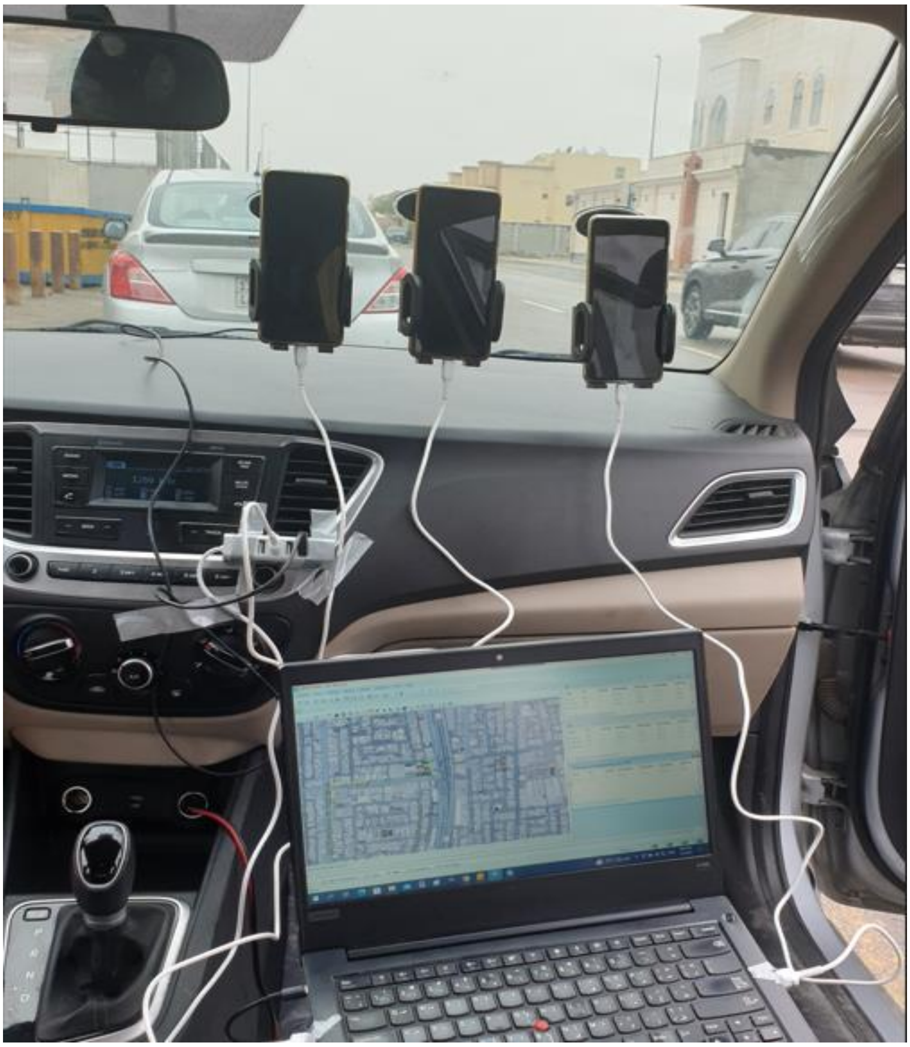

Figure 4.49. The tool setup for field drive test measurements.

The drive test log files are imported and post-processed using MapInfo Pro software [89], and the Rx levels for each technology are evaluated for pre-and-post measurements. Table 4.21 summarizes the results that show the average coverage level in dBm and the delta of Pre vs Post, it indicates that there is no major drawback in signal level in the whole cluster for all technologies.

Table 4.21. The Pre and Post Rx Levels from drive test measurements.

Measurement Layer		G 900 BCCH	U 900 RSCP	L 800 RSRP	L 1800 RSRP	L 2100 RSRP	N 2600 SS-RSRP
Average Rx Level (dBm)	Pre	-68.9	-72.1	-77.6	-82.9	-83.3	-79.2
	Post	-69.3	-71.3	-77.0	-82.0	-82.6	-79.6
	Delta (dB)	0.4	-0.8	-0.6	-0.9	-0.7	0.4

For example, in Figure 4.51 and 4.51, the Rx levels are plotted in the cluster map to display the details of the coverage levels and distribution for L800 and N2600 technologies. The results show the RSRP for L800 almost remains at the same average levels with -77.6 dBm at Pre and -77.0 dBm at Post with -0.6 dB delta, and have the same RSRP accumulated distribution among the cluster area. Also, the same results are obtained for N2600, the SS-RSRP almost remains at the same levels with -79.2 dBm at Pre and -79.6 dBm at Post with 0.4 dB delta. The minor differences in the measurements Pre vs Post are due to the rotation of the antenna directions where some locations have received higher signal levels and some have received lower levels compared to before applying the model depending on the antenna's main beam directions, mainly this due to the constructions in the area (the buildings and houses) as it remains in the same places while the antenna's directions have been changed which affect the signal propagation.

A B C

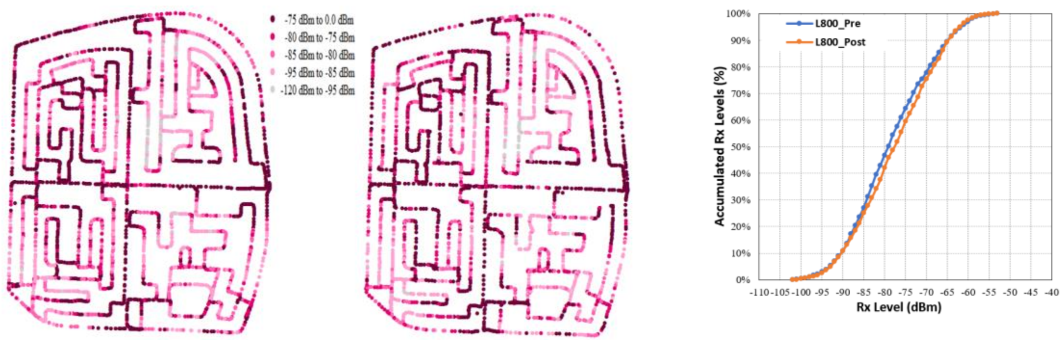

Pre: Average RSRP = -77.6 dBm Post: Average RSRP = -77.0 dBm Accumulated RSRP distribution

Figure 4.50. 4G Rx level: (A) Pre level, (B) Post level, (C) Accumulated RSRP.

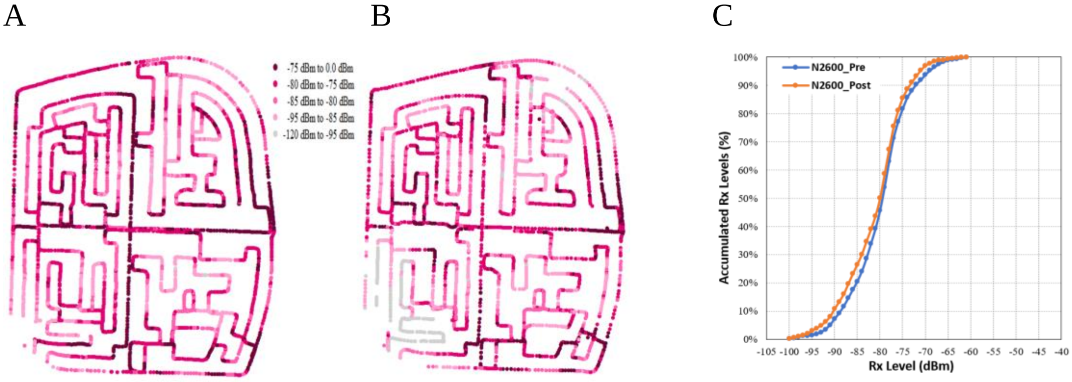

Pre: Average SS-RSRP = -79.2 dBm   Post: Average SS-RSRP = -79.6 dBm   Accumulated SS-RSRP distribution

Figure 4.51. 5G Rx level: (A) Pre level, (B) Post level, (C) Accumulated SS-RSRP.

4.3.2.4. OSS Performance Records

Operation support system for mobile network often uses system row counters and statistics typically refer to a variety of metrics and data records that aid in network performance management and monitoring [88]. In this work, some of OSS key performance indicators (KPIs) are employed to evaluate the behaviour of the cluster under this study before and after applying the antenna azimuth changes which were implemented on the 09th of January 2024. The daily data were recorded for a continuous six weeks, three weeks pre, and three weeks post to the date of the change.

Figure 4.52 shows the total daily carried traffic by the 5G N2600 for the whole cluster (4 sites), and also the system load percentage recorded based on the PRB utilization. The traffic trend shows no significant change after the implementation date where the average traffic was 1.16 TB and became 1.18 TB, and the PRB utilization was 14.4% and became 14.5% with 0.7% increment.

Also, for N2600, Figure 4.53 shows the daily total number of active connected users (simultaneous connection) and the user's throughput, the trend shows a very slight increase in connected users from an average of 295 to 305 users per day. And, there was almost no significant change in the user's throughput which was 78.7 Mbps and became 78.3 Mbps with -0.6% reduction.

Another two important metric performance indicators are collected, the admission call setup success rate (CSSR) and the HO success rate (HOSR), and for both the daily trend remains within the same average values as shown in Figure 4.54 where CSSR was 99.8% during Pre and Post, and the HOSS was 99.0% with slightly decreased to 98.9% with -0.1% reduction.

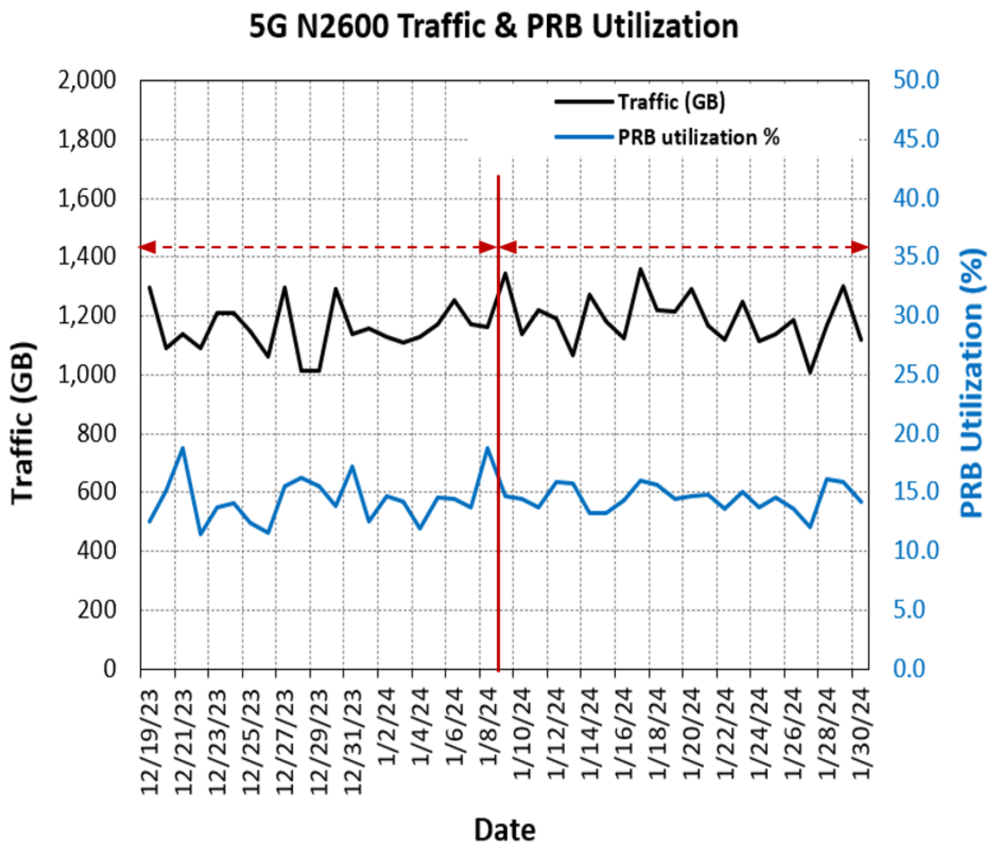

Figure 4.52. The traffic and PRB utilization of 5G N2600.

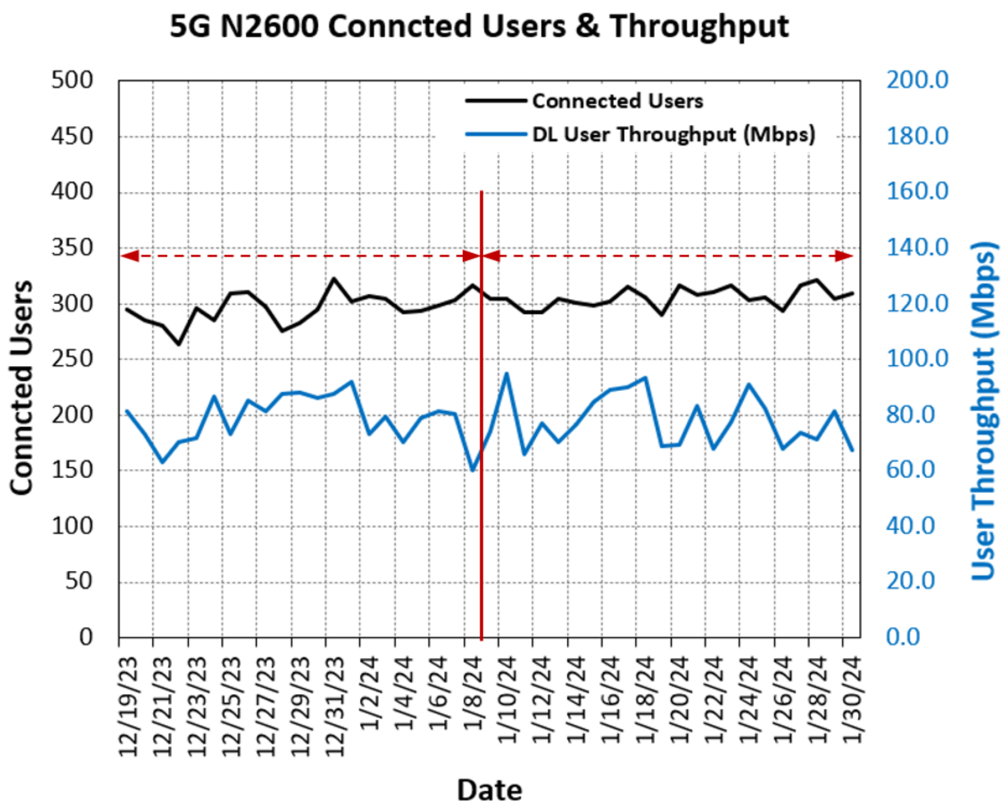

Figure 4.53. The connected users and throughput of 5G N2600.

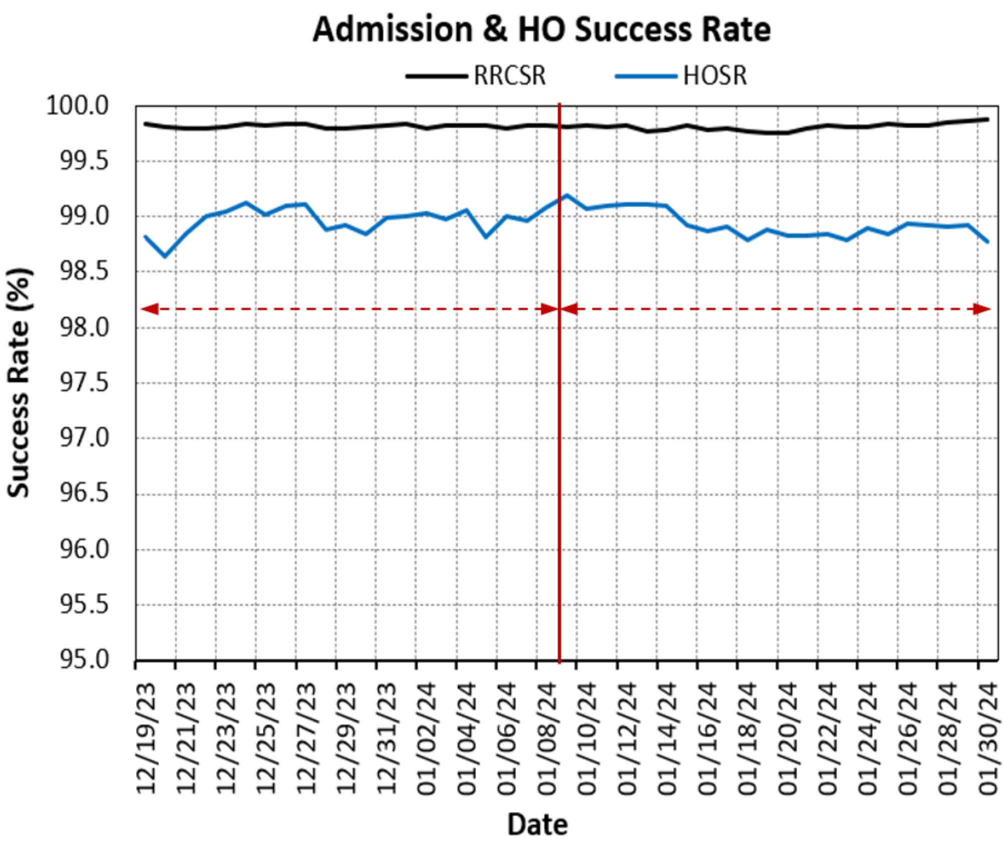

Figure 4.54. The CSSR and HOSC of the 5G N2600.

Very similar behaviour was observed for the 4G technologies from the OSS records which are collected for all LTE cells (including L800, L1800, and L2100) and combined to generate LTE reports for the whole cluster. Figure 4.55 shows the total daily carried traffic by the 4 LTE sites and their PRB utilization. The traffic trend displays no significant effect after the implementation date where the average traffic was 4.71 TB and became 4.72 TB with 0.5% increment, and the PRB utilization was 42.7% and became 42.5% with -0.4% reduction.

Likewise, Figure 4.56 shows the active connected users were 999 and became 1,008 users with a 0.9% increment. The user's throughput was 20.4 Mbps and became 20.3 Mbps with a -0.4% reduction. Also, Figure 4.57 displays that both CSSR and HOSR remain with the same percentages at 99.9% with no changes before and after the implementation date.

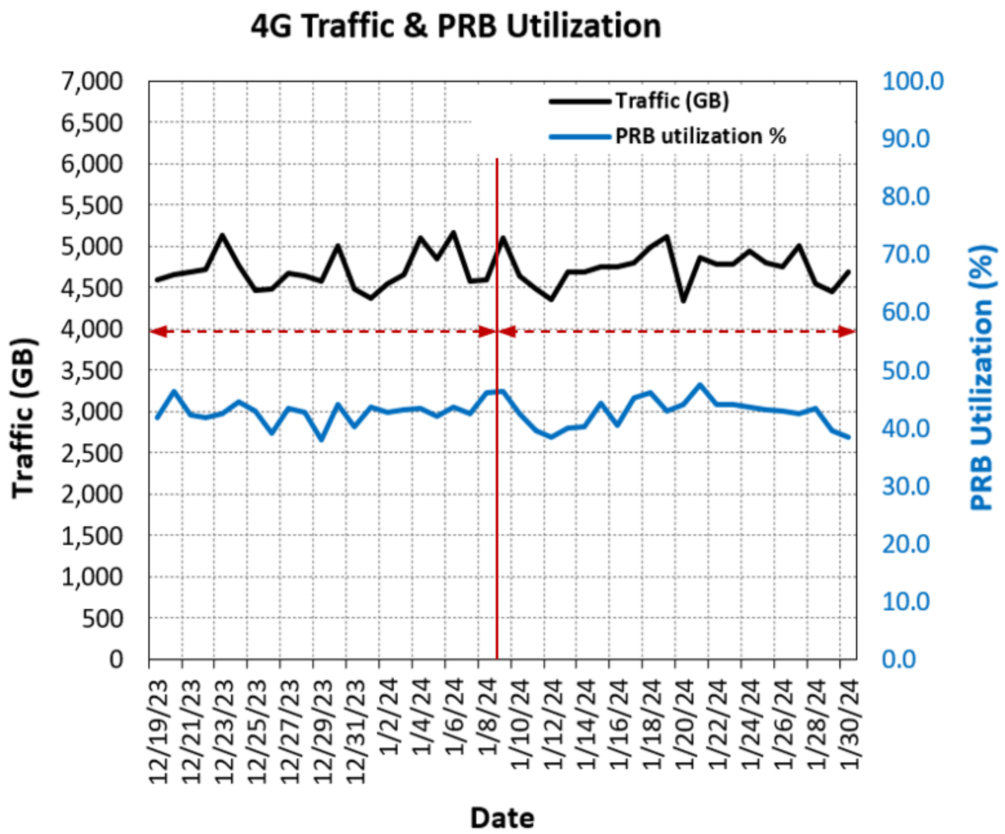

Figure 4.55. The traffic and PRB utilization of 4G LTE.

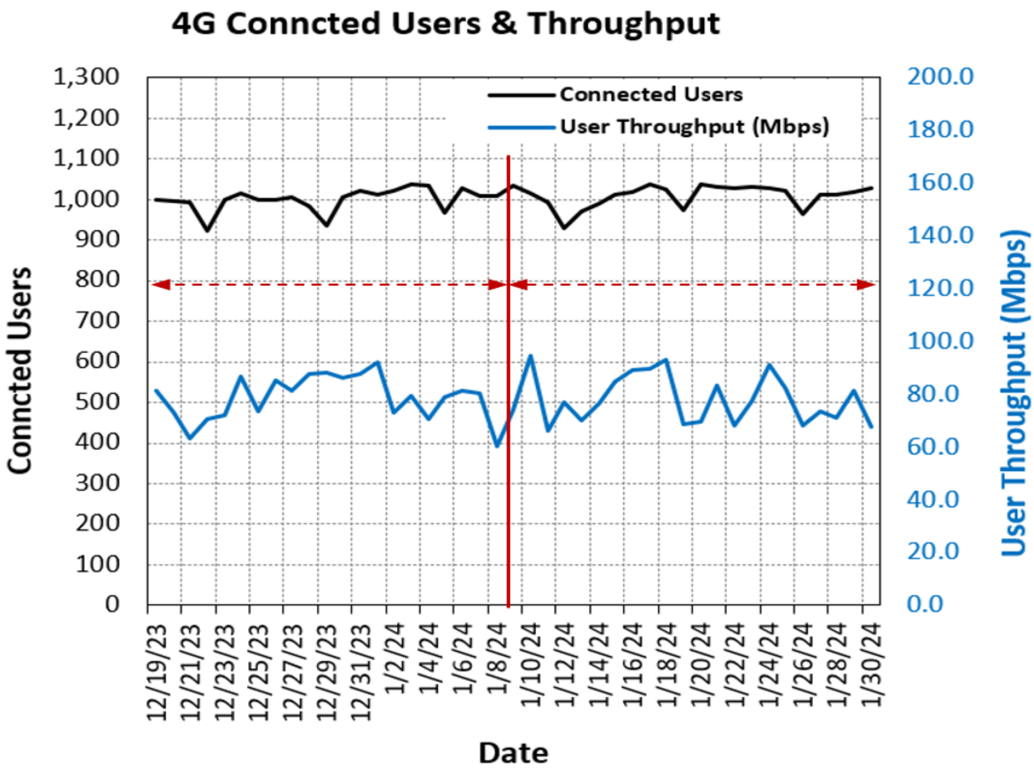

Figure 4.56. The connected users and throughput of 4G LTE.

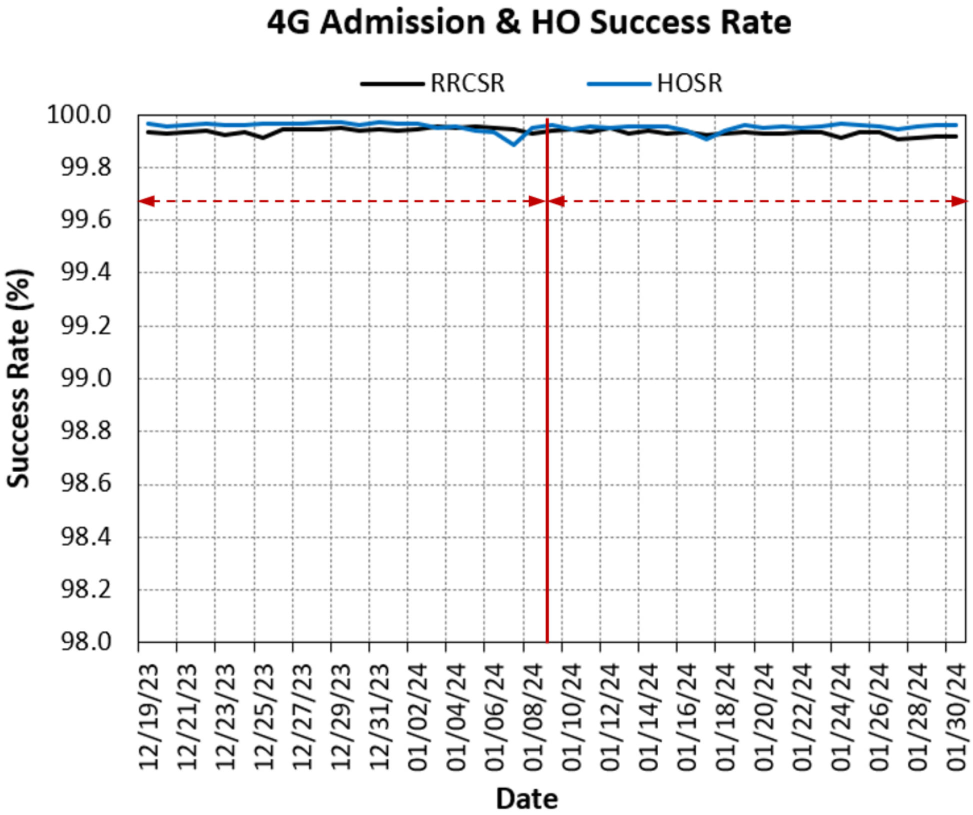

Figure 4.57. The CSSR and HOSC of the 4G LTE.

Although the 2G and 3G technologies are on the way to being switched off, it's still carrying some traffic in this cluster and it's included in the implemented antenna azimuths in this test. Similar to LTE and NR, the OSS records show no major change in 2G and 3G performance.

Figure 6.19 shows the total daily carried traffic by all 3G sites with CSSR and HOSR, the traffic trend displays no significant effect after the implementation date where the average traffic was 276 GB and became 277 GB with a 0.6% increment, and both CSSR and HOSR remains with the same percentages at 99.9%.

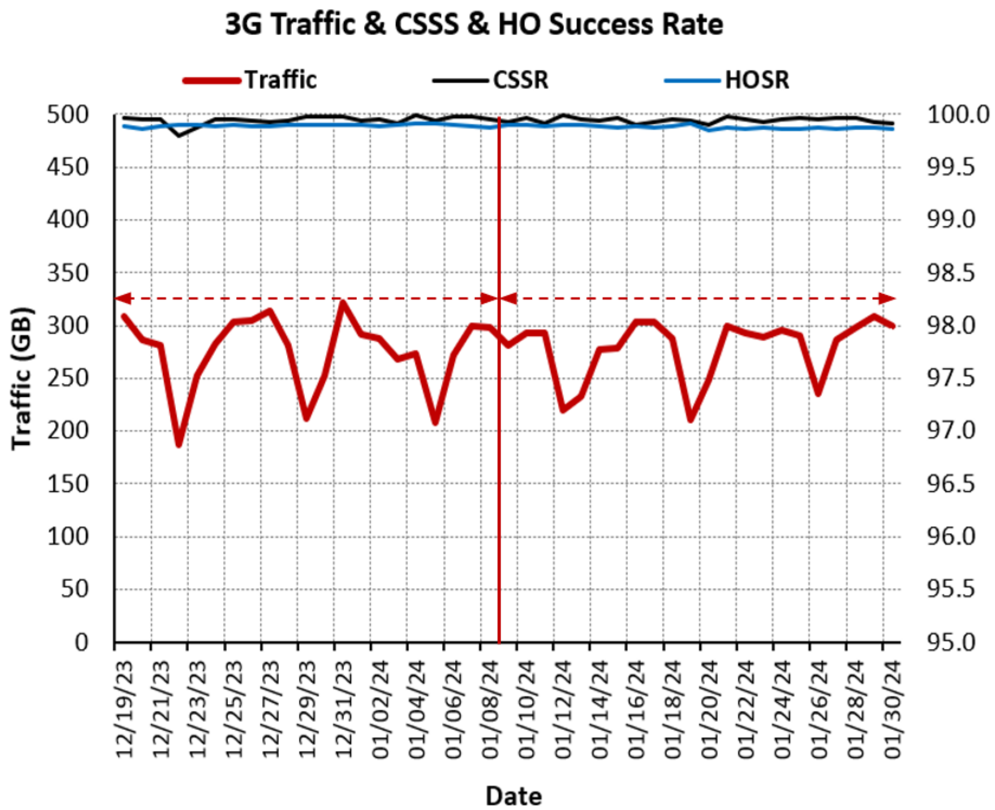

Figure 4.58. Traffic, CSSR, and HOSC for 3G UMTS.

Finally, for all 2G sites, Figure 6.20 shows the CSSR and HSSR trends with no major changes, and both remain with the same percentages at 99.9%.

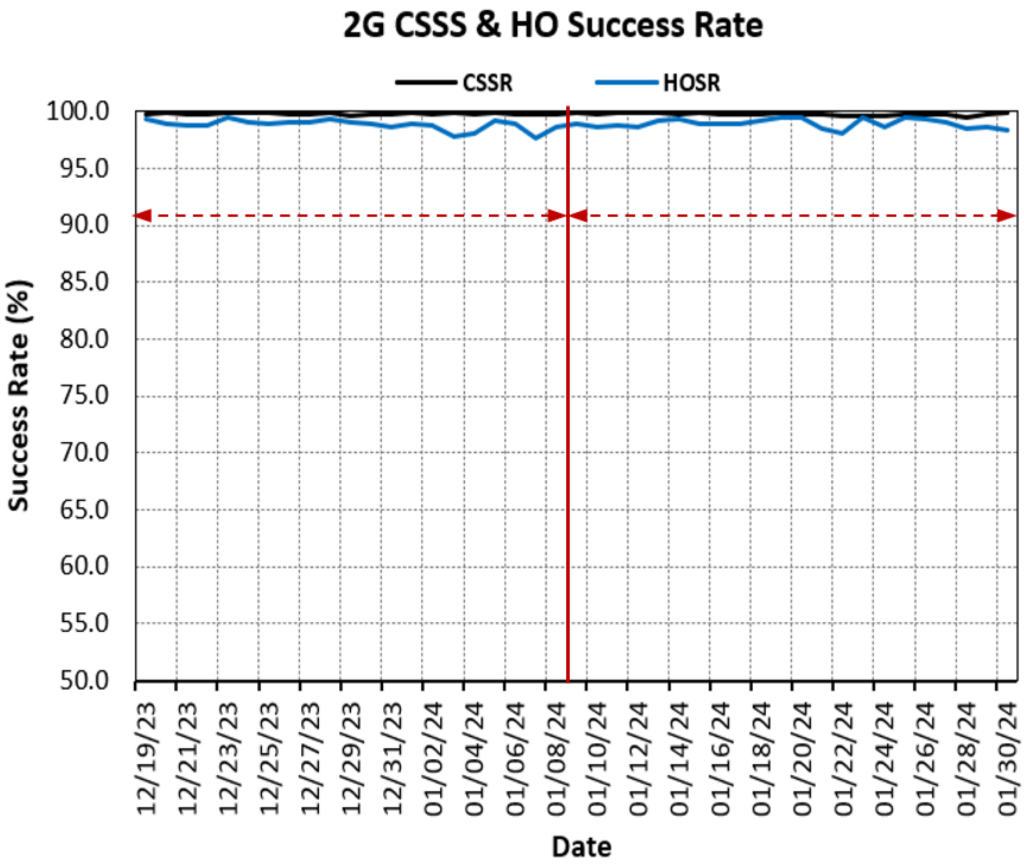

Figure 4.59. The CSSR and HOSR for 2G GSM.

4.3.3. Applications of the Proposed Reduction Solution

Reducing the TRE is the goal of the suggested method, and doing so will inevitably shorten compliance distances. On the other hand, neither the site performance nor the site coverage levels are impacted by the suggested approach.

Nearly all national regulators require that the compliance borders be exclusive, inaccessible areas for the general public and shall be marked with warning signs or other obstacles to keep people out. To implement the compliance requirement, it is necessary to determine the compliance distances. The easier it is for mobile operators to meet the standards, the lower the compliance limits. The authors see these requirements can be assessed in the design phase before implementation, and small adjustments to the antenna orientations can be made using the proposed model to shorten the compliance distances for the necessary cases, particularly for wall-mounted and rooftop sites where the antennas usually will be placed in close proximity to accessible areas.

Also, the mobile operators continue expanding their networks by adding and deploying new technologies such as the 5G NR into the existing on-air sites following the current sector's direction, this approach increases the total exposure ratio and consequently extends the compliance boundaries. For some sites, extending the compliance boundaries to bigger ranges might reach accessible areas specifically for some rooftop and wall-mounted sites. in these kinds of situations, the authors believe that the proposed solution is advantageous and can assist in reducing the compliance distances without affecting network performance or coverage.

4.3.4. Results Summary of the Exposure Reduction

A design model to de-concentrate and reduce the overall exposure ratio from sectorized antennas of the multi-technology base station was proposed in this study. The model uses the weighted antenna's azimuth to spread the total exposure by horizontally separating the installed antennas in the same sector. A set of simulations is carried out to calculate the reduction in total exposure for widely commonly used antenna deployment setups in multi-technology mobile networks. For three-sectors BS operating with six technologies, the simulation results show the compliance distance is reduced by -23% when using two antennas (two different azimuths) compared to using one azimuth, reduced by -35.9% using 3 azimuths, -39.8% using 4 azimuths, -41.3% using 5 azimuths, and by -43.4% when using 6 azimuths. A field test is done in a life network serving in a geographical cluster that consists of 4 sites, the results show that the TER is reduced by -19.23% after the antennas azimuths are changed with separation angles calculated using the proposed model. Further, the OSS system performance records and counters were analysed to evaluate the impact of the model on the network coverage and capacity. Overall, the system records show no significant impacts were registered on network coverage level and capacity performance for all transmitting technologies of the sites involved in the test. The proposed solution is beneficial and can help mobile operators minimize the compliance boundaries without impacting the network coverage and performance especially for rooftop and wall-mounted sites where the antennas are installed in close areas accessible to the general public.

4.4. Far Field Exposure Assessement Results

4.4.1. Assessment Process

A set of related activities are performed according to the process flow as shown in Figure 4.60. Field measurements were collected for selected sites, and the results were used to calibrate the simulation tool propagation model to achieve higher accuracy by fine-tuning the propagation model parameters and correction factor, both of which depend on the environment type. The simulation was performed to predict the Rx signal levels of each technology for selected sites. Using the predicted Rx level results for each technology (2G, 3G, 4G, IoT, and 5G), the exposure level emitted from each technology is calculated in terms of power densities, which are used as input to calculate the total exposure ratio (TER) and to analyze its related characteristics and behavior for different scenarios.

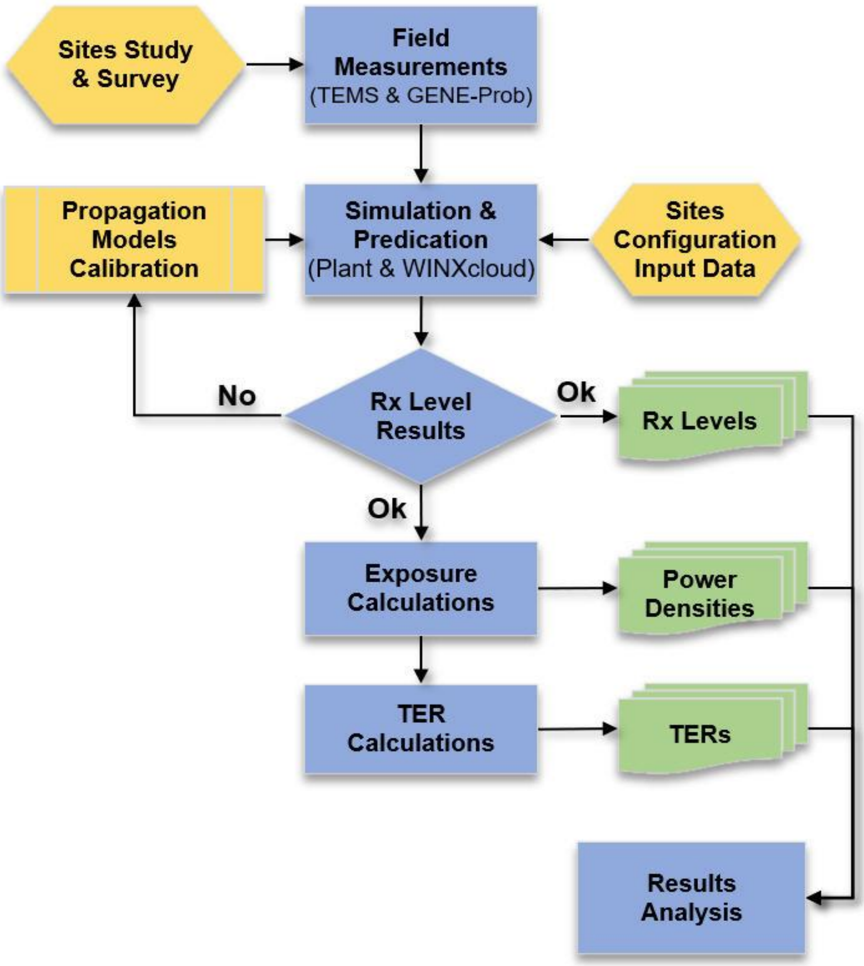

Figure 4.60. The process used for EMF exposure assessment.

4.4.2. In-Situ Description

Real network sites belonging to one operator in the Kingdom of Saudi Arabia (KSA) are used in this study, and all sites include multi-technology 2G/3G/4G/IoT/5G coexisting in the same site tower, and all are on-air in service at the same time. The used site configurations and related data are typical for the current operating network that provides actual results based on the actual setup, and this was our main purpose for using live network data. Of course, other networks might have different settings, which may lead to different results. To enrich this study, four sites were selected to represent four assessment scenarios. Site-1 is located in a dense area in the downtown of Dammam city in the eastern region, this site services dense commercial and residential areas. The antennas of all technologies are installed on the building rooftop at 20 m height from ground level. Figure 4.61. shows the site location on the Google Earth map, and Table 4.22 shows the site data and operating configurations.

Figure 4.61. The geographical location of Site-1 in the dense area.

Site-2 is located in an urban area in Khubar city in the eastern region. This site services mainly residential areas with some commercial area near the Arbian Gulf coast, and the antennas of all technologies are installed on the building rooftop at 25 m height from ground level. Figure 4.62 shows the site location on the Google Earth map, and Table 4.22 shows the site data and operating configurations.

Figure 4.62. The geographical location of Site-2 in the urban area.

Site-3 is located in a suburban area in Dhahran city (in eastern region, Kingdom of Saudi Arabia), which is a purely residential area. The antennas of all technologies were installed on the greenfield monopole tower at a height of 30 m from the ground level. Figure 4.63 shows the site location on the Google Earth map, and Table 4.22 shows the site data and operating configurations.

Figure 4.63. The geographical location of Site-3 in the suburban area.

Site 4 is located in a rural area on the highway to Dammam International Airport, which is located 30 km from Dammam city. This site services highway roads and is under the construction of new residential areas. The antennas of all technologies were installed on the greenfield tower at a 60 m height from the ground level. Figure 4.64 shows the site location on the Google Earth map, and Table 4.22 shows the site data and operating configurations.

Figure 4.64. The geographical location of Site-4 in the rural area.

4.4.3. Site Configurations Setup

In this study, the same configurations and setups were used for the four sites, including Tx/Rx hardware, equipment types, antenna gain, bandwidth, frequency ranges, and transmitting power. Except for the antenna heights, the antennas were installed at different heights in each scenario. These are the actual on-air operating configurations, and this was intentionally considered in this study to evaluate the radiation emissions based on actual scenarios. At each site, 3-sector BTS is installed per technology, and antenna azimuths were horizontally directed with a 120-degree spacing between every two sectors (each sector cover 120 degree).

At the four sites, the 2G GSM 900 MHz and 3G UMTS 900MHz were transmitted from the same radio remote unit (RRU) that was connected to the crossed-polarized antenna by a coaxial feeder. The RRU is connected down through the common public radio interface (CPRI) front-backhaul to the base-band unit (BBU) that handles and controls radio processing, as illustrated in Figure 3.6. The RRU power was spilled between the GSM and UMTS, and the final configuration setup is shown in Table 3.1.

Table 4.22. Configuration Setup of the Selected Sites

Site Setting	2G G900	3G U900	4G L800	4G L1800	4G L2100	5G NR2600
Freq. Band (MHz)	900	900	800	1800	2100	2600
Freq. BW (MHz)	400	4.2	10	10	20	60
Number of Tx	2T	1T	2T	2T	4T	64T
Number of Rx	2R	2R	2R	4R	4R	64R
Total Power (Watt)	40	40	80	40	40	96
System Utilization	95%	95%	95%	95%	95%	95%
Ant. Gain (dBi)	17	17	16.7	16.6	17	24.8
Horizontal BW	60º	60º	65º	65º	65º	65º
Vertical BW	7.5º	7.5º	7.8º	6º	6º	6.5º
Ant. Tilt Angle	-6º	-6º	-6º	-6º	-6º	-6º
Ant. Height. Dense	20 m	20 m	20 m	20 m	20 m	20 m
Ant. Height. Urban	25 m	25 m	25 m	25 m	25 m	25 m
Ant. Height. Sub-Urban	30 m	30 m	30 m	30 m	30 m	30 m
Ant. Height. Rural	60 m	60 m	60 m	60 m	60 m	60 m

Similar to the 4G LTE 1800 MHz 2100MHz, both were transmitted from the same RRU, which was also connected to the crossed polarized antenna by a coaxial feeder, and the RRU power was spilled between both. The 4G LTE 800 MHz was installed in a separate RRU connected to a separate antenna.

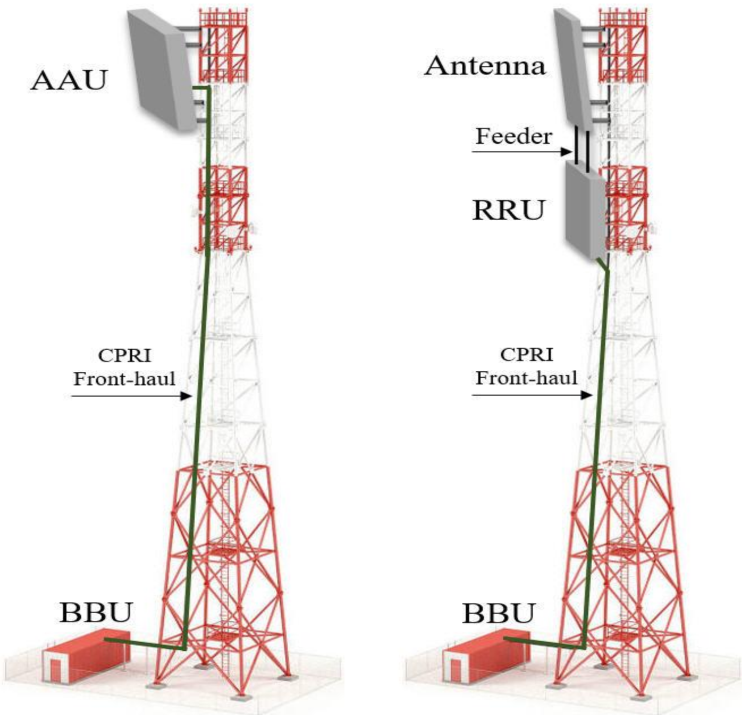

Figure 3.6. Connectivity setup of RRU used for 2G/3G/4G and the AAU used for 5G.

The 5G NR 2.6 GHz were transmitted from the massive-MIMO 64T/64R active antenna unit (AAU), which is a physical hardware unit consisting of an integrated radio unit with anantenna. Most technology vendors designed the AAU as a compact practical solution instead of using a large number of antennas, such as the 64 antennas required to transmit the 64T/64R massive-MIMO.

4.4.4. NB-IOT Configuration

The narrow band IoT (NB-IoT) allows access to network services via LTE [31] with a bandwidth-limited channel to a maximum of 200 kHz [32]. The investigated sites in this study transmitted NB-IoT at 800 MHz with a one-channel 180 kHz bandwidth that consists of 12 subcarriers each at 15 kHz and has the same LTE frame structure as one radio physical resource block (PRB). The NB-IoT is transmitted from the same 2T/2R RRU hardware used by the 4G FDD LTE 800 MHz (Frequency Division Duplexing) and connected to one antenna with a 17.6 dBi gain. The total power (80 W) of this IoT/FDD RRU is equally distributed over a total of 50 PRBs (one PRB for IoT, and 49 PRBs for FDD).

4.4.5. Field Measurements

Field measurements were conducted using two types of drive test tools in different fixed locations around the four selected sites. The first tool is the Test of Mobile System (TEMS®) Investigation v20 [33], and the second tool is the Huawei GENE-Prob-5. Both tools have software installed on a laptop PC and connected to three mobile user equipment (UE) and GPS antenna (Global Positioning System), and all were mounted inside a car in front of the dashboard at 1.3-1.5 m height, as shown in Figure 4.65. The tool collects the Rx signal levels from the 3 UEs for one technology at the same time (average results from 3 UEs are used later as input to calibrate the simulation tool). The measurements are recorded in log files with related time and GPS coordinates, and the measured samples were collected every 0.5 s for each UE with more than 2,500 measurement samples for each technology at each fixed location. The measurements were collected in fixed places located at different distances and covered the coverage area of the site. The collected measurement for 2G GSM900 includes the Rx level in dBm of the broadcast common control channel (BCCH), and for 3G UMTS900 includes the received signal code power (RSCP) levels in dBm. The 4G FDD LTE includes the reference signal received power

(RSRP) levels in dBm. 5G includes Secondary Synchronization Reference Signal Received Power (SS-RSRP) levels in dBm.

Figure 4.65. Photo of the car drive test tool used for field measurements.

3. 3. Results and Discussion

3. 3. A. Measurement Results and Simulation Calibration

The measurement data from the drive test (Rx Levels in dBm at different locations from the sites) were used to calibrate the simulation tool input [44], including the propagation model setup as described in section 3.4. The final simulated Rx-Level results for all technologies were compared with the measurement data though point-to-point comparison, and the measurements were found to be lower than the simulated results for all technologies, as shown in Figure 4.66. For example, in 5G NR at 2600 MHz, the average measured SS-RSRP is -78.4 dBm, and the simulated SS-RSRP is -71.6 dBm.

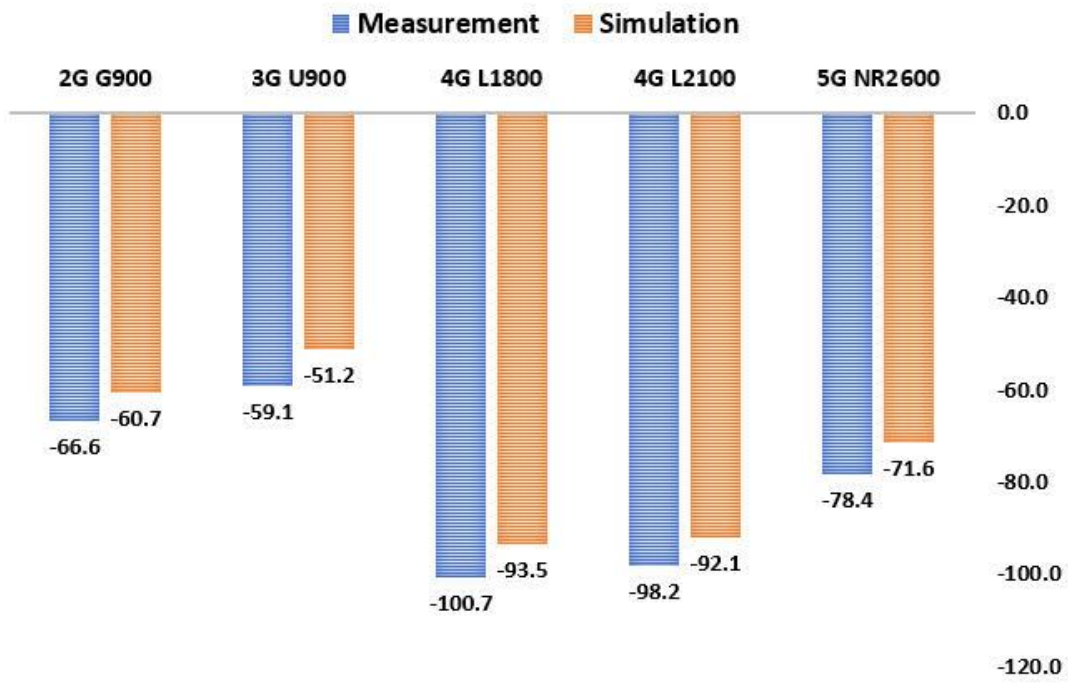

Figure 4.66. Measurement vs. simulation for Rx signal levels.

The difference between the measured and simulated values of the final calibrated tool was calculated in terms of the mean error in dB, which reflects the signal loss due to in-car penetration. Table 4.23 shows the mean error for each technology, which indicates that the lowest mean error is 6.0 dB for 2G GSM 900 MHz, and the highest is 7.2 for 4G LTE 1800 MHz. These results closely match and are in line with the results published in [45, 46].

Table 4.23. Mean Error between Measured and Simulated Signal Levels

Average Signal Level	2G G900	3G U900	4G L1800	4G L2100	5G NR2600
Measurement (dBm)	-66.6	-59.1	-100.7	-98.2	-78.4
Simulation (dBm)	-60.7	-51.2	-93.5	-92.1	-71.6
Mean Error (dB)	6.0	7.9	7.2	6.1	6.8

4.4.6. Rx Signal Level Prediction Results

The COST231-Hata propagation model of Equation (3.24) is used in the simulation to predict the RX level for the 2G GSM and 3G UMTS at 900 MHz. In addition, the UMa-4G propagation model of Equations (3.24 and 3.25) is used to predict the 4G LTE FDD (800, 1800, and 2100 MHz) RSRP level, and the UMa-5G propagation model of Equations (3.27 – 3.29) is used to predict the 5G NR (2.6 and 3.7 GHz) SS-RSRP levels. The calculations were performed for the 4 sites that represent dense-urban, urban, suburban, and rural cases. As an example, Figure 4.67 shows the RSRP level in dBm distribution for 5G NR at 2.6 GHz for the suburban area within a 1.5 km radius from the site.

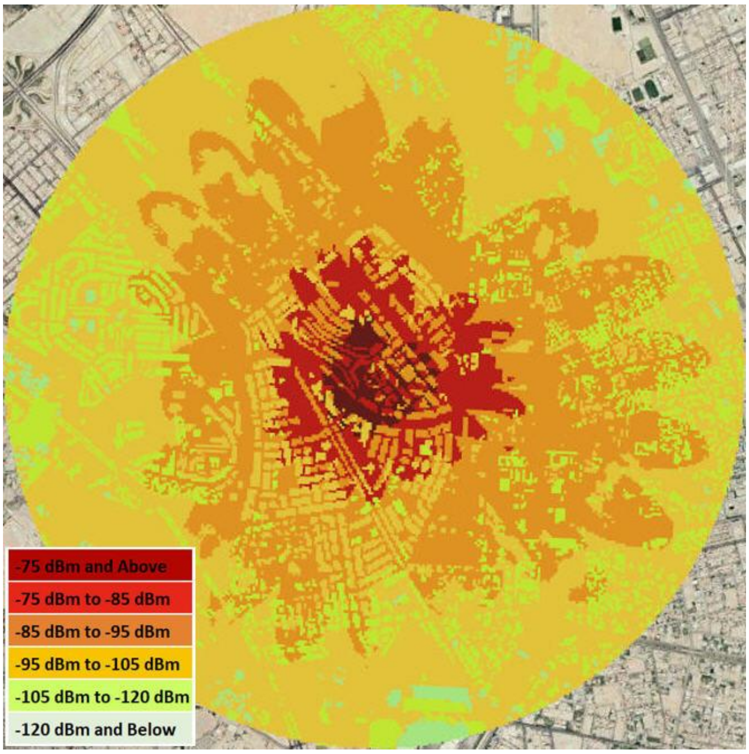

Figure 4.67. Site-1 (suburban area) simulated Rx RSRP (dBm) for 5G NR 2600 MHz.

The mentioned TX power in Table 3.3 is the total power in watt for all transmitters in each technology, for example the 2G G900 has 2 TRXs with a total power of 40 watts (each TRX transmit 20 watts). So, the actual used 5G EIRP (Equivalent isotropic radiated power) is 56.6 dBm which is the lowest one and 3G U900 has the highest EIRP (63 dBm. The simulation results of the predicted Rx signal levels were exported and processed to obtain the maximum levels at each 10 m distance step from the site (aggregated for all directions) up to a 1.5-km radius from the site. Figure 4.68 shows the Rx level for all technologies (dBm) for the site in the dense area scenario with the highest strength levels registered from 2G GSM and 3G UMT at 900 MHz and the lowest strength levels recorded from 4G FDD LTE at 1800/2100 MHz.

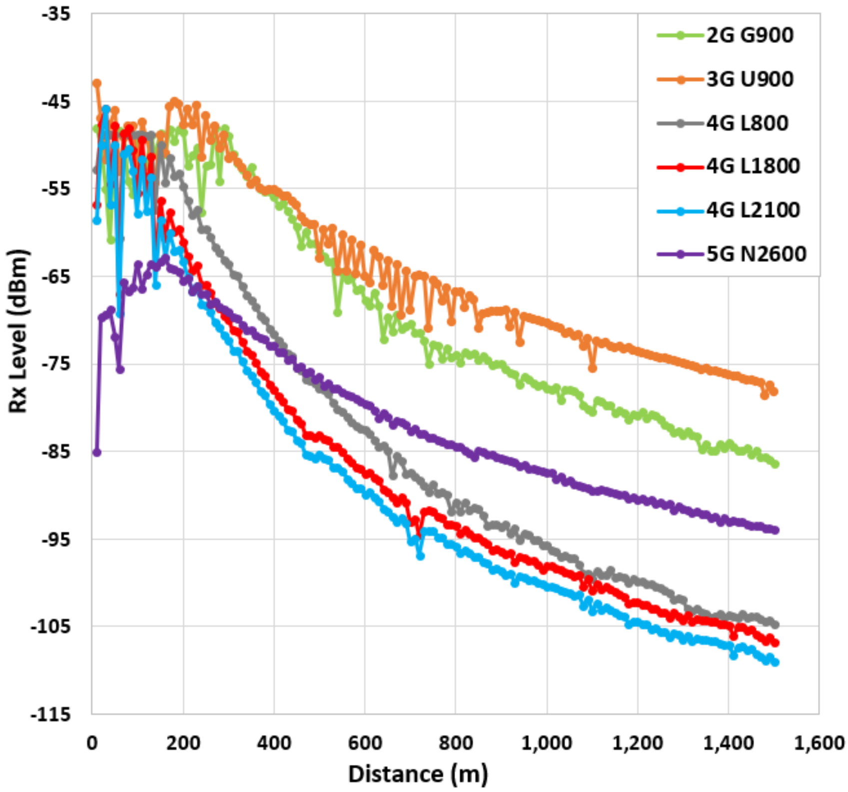

Figure 4.68. Site-1 (dense area) simulated Rx level (dBm) for all technologies.

The 5G NR 2.6 GHz results show that signal levels are low in the areas close to the site at a distance of less than 200 m, and the highest signal levels are registered after approximately 200 m. Then, Rx starts to degrade as the distance increases. For distances farther than 200 meters, AAU massive MIMO with beamforming shows good performance in the Rx signal degradation trend compared to 2G/3G/4G, which has a higher signal degradation rate. The simulation results and behaviors were similar for the urban and suburban sites, as shown in Figures 4.69 and 4.70. For the rural area site, the Rx levels were calculated for the entire coverage area of up to 6 km, as shown in Figure 4.71. The Rx signal degradation trend with increasing distance was found to be similar to the behavior of dense, urban, and suburban sites.

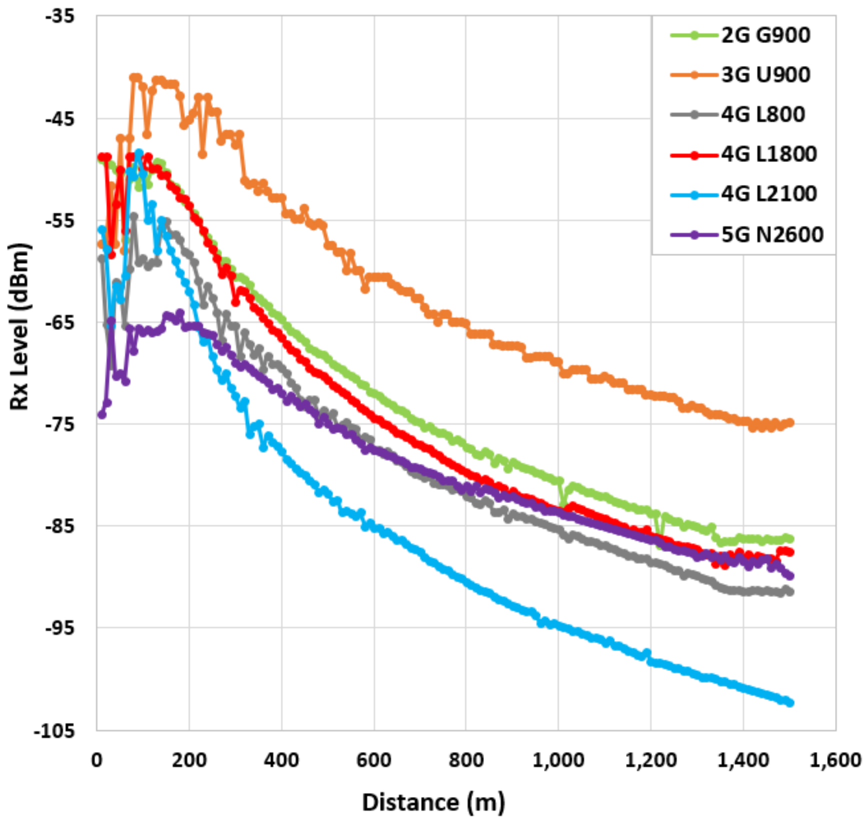

Figure 4.69. Site-2 (urban area) simulated Rx level (dBm) for all technologies.

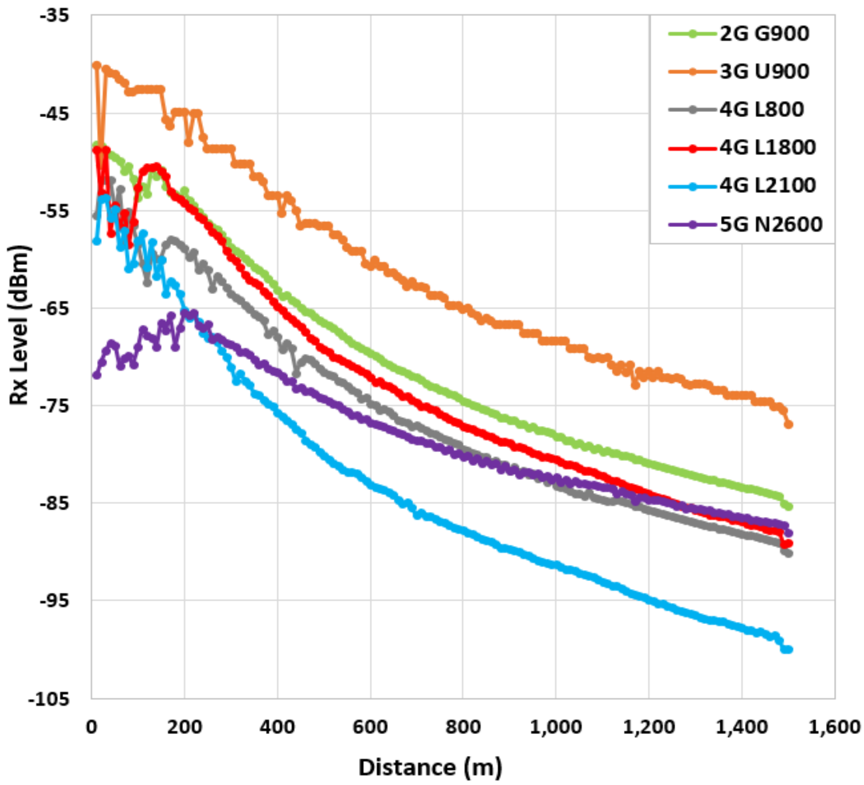

Figure 4.70. Site-3 (suburban area) simulated the Rx level (dBm) for all technologies.

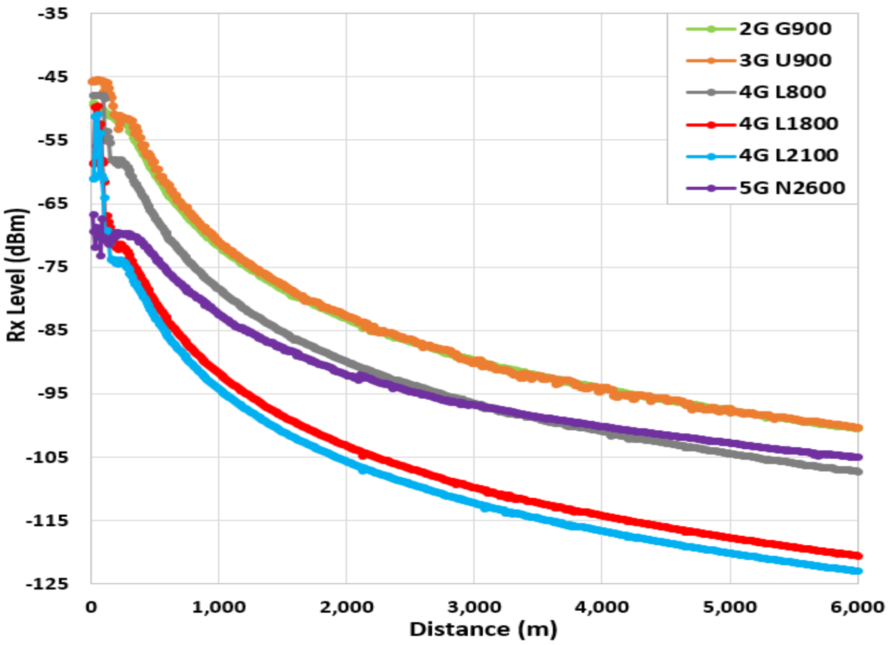

Figure 4.71. Site-4 (rural area 6 km) simulated the Rx level (dBm) for all technologies.

The used EIRPs are reflected in the results of Rx level simulation, for example in the dense area site, the RX signal level results show 2G 900 and 3G 900 have higher EIRP compared to 5G 2600 and 4G L800/L1800/L2100. But, the 5G that has massive MIMO with beamforming shows good performance in the Rx signal degradation trend compared to 2G/3G/4G, which has a higher signal degradation rate.

4.4.7. Power Density Results

The total power densities were calculated at each point around the site and for all technologies of technology. The predicted Rx levels of the simulation results were used as inputs for the power density calculations considering each technology configuration setup, as listed in Table 3.22. The 800 MHz results include the combined power density for both 4G-FDD-LTE and NB-IoT. For the four scenarios (dense, urban, suburban, and rural), the obtained results show that the power densities from all technologies (2G/3G/4G/5G) are low compared to the reference limit, which is consistent with the results of previously published studies [18, 23, 35, 41, 47-51] related to this work.

For the dense area site, as shown in Figure 4.72. the total power densities trend with increasing distance from the site. The evaluation of each technology shows that the whole average S_{inc} (power density) is recorded as the highest at 35.1 µW/m^2 for 5G, which is 0.0000351% from the ICNIRP reference level of 10 w/m^2, and this is only for 5G at 2.6 GHz technology but accumulation with other technologies is calculated using TER. Then, 15.4/8.5 µW/m^2 are recorded for 4G L2100/L1800, 5.2/4.4 µW/m^2 for 2G/3G 900, and 2.4 µW/m^2 for IoT/L800, as shown in Figure 4.73.

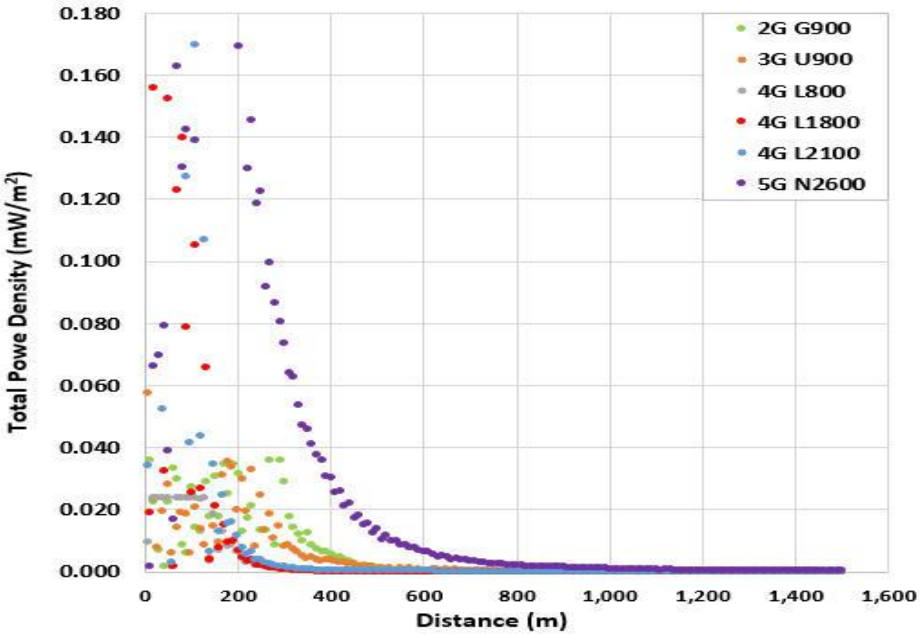

Figure 4.72. Site-1 (dense area) simulated the total power density per technology.

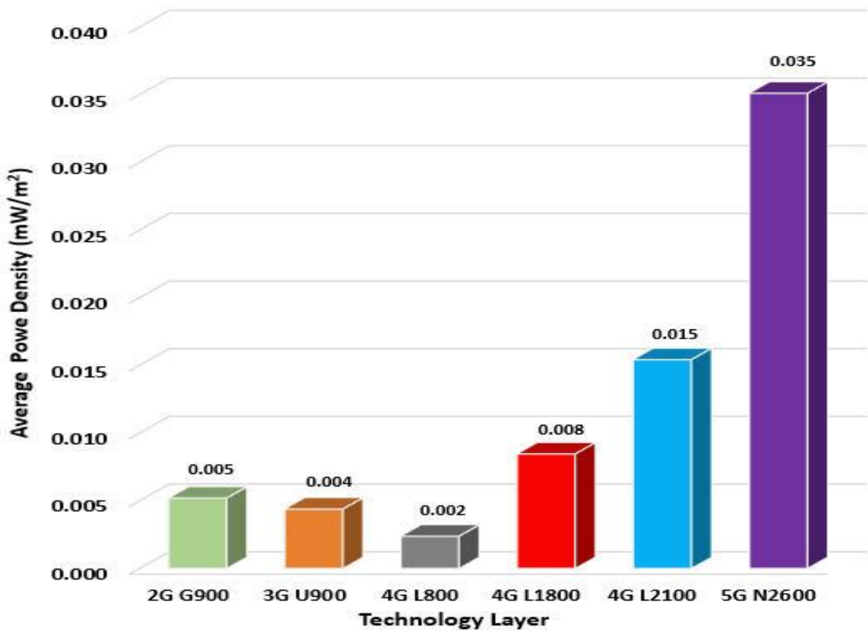

Figure 4.73. Site-1 (dense area) the simulated exposure ratios for all technologies.

For the urban area site, Figure 4.74. shows the total S_{inc} trend with increasing distance, and the evaluation results show that the highest average S_{inc} recorded value is 36.1 μW/m^2 for 5G, 12.0/11.0 μW/m^2 for 4G L1800/L2100, and 9.5/3.0 μW/m^2 for 3G/2G 900, and the lowest S_{inc} is 0.5 μW/m^2 for IoT/L800, as shown in Figure 4.75.

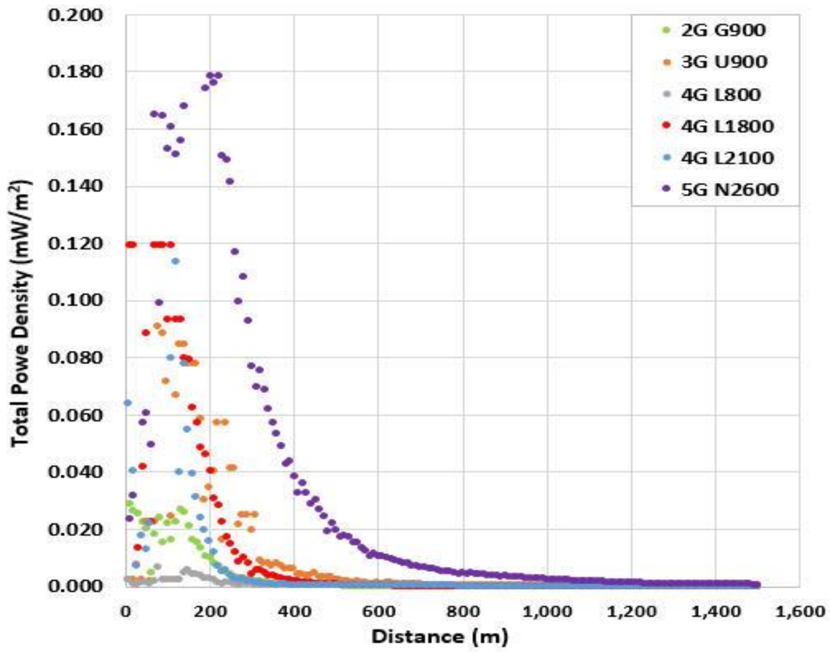

Figure 4.74. Site-2 (urban area) simulated the total power density per technology.

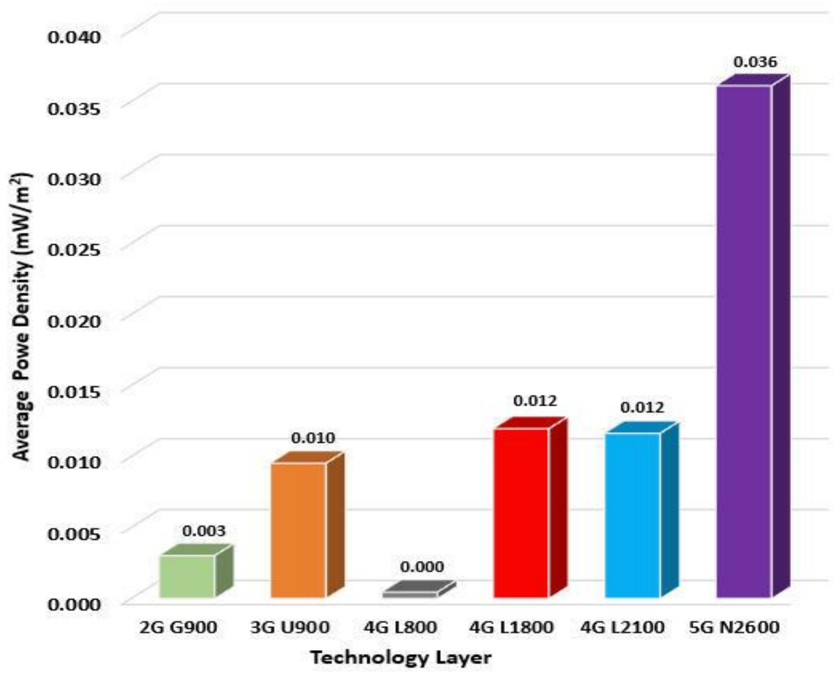

Figure 4.75. Site-2 (urban area) the simulated exposure ratios for all technologies.

For the suburban area site, Figure 4.76. shows the total S_{inc} trend with increasing distance, and the evaluation results show that the highest average S_{inc} recorded value is 29 µW/m^2 for 5G, 9.0/5.5 µW/m^2 for 4G L1800/L2100, and 10.4/3.1 µW/m^2 for 3G/2G 900, and the lowest S_{inc} is 0.8 µW/m^2 for IoT/L800, as shown in Figure 4.77.

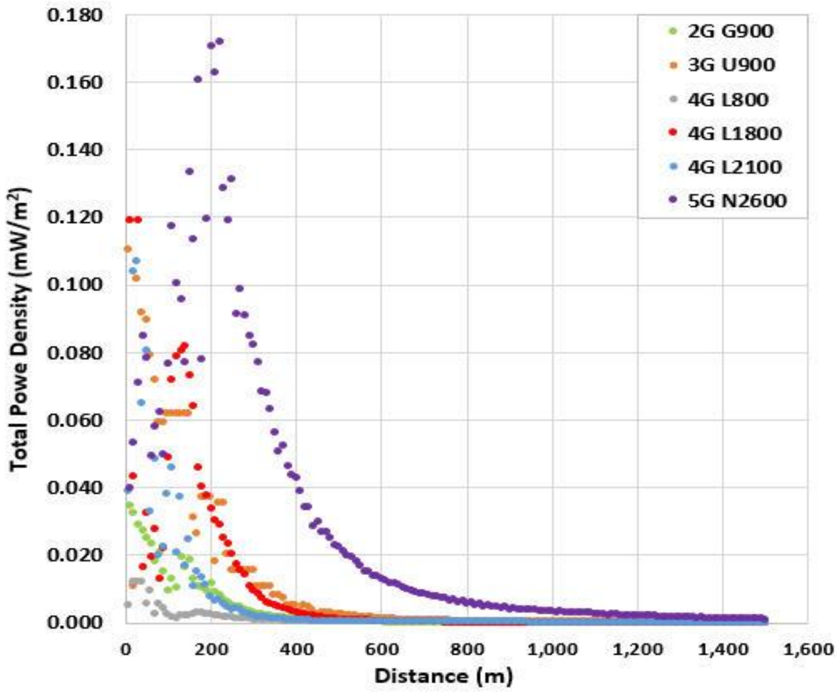

Figure 4.76. Site-3 (suburban area) simulated the total power density per technology.

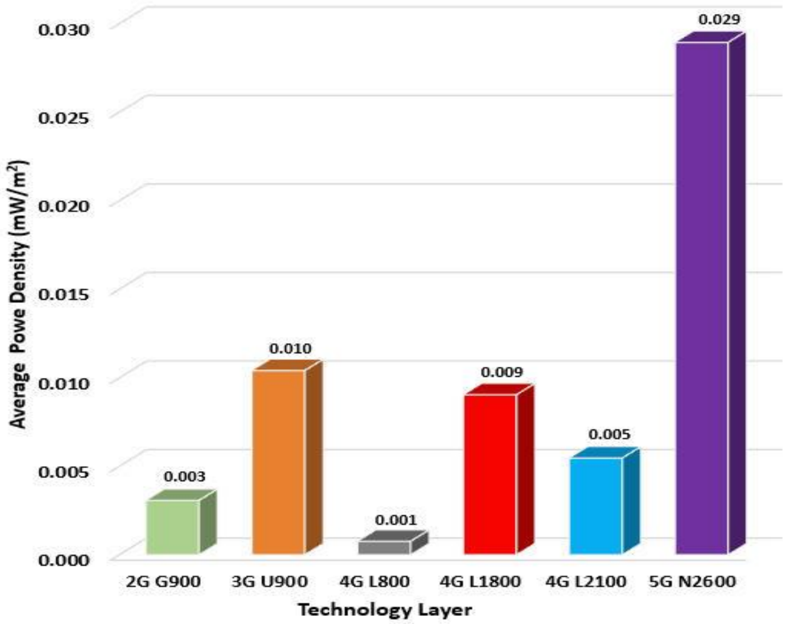

Figure 4.77. Site-3 (suburban area) the simulated exposure ratios for all technologies.

For the rural area site, the calculated S_{inc} is evaluated for two zones, within 1.5 km (Figure 4.78) and up to 6 km (Figure 4.79), and the evaluation results for 1.5 km show that the highest average S_{inc} recorded value is 22.6 µW/m^2 for 5G, then 4.6/2.5 µW/m^2 for 4G L2100/L1800, and 4.6/4.4 µW/m^2 for 2G/3G 900, and the lowest S_{inc} is 2.5 µW/m^2 for IoT/L800. The evaluation results for 6 km show that the highest average S_{inc} is 5.7 mW/m^2 for 5G, then 1.13/0.61 µW/m^2 for 4G L2100/L1800, and 1.14/1.08 µW/m^2 for 2G/3G 900, and the lowest S_{inc} is 0.63 µW/m^2 for IoT/L800 as shown in Figure 4.80.

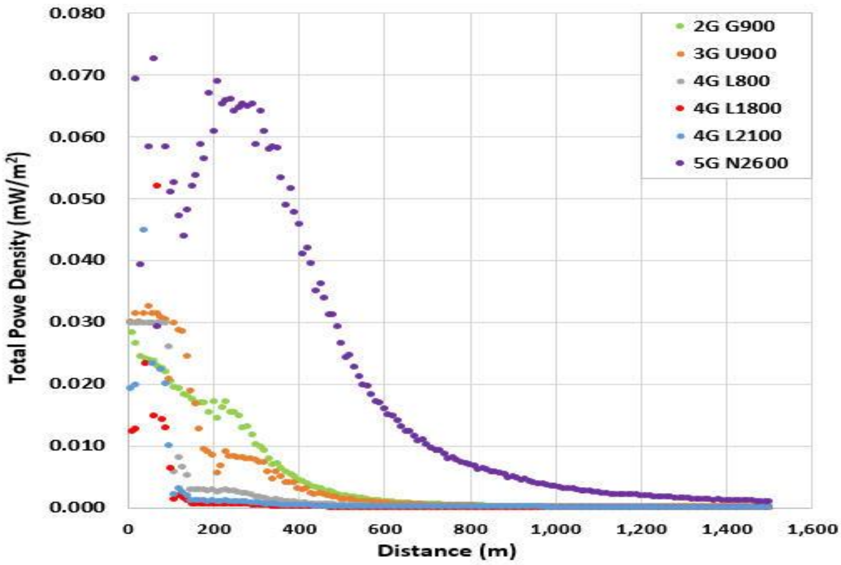

Figure 4.78. Site-4 (rural area) simulated total power density at 1.5 km.

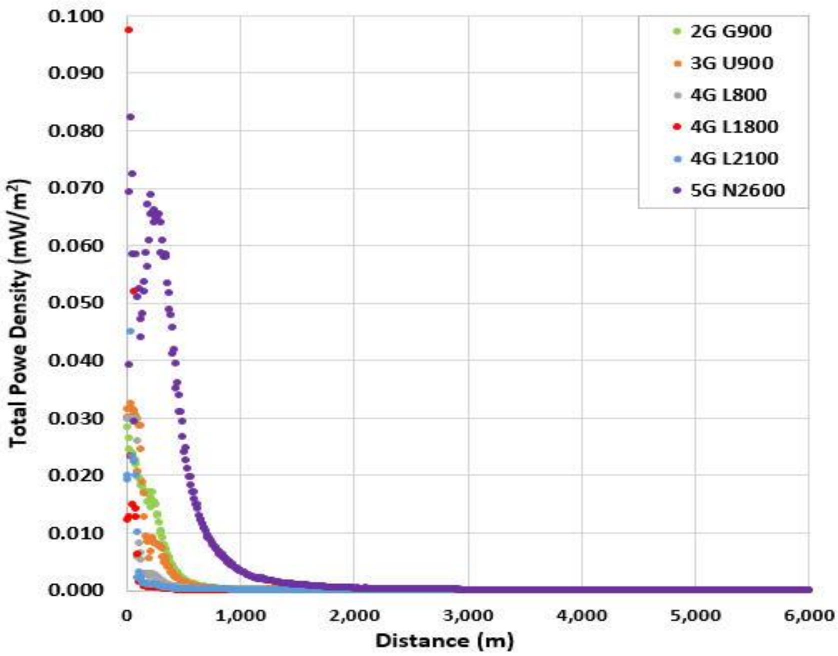

Figure 4.79. Site-4 (rural area) simulated total power density at 6 km.

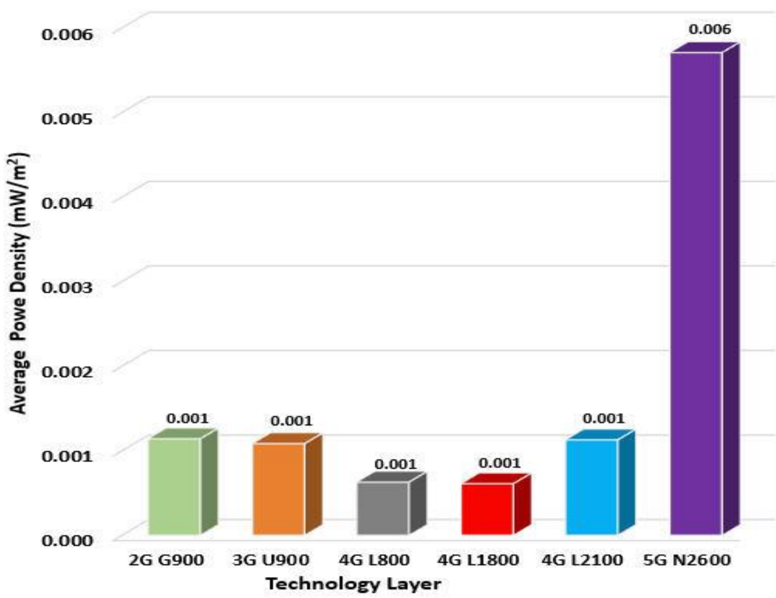

Figure 4.80. Site 4 (rural area) the simulated exposure ratios for all technologies.

4.4.8. Exposure Ratio and TER Results

The accumulated TER was calculated for the four scenarios, and the simulated power density S_{inc} results with reference standard limits. The obtained results show that the maximum TER is very low compared to the ICNIRP limit, specifically it is 10.5×10^{-5} for the dense area, 8.8×10^{-5} for the urban area site, 6.2×10^{-5} for the suburban area, and 5.6×10^{-5} for the rural area. These results are in agreement with the studies published in [18, 23, 35, 41, 47-51]. Of note, these studies were focused on assessment for one technology, and in this work, the results present the accumulated TER.

Furthermore, the TER is analyzed to evaluate the contribution of each technology, which addresses and provides indications about forecast radiation increases for future incoming technologies and expansions. Therefore, we added a second technology of 5G NR at a frequency of 3.7 GHz, which is expected to be deployed at the same sites, including 64T/64R AAU with 180 watts, 100 MHz bandwidth, and the same antenna heights as other technologies. The analysis of results for the dense area shows that TER is very low compared to the ICNIRP, with the highest being 0.0114% from the maximum limit. TER distribution Figure 4.81 shows that the addition of the first technology of 5G NR2600 (co-location with exiting 2G/3G/4G) raises the TER by 68% and the addition of the second technology of 5G NR 3700 raises the TER by 27%, so the total increase due to 5G technologies is 114%, which makes the 5G contribution to TER approximately 53%.

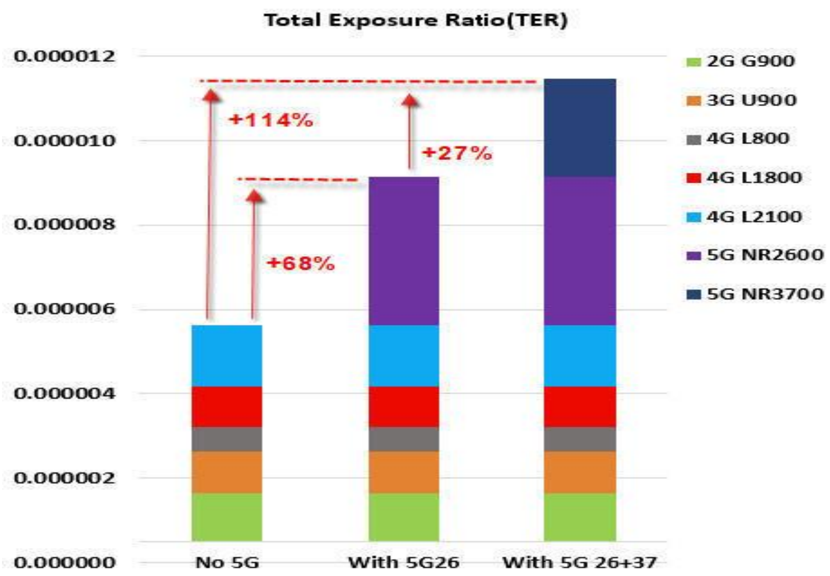

Figure 4.81. Site-1 simulated increments in TER due addition of 5G2600 and 5G3700.

The urban area analysis also shows that TER is very low compared to the ICNIRP, with the highest being 0.0104% from the maximum limit. TER distribution Figure 4.82 shows that the addition of the first technology of 5G NR2600 (co-location with exiting 2G/3G/4G) raises the TER by 68%. The addition of the second technology of 5G NR 3700 raises the TER by 76%; thus, the total increase due to both 5G technologies is 195%, which makes the 5G contribution to TER approximately 66%.

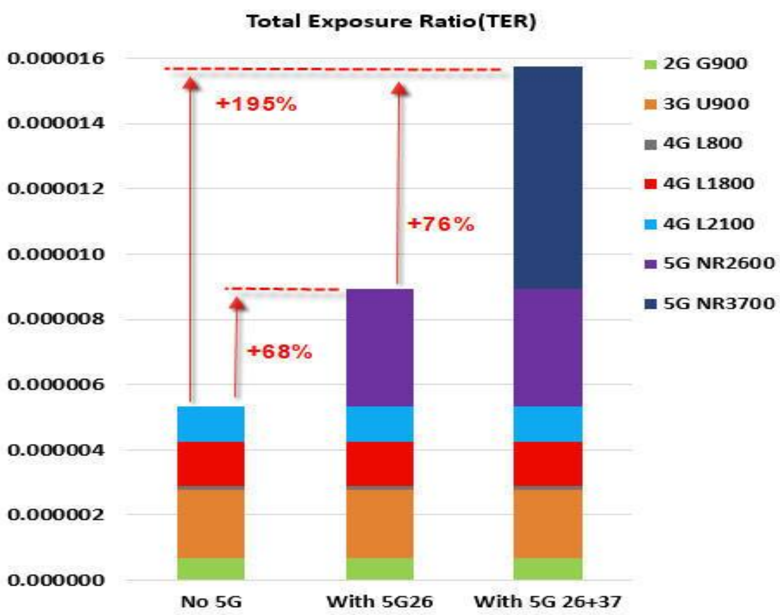

Figure 4.82. Site-2 simulated increments in TER due addition of 5G2600 and 5G3700.

The suburban area analysis also shows that TER is very low compared to the ICNIRP, with the highest 0.098% from the maximum limit. TER distribution Figure 4.83 shows that the addition of the first technology of 5G NR2600 (co-location with exiting 2G/3G/4G) raises the TER by 62% and the addition of the second technology of 5G NR 3700 raises the TER by 47%; thus, the total increase due to 5G technologies is 137%, which makes the 5G contribution to TER approximately 53%.

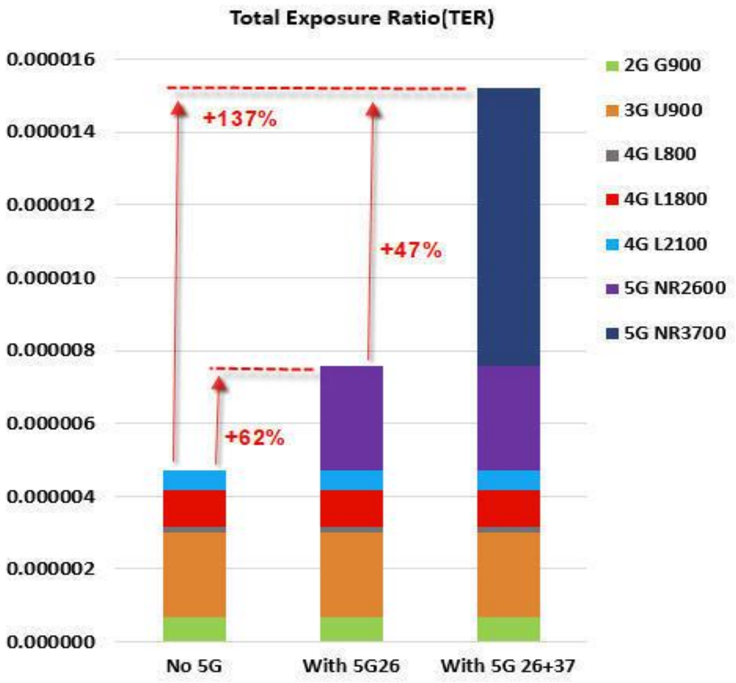

Figure 4.83. Site-3 simulated increments in TER due addition of 5G2600 and 5G3700.

The rural area analysis also shows that TER is very low compared to the ICNIRP, with the highest being 0.0066% from the maximum limit. TER distribution Figure 4.84 shows that the addition of the first technology of 5G NR2600 (co-location with exiting 2G/3G/4G) raises the TER by 68%. The addition of the second technology of 5G NR 3700 raises the TER by 64%; thus, the total increase due to both 5G technologies is 175%, which makes the 5G contribution to TER approximately 65%.

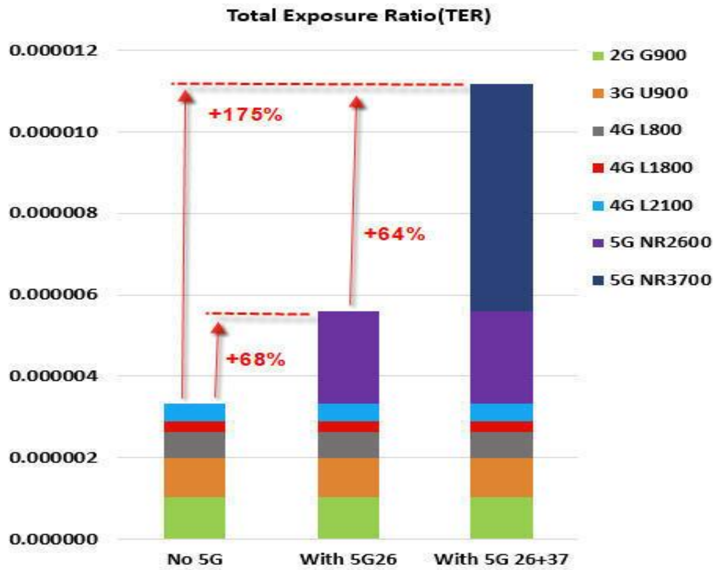

Figure 4.84. Site-1 simulated increments in TER due addition of 5G2600 and 5G3700.

4.4.9. Summary of Far-Field Assessment

This study assessed the EMF exposure radiation for specific single sites in dense, urban, suburban, and rural areas considering multi-technology simultaneously operating and co-located at the same site, including 2G, 3G, 4G, IoT, and 5G. The assessment was performed through simulation tools using propagation models to predict the Rx levels, and the tool was calibrated using field measurements. The Rx level results were used to calculate the power densities at different distances from the sites, and the total exposure ratios were calculated from the power densities. The obtained results show that the power densities and total exposure ratios are low for the four area scenarios compared to the ICNIRP standard reference limits. Further studies will be conducted to investigate and assess the RF-EMF radiation exposure at the near field for single sites and groups of sites and surrounding sites in the whole area considering multi-technology and multi-operator coexistence. Additionally, further studies are required to investigate the exposure considering other factors, such as traffic load (system utilization), time-averaged power and spectral efficiency.

Chapter Five: Conclusion and Recommendation

5.1. Conclusion

This study addressed an important problem related to total accumulated EMF radiation levels emitted from mobile network base station in the situation of the co-existing multi-technology transmitting from the same site, belwo are the conclusions summarized in four points:

1. The accurate calculations are essential in determining compliance distances from mobile tower base station sites to ensure that EMF exposures are within regulatory limits. This investigation of the EMF compliance safety boundary for multi-technology situation considered the real configuration scenarios and power reduction factor for 5G mMIMO technology. An enhanced formula is proposed to calculate the CD with more accurate results. The study examined macro site with typical GSM, UMTS, LTE, and NR operations. The GP zone's CD values were lower than the OW zone. The GP horizontal CD were 14.8m in accordance with ICNIRP. Additionally, the 5G NR 3,500 MHz has the greatest contribution with 34% from the TER at the horizontal CD. The results show that the horizontal CD was 2.9 m. The calculation involving the power weight ρ_w which gives horizontal CDs less by -34.5% compared to the original equation and less by -6.2% for vertical CDs. The research team will examine the CDs in the near future while taking into account the cumulative radiation contribution from nearby sites, and also will study the effective actions that mobile network operators can take to reduce the PD and minimize the EMF exposure while maintaining sufficient network coverage and capacity.

2. The EMF exposure compliance boundary for multi-technology, multi-operator site sharing was analyzed using calculations that considered realistic configurations. The EMF site sharing scale-up formula is developed to estimate the increase in CDs for N number of MNOs sharing the same sites and all MNOs use the same configuration. The evaluation is done for two types of site sharing: macro and indoor IBS sites. For the macro site with a single MNO, the general public's horizontal R_{CD} distances were 14.8 m and 13.8 m according to the ICNIRP and FCC, respectively. Furthermore, for a macro site shared by four MNOs, the R_{CD} distances were 29.61 m and 27.69 m according to the ICNIRP and FCC, respectively. In addition, the 5G N3500 MHz had

the highest contributions to the TER of 34% and 39% at the horizontal R_{CD} according to the ICNIRP and the FCC, respectively. For the indoor IBS site with a single MNO, the general public's horizontal R_{CD} distances were 0.87 m and 0.8 m according to the ICNIRP and FCC, respectively. In addition, for an IBS shared by four MNOs, the R_{CD} distances were 1.74 m and 1.6 m according to the ICNIRP and FCC, respectively. Moreover, for all shared IBS site scenarios, the 5G N3600 MHz had the highest contributions to the TER of 26% and 30% at the horizontal compliance distances according to the ICNIRP and FCC, respectively.

3. the increase in radiation levels due to the addition of future technologies leads to more restricted compliance distances which constrains the 5G deployment. A design model to de-concentrate the overall exposure ratio from sectorized antennas of the multi-technology base station was proposed in this study. The model uses the weighted antenna's azimuth to spread the total exposure by horizontally separating the installed antennas in the same sector. A set of simulations is carried out to calculate the reduction in total exposure for widely commonly used antenna deployment setups in multi-technology mobile networks. For three-sectors BS operating with six technologies, the simulation results show the compliance distance is reduced by -23% when using two antennas (two different azimuths) compared to using one azimuth, reduced by -35.9% using 3 azimuths, -39.8% using 4 azimuths, -41.3% using 5 azimuths, and by -43.4% when using 6 azimuths. A field test is done in a life network serving in a geographical cluster that consists of 4 sites, the results show that the TER is reduced by -19.23% after the antennas azimuths are changed with separation angles calculated using the proposed model. Further, the OSS system performance records and counters were analyzed to evaluate the impact of the model on the network coverage and capacity. Overall, the system records show no significant impacts were registered on network coverage level and capacity performance for all transmitting technologies of the sites involved in the test. The proposed solution is beneficial and can help mobile operators minimize the compliance boundaries without impacting the network coverage and performance especially for rooftop and wall-mounted sites where the antennas are installed in close areas accessible to the general public.

4. Determining and quantifying the increase in EMF exposure levels in terms of Total Exposure Ratio (TER) due to the addition of ongoing 5G mMIMO deployments on

existing sites as the situation of multi-technology co-located site, where most of the current related works (found in the literature) investigated the situation of single-technology. The study assessed the EMF exposure radiation for specific single sites in dense, urban, suburban, and rural areas considering multi-technology simultaneously operating and co-located at the same site, including 2G, 3G, 4G, IoT, and 5G. The assessment was performed through simulation tools using propagation models to predict the Rx levels, and the tool was calibrated using field measurements. The Rx level results were used to calculate the power densities at different distances from the sites, and the total exposure ratios were calculated from the power densities. The obtained results show that the power densities and total exposure ratios are low for the four area scenarios compared to the ICNIRP standard reference limits.

5.2. Contributions

Below are the major contributions achieved during this research:

A. In this research, an enhanced formula is proposed to calculate the CD with more accurate results considering more factor in the calculation such as the power reduction factor and the system load utilization.

B. The study investigated the compliance boundary for multi-technology, multi-operator site sharing, and proposed as site sharing scale-up formula to estimate the increase in CDs for N number of MNOs sharing the same sites.

C. The study proposed a design model to de-concentrate the overall exposure ratio from multi-technology base station. The proposed model uses the weighted antenna's azimuth to spread the total exposure by horizontally separating the installed antennas in the same sector.

D. The study provided answers (determined and quantified) for the amount of increase in EMF exposure levels in terms of Total Exposure Ratio (TER) due to the addition of ongoing 5G mMIMO deployments on existing sites as the situation of multi-technology co-located site.

5.3. Recommendation for Future Work

The EMF radiation and exposure is hot topic, and it's become more important with increase of installing more base stations for mobile networks specially with rise of the 5G deployment. Below are the suggested future works related to this research problem statement:

A. To investigate and assess the EMF radiation exposure for whole area considering the contribution from handset devices as source of EMF radiations.

B. To enhance the compliance distance calculation formula by considering more factors, such as mMIMO beamforming.

C. To develop smart technique to decrease the total exposure ratio by employing and auto-optimize the network soft features such as dynamic power control and traffic balancing.

D. To investigate and predict the overall exposure increase due to addition of upcoming future six generation (6G) in mobile network..

Published Papers and References

Published Papers

The following papers were published during the research period:

1. **Mohammed S. Elbasheir**, R. A. Saeed and S. Edam, "Measurement and Simulation-based Exposure Assessment at a Far-Field for a Multi-Technology Cellular Site up to 5G NR," in IEEE Access, 2022, doi: 10.1109/ACCESS.2022.3177732. https://ieeexplore.ieee.org/document/9781406

2. **Mohammed S. Elbasheir**, R. A. Saeed and S. Edam, "Electromagnetic field exposure boundary analysis at the near field for multi-technology cellular base station site". Wiley, IET Communication 1–17 (2023), doi.org/10.1049/cmu2.12711. https://ietresearch.onlinelibrary.wiley.com/doi/10.1049/cmu2.12711

3. **Mohammed. S. Elbasheir**, Rashid A. Saeed, and Salaheldin Edam. "Multi-Technology Multi-Operator Site Sharing: Compliance Distance Analysis for EMF Exposure", MDPI Sensors, 2023, no. 3: 1588. https://doi.org/10.3390/s23031588. https://www.mdpi.com/1424-8220/23/3/1588

4. **Mohammed S. Elbasheir**, R. A. Saeed, A. A. Z. Ibrahim, S. Edam, F. Hashim and S. M. E. Fadul, "A Review of EMF Radiation for 5G Mobile Communication Systems," 2021 IEEE Asia-Pacific Conference on Applied Electromagnetics (IEEE APACE 2021), 2021, pp. 1-6, doi: 10.1109/APACE53143.2021.9760689. https://ieeexplore.ieee.org/document/9760689

5. **Mohammed S. Elbasheir**, R. A. Saeed and S. Edam, "5G Base Station Deployment Review for RF Radiation" 2021 IEEE International Symposium on Networks, Computers and Communications (IEEE ISNCC 2021), 2021, pp. 1-5, doi: 10.1109/ISNCC52172.2021.9615689. https://ieeexplore.ieee.org/document/9615689

6. **Mohammed S. Elbasheir**, R. A. Saeed and S. Edam, "EMF Compliance Distance Calculation Enhancement for Multi-Technology Mobile Site," 2023 IEEE Third International Conference on Signal, Control and Communication (IEEE SCC 2023), Hammamet, Tunisia, 2023, pp. 1-6, doi: 10.1109/SCC59637.2023.10527498. https://ieeexplore.ieee.org/document/10527498

7. **Mohammed S. Elbasheir**, R. A. Saeed and S. Edam, "EMF Exposure De-Concertation Model for Multi-Technology Mobile Base-Station," IEEE 2024 6th Global Power, Energy and Communication Conference (IEEE GPECOM 2024), Budapest, Hungary, 2024, pp. 752-758, doi: 10.1109/GPECOM61896.2024.10582563. https://ieeexplore.ieee.org/document/10582563

8. **Mohammed S. Elbasheir**, R. A. Saeed and S. Edam, "Weighted Antenna's Azimuth for Minimal EMF With Sustainable KPIs of Multi-Technology BS," in IEEE Open Journal of the Communications Society, vol. 5, pp. 5436-5451, 2024, doi: 10.1109/OJCOMS.2024. https://ieeexplore.ieee.org/document/10654380

References

[1] A. Bajpai and A. Balodi, "Role of 6G Networks: Use Cases and Research Directions," 2020 IEEE Bangalore Humanitarian Technology Conference (B-HTC), 2020, pp. 1-5, doi: 10.1109/B-HTC50970.2020.9298017.

[2] M. Z. Chowdhury, M. Shahjalal, S. Ahmed and Y. M. Jang, "6G Wireless Communication Systems: Applications, Requirements, Technologies, Challenges, and Research Directions," in IEEE Open Journal of the Communications Society, vol. 1, pp. 957-975, 2020, doi: 10.1109/OJCOMS.2020.3010270.

[3] W. J. Koh and S. M. Moochhala, "Non-ionizing EMF hazard in the 21th century," 2018 IEEE International Symposium on Electromagnetic Compatibility and 2018 IEEE Asia-Pacific Symposium on Electromagnetic Compatibility (EMC/APEMC), 2018, pp. 518-522, doi: 10.1109/ISEMC.2018.8393832.

[4] ICNIRP (2020), "ICNIRP Guidelines for Limiting Exposure to Electromagnetic Fields (100 kHz to 300 GHz)". Health Phys 118(00):000-000; 2020. p. 483-524.

[5] ICNIRP, "Guidelines for limiting exposure to time-varying electric, magnetic, and electromagnetic fields (up to 300 GHz)". 1998. 74(4): p. 494-522.

[6] FCC USA, F.O.B., "Evaluating Compliance with FCC Guidelines for Human Exposure to Radiofrequency Electromagnetic Fields", 1997, in FCC OET Bulletin 65, FCC, Editor. 1997.

[7] W. El-Beaino, A. M. El-Hajj and Z. Dawy, "On Radio network planning for next generation 5G networks: A case study," 2015 International Conference on Communications, Signal Processing, and their Applications (ICCSPA'15), 2015, pp. 1-6, doi: 10.1109/ICCSPA.2015.7081315.

[8] C. Blackman and S. Forge, ‘‘5G deployment—State of play in Europe, USA and Asia,’’ Policy Dept. Econ., Sci. Qual. Life Policies, Eur. Parliament, Brussels, Belgium, Tech. Rep. PE 631.060, Apr. 2019.

[9] R. Werner, Phill Knipe, Steve Iskra, “A Comparison Between Measured and Computed Assessments of the RF Exposure Compliance Boundary of an In-Situ Radio Base Station Massive MIMO Antenna”, IEEE Access, Volume: 7, 2019.

[10] S. Sagar, S. M. Adem, B. Struchen, S. P. Loughran, M. E. Brunjes, L. Arangua, M. A. Dalvie, R. J. Croft, M. Jerrett, J. M. Moskowitz, T. Kuo, M. Röösli, “Comparison of radiofrequency electromagnetic field exposure levels in different everyday microenvironments in an international context,” Environmental International, vol. 114, pp. 297-306, May 2018.

[11] T. Rumeng, Shi Ying, Wu Tong, Zhu Wentao, “Electromagnetic field safety compliance assessments for 5G wireless networks”, 2020 IEEE 9th Power India International Conference (PIICON), 2020.

[12] A. Lee, Sang-Bong Jeon, Hyung-Do Choi, “EMF Levels in 5G New Radio Environment in Seoul, Korea”,Journal Article, IEEE Access, Volume: 9, 2021.

[13] G. Betta, G. Cerro, G. Miele, M. Salone D’Amata, D. Capriglione, ”Frequency Selective EMF Measurements and Exposure Assessment in Indoor Office Environments”, 2020 14th European Conference on Antennas and Propagation (EuCAP),2020, Conference Paper, IEEE.

[14] M. Celaya-Echarri, L. Azpilicueta, J. Karpowicz, V. Ramos, P. Lopez-Iturri and F. Falcone, "From 2G to 5G Spatial Modeling of Personal RF-EMF Exposure Within Urban Public Trams," in IEEE Access, vol. 8, pp. 100930-100947, 2020, doi: 10.1109/ACCESS.2020.2997254.

[15] L. Verloock, W. Joseph, A. Gati, N. Varsier, B. Flach, J. Wiart, and L. Martens, “Low-cost extrapolation method for maximal LTE radio base station exposure estimation: test and validation,” Radiation Protection Dosimetry, vol. 155, no. 1, pp. 11–15, 11 2012.

[16] A. Pathak, Ashok Jangid, “Measurement and Impact Assessment of Radio Frequency Electromagnetic Fields in Dayalbagh Educational Institute”, 2020 IEEE 9th Power India International Conference (PIICON), 2020.

[17] ITU-T Recommendation K.IOO, “Measurement of radio frequency electromagnetic fields to determine compliance with human expo sure limits when a base station is put into service” [S].20 18, ITU-R.

[18] R. Ramirez-Vazquez, I. Escobar, A. Thielens and E. Arribas, "Measurements and Analysis of Personal Exposure to Radiofrequency Electromagnetic Fields at Outdoor and Indoor School Buildings: A Case Study at a Spanish School," in IEEE Access, vol. 8, pp. 195692-195702, 2020, doi: 10.1109/ACCESS.2020.3033800.

[19] G. Betta, G. Cerro, G. Miele, M. S. D'Amata and D. Capriglione, "On the Reliability of Extrapolation Techniques for Verifying the Compliance of LTE Cellular Systems with RF Human Exposure Limits," 2020 IEEE International Instrumentation and Measurement Technology Conference (I2MTC), 2020, pp. 1-6.

[20] L. Chiaraviglio, Angela Sara Cacciapuoti, Gerardo Di Martino, Marco Fiore, Mauro Montesano, Damiano Trucchi, Nicola Blefari Melazzi, "Planning 5G Networks Under EMF Constraints: State of the Art and Vision", IEEE Access, volume 6, 2018. doi: 10.1109/ACCESS.2018.2868347.

[21] M. Koprivica, V. Slavkovic, N. Nešković, and A. Nešković, ''Statistical analysis of electromagnetic radiation measurements in the vicinity of GSM/UMTS base station installed on buildings in Serbia,'' Radiat. Protection Dosimetry, vol. 168, no. 4, pp. 489–502, 2015.

[22] ICNIRP, "The International Commission on Non-ionizing Radiation Protection. Guidelines for limiting exposure to time-varying electric, magnetic, and electromagnetic elds (up to 300 GHz)," Health Phys., vol. 75, pp. 494-522, 1998.

[23] B. Thors, A. Furuskär, D. Colombi and C. Törnevik, "Time-Averaged Realistic Maximum Power Levels for the Assessment of Radio Frequency Exposure for 5G Radio Base Stations Using Massive MIMO," in IEEE Access, vol. 5, pp. 19711-19719, 2017, doi: 10.1109/ACCESS.2017.2753459.

[24] S. Sagar, B. Struchen, V. Finta, M. Eeftens, M. Röösli, "Use of portable exposimeters to monitor radiofrequency electromagnetic field exposure in the everyday environment," Environmental Research, vol. 150, pp. 289-298, October 2016.

[25] W. H. Bailey, B. R. T. Cotts and P. J. Dopart, "Wireless 5G Radiofrequency Technology — An Overview of Small Cell Exposures, Standards and Science," in IEEE Access, vol. 8, pp. 140792-140797, 2020, doi: 10.1109/ACCESS.2020.3010677.

[26] K. R. Foster, S. Kodera, and A. Hirata, "5G communications systems and radiofrequency exposure limits," IEEE Futur. Networks Tech Focus, vol. 3, no. 2, pp. 1–10, 2019.

[27] Mohammed. S. Elbasheir, R. A. Saeed, A. A. Z. Ibrahim, S. Edam, F. Hashim and S. M. E. Fadul, "A Review of EMF Radiation for 5G Mobile Communication Systems," 2021 IEEE Asia-Pacific Conference on Applied Electromagnetics (APACE), 2021, pp. 1-6, doi: 10.1109/APACE53143.2021.9760689.

[28] Mohammed. S. Elbasheir, R. A. Saeed and S. Edam, "5G Base Station Deployment Review for RF Radiation," 2021 International Symposium on Networks, Computers and Communications (ISNCC), 2021, pp. 1-5, doi: 10.1109/ISNCC52172.2021.9615689.

[29] L. Chiaraviglio, A. Elzanaty and M. -S. Alouini, "Health Risks Associated With 5G Exposure: A View From the Communications Engineering Perspective," in IEEE Open Journal of the Communications Society, vol. 2, pp. 2131-2179, 2021, doi: 10.1109/OJCOMS.2021.3106052.

[30] V. Markovic, "5G EMF Exposure: Overview of Recent Research and Safety Standard Updates," 2021 15th International Conference on Advanced Technologies, Systems and Services in Telecommunications (TELSIKS), 2021, pp. 359-365, doi: 10.1109/TELSIKS52058.2021.9606262.

[31] H. Malik, H. Pervaiz, M. Mahtab Alam, Y. Le Moullec, A. Kuusik and M. Ali Imran, "Radio Resource Management Scheme in NB-IoT Systems," in IEEE Access, vol. 6, pp. 15051-15064, 2018, doi: 10.1109/ACCESS.2018.2812299.

[32] 3GPP-TS-36.302, Technical Specification Group Radio Access Network; Evolved Universal Terrestrial Radio Access (E-UTRA); Services provided by the physical layer (Release 16). 2020 3GPP.

[33] infovista. https://www.infovista.com/tems/investigation. 2021.

[34] infovista. https://www.infovista.com/5g-network/planet-rf-planning-software. 2021.

[35] V. S. Anusha, G. K. Nithya and S. N. Rao, "A comprehensive survey of electromagnetic propagation models," 2017 International Conference on Communication and Signal Processing (ICCSP), 2017, pp. 1457-1462, doi: 10.1109/ICCSP.2017.8286627.

[36] S. A. Siddiqui, N. Fatima and A. Ahmad, "Comparative Analysis Of Propagation Path Loss Models In Lte Networks," 2019 International Conference on Power Electronics, Control and Automation (ICPECA), 2019, pp. 1-3, doi: 10.1109/ICPECA47973.2019.8975464.

[37] 3GPP-TR-36.873, Study on 3D channel model for LTE. 2018.

[38] T. S. Rappaport, Y. Xing, G. R. MacCartney, A. F. Molisch, E. Mellios and J. Zhang, "Overview of Millimeter Wave Communications for Fifth-Generation (5G) Wireless Networks—With a Focus on Propagation Models," in IEEE Transactions on Antennas and Propagation, vol. 65, no. 12, pp. 6213-6230, Dec. 2017, doi: 10.1109/TAP.2017.2734243.

[39] 3GPP-TR-38.901, Study on channel model for frequencies from 0.5 to 100 GHz. 2018.

[40] Tataria, Harsh, Katsuyuki Haneda, Andreas F. Molisch, Mansoor Shafi, and Fredrik Tufvesson. "Standardization of Propagation Models for Terrestrial Cellular Systems: A Historical Perspective". Int J Wireless Inf Networks 28, 20–44 (2021). https://doi.org/10.1007/s10776-020-00500-9.

[41] A. -K. Lee, S. -B. Jeon and H. -D. Choi, "EMF Levels in 5G New Radio Environment in Seoul, Korea," in IEEE Access, vol. 9, pp. 19716-19722, 2021, doi: 10.1109/ACCESS.2021.3054363.

[42] A. Gati, E. Conil, M. Man-Faï Wong and J. Wiart, "Duality Between Uplink Local and Downlink Whole-Body Exposures in Operating Networks," in IEEE Transactions on Electromagnetic Compatibility, vol. 52, no. 4, pp. 829-836, Nov. 2010, doi: 10.1109/TEMC.2010.2066978.

[43] GSMA, Public Policy 2019, "https://www.gsma.com/publicpolicy/emf-and-health/emf-policy". 2019.

[44] C. Phillips, D. Sicker and D. Grunwald, "Bounding the error of path loss models," 2011 IEEE International Symposium on Dynamic Spectrum Access Networks (DySPAN), 2011, pp. 71-82, doi: 10.1109/DYSPAN.2011.5936271.

[45] D. G. Lopez, M. Ignatenko and D. S. Filipovic, "Eigenmode Prediction of High RF Exposure Frequency Region Inside Vehicles," in IEEE Transactions on Electromagnetic Compatibility, vol. 59, no. 1, pp. 43-47, Feb. 2017, doi: 10.1109/TEMC.2016.2593023.

[46] U. T. Virk, K. Haneda, V. -M. Kolmonen, P. Vainikainen and Y. Kaipainen, "Characterization of Vehicle Penetration Loss at wireless communication frequencies," The 8th European Conference on Antennas and Propagation (EuCAP 2014), 2014, pp. 234-238, doi: 10.1109/EuCAP.2014.6901733.

[47] T. Rumeng, S. Ying, W. Tong and Z. Wentao, "Electromagnetic field safety compliance assessments for 5G wireless networks," 2020 IEEE International Symposium on Electromagnetic Compatibility & Signal/Power Integrity (EMCSI), 2020, pp. 659-662, doi: 10.1109/EMCSI38923.2020.9191518.

[48] S. Aerts et al., "In-situ Measurement Methodology for the Assessment of 5G NR Massive MIMO Base Station Exposure at Sub-6 GHz Frequencies," in IEEE Access, vol. 7, pp. 184658-184667, 2019, doi: 10.1109/ACCESS.2019.2961225.

[49] A. Pathak and A. Jangid, "Measurement and Impact Assessment of Radio Frequency Electromagnetic Fields in Dayalbagh Educational Institute," 2020 IEEE 9th Power India International Conference (PIICON), 2020, pp. 1-5, doi: 10.1109/PIICON49524.2020.9113039.

[50] D. Colombi, P. Joshi, B. Xu, F. Ghasemifard, V. Narasaraju, C. Tornevik "Analysis of the actual power and EMF exposure from base stations in a commercial 5G network", Applied Sciences, 2020. 10(15): p. 5280.

[51] S. Q. Wali, A. Sali, J. K. Allami and A. F. Osman, "RF-EMF Exposure Measurement for 5G Over Mm-Wave Base Station With MIMO Antenna," in IEEE Access, vol. 10, pp. 9048-9058, 2022, doi: 10.1109/ACCESS.2022.3143805.

[52] M. Velghe, S. Aerts, L. Martens, W. Joseph, A. Thielens, “Protocol for personal RF-EMF exposure measurement studies in 5th generation telecommunication networks”. Environmental Health 20, no. 1 (2021): 1-10.

[53] M. Velghe, S. Shikhantsov, E. Tanghe, L. Martens, W. Joseph, A. Thielens, “Exposure to RF-EMF hotspots induced by maximum ratio field combining in 5th generation networks”, In Joint Annual Meeting of the Bioelectromagnetics Society and the European BioElectromagnetics Association (BioEM 2020), pp. 380-384. 2020.

[54] S. Aerts, W. Joseph, M. Maslanyj, D. Addison, T. Mee, L. Colussi, J. Kamer, J. Bolte. "Prediction of RF-EMF exposure levels in large outdoor areas through car-mounted measurements on the enveloping roads." Environment international 94 (2016): 482-488.

[55] A. B. Sharma, O. S. Lamba, A. Sharma and M. Sanadhya, "Investigation to Measure Risk Free Exposure from Mobile Base Station Antennas in Residential Area," 2018 2nd International Conference on Micro-Electronics and Telecommunication Engineering (ICMETE), 2018, pp. 64-70, DOI: 10.1109/ICMETE.2018.00026.

[56] L. Chiaraviglio et al., "How Much Exposure from 5G Towers is Radiated over Children, Teenagers, Schools and Hospitals?," in IEEE Open Journal of the Communications Society, 2022, DOI: 10.1109/OJCOMS.2022.3208938.

[57] IEC, “Determination of RF Field Strength and SAR in the Vicinity of Radio Communication Base Stations for the Purpose of Evaluating Human Exposure”, IEC Standard IEC 62232:2022, 2022-10.

[58] B. Thors et al., "On the Estimation of SAR and Compliance Distance Related to RF Exposure From Mobile Communication Base Station Antennas," in IEEE Transactions on Electromagnetic Compatibility, vol. 50, no. 4, pp. 837-848, Nov. 2008, DOI: 10.1109/TEMC.2008.2004605.

[59] A. Jain and P. Tupe-Waghmare, "Radiation measurements at repeated intervals for various locations of SIU campus and calculation of compliance distance from cell tower," 2016 International Conference on Automatic Control and Dynamic Optimization Techniques (ICACDOT), 2016, pp. 804-808, DOI: 10.1109/ICACDOT.2016.7877698.

[60] B. Thors, D. Colombi, Z. Ying, T. Bolin and C. Törnevik, "Exposure to RF EMF From Array Antennas in 5G Mobile Communication Equipment," in IEEE Access, vol. 4, pp. 7469-7478, 2016, DOI: 10.1109/ACCESS.2016.2601145.

[61] Sam Arets, Joe Wiart, Luc Martens, and Wout Joseph. "Assessment of long-term spatio-temporal radiofrequency electromagnetic field exposure" Environmental research 161 (2018): 136-143.

[62] Sam Aerts, Kenneth Deprez, Davide Colombi, Matthias Van den Bossche, Leen Verloock, Luc Martens, Christer Törnevik, and Wout Joseph. "In situ assessment of 5G NR massive MIMO base station exposure in a commercial network in Bern, Switzerland" Applied Sciences 11, no. 8 (2021): 3592.

[63] IEC TR 62669 ed2 106/463/cd, Case Studies Supporting, International Electromechanical Commission, IEC Standard 62232, Sep. 7, 2018.

[64] Narda Safety Test Solutions, SRM-3006 EMF Selective, “https://www.narda-sts.com/en/selective-emf/srm-3006-field-strength-analyzer/”, 2022.

[65] P. Baracca, A. Weber, T. Wild, and C. Grangeat, “A statistical approach for RF exposure compliance boundary assessment in massive MIMO systems," in Proc. 22nd Int. ITG Workshop Smart Antennas (WSA), 2018, pp. 1-6.

[66] M. Mahbub, and B. Barua, "Optimal Positioning of Macro Base Station: An Approach to Ensure Optimal Coverage of Small Cell in HetNet," 2021 IEEE International Conference on Electronics, Computing and Communication Technologies (CONNECT), 2021, pp. 1-4, DOI: 10.1109/CONECCT52877.2021.9622678.

[67] Mohammed S. Elbasheir, Rashed A. Saeed and Salahedin Edam, "Measurement and Simulation-Based Exposure Assessment at a Far-Field for a Multi-technology Cellular Site up to 5G NR," in IEEE Access, vol. 10, pp. 56888-56900, 2022, DOI: 10.1109/ACCESS.2022.3177732.

[68] R. Werner, P. Knipe, and S. Iskra, "A Comparison Between Measured and Computed Assessments of the RF Exposure Compliance Boundary of an In-Situ Radio Base Station Massive MIMO Antenna," in IEEE Access, vol. 7, pp. 170682-170689, 2019, DOI: 10.1109/ACCESS.2019.2955715.

[69] D. Pinchera, M. Migliore and F. Schettino, "Compliance Boundaries of 5G Massive MIMO Radio Base Stations: A Statistical Approach," in IEEE Access, vol. 8, pp. 182787-182800, 2020, DOI: 10.1109/ACCESS.2020.3028471.

[70] A. Thielens, G. Vermeeren, D. Kurup, W. Joseph and L. Martens, "Compliance boundaries for LTE base station antennas at 2600 MHz" 2012 6th European Conference on Antennas and Propagation (EUCAP), Prague, Czech Republic, 2012, pp. 889-892, doi: 10.1109/EuCAP.2012.6205926.

[71] F. Héliot, T. H. Loh, D. Cheadle, Y. Gui and M. Dieudonne, "An Empirical Study of the Stochastic Nature of Electromagnetic Field Exposure in Massive MIMO Systems," in IEEE Access, vol. 10, pp. 63100-63112, 2022, doi: 10.1109/ACCESS.2022.3182236.

[72] D. J. Cichon, T. C. Becker, and M. Dottling, "Ray optical prediction of outdoor and indoor coverage in urban macro- and micro-cells," Proceedings of Vehicular Technology Conference - VTC, 1996, pp. 41-45 vol.1, DOI: 10.1109/VETEC.1996.503404.

[73] Kang Jianfeng, Zhao Zhuyan, Guan Hao, B. Vejlgaard and Liu Guangyi, "TD-LTE network indoor performance with Micro and Femto deployment in a realistic metropolitan scenario," 2013 IEEE Wireless Communications and Networking Conference (WCNC), 2013, pp. 3948-3952, DOI: 10.1109/WCNC.2013.6555207.

[74] L. Huang, Y. Zhou, Y. Wang, X. Han, J. Shi and X. Chen, "Advanced coverage optimization techniques for small cell clusters," in China Communications, vol. 12, no. 8, pp. 111-122, August 2015, DOI: 10.1109/CC.2015.7224694.

[75] R. Atawia, M. Ashour, T. El Shabrawy and H. Hammad, "Optimized transmitted antenna power indoor planning using distributed antenna systems," 2013 9th International Wireless Communications and Mobile Computing Conference (IWCMC), 2013, pp. 993-1000, DOI: 10.1109/IWCMC.2013.6583692.

[76] E. S. Kim, M. Sung, J. H. Lee, J. K. Lee, S. -H. Cho and J. Kim, "Coverage Extension of Indoor 5G Network Using RoF-Based Distributed Antenna System," in IEEE Access, vol. 8, pp. 194992-194999, 2020, DOI: 10.1109/ACCESS.2020.3033592.

[77] Kopacz, T.; Heberling, D. "Impact of the Elevation Scanning Angle on the Vertical Compliance Distance of 5G Massive MIMO Antennas", In Proceedings of the 2019 13th European Conference on Antennas and Propagation (EuCAP), Krakow, Poland, 31 March–5 April 2019; pp. 1–5.

[78] Liu, S.; Onishi, T.; Taki, M.; Watanabe, S. "Radio Frequency Electromagnetic Field Exposure Compliance Assessments of Smart Surfaces: Two Approximate Approaches", IEEE Trans. Electromagn. Compat. 2022, 64, 963–974. https://doi.org/10.1109/TEMC.2022.3171044.

[79] Degirmenci, E.; Thors, B.; Tornevik, C. "Assessment of Compliance With RF EMF Exposure Limits: Approximate Methods for Radio Base Station Products Utilizing Array Antennas With Beam-Forming Capabilities", IEEE Trans. Electromagn. Compat. 2016, 58, 1110–1117. https://doi.org/10.1109/TEMC.2016.2550611.

[80] GSMA, Mobile Infrastructure Sharing. June 2019. Available online: https://www.gsma.com/futurenetworks/wiki/infrastructure-sharing-an-overview/ (accessed on).

[81] Frisanco, T.; Tafertshofer, P.; Lurin, P.; Ang, R., "Infrastructure Sharing and Shared Operations for Mobile Network Operators: From a Deployment and Operations View", In Proceedings of the 2008 IEEE International Conference on Communications, Salvador, Brazil, 7–11 April 2008; pp. 2193–2200. https://doi.org/10.1109/ICC.2008.419.

[82] Nokia, "Network Sharing: Delivering Mobile Broadband More Efficiently and at Lower Cost", Nokia Network Sharing White Paper. Available online: https://www.nokia.com/networks/solutions/network-sharing/#overview (accessed on).

[83] Blackman and S. Forge, ‘‘5G deployment—State of play in Europe, USA and Asia,’’ Policy Dept. Econ., Sci. Qual. Life Policies, Eur. Parliament, Brussels, Belgium, Tech. Rep. PE 631.060, Apr. 2019.

[84] Chiaraviglio, Luca, Cristian Di Paolo, and Nicola Blefari-Melazzi. "5G network planning under service and EMF constraints: Formulation and solutions." IEEE Transactions on Mobile Computing 21, no. 9 (2021): 3053-3070. DOI: 10.1109/TMC.2021.3054482.

[85] R. Joyce, D. Morris, S. Brown, D. Vyas and L. Zhang, "Higher Order Horizontal Sectorization Gains for 6, 9, 12 and 15 Sectored Cell Sites in a 3GPP/HSPA+ Network," in IEEE Transactions on Vehicular Technology, vol. 65, no. 5, pp. 3440-3449, May 2016, doi: 10.1109/TVT.2015.2446945.

[86] C. Weng, H. Wang, K. Li and M. N. S. Swamy, "Azimuth Estimation for Sectorized Base Station With Improved Soft-Margin Classification," in IEEE Access, vol. 8, pp. 96649-96660, 2020, doi: 10.1109/ACCESS.2020.2996417.

[87] K. Narongrit, P. Uthansakul and M. Uthansakul, "Performance analysis of MB-MIMO under 120 degree sector consideration for 5G communications," The 20th Asia-Pacific Conference on Communication (APCC2014), Pattaya, Thailand, 2014, pp. 463-467, doi: 10.1109/APCC.2014.7092858.

[88] Mohammed S. Elbasheir, Rashid A. Saeed, and Salaheldin Edam. "Electromagnetic field exposure boundary analysis at the near field for multi-technology cellular base station site." IET Communications 18, no. 1 (2024): 11-27.

[89] Mapbis . https://mapbis.com/mapinfo-pro/. 2024.

[90] F. K. Karo, A. Hikmaturokhman and M. A. Amanaf, "5G New Radio (NR) Network Planning at Frequency of 2.6 GHz in Golden Triangle of Jakarta," 2020 3rd International Seminar on Research of Information Technology and Intelligent Systems (ISRITI), Yogyakarta, Indonesia, 2020, pp. 278-283, doi: 10.1109/ISRITI51436.2020.9315504.

[91] M. Sousa, A. Alves, P. Vieira, M. P. Queluz and A. Rodrigues, "Analysis and Optimization of 5G Coverage Predictions Using a Beamforming Antenna Model and Real Drive Test Measurements," in IEEE Access, vol. 9, pp. 101787-101808, 2021, doi: 10.1109/ACCESS.2021.3097633.

[93] Y. An, C. Li, W. Duan, L. Sun and X. Cui, "Base station location determination model based on 5G network coverage," 2022 IEEE 5th International Conference on Information Systems and Computer Aided Education (ICISCAE), Dalian, China, 2022, pp. 736-740, doi: 10.1109/ICISCAE55891.2022.9927514.

[94] P. Rahmawati, M. I. Nashiruddin and M. A. Nugraha, "Capacity and Coverage Analysis of 5G NR Mobile Network Deployment for Indonesia's Urban Market," 2021 IEEE International Conference on Industry 4.0, Artificial Intelligence, and Communications Technology (IAICT), Bandung, Indonesia, 2021, pp. 90-96, doi: 10.1109/IAICT52856.2021.9532574.

[95] C. E. Garcia and I. Koo, "Coverage Prediction and REM Construction for 5G Networks in Band n78," 2023 15th International Conference on Computer and Automation Engineering (ICCAE), Sydney, Australia, 2023, pp. 125-129, doi: 10.1109/ICCAE56788.2023.10111476.

[96] H. Ganame, L. Yingzhuang, A. Hamrouni, H. Ghazzai and H. Chen, "Evolutionary Algorithms for 5G Multi-Tier Radio Access Network Planning," in IEEE Access, vol. 9, pp. 30386-30403, 2021, doi: 10.1109/ACCESS.2021.3058619.

[97] Ming Zhang and A. MacDonald, "Generalized cell planning technique applied for 4x12 frequency-reuse," 14th IEEE Proceedings on Personal, Indoor and Mobile Radio Communications, 2003. PIMRC 2003., Beijing, China, 2003, pp. 1884-1888 vol.2, doi: 10.1109/PIMRC.2003.1260444.

[98] G. V. Tsoulos, G. E. Athanasiadou, I. K. Valavanis and D. A. Zarbouti, "Green 4g radio network planning," 2017 11th European Conference on Antennas and Propagation (EUCAP), Paris, France, 2017, pp. 2212-2216, doi: 10.23919/EuCAP.2017.7928288.

[99] Z. Chen and E. Aksehirli, "Identifying Cell Sector Clusters Using Massive Mobile Usage Records," 2020 IEEE Wireless Communications and Networking Conference (WCNC), Seoul, Korea (South), 2020, pp. 1-6, doi: 10.1109/WCNC45663.2020.9120809.

[100] Dongdong Fan, Zhouyun Wu, Aiping Huang, Hangguan Shan and Hongcheng Zhuang, "Multi-sector joint beamforming for pilot coverage optimization," 2013 International Conference on Wireless Communications and Signal Processing, Hangzhou, China, 2013, pp. 1-5, doi: 10.1109/WCSP.2013.6677137.

[101] B. Xu, K. Zhao, S. He and Z. Ying, "Understandings of maximum spatially-averaged power density in 5G RF EMF exposure study," 2017 International Workshop on Antenna Technology: Small Antennas, Innovative Structures, and Applications (iWAT), Athens, Greece, 2017, pp. 115-117, doi: 10.1109/IWAT.2017.7915332.

[102] M. Bonato et al., "Human RF-EMF Exposure Assessment Due to Access Point in Incoming 5G Indoor Scenario," in IEEE Journal of Electromagnetics, RF and Microwaves in Medicine and Biology, vol. 5, no. 3, pp. 269-276, Sept. 2021, doi: 10.1109/JERM.2020.3042696.

[103] W. He, B. Xu, Y. Yao, D. Colombi, Z. Ying and S. He, "Implications of Incident Power Density Limits on Power and EIRP Levels of 5G Millimeter-Wave User Equipment," in IEEE Access, vol. 8, pp. 148214-148225, 2020, doi: 10.1109/ACCESS.2020.3015231.

[104] L. Chiaraviglio et al., "Massive Measurements of 5G Exposure in a Town: Methodology and Results," in IEEE Open Journal of the Communications Society, vol. 2, pp. 2029-2048, 2021, doi: 10.1109/OJCOMS.2021.3107287.

[105] B. Xu et al., "Power Density Measurements at 15 GHz for RF EMF Compliance Assessments of 5G User Equipment," in IEEE Transactions on Antennas and Propagation, vol. 65, no. 12, pp. 6584-6595, Dec. 2017, doi: 10.1109/TAP.2017.2712792.

[106] T. Panagiotakopoulos, Y. Kiouvrekis, L. -M. Misthos and C. Kappas, "RF-EMF Exposure Assessments in Greek Schools to Support Ubiquitous IoT-Based Monitoring in Smart Cities," in IEEE Access, vol. 11, pp. 7145-7156, 2023, doi: 10.1109/ACCESS.2023.3237970.

[107] L. Chiaraviglio et al., "Measuring EMF and Throughput Before and After 5G Service Activation in a Residential Area," in IEEE Open Journal of the Communications Society, vol. 4, pp. 1179-1195, 2023, doi: 10.1109/OJCOMS.2023.3277782.

[108] F. Héliot, T. H. Loh, D. Cheadle, Y. Gui and M. Dieudonne, "An Empirical Study of the Stochastic Nature of Electromagnetic Field Exposure in Massive MIMO Systems," in IEEE Access, vol. 10, pp. 63100-63112, 2022, doi: 10.1109/ACCESS.2022.3182236.

[109] J. M. Osepchuk and R. C. Petersen, "Safety standards for exposure to RF electromagnetic fields," in IEEE Microwave Magazine, vol. 2, no. 2, pp. 57-69, June 2001, doi: 10.1109/6668.924919.

[110] K. Li et al., "Intercomparison of Calculated Incident Power Density and Temperature Rise for Exposure From Different Antennas at 10–90 GHz," in IEEE Access, vol. 9, pp. 151654-151666, 2021, doi: 10.1109/ACCESS.2021.3126738.

[111] L. Mamushiane, L. Mboweni, H. Kobo, M. Mudumbe, J. Mwangama and A. A. Lysko, "4G RAN Infrastructure Sharing by 5G Virtualized Mobile Network Operators: A Tutorial," 2021 IEEE AFRICON, Arusha, Tanzania, United Republic of, 2021, pp. 1-7, doi: 10.1109/AFRICON51333.2021.9570937.

[112] L. Chiaraviglio et al., "EMF Exposure in 5G Standalone mm-Wave Deployments: What Is the Impact of Downlink Traffic?," in IEEE Open Journal of the Communications Society, vol. 3, pp. 1445-1465, 2022, doi: 10.1109/OJCOMS.2022.3200423.

[113] D. Harimurugan and G. S. Punekar, "Electric Field Reduction in an EHV Substation for Occupational Exposure via Transposition of Conductors," in IEEE Transactions on Power Delivery, vol. 33, no. 6, pp. 3147-3154, Dec. 2018, doi: 10.1109/TPWRD.2018.2860591.

[114] K. Lias, A. H. W. Teen, D. A. A. Mat, K. Kipli, A. S. W. Marzuki and M. H. Husin, "Biological Effect of 900MHz and 1800MHz Mobile Phones in SAR Weight," 2009 International Conference on Information and Multimedia Technology, Jeju, Korea (South), 2009, pp. 422-425, doi: 10.1109/ICIMT.2009.69.

[115] Kasumawati Bt Lias et al., "900MHz and 1800MHz mobile phone effect towards adult head in SAR distribution and SAR in weight," 2010 IEEE International Conference on Systems, Man and Cybernetics, Istanbul, Turkey, 2010, pp. 2239-2242, doi: 10.1109/ICSMC.2010.5641973.

[116] IEEE, "IEEE Standard for Safety Levels with Respect to Human Exposure to Electric, Magnetic, and Electromagnetic Fields, 0 Hz to 300 GHz - Corrigenda 2," in IEEE Std C95.1-2019/Cor2-2020 (Corrigenda to IEEE Std C95.1-2019) , vol., no., pp.1-15, 21 Oct. 2020, doi: 10.1109/IEEESTD.2020.9238523.

[117] L. Chiaraviglio, C. Lodovisi, S. Bartoletti, A. Elzanaty and M. Slim-Alouini, "Dominance of Smartphone Exposure in 5G Mobile Networks," in IEEE Transactions on Mobile Computing, vol. 23, no. 3, pp. 2284-2302, March 2024, doi: 10.1109/TMC.2023.3252662.

[118] Y. -D. Lin, H. -T. Chien, H. -W. Chang and C. -L. Lai, "Multi-operator Fairness in Transparent RAN Sharing," 2018 International Conference on Computing, Networking and Communications (ICNC), Maui, HI, USA, 2018, pp. 259-263, doi: 10.1109/ICCNC.2018.8390332.

[119] H. -T. Chien, Y. -D. Lin, H. -W. Chang and C. -L. Lai, "Multi-Operator Fairness in Transparent RAN Sharing by Soft-Partition With Blocking and Dropping Mechanism," in IEEE Transactions on Vehicular Technology, vol. 67, no. 12, pp. 11597-11605, Dec. 2018, doi: 10.1109/TVT.2018.2872042.

[120] B. Xu, D. Colombi, P. Joshi, F. Ghasemifard, D. A. Sanjurjo, C. Di Paola, et al., "A summary of actual maximum approach studies on EMF compliance of 5G radio base stations", Proc. 16th Eur. Conf. Antennas Propag. (EuCAP), pp. 1-5, Mar. 2022.

[121] C. Pisano et al., "Exposure System for Real-time 5G Electrophysiology Experiments: Numerical and Experimental Characterization," 2024 IEEE MTT-S International Microwave Biomedical Conference (IMBioC), Montreal, QC, Canada, 2024, pp. 155-157, doi: 10.1109/IMBioC60287.2024.10590365.

[122] H. Herssens and A. Thielens, "Focused Downlink Radiofrequency Electromagnetic Field Exposure at 26 GHz Using an Analytical Model," 2024 4th URSI Atlantic Radio Science Meeting (AT-RASC), Meloneras, Spain, 2024, pp. 1-4, doi: 10.46620/URSIATRASC24/SEMY1438.

[123] S. Goegebeur et al., "A Comparative Study of In Situ Methodologies for Assessment of RF EMF Exposure from a 5G FR2 Base Station," in IEEE Access, doi: 10.1109/ACCESS.2024.3424262.

[124] J. Liu et al., "Assessment of EMF Exposure Induced by Wireless Cellular Phones in Various Usage Scenarios in France," in IEEE Access, doi: 10.1109/ACCESS.2024.3424305.

[125] Y. Zhang et al., "Statistical Analysis of RF-EMF Exposure Induced by Cellular Wireless Networks in Public Transportation Facilities of the Paris Region," in IEEE Access, vol. 12, pp. 79741-79753, 2024, doi: 10.1109/ACCESS.2024.3410090.

[126] C. Bornkessel, A. Pikushina, L. -M. Schilling, T. Struck and M. A. Hein, "Reproducibility Studies of Instantaneous and 6-Minute Average Exposure Measurements Around 5G Massive-MIMO Base Stations," 2024 18th European Conference on Antennas and Propagation (EuCAP), Glasgow, United Kingdom, 2024, pp. 1-5, doi: 10.23919/EuCAP60739.2024.10501516.

[127] U. Roth, L. Selmane and S. Faye, "Measuring the EMF Exposure From Mobile Network Antennas: Experience From Luxembourg," in IEEE Access, vol. 12, pp. 57688-57710, 2024, doi: 10.1109/ACCESS.2024.3386432.

[128] N. Madawalage et al., "Blockchain-Enabled RF Radiation Exposure Level Measurement in Wireless Mobile Networks," 2024 IEEE 21st Consumer Communications & Networking Conference (CCNC), Las Vegas , NV, USA, 2024, pp. 392-395, doi: 10.1109/CCNC51664.2024.10454816.

[129] L. Senwen, W. Zhizhong, R. Yan, W. Huagang and C. Shaochuan, "Research on RF Characteristics and Electromagnetic Radiation Safety Compliance of 5G mmWave Base Station Based on OTA," 2023 IEEE 11th International Conference on Information, Communication and Networks (ICICN), Xi'an, China, 2023, pp. 432-440, doi: 10.1109/ICICN59530.2023.10393045.

[130] M. Rybakowski, K. Bechta, C. Grangeat and P. Kabacik, "Impact of Beamforming Algorithms on the Actual RF EMF Exposure From Massive MIMO Base Stations," in IEEE Access, vol. 11, pp. 141956-141964, 2023, doi: 10.1109/ACCESS.2023.3341623.

[131] Y. Yang et al., "RF Exposure Assessment in ITS-5.9 GHz V2X Connectivity and Vehicle Wireless Technologies: A Numerical and Experimental Approach," in IEEE Access, doi: 10.1109/ACCESS.2024.3435566.

[132] A. T. Ajibare and D. Ramotsoela, "A Radiofrequency Electromagnetic Wave Radiation Exposure Minimization Method in 5G Network: A Perspective of QoS Trade Offs," 2021 International Conference on Electrical, Computer and Energy Technologies (ICECET), Cape Town, South Africa, 2021, pp. 1-6, doi: 10.1109/ICECET52533.2021.9698800.

[133] S. Persia, C. Carciofi, S. D'Elia and R. Suman, "EMF evaluations for future networks based on Massive MIMO," 2018 IEEE 29th Annual International Symposium on Personal, Indoor and Mobile Radio Communications (PIMRC), Bologna, Italy, 2018, pp. 1197-1202, doi: 10.1109/PIMRC.2018.8580893.

[134] K. Li et al., "Intercomparison of Calculated Incident Power Density and Temperature Rise for Exposure From Different Antennas at 10–90 GHz," in IEEE Access, vol. 9, pp. 151654-151666, 2021, doi: 10.1109/ACCESS.2021.3126738

[135] K. Li et al., "Calculated Epithelial/Absorbed Power Density for Exposure From Antennas at 10–90 GHz: Intercomparison Study Using a Planar Skin Model," in IEEE Access, vol. 11, pp. 7420-7435, 2023, doi: 10.1109/ACCESS.2023.3238582.

[136] N. Miura, S. Kodera, Y. Diao, J. Higashiyama, Y. Suzuki and A. Hirata, "Power Absorption and Skin Temperature Rise From Simultaneous Near-Field Exposure at 2 and 28 GHz," in IEEE Access, vol. 9, pp. 152140-152149, 2021, doi: 10.1109/ACCESS.2021.3126372.

[137] A. T. Ajibare, D. Ramotsoela, L. A. Akinyemi and S. O. Oladejo, "RF EMF Radiation Exposure Assessment of 5G Networks: Analysis, Computation and Mitigation Methods," 2021 IEEE AFRICON, Arusha, Tanzania, United Republic of, 2021, pp. 1-6, doi: 10.1109/AFRICON51333.2021.9570865.

[138] H. G. Espinosa, D. V. Thiel and C. Brindley, "An assessment of simulation methodologies for the analysis of near-field radiation zones related to human exposure," 2014 International Workshop on Antenna Technology: Small Antennas, Novel EM Structures and Materials, and Applications (iWAT), Sydney, NSW, Australia, 2014, pp. 250-253, doi: 10.1109/IWAT.2014.6958651.

[139] C. -H. Wang, C. -J. Lee and X. Wu, "A Coverage-Based Location Approach and Performance Evaluation for the Deployment of 5G Base Stations," in IEEE Access, vol. 8, pp. 123320-123333, 2020, doi: 10.1109/ACCESS.2020.3006733.

[140] Z. Zhang, J. Chen and J. Hou, "Analysis of the Evolution Scheme of NSA RAN Sharing to SA RAN Sharing," 2021 International Wireless Communications

and Mobile Computing (IWCMC), Harbin City, China, 2021, pp. 204-211, doi: 10.1109/IWCMC51323.2021.9498959.

[141] M. Vincenzi, A. Antonopoulos, E. Kartsakli, J. Vardakas, L. Alonso and C. Verikoukis, "Cooperation incentives for multi-operator C-RAN energy efficient sharing," 2017 IEEE International Conference on Communications (ICC), Paris, France, 2017, pp. 1-6, doi: 10.1109/ICC.2017.7997131.

[142] X. Li et al., "Dimensioning of the shared transport network for collocated multiradio: LTE and HSDPA," 2012 IEEE 8th International Conference on Wireless and Mobile Computing, Networking and Communications (WiMob), Barcelona, Spain, 2012, pp. 308-315, doi: 10.1109/WiMOB.2012.6379092.

[143] M. Kassis, S. Costanzo and M. Yassin, "Flexible Multi-Operator RAN Sharing: Experimentation and Validation Using Open Source 4G/5G Prototype," 2021 Joint European Conference on Networks and Communications & 6G Summit (EuCNC/6G Summit), Porto, Portugal, 2021, pp. 205-210, doi: 10.1109/EuCNC/6GSummit51104.2021.9482466.

[144] M. De Ree, G. Mantas, A. Radwan, S. Mumtaz, J. Rodriguez and I. E. Otung, "Key Management for Beyond 5G Mobile Small Cells: A Survey," in IEEE Access, vol. 7, pp. 59200-59236, 2019, doi: 10.1109/ACCESS.2019.2914359.

[145] X. Chu, Y. Wu, D. Lopez-Perez and X. Tao, "On Providing Downlink Services in Collocated Spectrum-Sharing Macro and Femto Networks," in IEEE Transactions on Wireless Communications, vol. 10, no. 12, pp. 4306-4315, December 2011, doi: 10.1109/TWC.2011.101511.110237.

[146] V. B. Nikam, A. Arora, D. Lambture, J. Zaveri, P. Shinde and M. More, "Optimal Positioning of Small Cells for Coverage and Cost Efficient 5G Network Deployment: A Smart Simulated Annealing Approach," 2020 IEEE 3rd 5G World Forum (5GWF), Bangalore, India, 2020, pp. 454-459, doi: 10.1109/5GWF49715.2020.9221257.

[147] S. Sarkar, X. Zhang, A. Bhuyan, M. Ji and S. K. Kasera, "Uncoordinated Spectrum Sharing in Millimeter Wave Networks Using Carrier Sensing," in IEEE Transactions on Wireless Communications, vol. 21, no. 10, pp. 8368-8384, Oct. 2022, doi: 10.1109/TWC.2022.3165850.

[148] F. Héliot and T. W. C. Brown, "On the Exposure Dose Minimization of Multi-Antenna Multi-Carrier System Users," in IEEE Transactions on Vehicular Technology, vol. 71, no. 7, pp. 7625-7638, July 2022, doi: 10.1109/TVT.2022.3170606.

[149] F. Héliot and T. W. C. Brown, "Minimizing the exposure dose of Multi-Antenna Multi-Carrier System Users," 2021 Joint European Conference on Networks and Communications & 6G Summit (EuCNC/6G Summit), Porto, Portugal, 2021, pp. 170-175, doi: 10.1109/EuCNC/6GSummit51104.2021.9482420.

[150] C. Törnevik, T. Wigren, S. Guo and K. Huisman, "Time Averaged Power Control of a 4G or a 5G Radio Base Station for RF EMF Compliance," in IEEE Access, vol. 8, pp. 211937-211950, 2020, doi: 10.1109/ACCESS.2020.3039365.

[151] T. Wigren and C. Törnevik, "Coordinated Average EIRP Control of Radio Transmitters for EMF Exclusion Zone Computation," in IEEE Wireless Communications Letters, vol. 10, no. 9, pp. 2075-2079, Sept. 2021, doi: 10.1109/LWC.2021.3092190.

[152] N. Saba, L. Mela, M. U. Sheikh, K. Ruttik, J. Salo and R. Jäntti, "Measurements at 5G Commercial 26 GHz Frequency with Above and on Rooftop Level Antenna Masts in Urban Environment," 2021 IEEE 93rd Vehicular Technology Conference (VTC2021-Spring), Helsinki, Finland, 2021, pp. 1-5, doi: 10.1109/VTC2021-Spring51267.2021.9448983.

[153] J. Carlos Estrada-Jiménez, E. Pardo, U. Roth, L. Selmane and S. Faye, "Under the Hood of Electromagnetic Field Estimation and Evaluation in 5G Networks," in IEEE Access, vol. 12, pp. 88357-88369, 2024, doi: 10.1109/ACCESS.2024.3418301

[154] L. -M. Schilling, C. Bornkessel and M. A. Hein, "Analysis of Instantaneous and Maximal RF Exposure in 4G/5G Networks With Dynamic Spectrum Sharing," 2022 16th European Conference on Antennas and Propagation (EuCAP), Madrid, Spain, 2022, pp. 1-5, doi: 10.23919/EuCAP53622.2022.9769680.

[155] C. Bornkessel, T. Kopacz, A. -M. Schiffarth, D. Heberling and M. A. Hein, "Determination of Instantaneous and Maximal Human Exposure to 5G Massive-MIMO Base Stations," 2021 15th European Conference on Antennas and Propagation (EuCAP), Dusseldorf, Germany, 2021, pp. 1-5, doi: 10.23919/EuCAP51087.2021.9411089.

[156] K. Zhao, Z. Ying and S. He, "EMF Exposure Study Concerning mmWave Phased Array in Mobile Devices for 5G Communication," in IEEE Antennas and Wireless Propagation Letters, vol. 15, pp. 1132-1135, 2016, doi: 10.1109/LAWP.2015.2496229.

[157] Y. Qin, M. A. Kishk, A. Elzanaty, L. Chiaraviglio and M. -S. Alouini, "Unveiling Passive and Active EMF Exposure in Large-Scale Cellular Networks," in IEEE Open Journal of the Communications Society, vol. 5, pp. 2991-3006, 2024, doi: 10.1109/OJCOMS.2024.3390037

[158] E. Pardo, J. C. Estrada-Jimenez and S. Faye, "EMF-Aware User Association Optimization in 5G Networks," in IEEE Access, vol. 12, pp. 15946-15956, 2024, doi: 10.1109/ACCESS.2024.3355201.

[159] S. Q. Wali, A. Sali, J. K. Allami and A. F. Osman, "RF-EMF Exposure Measurement for 5G Over Mm-Wave Base Station With MIMO Antenna," in IEEE Access, vol. 10, pp. 9048-9058, 2022, doi: 10.1109/ACCESS.2022.3143805.

[160] V. Markovic, "5G EMF Exposure: Overview of Recent Research and Safety Standard Updates," 2021 15th International Conference on Advanced Technologies, Systems and Services in Telecommunications (TELSIKS), Nis, Serbia, 2021, pp. 359-365, doi: 10.1109/TELSIKS52058.2021.9606262.

[161] M. A. Jamshed, F. Héliot and T. W. C. Brown, "A Survey on Electromagnetic Risk Assessment and Evaluation Mechanism for Future Wireless Communication Systems," in IEEE Journal of Electromagnetics, RF and Microwaves in Medicine and Biology, vol. 4, no. 1, pp. 24-36, March 2020, doi: 10.1109/JERM.2019.2917766.

[162] F. Héliot, M. A. Jamshed and T. W. C. Brown, "Exposure Modelling and Minimization for Multi-antenna Communication Systems," 2020 IEEE 91st Vehicular Technology Conference (VTC2020-Spring), Antwerp, Belgium, 2020, pp. 1-6, doi: 10.1109/VTC2020-Spring48590.2020.9129510.

[163] F. Héliot and T. W. C. Brown, "On the Exposure Dose Minimization of Multi-Antenna Multi-Carrier System Users," in IEEE Transactions on Vehicular Technology, vol. 71, no. 7, pp. 7625-7638, July 2022, doi: 10.1109/TVT.2022.3170606.

[164] F. Mioc, L. Scialacqua, A. Scannavini, S. Anwar and L. J. Foged, "Power Density Evaluation of Simulated and Measured Data Based on Equivalent Currents Method," *2021 15th European Conference on Antennas and Propagation (EuCAP)*, Dusseldorf, Germany, 2021, pp. 1-4, doi: 10.23919/EuCAP51087.2021.9411062.

[165] B. Yin, W. Joseph and M. Deruyck, "RIS-Aided mmWave Network Planning Toward Connectivity Enhancement and Minimal Electromagnetic Field Exposure" in IEEE Access, vol. 11, pp. 115911-115923, 2023, doi: 10.1109/ACCESS.2023.3325678.

Appendix A

Electric and Magnetic Field Measurement

SRM-3006 Selective Radiation Meter

- Complete Solution for Selective Measurement of RF and Microwave Electromagnetic Fields
- Isotropic and Single-Axis Measurements from 9 kHz to 6 GHz
- Excellent Immunity for Operation in High Field Strengths
- Automatic Antenna and Cable Detection
- Results in V/m, A/m, Power Density, or Percentage of Permissible Limit
- Measures strength of single emitters in multiple emitter environments
- Ultra Wide Dynamic Range of 50 µV/m to 200 V/m (E-Field)
- Determines 5% Boundaries for FCC Compliance
- Resolution Bandwidths (RBWs) up to 20 MHz for UMTS and W-CDMA, 32 MHz (Level Recorder and SCOPE Modes)
- Designed for Outdoor Use: rugged, splash proof ergonomic design. Equipped with GPS and voice recorder to simplify survey reports
- Optional SCOPE, UMTS and LTE Modes

Features

The Selective Radiation Meter (SRM-3006) is our second generation, hand-held system for performing narrowband analysis of electromagnetic fields. Unlike our NBM series (broadband), the SRM-3006 has the ability to give you results of individual emitters and also generate a total of all emitters. The SRM-3006 allows you to verify compliance with the US FCC's "5% Rule" as well as accurately detect fields well below domestic and international standards. The SRM-3006 also has the ability to measure fields more accurately than broadband equipment and maybe more importantly, it is able to give you more information than just the total – like exactly what emitter or emitters are generating the most of the power.

38

narda Safety Test Solutions
TEL: (1) 631 231-1700 • FAX: (1) 631 231-1711
E-MAIL: NardaSTS@L-3com.com • www.narda-sts.us

SRM-3006 Selective Radiation Meter

No other measurement system gives you the information and accuracy that the SRM-3006 does. Narda Safety Test Solutions provides complete calibration information standard with every unit, just as you'd expect from the world leader.

The US version of the SRM-3006 consists of a basic unit (meter) and a 3-axis, E-field antenna. The meter is really an optimized spectrum analyzer covering 9 kHz to 6 GHz and modified to make accurate field strength readings with the help of our antennas. You can operate the meter with any type of antenna for special measurements (direction finding, DTV measurements, "Roberts' dipoles") but you'll be impressed by the performance of Narda's designs. We supply our SRM-3006 with a 3-axis design that covers 27 MHz to 3 GHz that is calibrated at 20 different frequencies and reliably works down to 200 µV/m . This portable, rugged and splash-proof system incorporates a highly readable color display, GPS receiver and microphone for voice recording. Also supplied is our full SRM-TS software package, a 1.5 meter cable to separate the antenna from the meter and charger, manual and other accessories inside a very protective carrying case.

Narda offers additional antennas that you'll find listed at the back of this data sheet. We have lower and higher frequency E-field antennas and some single axis designs that offer even higher accuracy. Narda can also supply single or 3-axis H-field antennas. Each antenna is individually calibrated and its factors are automatically accounted for as soon as the antenna is plugged in. We also offer longer cables for special measurement needs, non-metallic tripods, external or mobile battery chargers with extra battery packs, carrying pouches – basically everything you might need to get the survey done.

Every SRM-3006 has the ability to perform single or multiple measurements that can be averaged and/or stored in the meter for download to a computer. You can set-up the SRM-3006 the way you like and store a complete configuration for later use or repeated uses. You can set up parameters for time controlled storing that only logs the data you want above a certain threshold level. Each system has an embedded GPS receiver and microphone, so every stored reading is supplied with GPS coordinates and can have an audio description added.

Applications

The SRM-3006 has some special capabilities when it comes to RF safety measurements. In addition we have added some other operational modes (UMTS P-CPICH) for common engineering measurements. But if you simply want to perform safety measurements – the SRM-3006 makes it simple.

SAFETY EVALUATION MODE

Have you ever made a broadband measurement and wish you really knew what all the emissions all around you were really adding? The Safety Evaluation Mode is a very popular method to make a reading that simply separates emitters the way you would like them displayed. We include multiple sample tables in the meter we deliver to you that you can use as is, or modify for your own geographical area or interest. It's easy to make your own tables that quickly and cleanly show the total level of individual emitters or bands. You can display the results in common field strength or equivalent power density, or the easily understood "% of standard" units shown below. You can easily modify these tables and identify each frequency band or emitter by the name that you choose. You can add or remove entities as you see fit, thereby customizing the display for your area or need. We even offer two different displays, a common tabular listing as well as a bar graph listing, making evaluation of data quick and accurate.

This is a very powerful way to display multiple emitter data in a way that even non-technical persons understand and technical persons can appreciate.

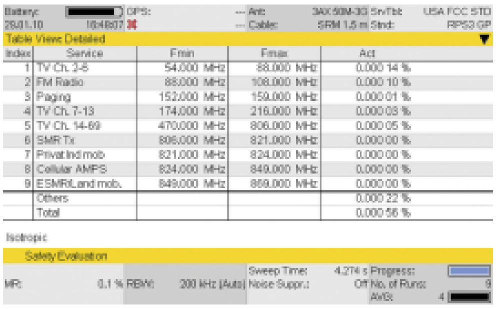
Table View Detailed

Index	Service	Fmin	Fmax	Act
1	TV Ch. 2-6	54.000 MHz	88.000 MHz	0.000 14 %
2	FM Radio	88.000 MHz	108.000 MHz	0.000 10 %
3	Paging	152.000 MHz	159.000 MHz	0.000 01 %
4	TV Ch. 7-13	174.000 MHz	216.000 MHz	0.000 03 %
5	TV Ch. 14-69	470.000 MHz	806.000 MHz	0.000 05 %
6	SMR Tx	806.000 MHz	821.000 MHz	0.000 00 %
7	Privat Ind mob	821.000 MHz	824.000 MHz	0.000 00 %
8	Cellular AMPS	824.000 MHz	849.000 MHz	0.000 00 %
9	ESMR/Land mob.	849.000 MHz	869.000 MHz	0.000 00 %
	Others			0.000 22 %
	Total			0.000 56 %

Overview with Safety Evaluation: The services to be checked are recorded in editable tables. There's no complicated evaluation needed in Safety Evaluation Mode. The numerical result shows the individual contributions of the services as well as the overall level in terms of the permitted limit value.

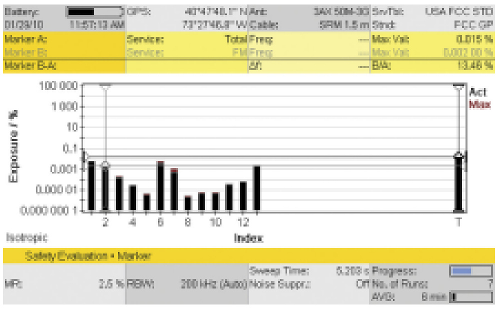

Safety Table Entries can also be displayed as bars on a graph, quickly identifying what service (or frequency) is providing the most power to your selected safety table.

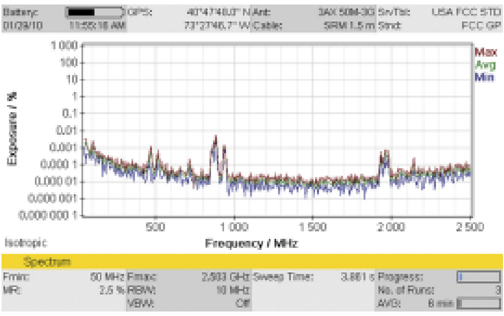

Classic Spectrum Analysis: *Result evaluation using markers and delta markers. For example, the integration function can be used to determine the channel power level. Special feature: Service Identification by means of pre-recorded service values.*

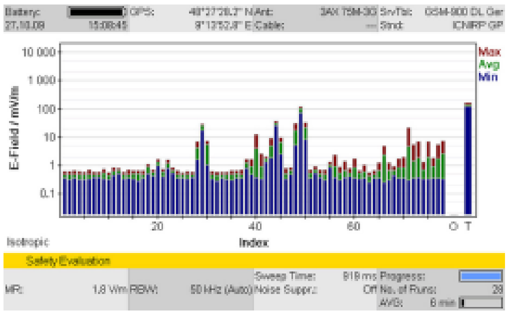

Safety Evaluation in the UMTS Range: *The individual channels with their channel numbers are shown next to each other in the bar graph display, just like a textbook. The "T" bar on the extreme right shows the total power density. The "O" bar shows the contributions from the frequency gaps (others) between the services*

SPECTRUM ANALYSIS MODE

Spectrum Analysis Mode makes finding "hidden" or "intermittent" emitters easy. Perhaps you didn't expect a certain frequency to be used in your area, but in this mode that emitter can be quickly and easily identified by the frequency and level it's operating at. This gives you the real story of what is happening right now – when and where you are performing the measurement. The SRM-3006 allows easy settings of frequencies and resolution bandwidths with a powerful "marker" function that lets you see each significant signal, set a marker on it and zoom to it in a rapid manner. When it comes time to save a spectrum view the SRM saves the entire dataset rather than just a picture. With the supplied SRM-TS software you are able to even post-process information thereby enhancing detected data for your survey reports.

When using the SRM-3006 to "direction find" or search out "cable leakage" the Spectrum Analysis Mode with our overall system design makes it a simple, portable task. First is the SRM's capability to add antennas into its memory. You can easily import calibration data of your existing antennas and/or cables and have the SRM account for them in its display.

SPATIAL AVERAGING

FCC license holders will find the built-in spatial averaging feature very powerful. Broadcasters can employ the 1.5m cable along with optional antenna holders and a non-metallic tripod to make accurate and repeatable measurements at their transmitter sites. GPS logs exactly where the measurement was taken and the narrowband performance means you just survey your emissions. Cellular operators can also use the fast time averaging for a quick vertical spatial average sweep, again logging just your emission out and beyond the "5%" distance.

LEVEL RECORDER MODE

Level Recorder Mode allows you to particularly watch one signal or band over a long time period. The display is optimized to give you four results, Maximum Peak, Actual Peak (present reading), Maximum RMS and RMS. RMS Actual is an average over a time that you choose from 0.48 seconds to 30 minutes. This makes long term monitoring of an emitter easy and supplies all the data you might need to fully evaluate its contribution to the overall site levels.

TIME CONTROLLED STORING

The SRM can store measurements under timer control by specifying the start date, start time, measurement duration, and other parameters.

Options

UMTS P-CPICH DEMODULATION

This option is useful for cellular phone companies and their consultants. The SRM-3006 automatically identifies every site and sector that it received a UMTS scrambling code from. The SRM-3006 can then measure the field strength (or power density) of the associated pilot channel (P-CPICH) at the same time. The SRM-3006 also shows the sum of all P-CPICH levels as an overall value (Total). The Analog measured value for the frequency channel is also shown for comparison. You can also set a factor that the SRM can use to extrapolate the field strength that would result if all channels were fully loaded. Therefore, instead of guessing what the UMTS signal is (at measurement time) and how it relates to the maximum possible signal strength that the site could generate, now you can measure and estimate with confidence.

SRM-3006 Selective Radiation Meter

SCOPE MODE

The Scope Mode incorporates a high speed oscilloscope that displays pulse modulated signals down to a resolution of 31.25 ns. This allows high speed characterization of WiMax signals along with any other pulsed signal below 6 GHz. This mode allows the communications engineer and technician an extended and powerful capability in a system that they needed already.

LONG TERM EVOLUTION (LTE) / 4G

LTE, also generally but less correctly known as 4G (4th generation wireless), can be utilized in the frequency ranges 700 MHz, 900 MHz, 1.8 GHz, 2.1 GHz and 2.6 GHz.

As with UMTS, LTE uses individual cells, which are differentiated by their cell numbers (cell ID, 0 to 503). Each cell can also use one, two or four antennas (multiple input – multiple output, MIMO).

LTE uses a special method of modulation called orthogonal frequency domain modulation access (OFDMA). This distributes the information across many sub-carriers spaced at intervals of 15 kHz, each of which is modulated by QPSK, 16 QAM or 64 QAM. Frequency division duplex (FDD) is generally used to separate the uplink and downlink directions (from the subscriber to the base station and vice versa), although time division duplex (TDD) is also possible.

The LTE option equips users for all the crucial measurement tasks on LTE systems with FDD. The SRM 3006:

- supports all LTE channel bandwidths from 1.4 MHz to 20 MHz
- automatically determines the cell ID and number of antennas used
- measures the average power values of the PSS and SSS
- measures the average power values of the Reference Signal, separately for each antenna, or as average power of all antennas used, or as maximum power of all antennas used
- offers automatic extrapolation using factors up to 10,000

All the usual SRM 3006 result types are available (see list, right), which users can select individually. Combined with the cell-specific power values, this gives up to 54 columns of results.

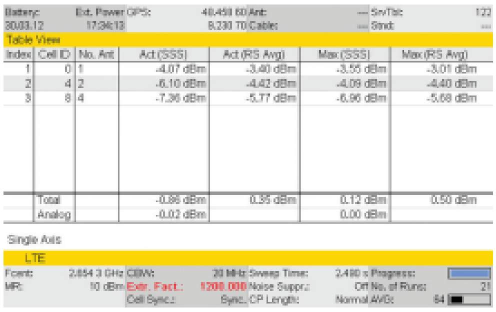

Result of an LTE measurement *with four cell-specific power values. The SRM 3006 shows the individual values obtained by demodulation and their total in the bottom line (Total) as well as the analog measured values (Analog) – similar to the UMTS option.*

Display of cell-specific power values:

PSS
Primary sync signal; average power

SSS
Secondary sync signal; average power

RS Avg
Reference signal; average power of all antennas used

RS Sum
Reference signal; sum power of all antennas used

RS Max
Reference signal; maximum power of all antennas used

RS 0, RS 1, RS 2, RS 3
Reference signal; average power of the individual antennas

Result types available:

- Actual, Act
- Maximum, Max
- Maximum Average, MxA
- Average, Avg
- Minimum Average, MnA
- Minimum, Min

Antenna Specifications

ANTENNA	Three Axis E-Field (supplied)	Three Axis E-Field 3502/01	Three Axis H-Field 3581/02	Single Axis E-Field 3531/01	Single Axis E-Field 3531/04	Single Axis H-Field 3551/02
Frequency Range [a]	27 MHz to 3 GHz	420 MHz to 6 GHz	9 kHz to 250 MHz	27 MHz to 3 GHz	9 kHz to 300 MHz	9 kHz to 300 MHz
Antenna Type	E-Field	E-Field	H-Field	E-Field	E-Field	H-Field
Sensor Type	Triaxial design with scanned axes	Triaxial design with scanned axes	Triaxial active magnetic loop design with scanned axes	Single axis passive wide band dipole	Single axis active broadband dipole	Single axis active magnetic loop
Dynamic Range [b]	0.25 mV/m to 200 V/m	0.14 mV/m to 160 V/m	2.5 µA/m to 560 mA/m	90 µV/m to 80 V/m	70 µV/m to 36 V/m	0.4 µA/m to 71 mA/m
CW Damage Level	435 V/m or 50 mW/cm²	435 V/m or 50 mW/cm²	250 A/m / f[MHz]	> 300 V/m or 25 mW/cm²	> 1000 V/m	> 2.65 A/m above 1 MHz
RF Connector [c]	N connector, 50 Ω					
Operating Temperature Range	-10° C to 50° C (same as SRM basic unit)					
Compliance: Climatic						
Storage [d]	1K3 (IEC 60721-3)					
Transport	2K4 (IEC 60721-3)					
Operating	7K2 (IEC 60721-3)					
Compliance: Mechanical						
Storage	1M2 (IEC 60721-3)					
Transport	2M3 (IEC 60721-3)					
Operating	7M3 (IEC 60721-3)					
ESD and EMC	EN 61326:2006					
Safety	EN 61010-1:2004					
CE (European Community)	Yes					
Air Humidity	< 29 g/m³ (< 93% at +30°C)					
Weight	450 g	400 g	470 g	450 g	550 g	450 g
Dimensions	450 mm length, 120 mm antenna head diameter	450 mm length, 120 mm antenna head diameter	450 mm length, 120 mm antenna head diameter	460 mm length, 135 x 90 mm antenna head dimension	460 mm length, 135 x 90 mm antenna head dimension	460 mm length; 43 x 100 mm antenna head dimension
Calibration The SRM applies linear interpolation between reference points.	20 reference points[e] 26, 45, 75, 100, 200, 300, 433, 600, 750, 900 MHz 1, 1.2, 1.4, 1.6, 1.8, 2, 2.2, 2.45, 2.7, 3 GHz	21 reference points[e] 420, 600, 750, 900 MHz 1, 1.2, 1.4, 1.6, 1.8, 2, 2.2, 2.45, 2.7, 3, 3.5, 4, 4.5, 5, 5.5, 5.8, 6 GHz	178 reference points[e]	24 reference points[e] 26, 30, 40, 50, 60, 75, 100, 200, 300, 433, 600, 750, 900 MHz 1, 1.2, 1.4, 1.6, 1.8, 2, 2.2, 2.45, 2.6, 2.8, 3 GHz	183 reference points[e]	183 reference points[e]
Calibration Interval	24 months (recommended)					

NOTES:

[a] The correction factors determined individually during calibration are stored in an EEPROM and are applied automatically when used in conjunction with the SRM basic unit.

[b] Typical measurement dynamic range for 10 dB signal to noise ratio (RBW = 1 kHz)

[c] Typical Values

[d] Extended to -10°C to +50°C

[e] The SRM basic unit applies linear interpolation between reference points

narda Safety Test Solutions
TEL: (1) 631 231-1700 • FAX: (1) 631 231-1711
E-MAIL: NardaSTS@L-3com.com • www.narda-sts.us